JAMES COOK UNIVERSITY

COLLEGE OF SCIENCE AND ENGINEERING

Wind Load Sharing and Vertical Load Transfer from Roof to Wall in a Timber-Framed House

Satheeskumar Navaratnam MSc (Eng)

DOCTORAL THESIS

Thesis submitted to the College of Science and Engineering in partial fulfilment of the requirements for the degree of

Doctor of Philosophy
(Civil Engineering)

August, 16th 2016

Statement of access

I, the undersigned, the author of this thesis, understand that James Cook University will make it available for use within the University Library and via the Australian Digital Theses network for use elsewhere.

I understand that as an unpublished work a thesis has significant protection under Copyright act and I do not wish to place restriction on access to this work.

16/08/2016

Satheeskumar Navaratnam Date

Statement of Sources

I declare that this thesis is my work and has not been submitted for another degree or diploma at any university or other institution of tertiary education. Information derived from published or unpublished work of others has been acknowledged in the text and a list of references given.

16/08/2016

Satheeskumar Navaratnam Date

Statement on the contribution of others

Grants: This research work was supported by CSIRO "Climate Adaptation Engineering for Extreme Events Cluster", managed by CSIRO Land and Water Business Unit. Additional funding was received from the College of Science and Engineering, and the Cyclone Testing Station (CTS) at James Cook University (JCU). A CSIRO Top-Up Scholarship was awarded for stipend (living allowance) and travel support, and additional travel stipend was also awarded by the Graduate Research School (GRS) at James Cook University to present the papers at international and national conferences.

Supervision: Prof. J.D. Ginger (JCU) was the principle supervisor of this work. Other supervision was provided by Dr. D.J. Henderson (JCU) and Dr. C-H. Wang (CSIRO).

Editorial Assistance: The editorial assistance was provided by Prof J.D. Ginger (JCU), Dr. D.J. Henderson (JCU), Dr. C-H. Wang (CSIRO) and Adjunct Prof. G.R. Walker (JCU).

Acknowledgements

I am extremely grateful and deeply indebted to acknowledge the valuable contributions of the many people who have helped to make this research possible. First and foremost thank Prof. John Ginger for his excellent, guidance, support, patience and encouragement throughout this research. I also thank Dr. David Henderson for his advice, guidance and invaluable discussions.

I acknowledge the funding support of CSIRO, Australia. I would like to thank Dr. Chi-Hsiang Wang (CSIRO) for his support, advice and feedback about this project.

I would like to thank Prof. Geoffrey Boughton and for many interesting discussions pertaining to his experiences with full-scale testing and damage investigations. I also thank Prof. George Walker for his advice and feedback about this project.

I also would like to thank staff and the technicians of Cyclone Testing Station for their support, assistance and advice. Specially, I would like to thank Mr. Dennis Smith and Mr. Don Braddick for their support on the construction of the test structure.

Many thanks go to fellow post graduate student at JCU, Mr. Mitchell Humphreys for his support to setting up and assisting with conducting the structural tests.

Finally, I would like to thank my family and friends for their steady support and encouragement. I am especially thankful to my mum, Mrs Indiradevi, for her patience and support.

ABSTRACT

Windstorms are one of the major causes of severe damage to houses and other infrastructure. Damage investigations indicate that the roof is the most vulnerable part of a timber-framed house, and that failures take place at inter component connections; hence there is a need to study the load sharing and structural response of these timber-framed house structural systems to assess their performance. Contemporary houses in many parts of Australia are brick veneer structures with metal or tile clad roofs that are built to National Construction Code of Australia's design specifications.

Full-scale tests were carried out on a representative part of a brick veneer contemporary house to assess the loading effects on roof to wall connections and load sharing. Tests were conducted for each stage of construction: bare frame followed by the installation of roof battens and cladding, wall lining, ceiling, etc. These construction stages were used to assess the contribution of the structural and lining (i.e. ceiling, ceiling cornice and wall lining) elements to the load sharing and response of the timber-framed house structure to wind loading. Results show that the vertical load sharing of the timber-framed house through the roof to wall connection depends on the stiffness of the roof to wall connection and the truss location (i.e. whether located at the end or middle). The contribution of the lining elements to the vertical load sharing is about 15% to 20%.

In addition, individual component tests were conducted on the roof to wall framing anchor (i.e. triple grip and truss grip) connections to examine their structural response to loading. This study also showed that construction defects in roof to wall connections influence the design uplift capacity. Two missing nails out of ten in the hand nailed triple grip connection (i.e. one nail from the truss and other one from the top plate) reduces the design uplift capacity by about 40 % of the "Ideal" hand nailed triple grip connection. Finite element models were also developed for part of the timber framed house and roof to wall connections (i.e. triple grip and truss grip connections) using ABAQUS finite element software. Results obtained from the finite element models were compared with the experimental tests, showing good agreement. This finite element model can be used to predict the roof to wall connection response and truss hold-down force variation with a range of construction defects and truss bay configurations. The overall outcomes can be used to evaluate house structure vulnerability to wind loading, and to improve the design and standards of timber-framed houses.

Table of Contents

List of Figures

List of Tables

NOMENCLATURE

A_i	Tributary Area
C_p	Pressure Coefficient
C_N	Dimension-Less Hold-Down Force
C_{dyn}	Dynamic Response Factor
C_{fig}	Aerodynamic Shape Factor
COV	Coefficient of Variation
CTS	Cyclone Testing Station
DAQ	Data Acquisition
FE	Finite Element
FEM	Finite Element Model
G_u	Gust Factor
I_{uu}	Turbulent Intensity
JCU	James Cook University
LVDT	Linear Variable Displacement Transducer
MGP	Machine Graded Pine
PLA	Pressure Load Actuator
RWC	Roof to Wall Connection
SPM	Superposition Method
$\overline{U}_h$	Mean Wind Velocity at Mid Roof Height *h*
UWO	University of Western Ontario, Canada
$V_{des,\theta}$	Design Gust Wind Speed at Mid Roof Height *h*
VRC	Vertical Reaction Coefficient
(t)	Fluctuating Reaction Force at Time *t*
ρ	Density of Air
β_i	Influence Coefficient

LIST OF PUBLICATIONS

Journal Publications

- Satheeskumar, N., Henderson, D. J., Ginger, J. D. and Wang, C.H. (2016). "*Wind Uplift Strength Capacity Variation in Roof-to-Wall Connections of Timber-Framed Houses*." Journal of Architectural Engineering, 10.1061/(ASCE)AE.1943-5568.0000204 , 04016003.

- Satheeskumar, N., Henderson, D. J., Ginger, J. D., Humphreys, M.T. and Wang, C.H. (2016). "*Load Sharing and Structural Response of roof-wall system in a Timber-Framed House*." Engineering Structures 122:310-322.

- Satheeskumar, N., Henderson, D. J., Ginger, J. D. and Wang, C.H. (2016). "*Finite Element Modelling of the Structural Response of Roof to Wall Framing Connections in Timber-Framed House*s." Engineering Structures 134:25-36.

- Satheeskumar, N., Henderson, D. J., Ginger, J. D. and Wang, C.H. (2016). "*Three-Dimensional Finite Element Modelling and Validation of a Timber-Framed House to Wind Loading*." Paper submitted to Journal of Structural Engineering (ASCE).

Conference Publications

- Satheeskumar, N., Henderson, D. J., Ginger, J. D. and Wang, C.H. (2015). "*Loading Effects on Timber Truss to Wall Connection in a Contemporary House*". 17th AWES Workshop, Wellington, NZ in February 2015.
- Satheeskumar, N., Henderson, D. J., Ginger, J. D. and Wang, C.H. (2015). "*Wind Loading Effects on Roof to Wall Connection in a Timber Frame Structure*". 14th ICWE, Porto Alegre, Brazil – June 21-26, 2015
- Satheeskumar, N., Henderson, D. J., Ginger, J. D. and Wang, C.H. (2015). "*Load Sharing and Structural Response of Timber-Framed House*", Second International Conference on Performance-based and Life-cycle Structural Engineering (PLSE 2015), Brisbane, Australia, 9-11 December 2015.
- Satheeskumar, N., Henderson, D. J., Ginger, J. D. and Wang, C.H. (2016). "*Three-Dimensional Modelling of the Timber- Framed Houses to Uplift Loading*". 24th Australian Conference on the Mechanics and Structures and Materials (ACMSM24), Perth, Australia, December 6-10, 2016.

CHAPTER 1: INTRODUCTION

Windstorms have caused billions of dollars in damage to infrastructure (buildings, houses, transport etc.), significant insurance payouts and loss of lives to coastal regions around the world. Two extreme wind events that led to significant changes in building codes were; Cyclone Tracy which caused extreme damage in Darwin, Australia (Walker, 1975), and Hurricane Andrew in the United States (US) (Department of Housing and Urban Development, 1993). During Cyclone Tracy, the loss of roof cladding in houses resulted in extreme damage, leading to a significant loss of strength in house structure, which resulted in progressive collapse (Walker, 1975). These failures have shown that timber-framed residential structures can be highly vulnerable to windstorms. After Cyclone Tracy, all levels of government, researchers, insurance companies and structural engineers raised questions about the vulnerability of the timber-framed houses in Australia. As a result, research studies and investigations were conducted by way of wind tunnel testing, wind climate measurements and modelling, structural analysis, full-scale field testing and full-scale laboratory testing in order to assess the strength, revise the design codes and improve the structural stability of the house structure.

Individual components' (i.e. wall, ceiling, connections, etc.) laboratory tests were carried out at the Cyclone Testing Station (CTS), James Cook University by Walker and Gonano (1981, 1982 and 1983) and Reardon (1979) to evaluate the load transmission, strength and stiffness of timber-framed houses and their structural and non-structural elements. Two basic forms of load transmission were found from these laboratory tests: (i) transmission of vertical uplift loads from the roof to the foundations, primarily achieved by ensuring a direct load path from the main roof structure to the foundations, and (ii) transmission of lateral loads. To evaluate vertical transfer, most experiments focused on testing various types of connections between roof cladding and battens, between battens and trusses, between trusses and the top-plates, and between the top-plates and the foundations.

Transmission of lateral loads was more complex, involving transmission of the lateral loads on the walls, and the lateral component of roof loads to transverse walls by diaphragm action of the ceiling linings. These forces were transmitted to the foundations by diaphragm action of the transverse walls. In each case (i.e. vertical and lateral loads' transmission) connections were a very important part of the structural system to transfer

the loads. These individual components' tests were 'deemed-to-comply' with construction standards for wind loading, which were developed to cover most conventional forms of houses. All the members, including the connections, ceiling diaphragm and transverse walls, were assumed to transmit the loads and were regarded as structural elements. The members were rated in terms of strength, and the structural transmission was assumed to be taken by a limited number of walls designed to meet these requirements, with the rest of the walls regarded as non-structural.

The full-scale house tests under simulated wind loads, including houses designed for cyclone areas, were carried out at the CTS by Boughton and Reardon (1982, 1983a, 1983b, and 1984). Houses were tested to failure, with the failure loads compared with design loads. The full-scale test results showed that the new design approach was mostly conservative in terms of assumed structural behaviour, as Boughton and Reardon (1982) found there were inherent redundancies in the structural behaviour of houses as a whole unit. Based on the simplifications of load transmission assumed in the design, these redundancies provided more wind resistance in houses than estimated. The complexity of the actual load transmission was difficult to incorporate in design, without full-scale testing of individual house designs. The full-scale tests (Boughton and Reardon, 1982, 1983 and 1984; Reardon, 1986 and 1990; Reardon and Mahendran, 1988; Reardon and Henderson, 1996) qualitatively showed the strength, stiffness and load transfer of the house system subjected to wind load, with various structural and lining components such as wall lining, ceiling and ceiling cornice. Therefore, quantitative analysis of load sharing and contribution of the structural and lining elements to the load sharing of the timber-framed house structure are needed.

Recently, several other full-scale house tests have been carried out to evaluate the structural response and load transmission of the North American and Canadian residential houses (Morrison, 2010; Datin et al., 2007; Doudak et al., 2012; Canino et al., 2011). However, the usefulness of these experimental results to assess the structural response of Australian residential house is limited, as their construction types are different. In non-hurricane regions of North America, houses are generally light-framed wood structural systems and have wood sheathing on the walls and roof, and roof trusses are toe-nailed to the wall top-plate. Modern houses in non-cyclone regions of Australia are brick veneer wall, metal roof cladding and roof trusses that are tied with triple grip connections to the

wall top-plate. These variations in construction result in differences in their structural response to wind load. Both the full-scale and individual components' test (Boughton and Reardon, 1982, 1983 and 1984; Reardon, 1986 and 1979; Reardon et al, 1988; Walker and Gonano, 1981, 1982 and 1983) results assisted in the developing building standards for housing and recommendations that houses should be structurally designed to resist extreme winds in cyclone prone areas. The recommendations were largely implemented by the early 1980's, and by the early 1990's had been extended Australia-wide through the Building Code of Australia and a range of standards (AS 1684.1, 2002; AS 1684.2, 2010; AS 1684.3, 2010; AS 1720.1, 2010). Similar process were adopted around the same time in respect of earthquakes in New Zealand. In the 1990's, following damage from Hurricane Andrew, similar type of recommendations were adopted in many hurricane prone areas of the US (Khan et al., 1993; Gurley et al., 2006).

In very broad-brush terms, houses in Australia are categorised into two types: Pre1980s and Post 1980s. Pre1980s houses were generally built by skilled labourers and builders, with limited engineering design input, and their sizes were smaller compared to post 1980s houses. Post 1980s houses (contemporary houses) are built by trained builders, using skilled and/or semi-skilled labourers to engineering design specifications (i.e. AS 4055, 2012). Houses are constructed using a range of structural components (battens, trusses, top and bottom plates, wall, roof cladding, foundation, etc.) and connected by inter-component connections, which are usually cladding to batten, batten to truss, truss to wall and wall to foundation connections. Differences in design and construction will cause variable damage to houses within a community during windstorms as shown recently in Australia after Cyclone Yasi, Cyclone Larry and the Brisbane Thunderstorms.

The roof of a house generally experiences the highest wind loads, and has typically been the most vulnerable part of a house to wind loads. Post windstorm disaster investigations (Walker, 1975; Boughton et al., 2011; Leitch et al., 2009; Shanmugasundaram et al., 1995 and 2000) indicated that failures of many house structures were due to loss of the roof cladding system. These type of failures were due to the high internal pressure generated by a dominant opening on the windward wall (resulting from wind pressure or windborne debris impact) and construction defects. The damage investigations and research have clearly shown that the wind introduced external and internal pressure on a building, construction defects (i.e. missing fasteners, overdriving of nails and improper placement

of anchor bolts) and the resulting structural response must be accurately determined, in order to assess the fragility of structural components in houses. The damage in recent windstorms, such as in Cyclone Marcia (2015, Figure 1.1), Cyclone Olwyn (2015), the Brisbane Severe Storm (2014), and the Tornado in Oklahoma (2015, Figure 1.2) show the roof structure failures due to the high wind speed, which caused cascading failure. These failures indicate that timber-framed houses remain vulnerable in cyclonic and non-cyclonic regions.

Figure 1.1. Roof removed and exterior walls collapsed in a pre1980's house at Yeppoon (photo courtesy of CTS)

Figure 1.2. A metal-clad building with wood post frame construction destroyed (Prevatt et al., 2015)

Post 1980s houses of Australia are designed and built for a low internal pressure in non-cyclonic regions, whilst the houses in cyclonic regions are designed and built to the high internal pressure resulting from dominant opening (AS 4055, 2012). Therefore, potentially Post1980s houses in non-cyclonic regions of Australia are more vulnerable than those in cyclonic regions (Ginger et al., 2015) when a dominant wall opening is created. As a result, there has been an increasing focus within the structural engineering research community to assess the actual performance of structures under extreme events, particularly timber-framed houses because of their importance in respect of disaster mitigation.

The wind disaster mitigation policies for residential houses are specified based on the investigation of the vulnerability of a houses, damage estimation and cost of repair or replacement (Walker, 2011; Smith et al, 2015; Pinelli et al, 2008). Damage estimation in terms of loading depends on the load on each structural member and the inter-component connection along with their capacities. This requires a good understanding of their structural response to wind loading. Several studies have been conducted to evaluate the response and behavior of many of the components (i.e. roof to wall connection, cladding to battens connection, battens to truss connection) of timber house structures. However, there is only limited data available on the load distributions through inter-component connections, and progressive damage due to connection failure to wind loading. Moreover, construction defects and lack of knowledge in load sharing systems also increases the probability of structural failures in extreme wind events.

The evaluation of the structural adequacy of house design to windstorms is also needed due to the introduction of new materials, and the type of construction with new and old materials in current house construction (i.e. similar to retrofitted house after damage) (Dorey and Schriever, 1957; Smith et al, 2015). To assess the structural adequacy of house design, more sub-assembly tests on the structural elements and inter-component connections as well as full-scale house tests are required. Recent studies at the CTS, James Cook University, investigated the response of roof cladding to batten connection by Henderson (2010) and Lovisa (2015), and batten to truss connections by Jayasinghe (2012) in the vertical load path of the house (Figure 1.3) by testing sub-assembly systems. One of the unresolved issues pertaining to timber-framed residential structures is the load

sharing between adjacent trusses and roof to wall connections during uplift loading (Henderson et al., 2013).

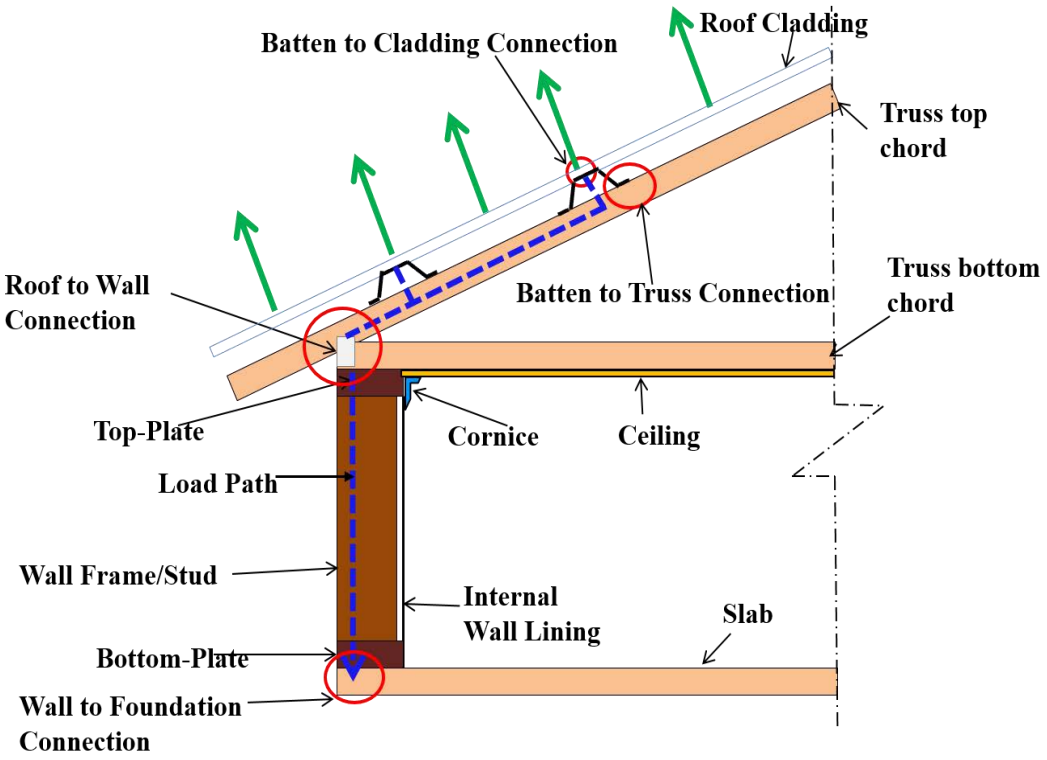

Figure 1.3. Schematic diagram of the vertical load path of the timber-framed house

The current study, investigates the "response of roof structure and its connections to the wall of a house to wind loading". Wind tunnel model test, full-scale test, individual joint tests (i.e. roof to wall connections and glued and screwed fastener joints between the plasterboard and timber) and numerical model analysis are used assess the structural response of contemporary house to wind loads.

1.1 Objective

The aim is to quantify the load sharing and transfer of the load from roof to wall through the truss to wall connection of a timber-framed house. The load sharing and load transfer of the timber framed house are dependent on the structural response and capacity of their inter-component connections and, structural (i.e. truss, cladding, battens, studs, etc.) and lining elements (i.e. ceiling, ceiling cornice and wall lining).

Full-scale tests were conducted on the general truss region of a contemporary representative house to determine the influence coefficients for critical load effects, and evaluate the contribution of the structural and lining elements to the load sharing in timber-framed house. In addition, following supplementary tasks were used to achieve these objectives;

- Define the contemporary representative house and its inter-component connections and construction types from the field survey.
- Investigate the roof to wall connections' structural response by conducting sub assembly tests.
- Develop a finite element model (FEM) of the full-scale tested structure, and validate the model using full-scale test results. The model was developed to represent a real house.
- Evaluate the wind loading on a part of contemporary representative house using wind tunnel studies and FEM.

1.2 Thesis outline

The contents of this thesis are:

Chapter 2 reviews the fundamental concepts in wind load distributions and timber-framed house structural system design and construction. This Chapter also reviewed the full-scale tests and numerical modelling of the timber-framed structure and inter-component connections.

Chapter 3 presents details of the field survey and defines the contemporary representative house and its common roof to wall connections and construction defects. The experimental investigation on the individual joints, such as common roof to wall connections with and without construction defects and, glued and screwed joint between the timber and plasterboard are discussed in Chapter 4.

Chapter 5 reports the findings of full-scale tests on the representative contemporary house's general truss region. The load sharing and the contribution of the structural and lining elements to the load sharing are also detailed in this Chapter.

The FEM development, analysis and validation for the full-scale test structure are presented in the Chapter 6. This Chapter also discusses the FEM of the representative house, and the influence coefficients at the roof to wall connection.

Chapter 7 describes the wind tunnel model studies on the contemporary representative house and the wind pressure distribution on the full-scale test structure. This chapter also revealed the comparison of the truss hold-down force between the standards and full-scale test results.

Chapter 8 highlights the major conclusions drawn from this research, recommendations and potential areas for further research.

Appendix A reports the method to determine the design uplift capacity from laboratory test results. The calibration details of the measuring devises and full-scale test setups are presented in Appendix B. The FEM development and validation for the roof to wall connection, and additional results from the FEM of full-scale test structure are presented in Appendix C and D, respectively. Appendix E describes the sample wind load calculation.

CHAPTER 2: LITERATURE REVIEW

2.1 Introduction

The design approach to ensuring stability of a house structure under wind loading is to transfer wind loads from the roof and wall structure to the foundation, through secure inter-component connections. Although this approach has been shown as adequate, the complex structural system in a house (i.e. compared to other buildings) may result in non-optimal design (Walker and Reardon, 1987). Timber-framed construction is widely used for residential building in Australia. The design and construction of contemporary houses in Australia is based on the wind region (Figure 2.1) and wind classification. The wind load Standard and Building Codes of Australia (AS/NZS 1170.2, 2011; BCA, 2011) provide the parameters such as design wind speed and aerodynamic shape factors to determine wind loads on buildings.

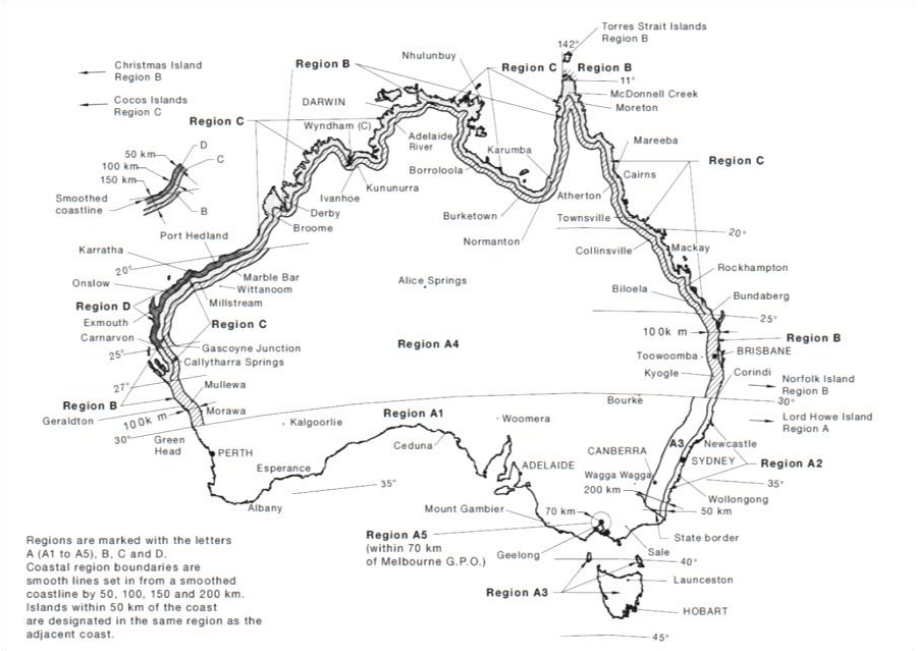

Figure 2.1. Wind regions of Australia (AS/NZS 1170.2, 2011)

The design of a timber-framed house structure aims to contest the strength (i.e. capacity) of structural components and connections with the loads applied during a windstorm, is sufficient to avoid structural failure. Prevention of structural damage to houses due to wind loading requires the connections to be robust and structural components able to transfer the fluctuating wind load.

The failure of components (i.e. wall, roof, etc.) and the modes of progressive damage are dependent on the load distribution, structural response, load sharing and the strength of structural members and connections. The load sharing of the timber-framed house structure is influenced by the type of roof system, geometry, cladding, battens, truss, ceiling, wall, and types of inter-component connections. This literature review examines the timber-framed house structural system design and construction, load distribution, structural response and load sharing.

2.2 Windstorm damage

Windstorms in Australia (Cyclone Tracy, Cyclone Yasi, Cyclone Larry, Brisbane Thunderstorms, Cyclone Marcia, etc.) have caused severe damage to houses due to high gust wind speeds. After these events, research and investigations were conducted in order to assess design and structural strength of timber-framed houses (Walker, 1975; Boughton and Reardon, 1982, 1983, 1984; Leitch et al., 2009; Boughton et al., 2011). During Cyclone Tracy, the loss of roof cladding led to extreme damage, a subsequent significant loss of strength in connections, creating progressive collapse (Walker, 1975). Walker (1975) also found that engineered structures performed better compared to non-engineered structures. His report strongly recommended that houses in Australia be engineered, and their structural design should be certified by a structural engineer and to have their construction adequately supervised.

More recently Cyclone Yasi caused failures of roof, roofing components (batten to cladding connection, the batten to rafter connections, etc.) and roller doors especially in older houses (i.e. built before 1980s). Boughton et al (2011) found that the reason for these types of failures was due to the high internal pressure created by a dominant opening on the windward wall (resulting from wind pressure or windborne debris impact) as shown in Figure 2.2. This type of failure was also found in Cyclone Tracy (Walker, 1975) and the Brisbane Thunderstorms (Leitch et al., 2009). In addition, Boughton et al (2011) also found that there were hidden or partial failures of the structural connections within the roof (Figure 2.3). These hidden failures reduced the strength and stiffness of the connections. This stiffness reduction in the connections will affect the load sharing and creates progressive failures (Morrison, 2010). Hence, these hidden failures should be repaired otherwise they will cause significant damage to the timber-framed house structure in future events (Boughton et al., 2011).

Figure 2.2. Roof loss after failure of door on the windward wall (Boughton et al., 2011)

Figure 2.3. Partial withdrawal of nails in batten to rafter connection (Boughton et al., 2011)

Hurricane Andrew (1992) and Hurricane Katrina (2005) caused severe damage to houses in the US, with most of the failures being the roof sheathing. Hurricane Andrew estimated that about 77% of houses had failures of roof covering and about 64% of houses had failure of windows and/or doors (Department of Housing and Urban Development, 1993). These window and door failures increased the internal pressure and that caused most of roof failures (Keith and Rose, 1994). Hurricane Katrina's damage indicated that more detailed concern needs to be paid to all connections, especially the correct use of all straps and ties to securely convey the load from roof to foundation (Van de Lindt et al., 2007). These research studies and damage investigations showed that the roof, roofing components and connections are the most vulnerable structural elements in the timber-framed house structural system. Furthermore, a detailed knowledge of the wind load distribution and load sharing from the roof to foundation is required to assess the performance of houses to windstorms.

2.3 Contemporary house structural system

The structural system of timber-framed houses vary from country to country and region to region, and have developed over time. In most parts of Australia, residential structures are a timber-framed construction, which enables quicker construction. Depending on the location (Figure 2.1), Australian houses can be categorised into two types: cyclonic region and non-cyclonic region houses. Moreover, houses can be catergorised as Pre1980s and Post 1980s houses. Pre 1980s houses in cyclonic regions are generally timber-framed nail constructions with studded walls and inset diagonal timber bracing and that had limited engineering inputs. Roofing is bolted truss or orthodox framing construction with galvanized-iron sheeting and diagonal timber bracing. Houses built between 1968 and 1972 were structurally similar, except for the use of gang-nails on trusses and triple-grips for the connection between purlin and truss (i.e. strap type connectors were replaced with simple nail connections).

Since then, trusses have become the dominant roofing structural system, but bracing between trusses has been largely removed (Walker, 1975), under the supposition that the roof sheeting resisted the wind load and acted as bracing. Houses built towards the end of this era incorporated cyclone provisions such as more effective use of cyclone rods and the use of screws instead of nails for fixing roofing material. Post 1980s houses in cyclonic regions are generally engineered structures that are designed to standards (AS

1684.3, 2010; AS 4055, 2012); consisting of a slab on the ground, one storey, and timber-framed or reinforced masonry block wall houses with steel clad low roofs with short eaves. These types of houses were the most commonly built immediately after Cyclone Tracy. The layout of a timber-framed house structural system in Australia is shown in Figure 2.4.

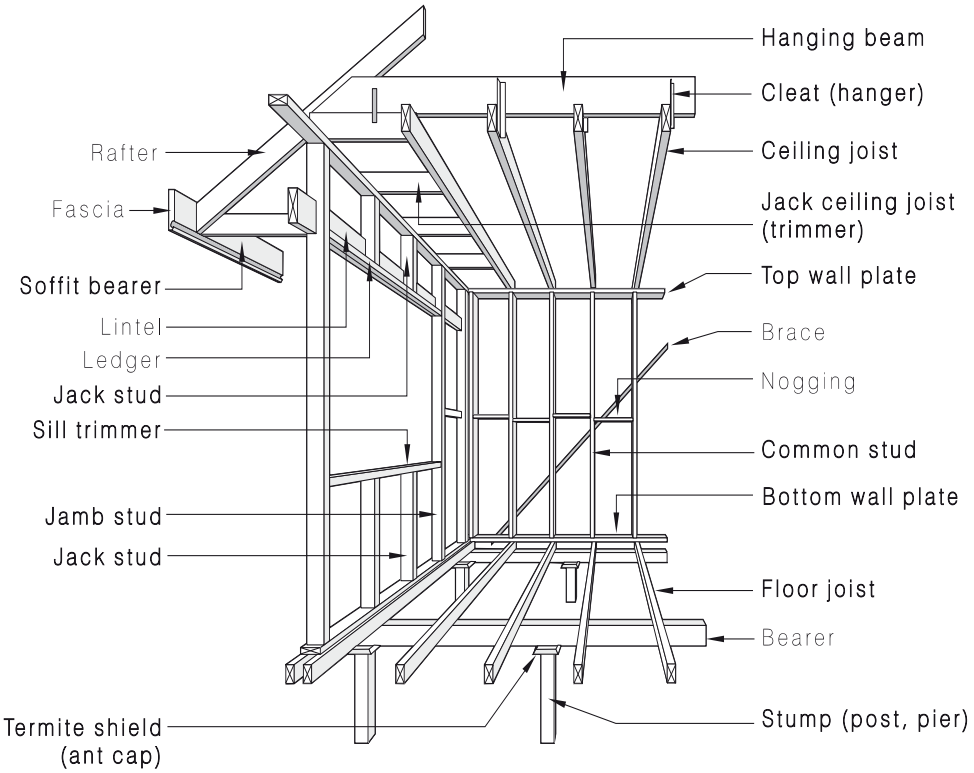

Figure 2.4. Typical arrangement of timber-framed house, (AS1684.3, 2010)

Contemporary houses in cyclonic regions of Australia are generally masonry block construction systems (Jayasinghe, 2012). This type of house is constructed on a concrete slab on the ground and concrete filled masonry blocks with regular spaced continuous reinforcement from slab to bond beam. The roof shapes of these cyclonic region houses are gable or hip, or a combination of both.

The contemporary houses in non-cyclonic regions are generally brick veneer (i.e. external wall cladding) construction systems with the roof shapes similar to cyclonic region houses. Tiles and metal cladding are used in these non-cyclonic region house roofs, the tiles are attached to timber battens, and the metal cladding is fixed to metal top-hat battens. Shear walls in these contemporary house are based on the length of the house and

wind speed. The schematic diagram of a brick veneer contemporary house structural system is shown in Figure 2.5.

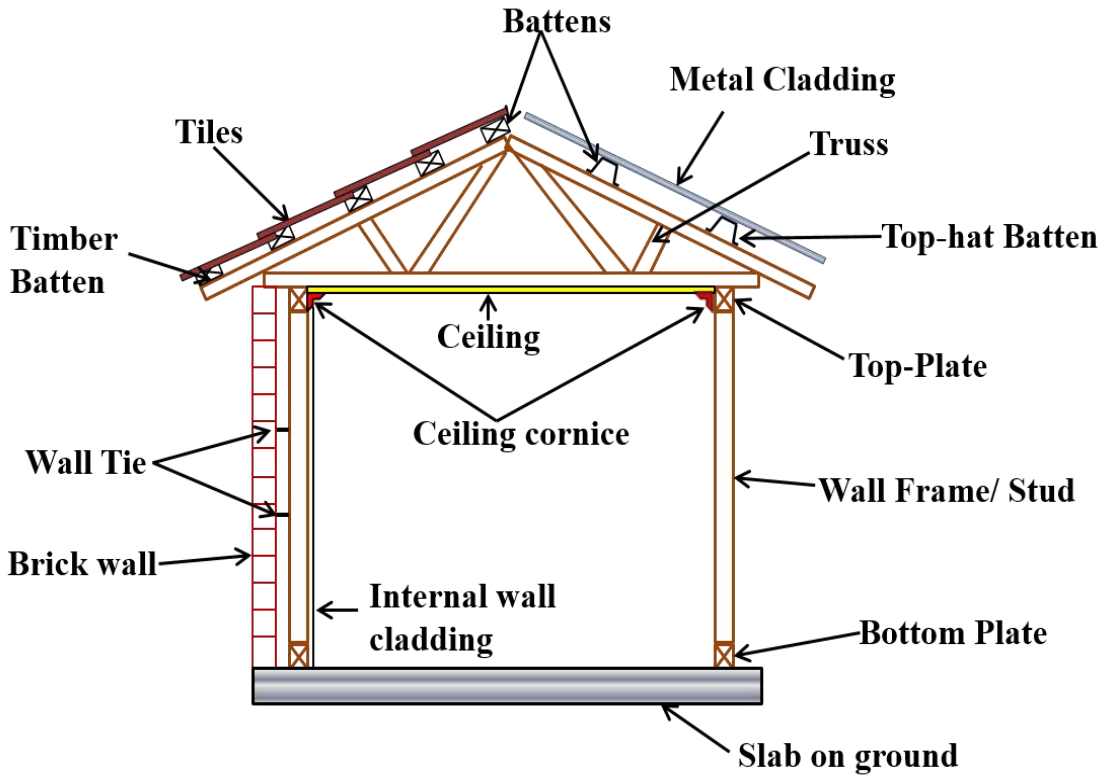

Figure 2.5. Schematic diagram of a brick veneer contemporary house structural system

2.3.1 Roof structure

The roof system of a timber-framed house consists of cladding, battens, trusses, top-plates, etc. Tiles and metal cladding are the common roof cladding materials used in Australia, and are dependent on the climate and aesthetics. The installation of roof tiles is specified in Australian Standard AS 2050 (2002), which strongly recommends that every full tile should be mechanically fastened according to wind classification AS 4055 (2012). The structural response of the roof structural system to windstorm is strongly influenced by the connections: cladding to batten, batten to trusses and truss to top-plate. In addition, response of the roof structure also depends on the ceiling and ceiling cornice, which distributes or transfers the wind loads from the roof structure to wall.

2.3.2 Wall structure

The wall structure plays an important role in the timber-framed house, resisting racking loads as well as vertical loads by transfer of the loads to the foundation. Plywood sheathing, plasterboard, brick veneer, metal cladding and reinforced masonry blocks are commonly used in Australian house wall structures. The structural behavior and response of plywood sheathing walls to wind loading mainly depends on the nail force-slip characteristics. Moreover, plywood sheathing's structural response also depends on studs and the sheathing stiffness and strength (Gupta et al., 1985). Commonly, this type of wall structure is used in the US, Canada, UK and Australia, while brick veneer type walls are commonly used in low rise buildings in some part of the world (i.e. Australia, US, India, France, China, etc.). The brick veneer is used in conjunction with inner timber frame units, where brick ties are used to connect the timber frame to the brick veneer. The advantage of a brick veneer wall is excellent thermal performance and prevention of water penetration. This brick veneer is not designed to carry lateral loads but it can convey the lateral loads through the brick ties to the frame (Reardon et al., 1988; Choi et al., 2004).

Masonry block wall constructions are popular in the cyclone regions of Australia. Masonry blocks have large hollow cores allowing steel reinforcing to run through walls, and some cores to be filled with concrete. Normally, brick veneer construction and masonry blocks are built onto the slab with starter bars running through the cores. Horizontal steel reinforcement is used along with shear ties in the concrete bond beam at the top of the walls, and vertical reinforcing steel is tied to the starter bars and runs the entire height of the wall.

2.3.3 Inter-component connections

In a house structural system, connections are designed to transfer uplift and lateral loads during a strong wind event, and should provide a continuous load path from the roof to the foundation. Common types of connections used in timber-framed construction are cladding to batten, batten to truss, truss or rafter to top-plate, top-plate to wall frame, and wall to foundation connections. The strength of the connections varies with type, design, material, construction practices and workmanship (Jayasinghe, 2012). The inter-component connections of timber-framed houses are commonly made by nails, nail plates, bolts and nuts, screws, glue and straps, or a combination of these. They are simple

to install but their response to wind loads are more complex compared to other building connections (i.e. steel joints, concrete and steel connection, etc.) (Guha et al., 2012).

Many windstorm damage investigations including those by Boughton et al (2011), Walker (1975), and Shanmugasundaram et al (1995) have shown that the failure of connections between structural components is mainly responsible for major damage to timber-framed houses. The failure of connections can often be attributed to construction defects which result from inadequate quality assurance, missing fasteners, overdriving of nails and improper placement of anchor bolts (Leitch et al., 2009).

2.3.3.1 Cladding to batten connection

The number and type of fasteners for cladding to batten connection are specified in the standard (AS 1684.2, 2010; AS 1684.3, 2010) and manufacturer's specifications. This cladding to batten connection is designed to transfer the wind load to the battens. A common failure in the metal roof cladding system is fatigue failure (Mahendran, 1995; Walker, 1975; Boughton et al., 2011). The large number of low level load cycles or fewer cycles at a level closer to the ultimate static capacity can create this fatigue failure (Henderson, 2010; Henderson and Ginger, 2005). In addition, metal roof cladding may cause tearing of sheeting due to the profile of the roof cladding carrying part of the racking forces (Mahendran, 1998).

Boughton et al (2011) found that the performance of the metal roof cladding is better than the tile roof in a house during windstorm. In the case of tile roof cladding systems, half the tiles are tied down by use of metal clips. However, "Clips may suffer from a low cycle fatigue failure under the fluctuating wind loading, which results in the loss of tiles" (Boughton et al., 2011). A study by Henderson (2010) showed that the roof cladding system construction and design require improvements to enable innovative, efficient and economic use of materials. Such as additional screws in highly loaded corners and gable ends and reduced the number of screws in central area of roof. Henderson (2010) also suggested that manufactures' load span design tables should be improved to incorporate the peak loading pressures that are underestimated in AS/NZS 1170.2 (2002).

2.3.3.2 Batten to truss connection

Battens are located immediately under the roof cladding, and are fixed to the rafters or trusses in house structural systems. Screws, nails and metal straps, either singly or in combination, are commonly used to fix battens and trusses or rafters. Recent research studies carried out by Jayasinghe (2012) found that loads on the batten to truss connection are strongly influenced by the behaviour of the structural system and the wind pressure distribution on the roof. Moreover, Jayasinghe (2012) found that the conventional connection tributary area used in normal design practice can be unreliable, and can lead to underestimation of the connection load. In cyclonic regions, the batten to truss connection may suffer from fatigue failure due to the battens' locations experiencing the high wind load (Mahendran, 1995).

2.3.3.3 Roof to wall connection (RWC)

The roof to wall connection (RWC) is another vulnerable structural component in the load path of a house structural system. This connection should provide a continuous load path from the roof to the wall. Discontinuity in the load path will cause severe damage to the roof structure in extreme windstorm events (Guha et al., 2012). Common RWCs are made by nails, metal plates and clips connected with nails. The RWC should be designed to resist the uplift load as well as the lateral load component. Several experimental studies and numerical analyses were conducted to evaluate the performance of RWCs (Guha et al., 2012; Shanmugam et al., 2009; Cheng et al., 2003; Reed et al., 1997; Morrison et al., 2012; Henderson et al., 2013; etc.). Some of these studies applied static loads and cyclic loads which were able to capture the hysteretic and normal behavior of the connections at low levels of deformation.

Figures 2.6 and 2.7 show the roof loss due to RWCs failures during Cyclone Marcia. Figure 2.6 illustrates the roof to wall triple grip connection failure of the roof. The house's open veranda roof structure was held by timber posts and the veranda region was exposed to the windward direction. During cyclone Marcia, the high wind speeds initiated the failure of the connection between the floor and timber post. The failure of this floor to the timber post's connection created the cascading failure to the veranda RWCs, conveying it to the whole roof.

Figure 2.6. Roof loss after failure of windward side timber post (located at veranda) connection at floor (Photo courtesy of CTS**)**

Figure 2.7 shows the whole roof loss of a house during Cyclone Marcia. This is an old house where the roof structure's cladding, battens, batten to truss connections and batten to cladding connections were replaced recently. The RWCs were not replaced or repaired and that resulted in the whole roof failure during Cyclone Marcia. These failures indicate poor construction practice and high gust wind speed increase the probability of these RWCs failures.

Figure 2.7. Roof loss due to the RWCs failure (Photo courtesy of CTS)

2.3.3.4 Wall to foundation connection

The major contribution of this type of connection in a timber-framed structural system is to transfer the total lateral and uplift loads from the wall to the foundation. Full-scale studies by Tuomi et al (1974) found that the wall to foundation connections needed strengthening to provide adequate racking resistance for houses. Removal of an entire house's structural system is a result of the foundation failures in a windstorm (Walker, 1975). However, this type of failure due to windstorms is very rare for contemporary houses because the uplift on the roof and ceiling combination must be greater than the weight of the entire house. Moreover, it may happen only when the roof is well secured to the walls and without the walls being secured to the foundation (Liu, et al., 1989). Adequate anchorage of the structure to the foundation will reduce the wall to foundation connection failure.

2.4 Wind loading on houses

Fluctuating wind velocity in the approach flow, and the flow around the building generates a spatially and temporally varying pressure field on the external surface. This varying wind pressure generates fluctuating wind loads and fluctuating stresses on the structure (Holmes, 2002). The fluctuating pressure generally creates the high suction pressure found on a roof, especially on the roof corners and wall edges. Thus, it is essential to thoroughly understand the spatial and temporal characteristics of the pressure on this area. This fluctuating and increasing wind speeds can produce progressive damage to the timber-framed structures.

Wind tunnel studies are the most common way to obtain pressure distribution on timber-framed houses. The geometry of the roof is the main characteristic to dominate the pressure distribution of a house. Meecham et al (1991) indicated that the roof of a house should be designed based on the relationship between the pressure distribution and the underlying structural framing. In addition, their study found that the pressures on the full span trusses of the gable roof can be approximately twice those of the full span hip roof trusses at the same wind speed. Previous studies and research (Holmes, 1979; Uematsu et al., 1999; Stathopoulos et al., 1979; Vickery, 1986, 1991, 1992, 1994; Surry, 1991; Scruton, 1971; Kopp et al., 2008; Tieleman, et al., 1996; Ginger, 1997; McKinnon,2003; etc.) clearly show that the proper evaluation of internal and external pressure is important for calculating the wind load on the house, otherwise it will initiate damage on the vulnerable part of house structures (connections, roof, wall, ceiling, etc.).

The internal pressure mainly depends on the external pressure and the sizes and positions of the openings in the envelope of the building. The failure of a door or window in a windstorm can produce a dominant opening and generate large internal pressures. This type of failure had been observed during the Cyclone Tracy (Walker, 1975), Cyclone that hit South India in November 1996 (Shanmugasundaram et al., 2000), when Hurricane Andrew hit the Florida District of the US in 1992 (Shanmugasundaram et al., 1995) and Cyclone Yasi (Boughton et al., 2011). Recent windstorm damage to contemporary houses in non-cyclonic regions of Australia indicates that the failures are mostly contributed by the high gust wind speed and internal pressure. Moreover, in non-cyclonic region houses are designed for low internal pressure (AS 4055, 2012); this highlights the magnitude of

the external and internal pressure is the important factor in determining the wind load on the timber-framed house.

The quasi-steady method is used to design such "static" structures based on AS/NZS 1170.2 (2011). This approach produces the equivalent static loads based on a quasi-steady wind pressure and gust wind speed (Ginger et al., 1998). Davenport (1961) indicated that "this simplification was convenient in that pressures could then be regarded as static, and can be determined from simple wind-tunnel experiments on models in a steady airstream". AS/NZS 1170.2 (2011) provides design wind load data for buildings in Australia. Wind loads on the houses depend on many parameters: geometry, terrain categories, topographic classes and wind classes, pressure coefficients, etc. (AS/NZS 1170.2, 2011). Design approaches apply pressure on a given surface multiplied by the tributary area to obtain the total force on the surface.

2.4.1 Load Path

The fundamental design objective and task of a house's timber-framed structural system is to securely transfer the loads from roof and walls to the foundation. A good understanding of the load path is essential to evaluate the structural response of a house to windstorms. Uplift or vertical load transmission and lateral load transmission are the two basic types of wind load transmission in a timber-framed house structure. The vertical load transmission mainly depends on the structural response of the roof structure (i.e. roof cladding, batten, truss, ceiling, ceiling cornice, etc.) and its component connections (i.e. batten to cladding, batten to truss, and roof to wall connections). The lateral load transmission mainly depends on the structural response of the wall and ceiling and ceiling cornice and their fasteners and adhesive.

Several research studies associated with load path have been conducted worldwide (e.g., Rosowsky and Elingwood, 1991; Bulleit et al., 1993; Rosowsky et al., 1998, 1999, 2000, 2005; Wolfe and LaBissoniere, 1991; Reed et al., 1997; Taly, 2003; Mensah et al., 2011; Khan, 2012, Shivarudrappa, et al., 2013), which have provided some qualitative information of the load sharing of house structural systems. However, there is a lack of qualitative data on load sharing of timber-framed house construction, as it is very complex. There are several factors affecting the load sharing in timber-framed construction, such as spacing of the roof trusses, stiffness of member, fascia beams, roof

sheathing type and orientation, etc. (Henderson et al., 2013). Figure 2.8 shows the complex ways of the wind load transmission from roof to foundation in a timber-framed structure. The typical idealised vertical load path layout in a low rise light framed structure is shown in Figure 2.9.

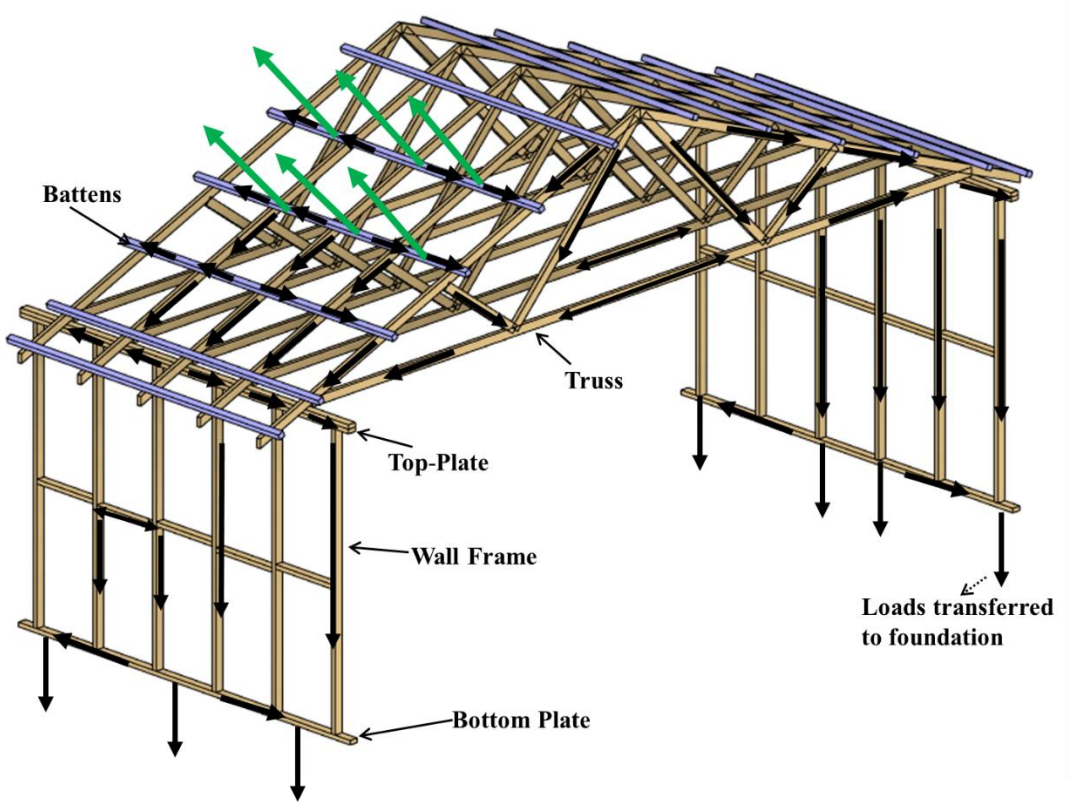

Figure 2.8. Schematic diagram of wind load transmission from roof to foundation in a timber-framed structure

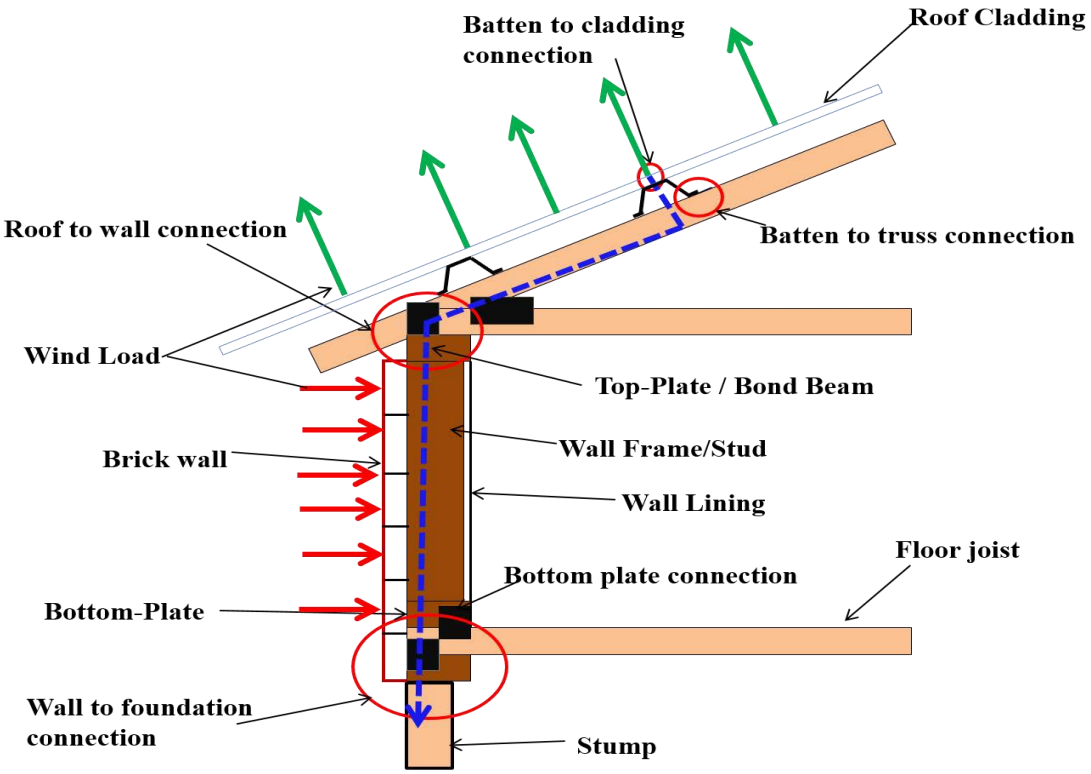

Figure 2.9. Schematic diagram of idealised vertical load path of low rise timber-framed structure (highlighted in blue dash line)

2.5 Full-scale testing

An understanding of load sharing and interaction between structural components on load paths are important to house structural response to wind loading. A full-scale test and numerical model analysis can be used to obtain the structural response of a house to wind loading. Boughton and Reardon (1982, 1983, and 1984) carried out a range of full-scale tests on houses at the CTS (Figure 2.10). Boughton and Reardon (1982) tested a forty-year-old house by applying wind load using hydraulic ram systems. The test focused on the strength and stiffness of wall stud and roof (uplift strength). In addition, a laboratory test was conducted on the internal walls and section of ceiling, complete with battens and joist. Load cells and hydraulic pressure gauges were used to measure the loads, and deflection gauges were used to measure deflections. Approximately 200 deflection readings were observed. This test showed how the forces are transmitted throughout a house.

Boughton and Reardon (1983 and 1984) tested a high-set house designed according to Australian standard for a wind speed of 42m/s. This study highlighted the connection failure modes when exposed to increasing static and cyclic loading, and identified the need for further research into ceiling and roof sheeting diaphragm action. This work led to further studies at the CTS, such as those by Reardon (1986 and 1990), Reardon and Mahendran (1988), Reardon and Henderson (1996), Henderson (2010) and Jayasinghe (2012). Some of these studies focused on the structural response by testing subassemblies of houses (Mahendran, 1989; Henderson, 2010; Jayasinghe, 2012), and showed that the results of subassemblies of the houses must be validated with available full-scale test results.

Figure 2.10. Full-scale tested houses at CTS (Photo courtesy of CTS)

Reardon and Mahendran (1988), and Reardon and Henderson (1996) showed interactions between the various structural and non-structural components of a house structure subjected to wind loads. Reardon and Henderson (1996) also showed improvement in the strength and stiffness of the house system subjected to wind load resulting from the contribution of various structural and lining components such as ceiling and ceiling cornice, and wall lining, as shown in Figure 2.11. This figure shows when the lining

elements were installed (i.e. wall lining and ceiling) in the structure, the lateral stiffness of the timber-framed house was increased by about 10 times more than that of the structure with only structural elements (i.e. frame and stairs). This lateral stiffness was increased further by about a factor of five when the ceiling cornice was installed in the structure. However, Reardon and Henderson's (1996) study did not investigate the vertical load sharing and the contribution of structural and lining elements to the vertical load sharing. Thus, the vertical load sharing and the contribution of the structural and lining elements to the vertical load sharing are yet to be determined for assessing the response of timber-framed houses.

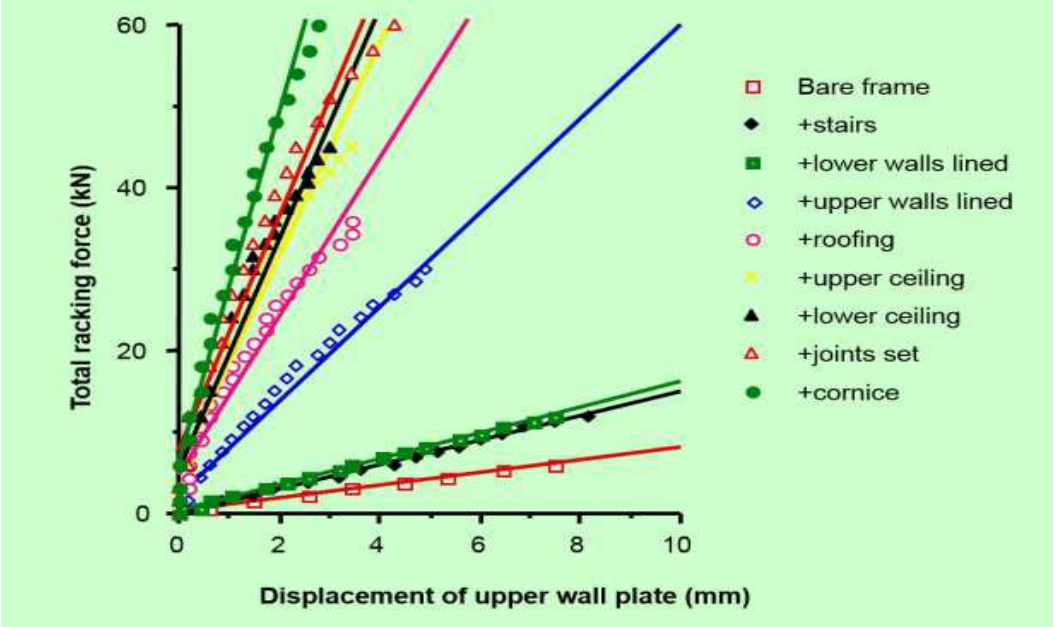

Figure 2.11. Change in lateral response with addition of elements (Reardon and Henderson, 1996)

Recently, a full-scale two storey house, shown in Figure 2.12, was built in accordance with the Ontario building code and tested by Morrison (2010), at the University of Western Ontario (UWO), Canada. The aim was to determine the response of a two-story residential house under realistic fluctuating wind loads. In addition, a subassembly of toe-nailed roof to wall connection was tested. This type of connection is commonly used in the US and Canadian residential houses. In this test, Morrison (2010) used Pressure Load Actuators (PLAs), which are able to reproduce realistic fluctuating wind load on a building structure as the loading system, to apply temporally and spatially varying

pressures to the building surfaces. In his study, applied loads to the roof of the house on a per connection basis that were significantly larger than the mean maximum capacity determined from the individual connection experiment.

Morrison (2010) showed that depending on the structural stiffness and the load sharing through the roof of the house, the failure did not initiate at a single connection but over many connections, on the entire roof. A significant hysteresis (i.e. energy dissipated during loading and unloading) was observed during the movement of the toe-nails during the full roof tests, while it was not observed in the single toe-nail tests. The connection in the full-scale test experienced tri-axial force (i.e. vertical, lateral and horizontal) but in the single toe-nail tests, the loads were applied in one direction (i.e. vertical). This could be the reason for the significant hysteresis observed in the full-scale tests of Morrison (2010). This indicates that the subassembly tests needs to be validated with a full-scale test.

Figure 2.12. The full-scale test house at UWO (Morrison, 2010)

Chowdhury et al (2013) carried out full-scale testing on a small one-story gable end roof wood-framed house model to evaluate the three-dimensional (3D) aerodynamic loading data on RWCs. The model was built based on the American style construction and the

dimensions were 3 x 3 x 2.4 m (i.e. width, length and eave height respectively). The roof slope of model was 4:12 and consisted of three trusses spaced at 1.5 m. The test was conducted at the six-fan Wall of Wind (WoW) facility at Florida International University. This WoW is capable of generating aerodynamic characteristics (i.e. atmospheric-boundary layer wind speed profiles and turbulence characteristics) similar to real tropical cyclones. The data collected from the full-scale field studies by the Florida Coastal Monitoring Program during the passage of hurricanes Ivan (2004) and Lili (2002) were used to generate the aerodynamic characteristics. The test were conducted for five wind angles of attack (i.e. 0^o, 30^o, 45^o, 60^o and 90^o) with high wind speed to ensure the simulation of high Reynolds number up to 8 $x10^6$. The load transfers were measured by the six degree-of-freedom load cells (JR3 model 75E20S4) sandwiched between the truss and top-plate at the RWC locations. The results show that the capacity of RWC was significantly reduced by maximum about 50% under triaxial load tests compared with that capacity estimated under uniaxial load tests. The RWC (i.e. toe-nailed connection) used in the study is different from the RWC (i.e. triple grip connection) of contemporary house in Australia. Therefore, the combination loading effects on the uplift capacity and structural response of RWC's of Australian contemporary houses need to be evaluated.

A full-scale test was carried on a typical North American single-story structure with platform construction (i.e. post and beam construction) by Doudak et al (2012), as shown Figure 2.13. The aim of this full-scale test was to measure internal force flows throughout the house. Concentrated horizontal loads and patches of gravity loads were applied normal to walls and roof surfaces respectively. Fifteen triaxial load cells were located between the floor platform and the foundation to measure the reaction forces at the foundation. In addition, six single-axis load cells were represented as the RWCs to measure the vertical reaction forces for some of the roof trusses. This study showed that the top of the foundation around the entire wall perimeter of the building footprint were reacted when horizontal loads were applied near eave level or to the roof. This study also indicated that the building superstructure was sufficiently rigid for nonsymmetric applied forces to cause significant redistribution of the applied load. However, the usefulness of this full-scale test results to assess structural response of Australian house is limited, as their construction types were different. Moreover, the Doudak et al (2012) study used the single-axis load cell as roof to wall toe-nailed connection and confirmed their stiffness is similar to the roof to wall toe-nailed connection from the laboratory testing of isolated

connection. However, the RWC structural response could be different compared to the single-axis load cell and could create the different load transmission and load redistribution.

Figure 2.13. The full-scale test house of Doudak et al (2012) study

An experimental study on a 1/3rd scale timber-framed house with twenty RWCs and wall to foundation connections was carried out by Datin (2010) to evaluate the vertical structural load paths due to wind loading on the roof of a low rise timber-framed house. In their study, the usefulness of the database assisted design methodology, which is used to predict the structural response of timber-framed structures subjected to fluctuating wind pressure, was investigated. Using this database assisted design method requires the structural influence coefficients and wind tunnel-derived pressure coefficients. In order to find the influence coefficient, the loads were applied at eighteen points per truss and the reaction forces measured by the load cells located at the RWCs of the 1/3rd scale timber-framed house. A FEM of a 21-truss roof was also developed to investigate the effects of dynamic loads on the roof in their study.

This FEM analysis was used to determine the first vertical mode of vibration based on the fundamental frequency analysis performed on the roof and various roof components. From this frequency analysis, Datin (2010) showed that the fundamental vertical

frequencies of the entire roof and the individual components were (i.e. between 8.6 Hz to over 40 Hz) higher than the dominant frequencies from the natural wind flows (i.e. up to 1 Hz). Thus, the roof of a timber-framed house will not be excited near resonance by the wind. Therefore, the influence coefficients derived from the static loads were equal to those used for dynamic load. Based on the experimental and FEM analysis, Datin (2010) study concluded that the static influence coefficients are valid to predict the structural response of timber-framed structures.

Overall, these full-scale, model scale and sub-assemblies of house tests have shown that the stiffness of the structural system plays an important role in the response (including failure) of the entire roof, furthering the understanding of the interaction of the wind loads and the structural system of houses. These studies also indicated that FEMs can be used to study the structural response of the overall structural systems.

2.6 Numerical model analysis of house structural system

Evaluation of the house structural performance requires the development of a numerical model simulation because full-scale laboratory testing is highly time-consuming and expensive. Through the development of computer technology and the Finite Element software, valuable analysis results can be obtained. There are a few numerical model analysis methods that have been developed to predict the structural performance of an entire building (Gupta and Kuo, 1987; Kasal et al., 1994, 1999; He et al., 2001; Thampi, 2011; Guha and Kopp, 2013).

Gupta and Kuo (1985) analysed the behavior of shear walls by using an experimental and numerical model. Their study indicated that the finite element analysis results are in good agreement with those from the experimental test. This prompted the development of a simple linear elastic building model (Gupta and Kuo 1987). This model was created with nine global degrees of freedom and seven “superelements”, which represent shear walls, flange walls, roof diaphragms, and ceilings. The model was validated with test house results of Tuomi-McCutcheon (1974), and model results were in good agreement with the experimental test. This indicates that “superelements” can be used to develop a FEM to assess the structural response of the timber-framed house.

Kasal et al (1994) have analysed a nonlinear FEM of a complete light-frame wood structure using ANSYS finite element software. The model was an assembly by

“superelements” and “quasisuperelements” and loaded by static loads. The linear “superelements” represented the floor and roof, and non-linear “quasisuperelements” represented walls and inter-component connections. This model was also considered for load sharing among wall components. The model was validated with a full-scale test of a one-story wood-frame building (4.9m x 9.8 m) under cyclic loads, and the experimental and analytical results closely agreed. However, the model predicted reaction forces and deformations at the boundaries that are less accurate for small loads and walls distant from the acting force. In this model, the structural properties for the substructure were obtained from the analytical model and this analytical model might give inaccurate values, which could be the reason for the less accurate results obtained at the boundaries. This indicates that to improve the model accuracy, actual material and structural properties for each element is required.

He et al (2001) investigated the performance of three-dimensional timber light-frame buildings under static loading conditions. In this model, shown in Figure 2.14, there was an assembly of three types of elements: panel element, frame element, and connection element. Panel elements are approximated as thin plate elements and a frame element modeled as a 3D beam element with inelastic material properties. The connection element consisted of a nail, the surrounding area on the panel, and frame members contacting with the nail, which is represented by non-linear spring elements. This numerical model produced an effective prediction of load sharing among structural components and load paths within the entire wood-frame structural system. The uniqueness of this model was that a mechanics-based nail model was implemented by using basic material properties of the nail connector and the embedment characteristics of the surrounding wood medium. This approach has led to easily modeled structures with varied connections in timber-framed house structural systems.

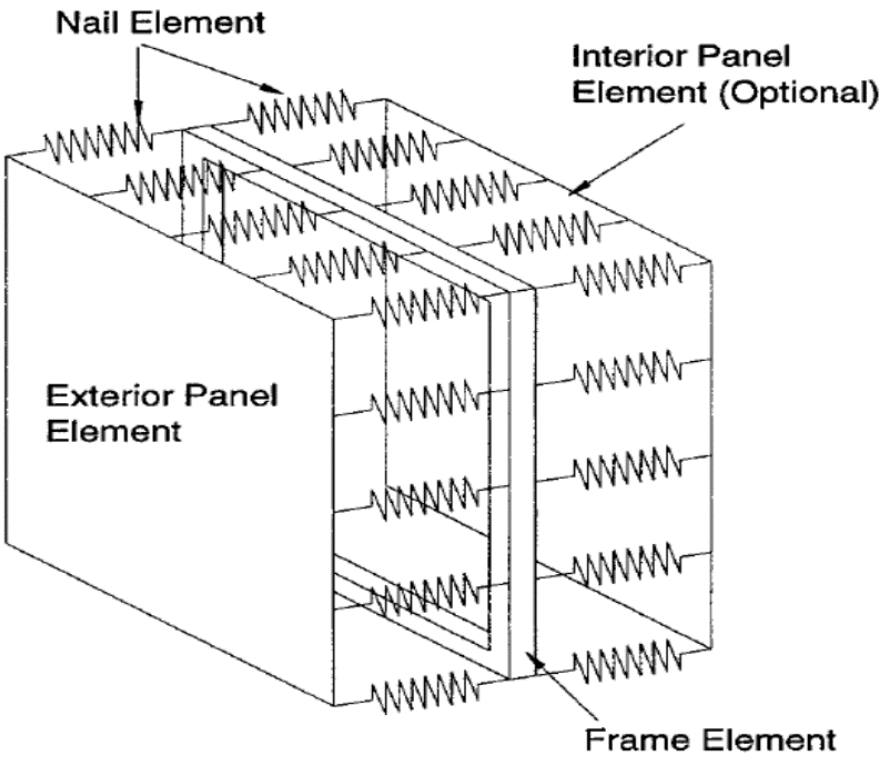

Figure 2.14. Basic Element Unit in He et al (2001) model analysis

Recently, a combined load sharing, nail-slip model was used to predict the failure of roof-to-wall toe-nail connections in residential wood-frame buildings, was presented by Guha and Kopp (2013). This model used the elastic beam theory of statically indeterminate continuous beams with the roof elements, which is represented as an equivalent two-dimensional (2D) beam. The Slope-Deflection method was used in combination with the nail-slip model to predict the connection responses. The outcome of the connection responses in the model is similar with the outcomes of controlled load sharing experiments. In addition, a piece-wise linear load-displacement curve was used to describe the observed progressive failure mechanism of nails subjected to realistic wind loads, and the results showed good agreement with experimental results of individual toe-nails. The most important outcome in this model was the progressive withdrawal and damage to the connections as well as the overall failure of the roof.

The experimental studies and numerical model analysis developed by Guha and Kopp (2013) and He et al (2001) were focused on US house structural systems. There, houses have wood sheathing on the wall and roof, and roof trusses that are toe-nailed to the wall

top-plate with a fascia board supported at the end of truss, whilst houses in Australia generally have brick veneer wall, metal roof cladding and roof trusses that are tied with triple grip connections to the wall top-plate. These types of differences in house structural systems cause a difference in the stiffness and deformation of structural system to wind load. Thus, the implementation of these numeric modeling techniques to Australian house structures need to be developed.

2.7 Summary of the literature survey

The review of research and windstorm damage evaluations indicate that the failure of components (i.e. wall, roof, etc.) and the modes of progressive damage are dependent on the load distribution, structural response, load sharing and the strength of components and connections. The contemporary houses may be resistant to wind loads than their design criteria as the load sharing not accounted in their design. Moreover, houses in non-cyclonic region of Australia are designed for low internal pressure and are more vulnerable to failure. Therefore, more research is needed to evaluate the structural sufficiency and load sharing of houses that are being built in the non-cyclonic region of Australia.

Full-scale tests and numerical model analysis are the most reliable methods to investigate the structural response and load sharing of the timber-framed structure. Based on the applied load and displacement, full-scale tests by the CTS qualitatively showed the strength, stiffness and load transfer of the house system subjected to wind load, with various structural and lining components such as wall lining, ceiling and ceiling cornice. Their studies do not provide a quantitative analysis of load sharing under uplift wind loads. Therefore, a detailed quantitative analysis of load sharing and contribution of the structural and lining element to the load sharing of the timber-framed house structure are needed.

CHAPTER 3: REPRESENTATIVE CONTEMPORARY HOUSE

3.1 Introduction

A field survey of contemporary houses under construction in non-cyclonic regions of Australia, near Brisbane and Melbourne, as shown in Figures 3.1 and 3.2, was conducted by a team from the CTS, to determine representative houses and their structural systems. Eighty-seven houses were surveyed in detail and the data compared with their certified engineering drawings. An additional thirty-seven certified engineering drawings were also analysed and the details are described in Ginger et al., 2015. The surveyed features included the overall dimensions of house, roof slope, shape and type of construction. In addition, the field survey also recorded construction defects. Based on the analysed survey data, the CTS team identified that houses in Melbourne are of similar size and shape and construction type to houses in the Brisbane region. The CTS team also defined a common representative house for both Melbourne and Brisbane regions, which is a one and two storey brick veneer timber-framed house (Ginger et al., 2015). The roof shapes and their roof structural systems were similar in both the one and two storey representative house.

Figure 3.1. House under construction in Brisbane (photo courtesy of CTS)

Figure 3.2. House under construction in Melbourne (photo courtesy of CTS)

This study focuses on the one storey representative house, with an objective to evaluate the load transmission from the roof to wall and the structural response of RWC. The field survey was analysed to find the structural systems, connection types the contemporary house.

3.2 Representative one storey Brisbane/ Melbourne house

The houses' construction types in both Melbourne and Brisbane are brick veneer with timber trusses and timber wall framing. These houses were designed and constructed to wind classification N1 and N2 from the AS 4055 (2012). Based on the wind load classification, the RWC used in houses of each region was different due to their reginal gust wind speed. In Brisbane, the triple grip and structural tie down strap were used whilst truss grip, triple grip and structural tie down strap were used to connect the roof to wall in the Melbourne region. Figure 3.3 shows the representative contemporary house for Brisbane and Melbourne regions of Australia. This house is a single storey, timber-framed, brick-veneer construction, with 21.5^{o} pitch hip-end roof.

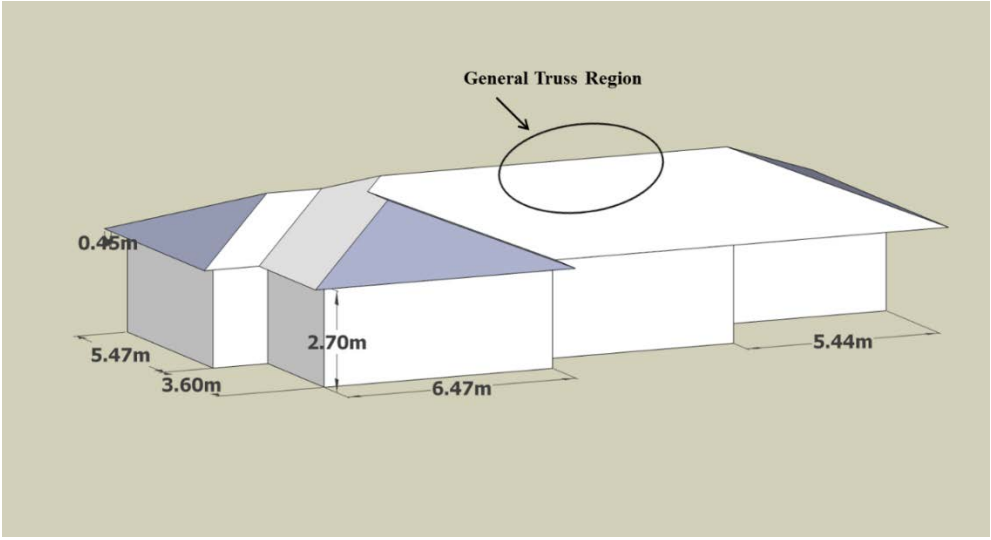

Figure 3.3. Representative contemporary house

3.2.1 Structural system of the representative contemporary house

The roof structure of the representative house is constructed with general trusses (Figure 3.4a) at the middle, truncated (Figure 3.4b) and jack trusses (Figure 3.4c) at the hip end of the roof, spaced at 600 mm, and were connected to the wall top-plates (Figure 3.4).

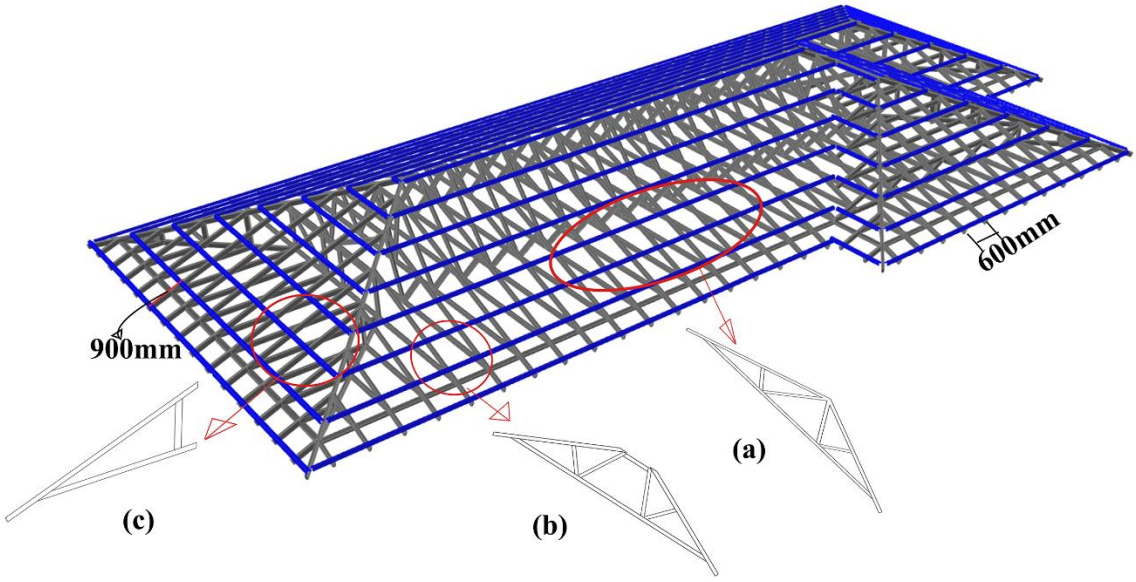

Figure 3.4. Schematic diagram of the truss layout of representative contemporary house: a) General truss, b) Truncated truss and c) Jack truss

Trusses are prefabricated with 90 x 35 mm Machine Graded Pine (MGP) 10 soft timber. The general trusses are generally connected to the top-plates with triple grips (Figure 3.5a) or truss grips (Figure 3.5b), whilst truncated trusses are fixed to the top-plates with two skew nails and a 30 x 0.8 strap (Figure 3.5c) with four nails per leg. Corrugated metal sheets or concrete tiles are used for the roof cladding. The metal roof cladding is attached to metal top-hat battens (40 x 40 x BMT 0.55) with three M6-11x50 Hd/Seal screws per corrugated metal sheet, whilst tiles are connected to the 40 x 25 mm timber batten with wire clips. The metal top-hat battens are connected to the trusses with M5.5 x 40 mm Hex Hd screws spaced at 900 mm, whilst timber battens are fixed with 65 x 3.15 mm twisted shank gun nails spaced at 900 mm to every truss.

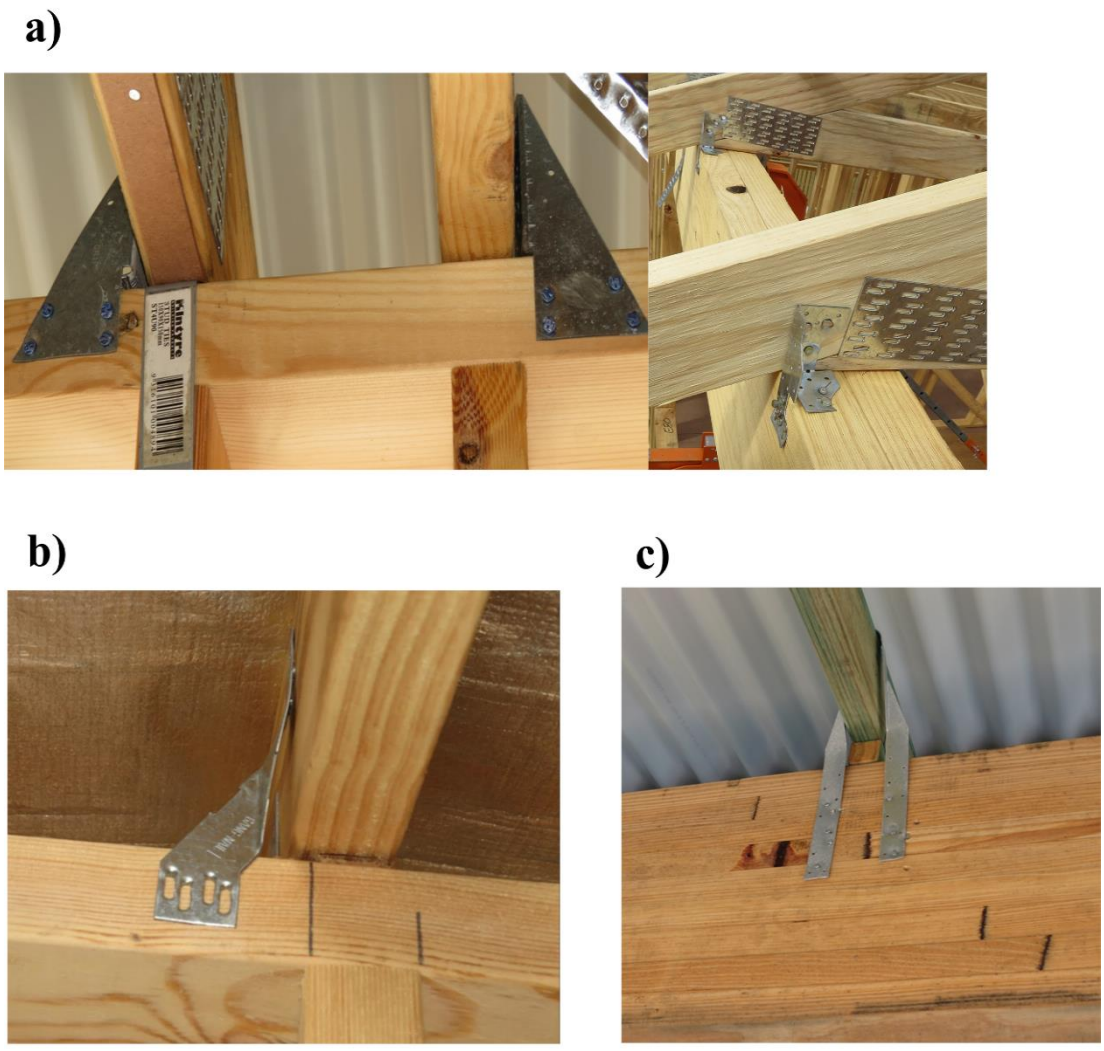

Figure 3.5. Common RWCs of representative contemporary house: a) Triple grip connection, b) Truss grip connection and c) strap connection

Wall frames are constructed with 90 x 35 mm MGP10 ribbon top-plates, bottom plates and studs. The wall studs are connected to the top-plate and bottom plate with skew nails at 600 mm apart, and the bottom plates are secured to the concrete floor slab with concrete nails spaced nominally at 900 mm. The brick veneer wall cladding is used for external wall lining and wall ties are used to connect the timber wall frame to external brick wall. Plasterboard is used for the ceiling and internal wall lining, and the ceiling is attached directly to the bottom chord of the trusses. The plasterboard sheets are fastened to the wall frame and bottom chord of the trusses with 8G x 40 mm bugle head power driven screws and walnuts of adhesive (glue) at regular intervals. Ceiling cornices are used to connect the ceiling and internal wall lining in the house. The cornice cement was used for adhesion between the cornice and ceiling and wall lining. The bracing wall or shear wall timber frames are constructed with similar timber members as the wall frames. Four mm thick plywood sheets are used for the external and internal lining for the shear wall, and are secured with 30 x 2.8 mm gun nails spaced at 50 mm along the top and bottom plates and spaced 150 mm vertically along studs.

3.2.2 Common construction defects in the RWCs

Based on the standard AS 1684.2 (2010) and the manufacturer's specifications, ten nails (i.e. four nails on the vertical side of truss chord, two nails on the top-plate top surface and four nails on the side surface of the top-plate) should be used in this roof to wall triple grip connection. The field survey data analysis also showed common construction defects on the RWCs, such as missing nails, grouping nails, bending framing anchors, and partially driven nails and nail teeth, as shown in Figure 3.6. These types of construction defects were observed in every surveyed house. The house survey data also showed that the roof structure of the contemporary house was constructed with at least a six general trusses and four truncated trusses. In every surveyed house, at least three of these general trusses RWCs had some common construction defect. Missing nails were the most common construction defect, as shown in Figure 3.6a, with all surveyed houses displaying this type of construction defect.

a)

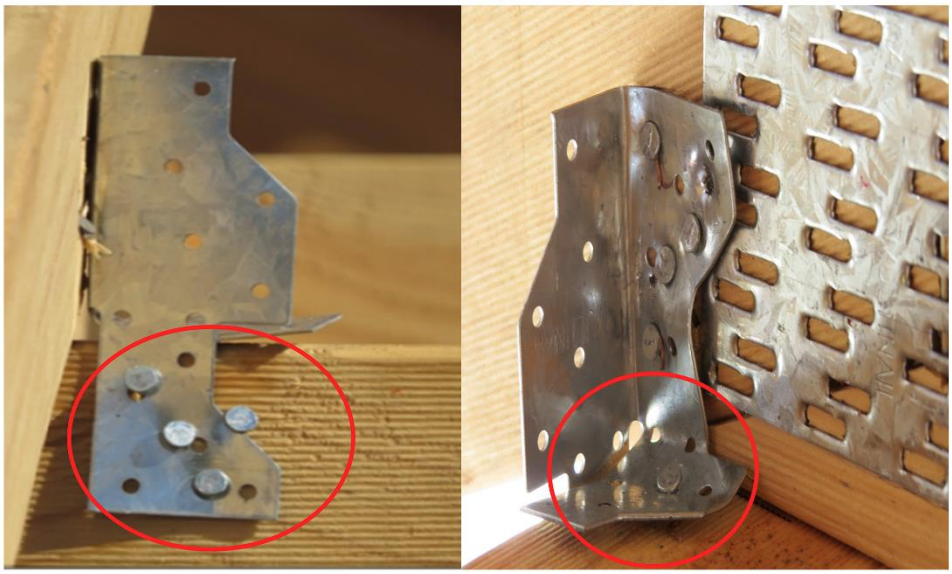

b)

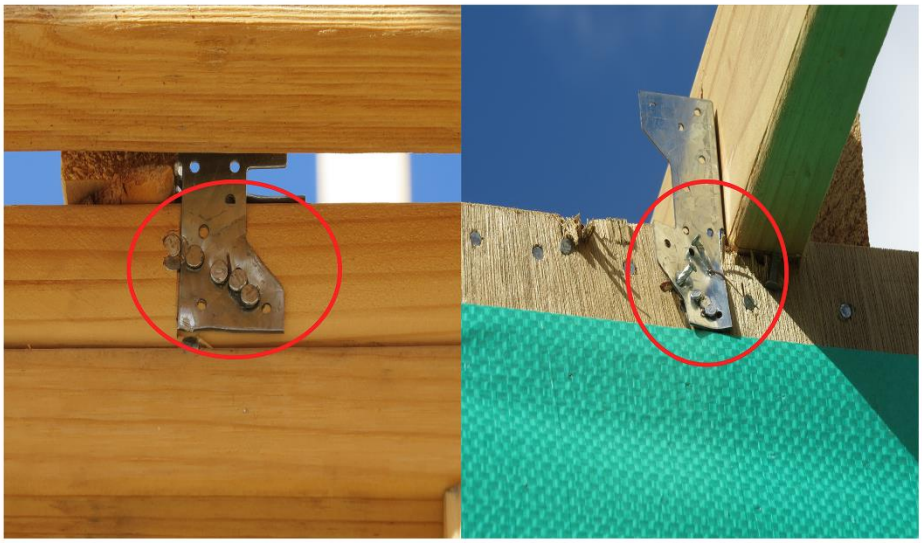

Figure 3.6. Common construction defects on the roof to wall triple grip connection: a) Missing nail and triple grip bending, and b) Grouping nails and nail bending

Figure 3.7 illustrates the common construction defect on the truss grip type roof to wall connection in the houses in Melbourne. Partially driven nail teeth were commonly observed as a construction defect on this type of connection.

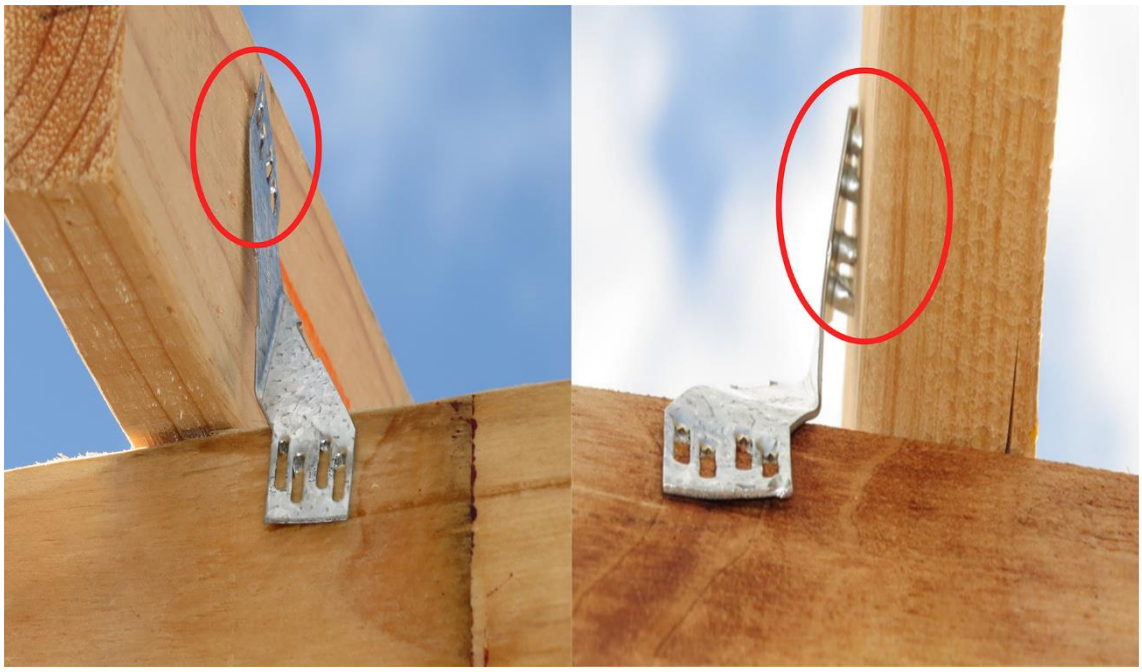

Figure 3.7. Common construction defects on the roof to wall truss grip connection

The common construction defects on the roof to wall strap connection were missing nails, grouping nails together and pre-punched nail hole, as shown in Figure 3.8. These grouped nails and pre-punched holes caused tearing of the strap, especially at the location of the grouped nails.

Figure 3.8. Common construction defects on the roof to wall strap connection

3.3 Summary and discussion

Contemporary houses in Melbourne and Brisbane are brick veneer timber-framed construction. The construction type, structural system and roof shapes are similar in both Brisbane and Melbourne region houses but the connections used between the roof and wall are different. The common RWC in the Brisbane region houses are triple grip connection whilst truss grip connection is commonly used in Melbourne region's houses. Missing nails and grouped nails were the most common construction defects in the roof to wall triple grip connections, and the partially driven nail teeth were the common construction defect in the truss grip connections.

- The effect of these common construction defects on the RWC uplift capacity will be investigated by conducting laboratory tests and detailed in the Chapter 4. This Chapter also discusses the RWC uplift capacity variation with different types of timber (radiata pine, spruce pine), nail (hand, gun) and framing anchor (triple grip, universal triple grip).
- The load sharing and structural response of the contemporary representative house will be assessed by conducting the full-scale tests and FEMs, and detailed in Chapters 5 and 6.

CHAPTER 4: EXPERIMENTAL TESTS ON INDIVIDUAL CONNECTIONS AND JOINTS

4.1 Introduction

The structural response and failure mode of the common RWCs and the joints between the plasterboard (i.e. ceiling or wall lining) and timber (i.e. stud or bottom chord of truss) of contemporary representative houses are individually assessed using laboratory tests. This Chapter presents the individual components experimental test details and results.

The RWC is a potential source of vulnerability in the load path of a house's structural system. Reed et al (1997) and Morrison (2010) showed that a discontinuity in the load path may cause severe damage in an extreme windstorm. The RWC should be designed to resist the uplift load as well as the lateral load components. The roof trusses of modern houses in non-cyclone regions of Australia are generally fixed with triple grips and truss grips to the wall top-plate, but in non-hurricane regions of North America are toe-nailed to the wall top-plate. These will result in differences in their stiffness and deformation of the structural systems to wind loading. Reed et al (1997), Cheng (2004), Shanmugam et al (2009), Ahmed et al (2011), Canino et al (2011), Guha et al (2012), Morrison et al (2012) and Henderson et al (2013) studied the performance of the RWC in North American houses using experiments and numerical model analyses. Ahmed et al (2011) showed that the uplift capacity of RWCs may be overestimated in current design practice. Their study also showed that adding two or more hurricane clips to an individual connection does not change the uplift capacity but it does change the failure mode of the connection. Some of these studies also investigated the effect of material variability (i.e. different timber species) on the RWC uplift capacity. However, these studies have not revealed the effect of construction defects on the connections. The response of the roof to wall triple grip and truss grip connections to loading depends on the metal plate, nails and type of timber.

The design procedure of the RWC is mainly based on the uplift capacity as specified in Australian standard AS 1684.2 (2010), but this standard does not account for construction defects. Little is known about the interdependencies between uplift capacity and constructions defects. Therefore, this Chapter focuses on the response and uplift capacity

variation of typical RWCs (i.e. triple grip and truss grip connection) with and without a range of common construction defects.

4.2 Test set-up for RWCs

Experimental tests were carried out to assess the strength and stiffness of RWCs with and without construction defects. Truss grip and triple grip connections were tested in an Instron testing machine. The specimens were stored at 25ºC and 65% relative humidity for 24-hours prior to testing. Figure 4.1 illustrates the test set-up for a triple grip connection. The resultant forces and vertical displacements (i.e. the relative displacement of the crosshead of Intron machine) were measured.

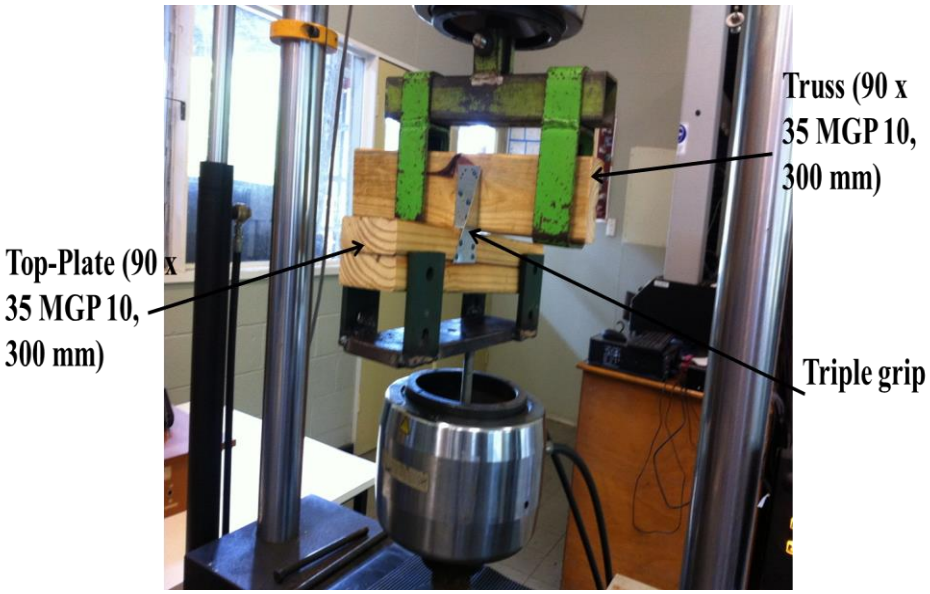

Figure 4.1. Triple grip connection test arrangements

4.2.1 Detail of "Ideal" triple grip connection test specimens

The triple grip test specimens consisted of 90 mm x 35 mm x 300 mm ribbon top-plate, 35 mm x 90 mm x 300 mm truss chord and Galvanized G300 (Z275) steel triple grip (1 mm thickness) with galvanized nails. Ten samples were tested and the results were used to predict the design uplift capacity of this type of connection. Five different types of "Ideal" triple grip connections (i.e. Types A, B, C, D and E), assembled with different timber species, nail type and framing anchor, and the number of tests conducted on each type are detailed in Table 4.1. Tests were carried out using the Instron testing machine at

a loading rate of 8 kN/min. Figures 4.2 and 4.3 show the five specimen types. The configuration of connection Types A, B and C (Figures 4.2a, 4.2b and 4.2c respectively) were assembled with hand driven nails (Figure 4.2d) and constructed based on the manufacturer's specifications and AS 1684.2 (2010). Types D (Figure 4.3a) and E (Figure 4.3b) were assembled with gun nails (Figure 4.3c) and constructed based on the manufacturer's specifications (MiTek Australia, 2014). The number of nails and their locations were similar in both Triple-Grip (i.e. Type A) and Universal Triple-Grip (i.e. Type B) connections, with the geometry of the framing anchor being the only difference, as shown in Figure 4.2. Figures 4.2 and 4.3 also show the different types of nails used to construct the test specimens. These specimens were used to obtain a range of responses (i.e. strength and stiffness) of ideal connection with different types of timber species, nail and framing anchor. This will enable the assessment of design uplift capacity variation of the RWC with material variability so that the results can be used to assess the design and vulnerability of houses subjected to windstorms.

Table 4.1. Detail of the "Ideal" triple grip connections test specimens

a) Hand nail connections				
Test Specimens	**Nail (Galvanized)**	**Timber species (MGP 10)**	**Framing anchor**	**Number of Tests**
Type A	30 mm x 2.8ϕ hand nails	Australian radiata pine	Triple grip	20
Type B	30 mm x 2.8ϕ hand nails	Australian radiata pine	Universal triple grip	10
Type C	30 mm x 2.8ϕ hand nails	spruce pine	Triple grip	10
b) Gun nail connections				
Type D	32 mm x 2.5ϕ Gun nails	spruce pine	Triple grip	10
Type E	32 mm x 2.5ϕ Gun nails	Australian radiata pine	Triple grip	10

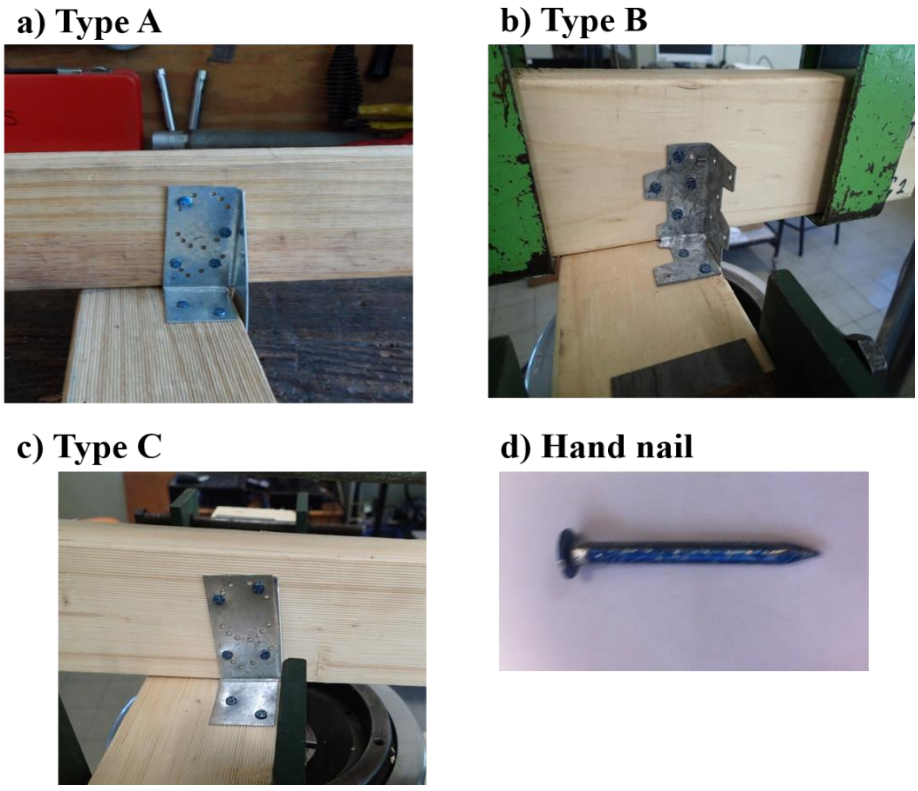

Figure 4.2. Hand nailed triple grip connection specimens: a) Type A, b) Type B, c) Type C, and d) hand nail (2.8 x 30 mm)

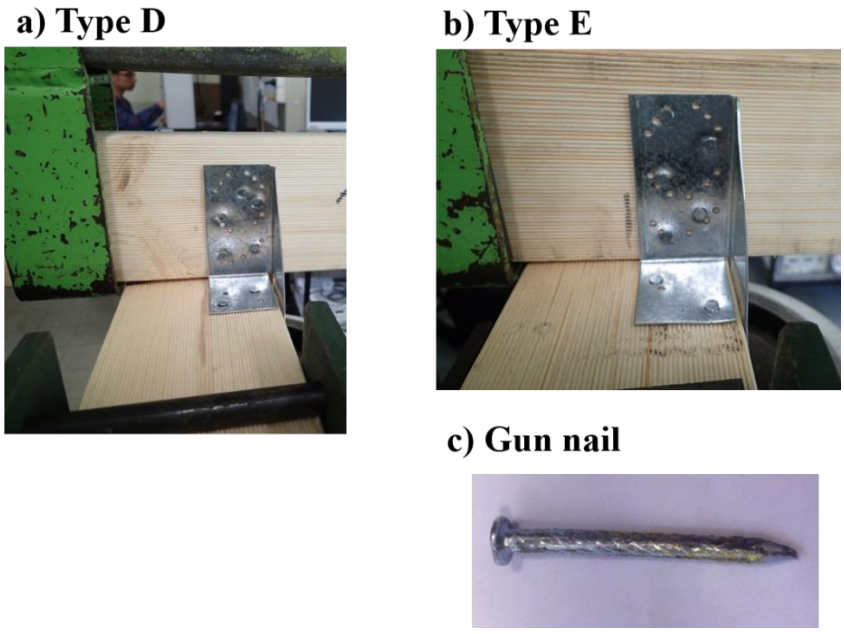

Figure 4.3. Gun nailed triple grip connection specimens: a) Type D, b) Type E, and c) gun nail (2.5 x 32 mm)

4.2.2 Triple grip connection with construction defects

Experiments were also carried out on triple grip connections with a range of construction defects to assess their connection strength and compared with the "Ideal" triple grip connections. Five types (i.e. Type A-N1, A-N6, A-N9, A- (N1-N6) and A-(N1-N8)) of triple grip connections, as described in Table 4.2a, were assembled with construction defects, such as nails missing in different locations. These five connection types are based on a nail missing from the "Ideal" connection Type A, as shown in Figure 4.4. As described in Table 4.2b, three additional types of connections were constructed with construction defects on the "Ideal" connection Type E (i.e. Types E-1, E-2 and E-3), as shown in Figures 4.5a, 4.5b and 4.5c respectively. The tests were carried out by using the Instron testing machine with a crosshead movement of 2.5 mm/min based on the Australian standard AS 1649 (2001).

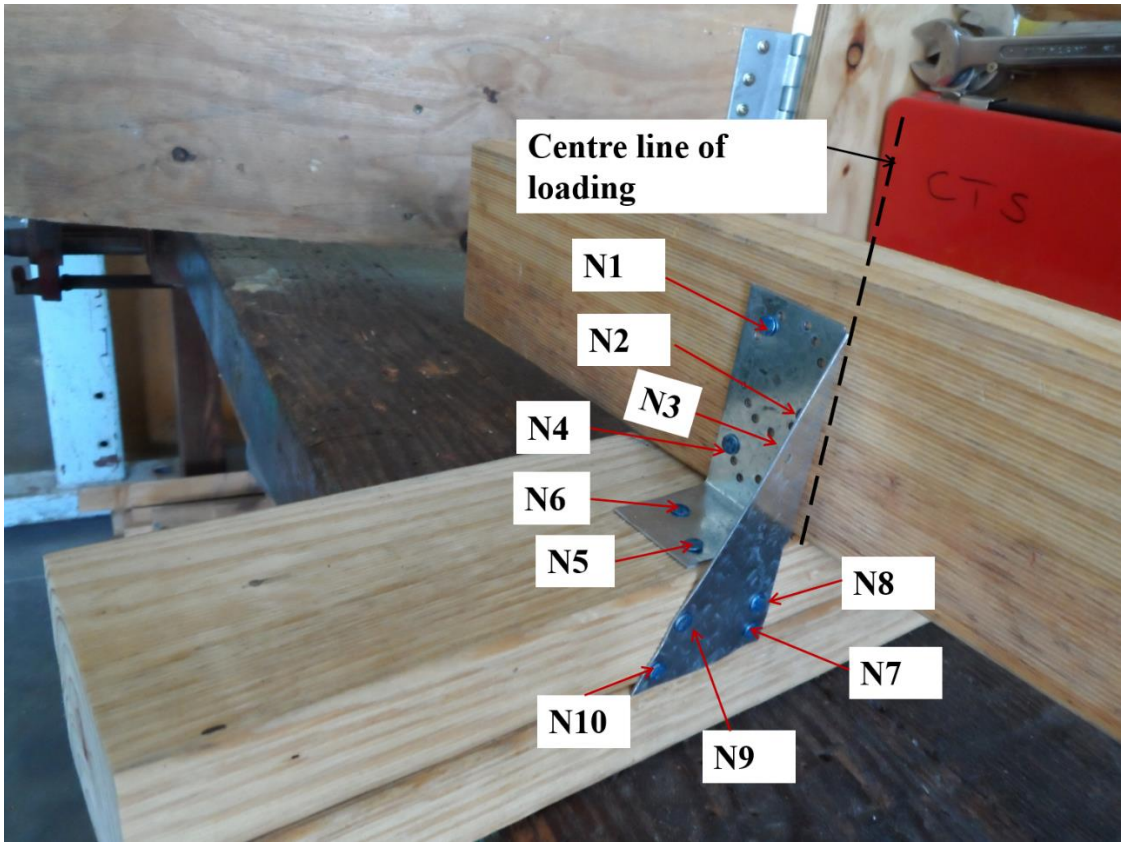

Figure 4.4. Test specimen Type A -showing Nails N1 to N10

a) Type E-1

b) Type E-2

c) Type E-3

Figure 4.5. Defective gun nailed triple grip connection specimens: a) Type E-1, b) Type E-2, and c) Type E-3

Table 4.2. Detail of the triple grip connections with construction defects

2a) Hand nail connections with defects				
Test Specimens	**Nail (Galvanized)**	**Timber species (MGP 10)**	**Framing anchor**	**Number of Tests**
Type A-N1, (missing nail N1)	30 mm x 2.8ϕ hand nails	Australian radiata pine	Triple-Grip	10
Type A-N6, (missing nail N6)	30 mm x 2.8ϕ hand nails	Australian radiata pine	Triple-Grip	10
Type A-N9, (missing nail N9)	30 mm x 2.8ϕ hand nails	Australian radiata pine	Triple-Grip	10
Type A-(N1-N6), (missing nail N1& N6)	30 mm x 2.8ϕ hand nails	Australian radiata pine	Triple-Grip	10
Type A-(N1-N8), (missing nail N1&N8)	30 mm x 2.8ϕ hand nails	Australian radiata pine	Triple-Grip	10
2b) Gun nail connections with defects				
Type E-1, (nails on the truss are in a line along an edge of the triple grip)	32 mm x 2.5ϕ Gun nails	Australian radiata pine	Triple-Grip	10
Type E-2, (nails on the truss are grouped)	32 mm x 2.5ϕ Gun nails	Australian radiata pine	Triple-Grip	10
Type E-3, (nails on the top-plate are grouped)	32 mm x 2.5ϕ Gun nails	Australian radiata pine	Triple-Grip	10

4.2.3 Results and analysis of the roof to wall triple grip connections

The experimental results for triple grip connection tests were presented in Figures 4.6, 4.7 and 4.8. These figures give the "average" applied force-displacement relationship for each type of connection. These results were obtained by averaging the data from the number of tests in each type. The experiments showed that the average peak load is 4.85 kN for the connection Type A, which is the average of the maximum load resisted by each test specimen. Additionally, ten specimens of the Type A connection were tested with a displacement rate of 2.5 mm/min to compare the structural response with that obtained by controlling the loading rate. As shown in Figure 4.6, the responses and peak

loads of connection Type A with loading and displacement control are similar. This indicates that both the displacement and load control methods produce a similar connection response.

The average force-displacement behaviour of connection Types A, B and E are similar, while that of Types C and D are similar. This shows that differences in the framing anchor do not cause significant differences in peak loads of the RWC. However, the material variability in timber does change the peak load of the RWC (Types A and C). Changing the timber material from MGP10 Australian radiata pine to spruce pine in the connection gives about 25% reduction in peak load. Figure 4.6 also shows that the different types of nails in the connections (Types A and E) also create variations in the peak load. The variation of peak load between the hand nailed and the gun nailed connection is about 25%. The average applied force versus displacement of the "Ideal" triple grip connections show that the stiffness of the hand nailed connection (i.e. Types A, B and C) is higher than the gun nailed connection (i.e. Types D and E). Eight of the 10 nails (i.e. N1, N2, N3, N4, N7, N8, N9 and N10) in the triple grip connection experience lateral (i.e. shear) load when the connection was subjected to uplift load. Under this condition, the lateral strength of the nail joint is mainly dependent on the nail diameter rather than the nail mechanical properties, as shown by Chui et al (2000). The hand nail diameter (2.8 mm) is higher than that of the gun nail (2.5 mm), and this could reason for the stiffness difference between the hand and gun nailed connections.

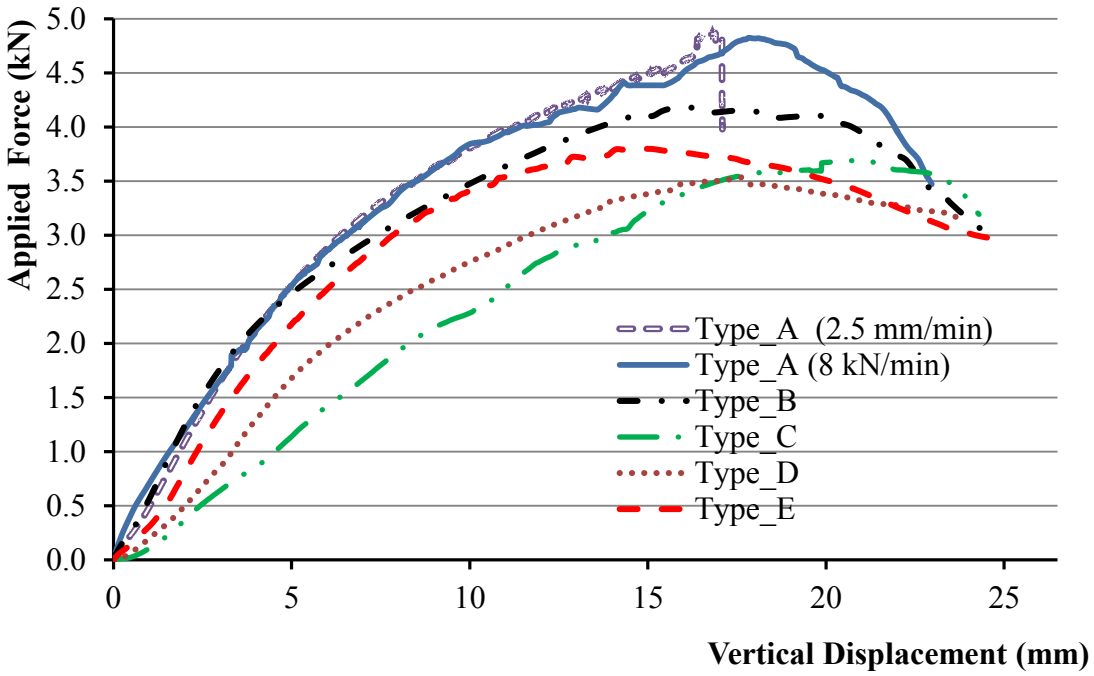

Figure 4.6. Average applied force-displacement relationships for "Ideal" Triple Grip connections

Figure 4.7 shows the comparison of the average applied force-displacement curves of the defective hand nailed connections, listed in Table 4.2a (Types A-N1, A-N6, A-N9, A-(N1-N6) and A-(N1-N8)), with the force-displacement curve of "Ideal" Type A (Figure 4.4). This figure and Table 4.3 illustrate that the average peak loads of the Types A-(N1-N6) and A-(N1-N8) of 3.10 kN and 2.78 kN respectively, are less than the "Ideal" connection Type A. This clearly indicates that when a nail is missing on both the truss and top-plate (i.e. Types A-(N1-N6) and A-(N1-N8)), the strength of the "Ideal" connection triple grip connection is significantly reduced by about 40%. Table 4.3 shows that the connection Types A-N6 and A-N9 have 90% of the strength of the "Ideal" connection (i.e. Type A). This indicates that missing either nail N6 or N9 has a lesser impact on the strength of the triple grip connection. The nails (N6 and N9) were located away from the lone of loading action compared to other nails, which is the reason for these nails to have less influence on the strength of the triple grip connection.

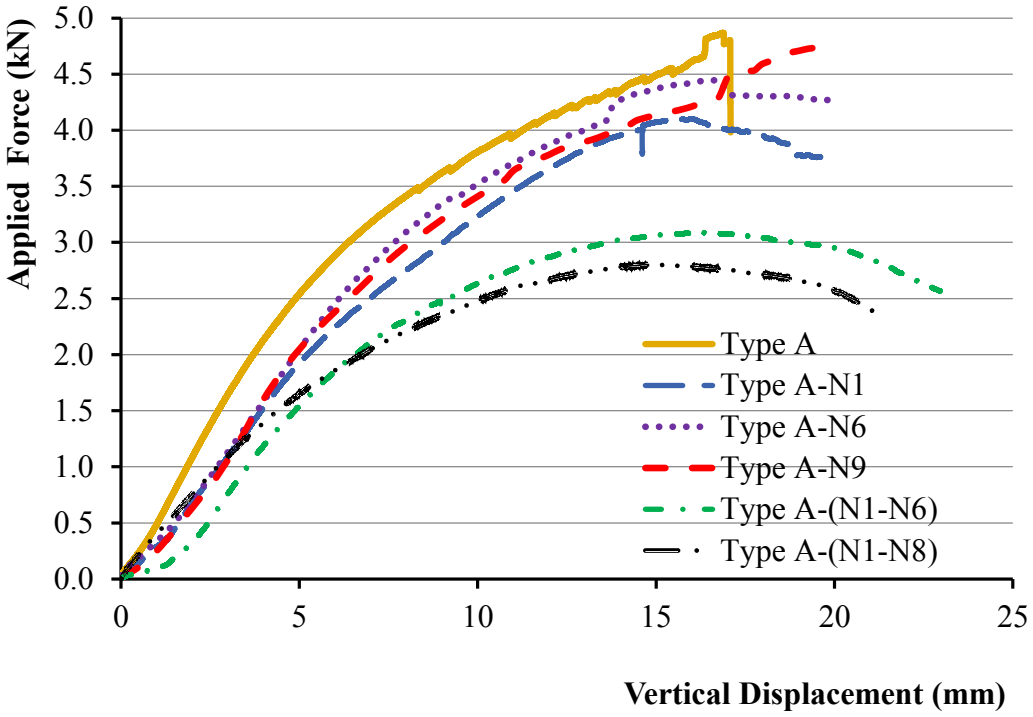

Figure 4.7. Average applied force-displacement relationships for triple grip connection Type A with construction defects

Figure 4.8 presents the comparison of the average applied force variation with a displacement for the defective gun nailed connection Types E-1, E-2 and E-3 with the "Ideal" connection Type E. This figure shows that the peak load of the connection Type E-3 is less than the other defective connections (i.e. Types E-1 and E-2), indicating that the grouping of nails together on the top-plate will reduce the connection strength and stiffness. This figure also shows that the stiffness of the connection Types E-1 and E-3 are similar and less than the connection Types E and E-2.

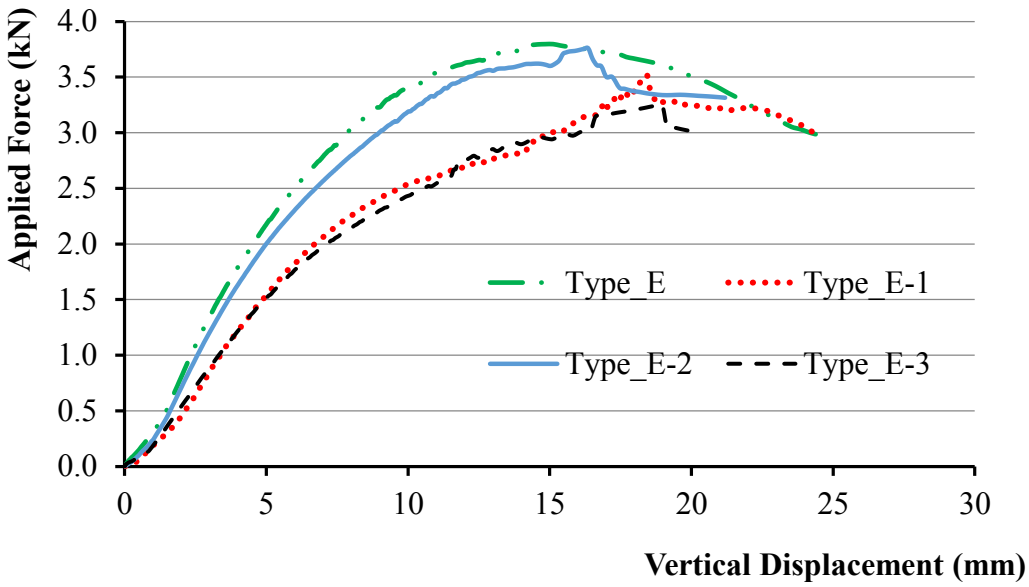

Figure 4.8. Comparison of the force-displacement relationships for the triple grip connection Type E with construction defects

The probability distribution function for the strength of each connection type was defined by fitting to the data with various distributions (i.e. normal, lognormal, Rayleigh), and the Chi-square test was applied to assess the goodness of fit (Figure A.1, A.2, A.3 and A.4 in Appendix A). Based on the goodness of fit test, the lognormal distribution was the best fit for the all the connection types. The goodness of fit test results showed, that there is significant variation in the strength of the RWC when changing the timber species from radiata pine to spruce pine, the connector from hand nail to gun nail, and the construction defects from missing nails to the "Ideal" connection. The standard deviation, coefficient of variation (COV) of the peak load and strength reduction factor, as specified in AS1720.1 (2010), were used to determine the design uplift capacity, with details described under Section 4.3. Table 4.3 shows that the COV of peak loads obtained for hand nailed defective connections was lower than the "Ideal" hand nailed connection. As the hand nails changed to gun nails in the connection, the variation of peak loads becomes lower than the variation of the "Ideal" hand nailed connection. Defective gun nailed connections (i.e. Types E-1 and E-3) show high peak load variability approximately twice that of a variation given by the "Ideal" gun nailed connection (i.e. Type E).

Table 4.3. The average peak load of the roof to wall triple grip connections

Test Specimens	Average Peak load (kN)	Standard deviation of peak load (kN)	Coefficient of variation (%)
Hand nail connections			
Type A	4.85	0.53	11.0
Type A-N1, (missing nail N1)	4.07	0.14	3.3
Type A-N6, (missing nail N6)	4.45	0.34	7.8
Type A-N9, (missing nail N9)	4.75	0.5	10.5
Type A-(N1-N6), (missing nail N1& N6)	3.10	0.32	10.2
Type A-(N1-N8), (missing nail N1&N8)	2.78	0.27	9.7
Type B	4.24	0.47	11.1
Type C	3.69	0.43	11.8
Gun nail connections			
Type D	3.53	0.46	12.9
Type E	3.80	0.4	10.5
Type E-1, (nails on the truss are in a line along an edge of the plate)	3.51	0.79	22.6
Type E-2, (nails on the truss are grouped)	3.75	0.48	12.7
Type E-3, (nails on the top-plate are grouped)	3.26	0.57	17.5

4.2.3.1 Failure modes of roof to wall triple grip connections

The failure modes of each triple grip connection were varied depending on various factors such as nail locations, material nonlinearity and construction practice. They all showed nail pull out, nail bending, triple grip bending and timber splitting. The nail deformation sizes and nail pull out displacements varied in each type of connection test and failures were observed in a different nail in each type of triple grip connection. Figure 4.9 shows that, for Types A, B and C, nails in the truss (N1, N2, N3 and N4) were pulled out and bent down, and timber splitting occurred, while nails in the top-plate (N5, N6, N7, N8,

N9 and N10) were pulled out but those were not bent. In contrast, Figure 4.10 shows that for Types D and E, nails (i.e. gun nails) in the top-plate were completely pulled out but with minimal bending; their triple grips suffered from severe deformation compared to Types A, B, and C. This could be the reason for the gun-nailed connections having lower stiffness than the hand-nailed connections, as observed in Figure 4.6.

A comparison of the tested specimens revealed that failures of hand-nailed connections eventuate on the part connected to the truss, whereas failures of gun-nailed connections eventuate on the part fixed to the top-plate. The length of the gun nail is almost equal to the width of the truss (Truss 35 mm and Gun nail 32 mm) and the nails on the truss are perpendicular to imposed load, consequently, these nails have more grip than other nails on the gun nailed triple grip connection. This could be contributing to the failure mode variation between the gun and hand nailed triple grip connections.

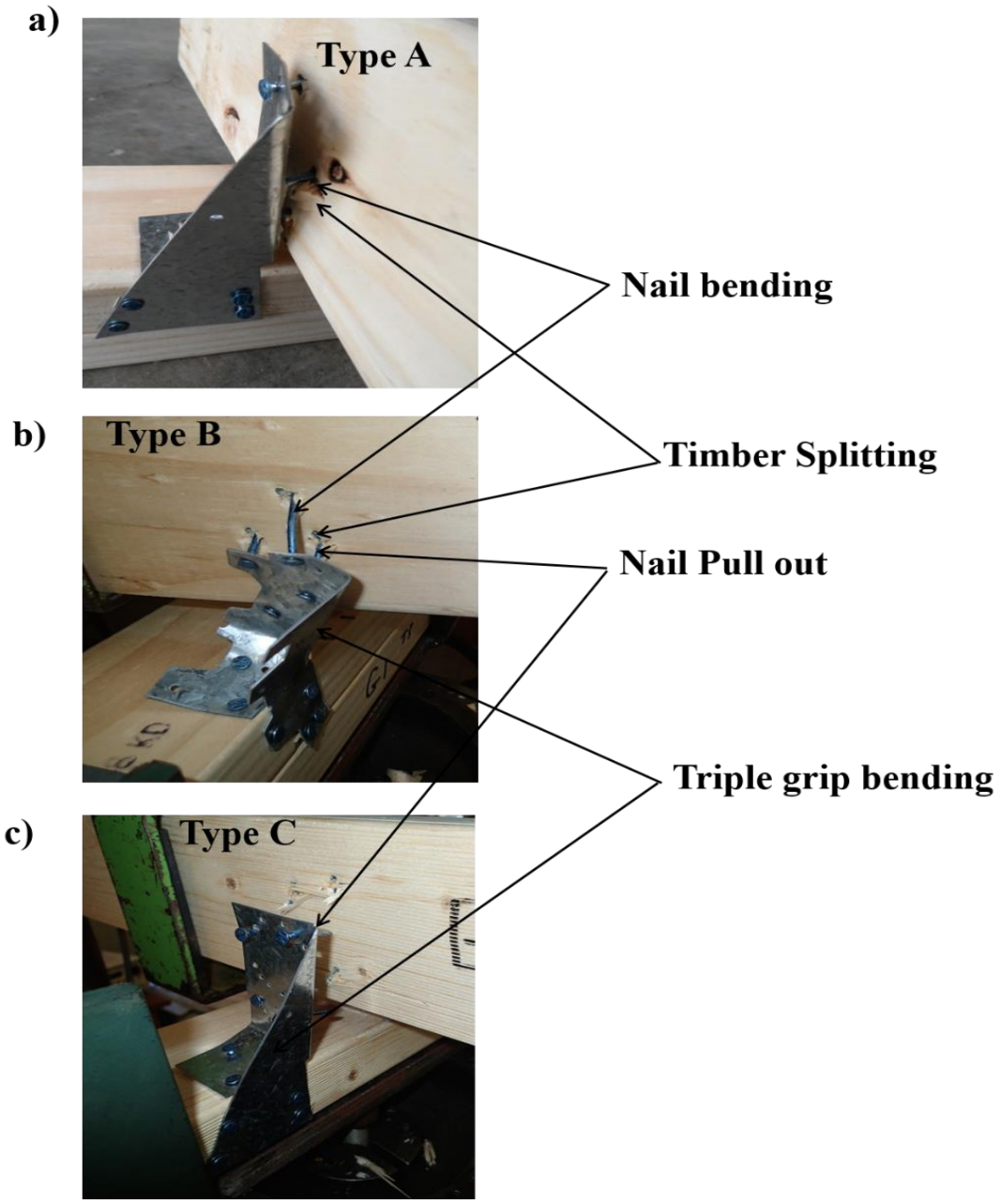

Figure 4.9. Most common failure modes of hand nailed "Ideal" triple grip connections: a) Type A, b) Type B, and c) Type C

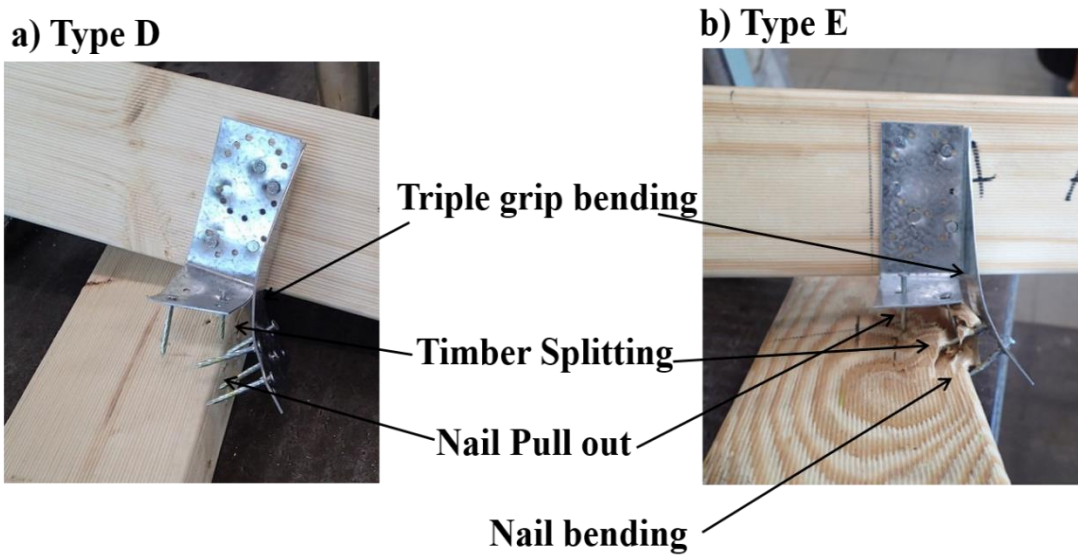

Figure 4.10. Failure modes of gun nailed "Ideal" triple grip connections: a) Type D, and b) Type E

Figures 4.11 and 4.12 illustrate the most common failure modes of defective hand nailed triple grip connection Types A-N1, A-N6, A-N9, A-(N1-N6) and A-(N1-N8). Compared to the failures of the "Ideal" connection Type A, the triple grips in these defective connections were more severely deformed, and nails N2, N3, N7, and N8 experienced more severe pull out and bending, mainly due to increased loads as a result of missing nearby nails. This indicates missing nails closer to the centre line of the loading will change the failure mode and reduce the strength of the connection; consequently, this will affect the load sharing and transfer of the timber-framed house to wind loads.

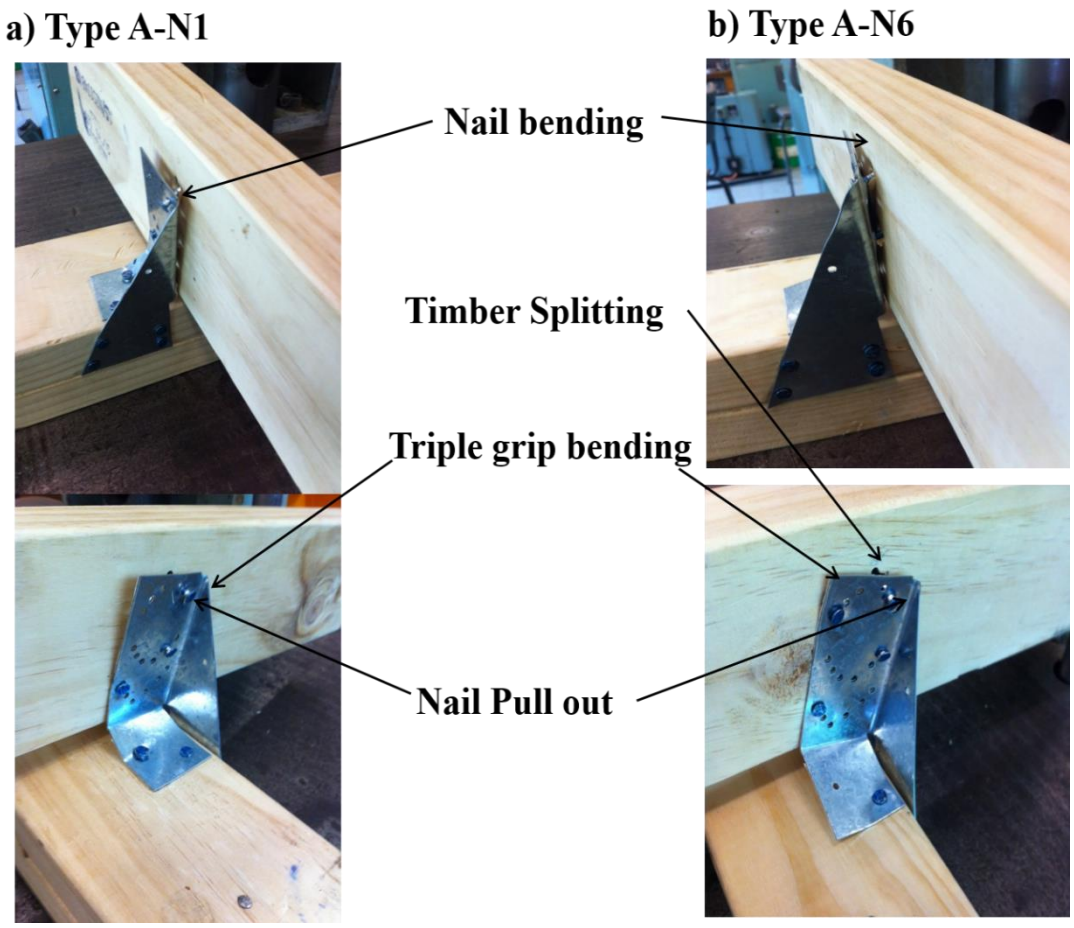

Figure 4.11. The most common failure modes of defective hand nailed triple grip connections: a) Type A-N1, and b) Type A-N6

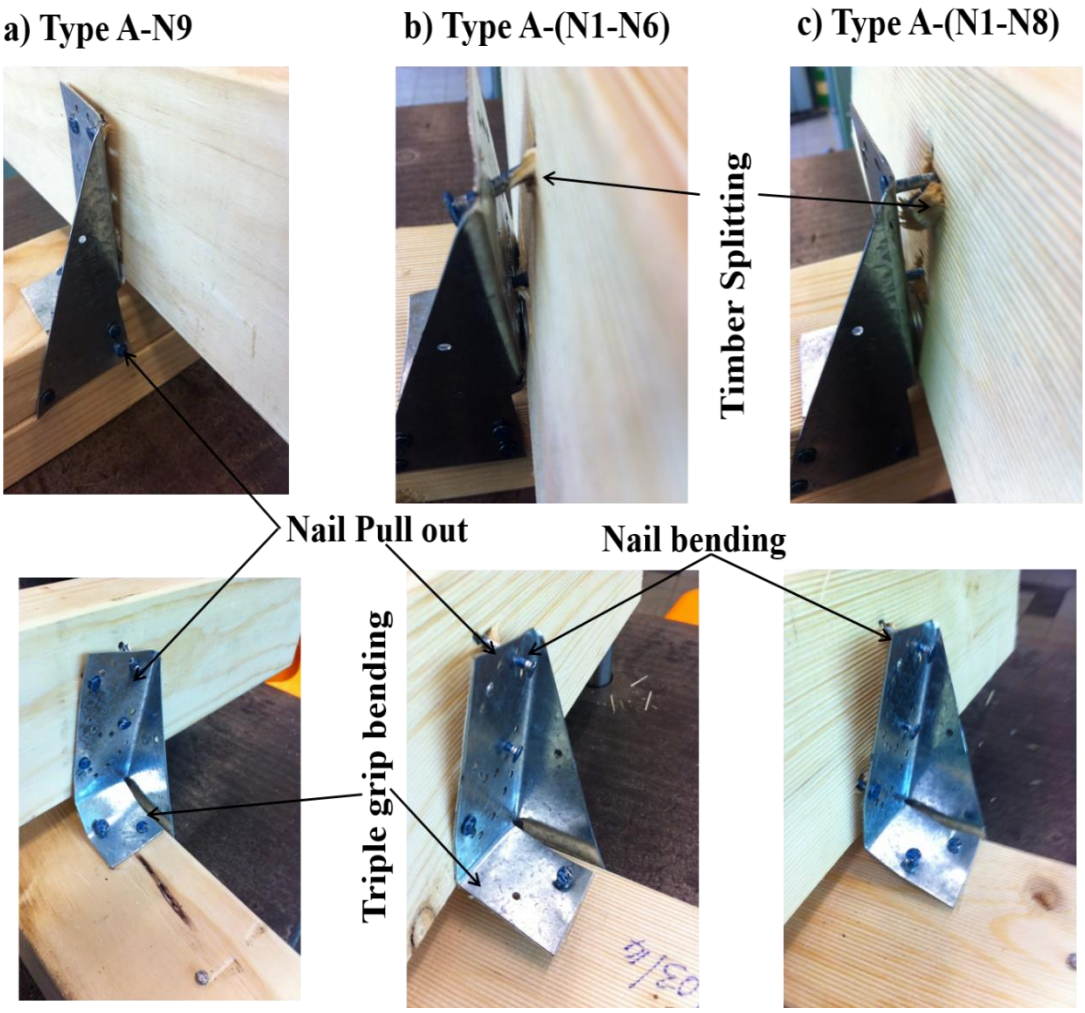

Figure 4.12. Most common failure modes of defective hand nailed triple grip connections: a) Type A-N9, b) Type A-(N1-N6), and c) Type A-(N1-N8)

The failure modes of defective gun nailed triple grip connection Types E-1, E-2 and E-3 are given in Figure 4.13. This figure shows the nails on the top-plate in the connection Types E-1 and E-2 were pulled out causing the splitting of the top-plate timber. This figure also shows that the nails on the truss in connection Types E-1 and E-2 have a considerably minimal affect compared to other nails on these connections to imposed loads. The failure mode of Type E-3 was different to the other defective gun nailed connections, showing the nails on the truss were pulled out. This indicates that the grouped nails on the top-plate changed the failure modes from the top-plate to truss. This is the reason for the lower stiffness obtained in connection Type E-3 (See Figure 4.8) compared to other gun nailed connections. This stiffness reduction of the RWC indicates

the grouping of nails on the top-plate could affect the load sharing and load transfer of the timber-framed house.

The deformed shape of the triple grip framing anchor of connection Types E-2 and E-3 were similar, but the size of deformation was variable. In Type E-2, nails were pulled out from the top-plate while nails were pulled out from the truss in Type E-3. This could be the reason for the difference in these connections' deformed size of the triple grip. Figure 4.13 also shows that the triple grip twisted about the nails on the truss of the Type E-1 connection. The nails located on the truss of the connection Type E-1 were near the edge of the triple grip and parallel to the center line of loading action. There was an equal eccentricity between each nail on the truss and center line of loading action. This eccentricity created the moment on the connection during loading, causing the triple grip to twist.

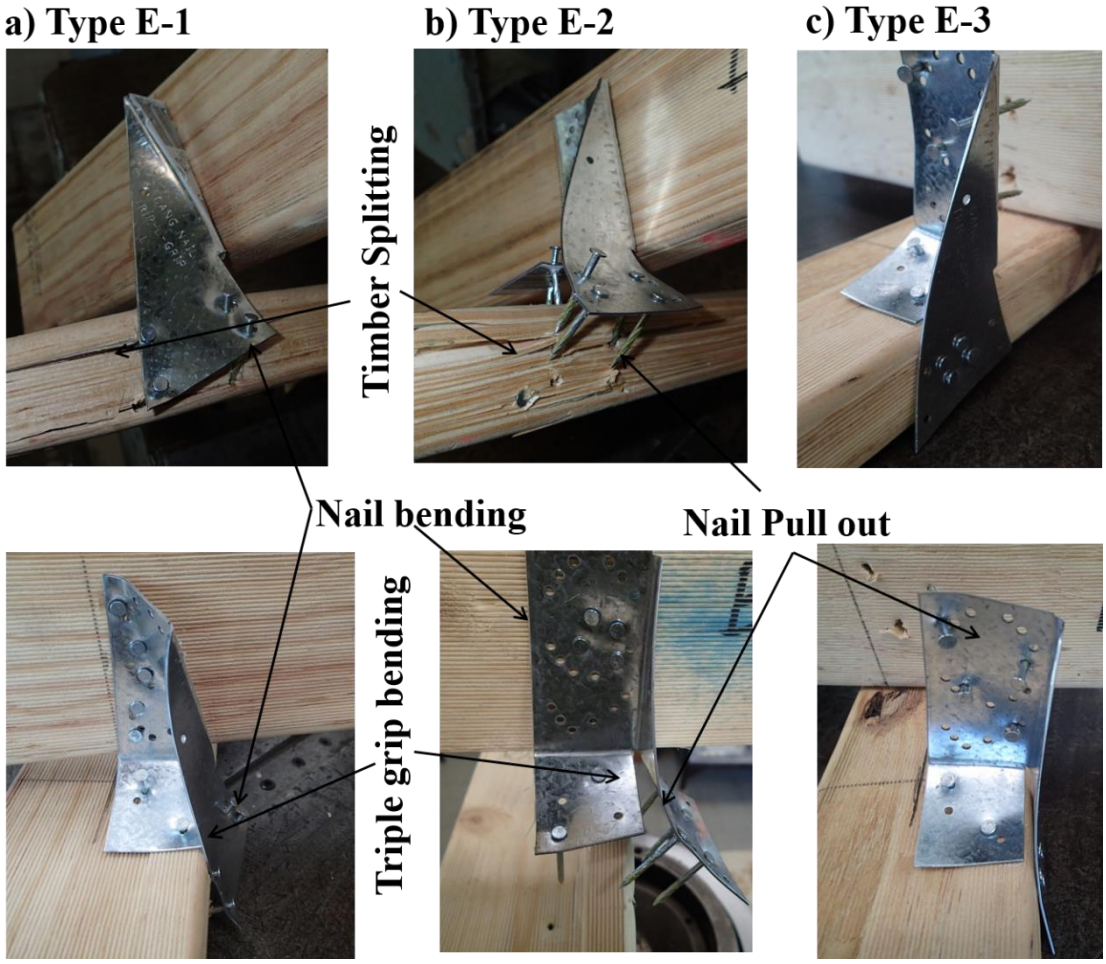

Figure 4.13. Common failure modes of defective gun nailed triple grip connections: a) Type E-1, b) Type E-2, and c) Type E-3

4.2.4 Detail of truss grip connection test specimen

Truss grip test specimens consisted of 90 mm x 35 mm x 300 mm top-plate, 35 mm x 90 mm x 300 mm truss chord and Galvanized G300 (Z275) steel truss grip (1 mm thickness), as shown in Figure 4.14. Ten samples were tested and the results were used to predict the design uplift capacity of this type of connection.

Figure 4.14. Truss grip connection test specimen

4.2.5 Test results and analysis of the roof to wall truss grip connection

Figure 4.15 presents the applied force versus vertical displacement of each of the truss grip connection tests. This figure shows that the maximum and minimum peak load of the truss grip connection were 1.27 kN and 0.94 kN. This peak load variation was due to the construction of the test specimens and density variation in the timber species. This figure also shows that the average peak load was 1.12 kN at a vertical displacement of 4.95 mm.

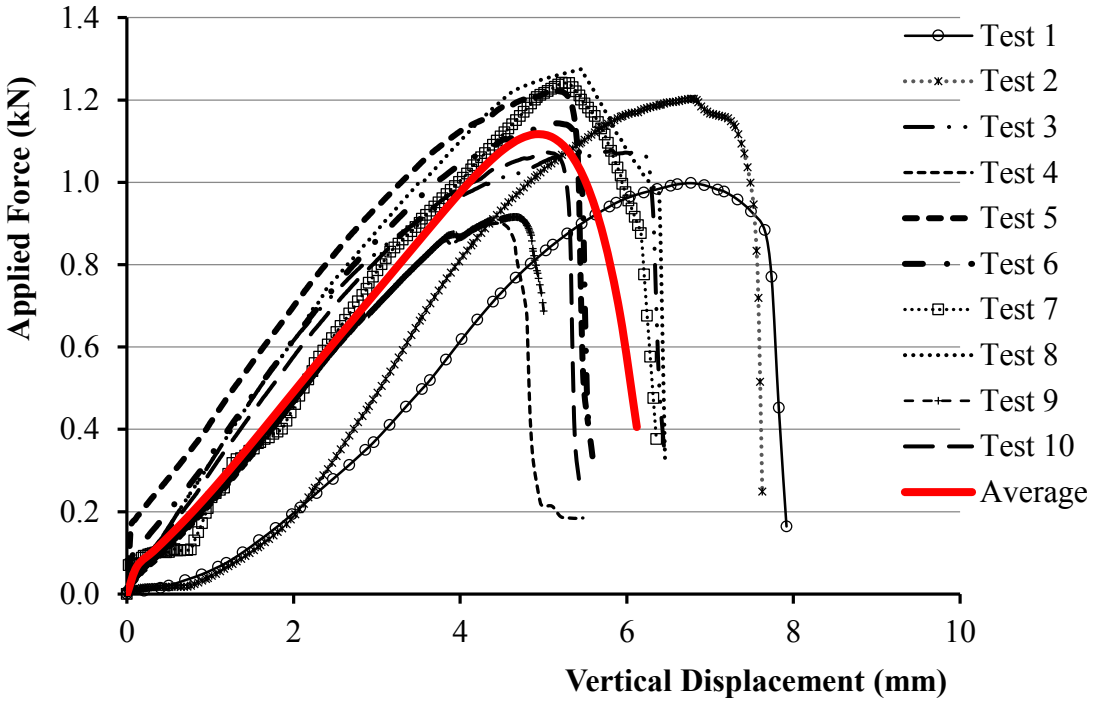

Figure 4.15. Applied force-displacement relationship for the Truss grip connection

Figure 4.16 shows the failure mode of the roof to wall truss grip connection. The illustration shows the deformed truss grip with nail teeth on the truss were pulled out and bent up and down, and the timber split in the truss. This figure also shows that the nail teeth on the top-plate have not pulled out. This indicates these nail teeth have more grip with top-plate and that causing the deformation on the truss grip framing anchor when loading.

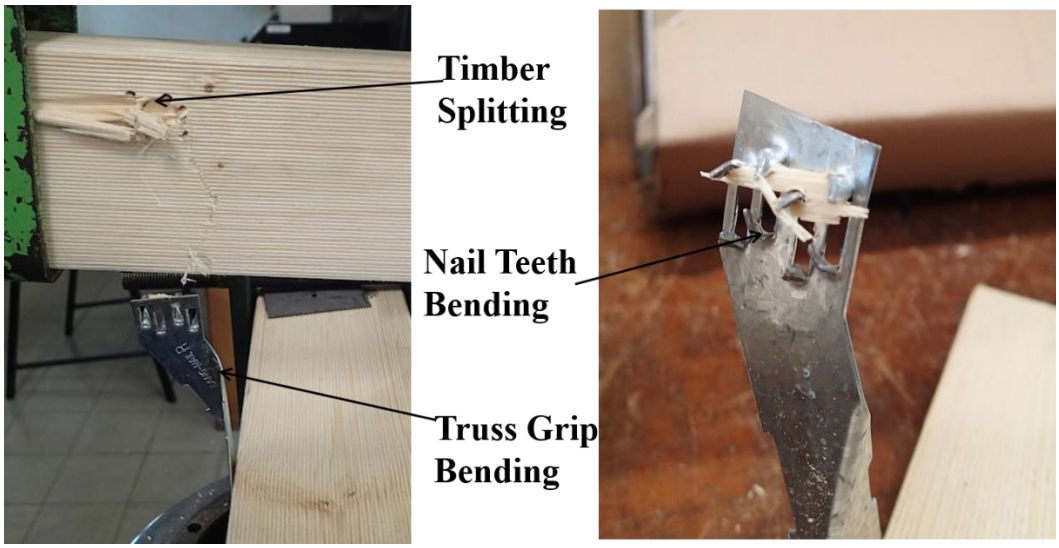

Figure 4.16. Common failure modes of truss grip connection

4.3 RWCs design uplift capacity

The standard AS 1684.2 (2010) and the manufacturer's specifications provide design uplift capacities for the RWCs, based on the strength and joint group classification. These groups are specified in Appendix H of the standard AS 1720.1 (2010) for common softwood species. These joint groups are based on the density and moisture condition (i.e. whether seasoned or unseasoned timber species). The average densities of the seasoned timber species used in each connection test were 510 kgm^{-3} and 450 kgm^{-3} for radiata pine and spruce pine respectively. According to AS 1720.1 (2010), radiata pine is classified as JD4 and spruce pine as JD5 joint group. Based on these groups, the design uplift capacity of roof to wall triple grip connection derived from AS 1648.2 (2010) and manufacturer specification (MiTek, 2014) are specified in Table 4.4. AS 1648.2 (2010) does not provide a design uplift capacity for the roof to wall triple grip connection with gun nails and/or the truss grip connection. However, the design uplift capacity of these connections can be obtained from the manufacturer's specification (MiTek, 2014), and are given in Table 4.4.

Appendix D in the standard AS1720.1 (2010) specifies methods for determining the design uplift capacities of these connections from the peak load of experimental results. This design uplift capacity was calculated from the fitted probability distribution, which was based on the peak load, number of samples and also using the duration of the test and

some strength reduction factors. These strength reduction factors depended on the failure of a constituent element (i.e. the failure of timber element or metal fastener) and the time required to reach the peak load. The effect of these codified factors resulted in a combined "material and test reduction factor" of between 0.66 and 0.83. A minimum of ten samples were tested for each type of connection to determine the design uplift capacity according to AS 1649 (2001). Based on the experimental test results, the design uplift capacity of triple and truss grip connections were obtained in accordance with AS1720.1 (2010) and listed in Table 4.4. This table also provides the design uplift capacities of the defective triple grip connections.

Based on the experiments, the design uplift capacities of "Ideal" triple grip connections (i.e. Types A, B, C, D and E) were higher than the manufacturer's (MiTek, 2014) specified uplift capacity and were in good agreement with the AS 1648.2 (2010. However, two nails missing on the hand nailed triple grip connection (i.e. Types A-(N1-N6) and A-(N1-N8)) had a significant effect on the design uplift capacity, giving about 40% reduction compared with the "Ideal" hand nailed triple grip connection (i.e. Type A). The grouping of nails on truss (i.e. Type E-2) in the gun nailed triple grip connections did not reduce the design uplift capacity but the grouping of nails together on the top-plate (i.e. Type E-3) reduced the design uplift capacity by about 20% of the "Ideal" gun nailed triple grip connection (i.e. Type E). Table 4.4 also shows that the design uplift capacity of the truss grip connection was less than the manufacture specified uplift capacity.

Table 4.4. Design uplift capacity of different types of RWCs

Design uplift capacity (kN)			
Detail	From AS1720.1 (2010) by using experimental test	From AS 1648.2 (2010)	From MiTek (2014)
Hand nail connections			
Type A	4.04	3.50	3.10
Type A-N1, (missing nail N1)	3.39	-	-
Type A-N6, (missing nail N6)	3.96	-	-
Type A-N9, (missing nail N9)	3.71	-	-
Type A-(N1-N6), (missing nail N1& N6)	2.58	-	-
Type A-(N1-N8), (missing nail N1&N8)	2.32	-	-
Type B	3.53	3.50	3.10
Type C	3.08	2.90	2.60
Gun nail connections			
Type D	2.94	-	2.60
Type E	3.17	-	3.10
Type E-1, (nails on the truss are in a line along an edge of the plate)	2.93	-	-
Type E-2, (nails on the truss are grouped)	3.13	-	-
Type E-3, (nails on the top-plate are grouped)	2.72	-	-
Truss grip connection			
Truss grip	0.93	-	1.10

4.4 Experimental tests on the joint between the timber and plasterboard

In the contemporary house, brick veneer is used for the exterior wall cladding and the plasterboard used as the interior lining. Plasterboard is also used for the ceiling and shear/bracing wall of contemporary houses in Australia. This plasterboard is fixed to the timber frame with either screws or nails and glue. The glue is not used for the top-plate, bottom plate and end-stud in the wall structure because, the glue makes a brittle failure at

the joint and, the durability of the glue may affect the design life of the structure (Liew et al, 2002).

Barton et al (1995), Reardon et al (1988), Gad et al (1999,1995), Wolfe (1982) and McCutcheon (1985) have shown that plasterboard lined walls significantly contribute to the lateral strength and stiffness of the timber-framed structures. Reardon (1988 and 1990) have shown that the main structural elements and the so-called non-structural components, particularly plasterboard lining, constitutionally contributes to the overall lateral behaviour of the timber-framed structure. Reardon (1990) also found that the plasterboard ceiling system acts as a rigid diaphragm relative to the walls. Moreover, the plasterboard also provides lateral bracing strength to the timber-framed house. The standard, AS1684.1 (2002) stipulates the bracing strength of 0.45 kN/m and 0.75 kN/m for plasterboard cladding on one and two side walls respectively. These bracing strengths depend on the strength and stiffness of the plasterboard, wall frame, and fasteners (i.e. screws or nails and glue).

The lateral and vertical loads are transferred from the roof to the walls (i.e. internal, external and shear walls) and then to the floor through the wall structure (i.e. wall frame, wall cladding and their fasteners). The loads' transmission within a wall depends on the connections to the ceiling, ceiling cornice, wall cladding, adjacent walls and the floor. Wind loads on the roof are generally transferred to the foundation in two ways. The first way is that the loads are transferred to the bottom chord of truss and RWCs then to the top-plates of the wall and subsequently along the following pathways: (i) to the plasterboard via connecting fasteners and glue, then conveyed to the bottom plates and foundation; (ii) to wall studs, then conveyed to the bottom plates and foundation. The second way is when loads are transferred to the bottom chord of the truss and then to the ceiling, subsequently conveyed to the ceiling cornice. From there, the loads are transferred directly to the wall plasterboard, and conveyed to the foundation in a similar manner to the first pathway.

These load transmission paths indicate that the connection between the plasterboard and timber inherently contributes an important role to the wind load sharing of the timber-framed house. Therefore, an evaluation of the structural response of this joint is needed in order to assess the load sharing and structural response of the timber-framed house and develop an FEM model of the full-scale test structure (Chapter 6). Laboratory tests were

conducted on these connections between timber and plasterboard to evaluate the stiffness and strength of the connections.

4.4.1 Experimental test set-up for the timber to plasterboard joints

The glue and screw joints were tested in a United testing machine. The specimens were stored at 25ºC and 65% relative humidity for 48-hours prior to testing. Figure 4.17 illustrates the test set-up for glue and screw joints. The resultant forces and vertical displacements (i.e. the relative displacement of the crosshead of United machine) were measured. Two types of tests, tension and shear load, assessed each glue and screw joint, Table 4.5 presents the test specimens' details and types.

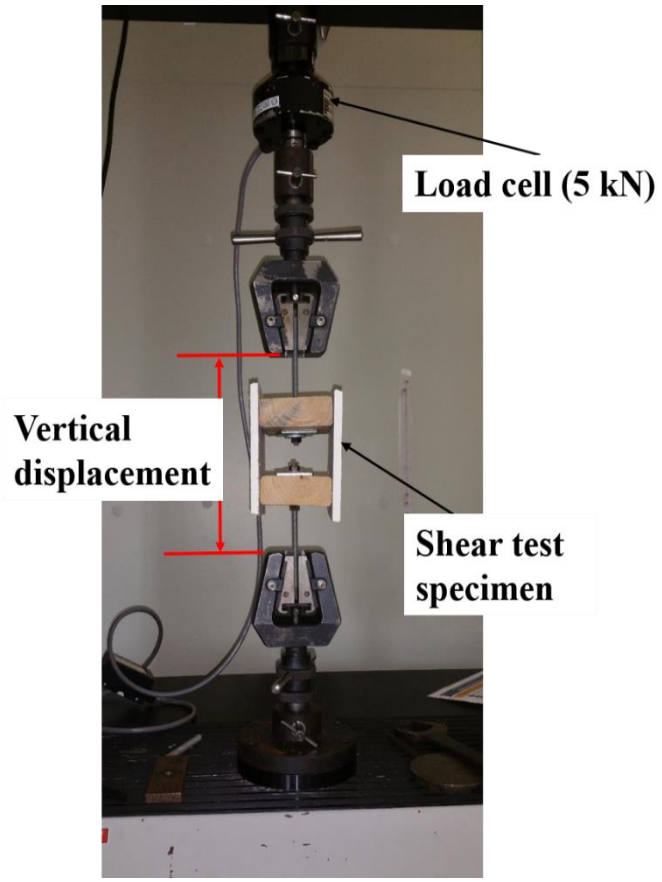

Figure 4.17. Timber to plasterboard shear joint test arrangements

Table 4.5. Test specimens' details for the timber to plasterboard

Shear load test			
Test Specimens	**Timber species (MGP 10)**	**Fixing type**	**Number of Tests**
Type S.G	Australian radiata pine	Walnuts of Gyprock Acrylic Stud adhesive	10
Type S.S	Australian radiata pine	Four , 8G x 40 mm bugle head screws	10
Tension load test			
Type T.G	Australian radiata pine	Walnuts of Gyprock Acrylic Stud adhesive	10
Type T.S	Australian radiata pine	One, 8G x 40 mm bugle head screw	10

Figure 4.18 shows the shear load test specimens and loading direction, whilst Figure 4.19 shows the tension load test specimens and loading direction.

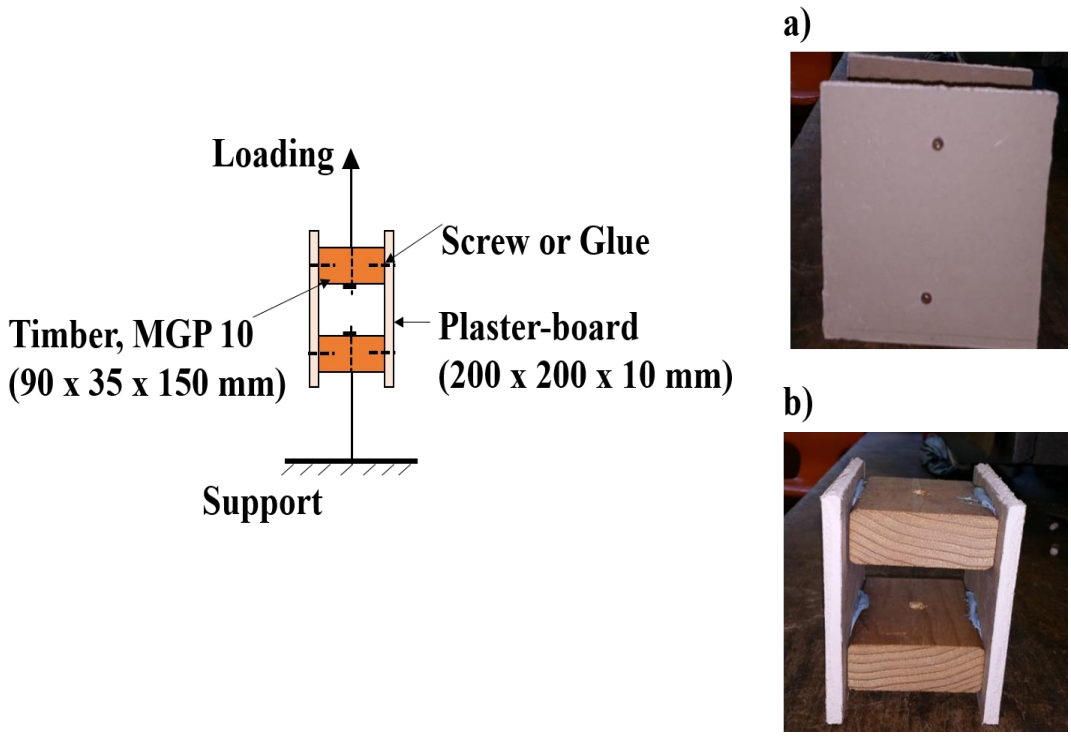

Figure 4.18. Shear load test specimens: a) Type S.S, and b) Type S.G

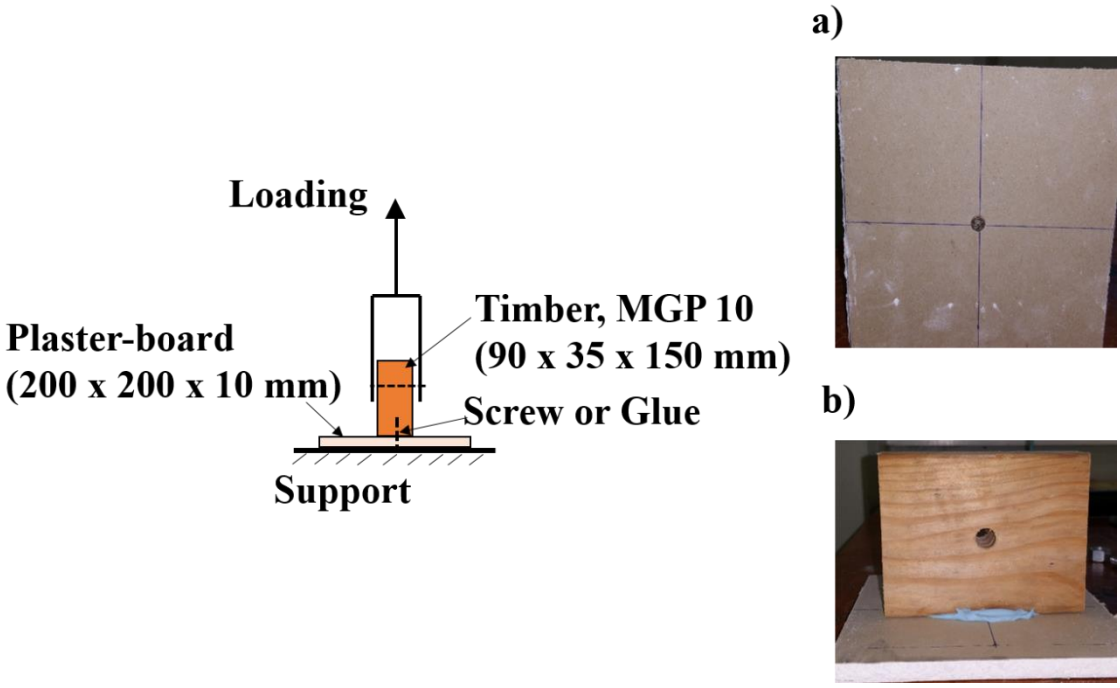

Figure 4.19. Tension load test specimens: a) Type T.S, and b) Type T.G

4.4.2 Results and analysis

The average applied load versus vertical displacement relationship for the shear load test specimen Types S.G and S.S were calculated by averaging the applied loads and displacements of each test sample (i.e. 10 number of tests). These average applied load versus vertical displacements were divided by four to determine the load displacement relationship for a single glue or screw joint (Figure 4.20). Figure 4.20 shows the maximum average load, 680 N, was obtained at a vertical displacement of 0.7 mm, then the load dropped to zero at 0.75 mm for Type S.G. For Type S.S, the maximum average load, 200 N, was obtained at vertical displacement of 1 mm where the applied load trend was constant up to a vertical displacement of 2 mm, and then dropped. This indicates that the glue joint's (i.e. Type S.G) maximum stiffness was about five times higher than that of the screw joint (i.e. Type S.S). Figure 4.20 also indicates that the glue joint's was more brittle, whilst the screw joint behaved as ductile to shear loading. This indicates that brittle failure on the glue joint will affect the load transfer through the wall lining, as they experienced a high shear load compared to the ceiling during a windstorm.

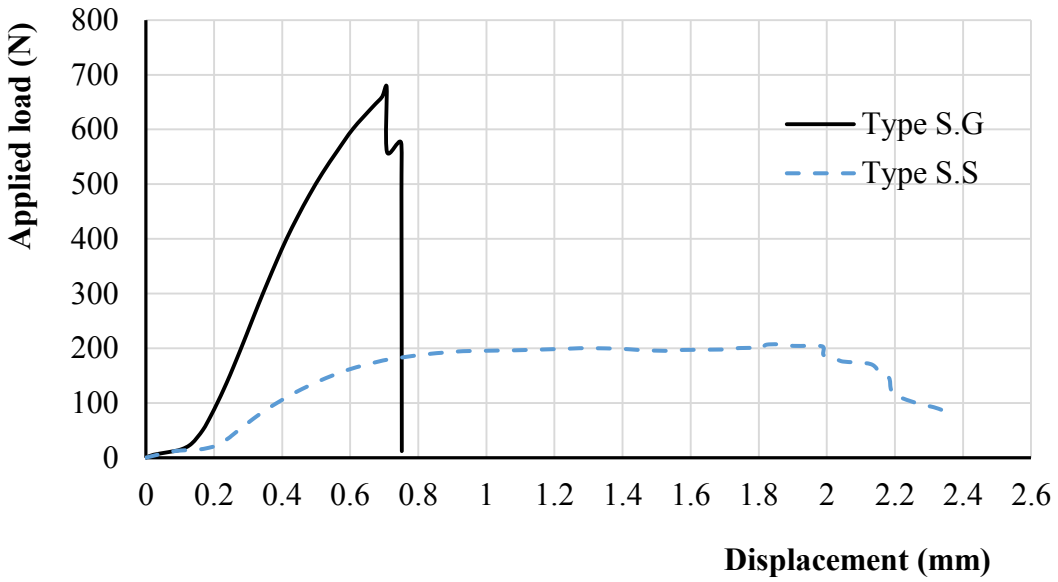

Figure 4.20. The applied load versus vertical displacement for Types S.G and S.S

The most common failure modes observed in the shear load test specimen, Type S.G were the plaster crushed (Figure 4.21a), tearing the paper liner on the plasterboard, causing glue separation from the plasterboard (Figure 4.21b). This glue separation from the plasterboard was the reason for this joint behaving in a brittle manner. Figures 4.21c and 4.21d illustrate the common failure modes for Type S.S joints. The most common failure for Type S.S joint tests was the plasterboard torn by the screws along the loading direction (Figure 4.21c), and the plaster compressed and crushed at the surrounding area of the fastener (Figure 4.21d). The plasterboard tearing and torn by the screws were the reason for lower stiffness found in the screw joint (Figure 4.20).

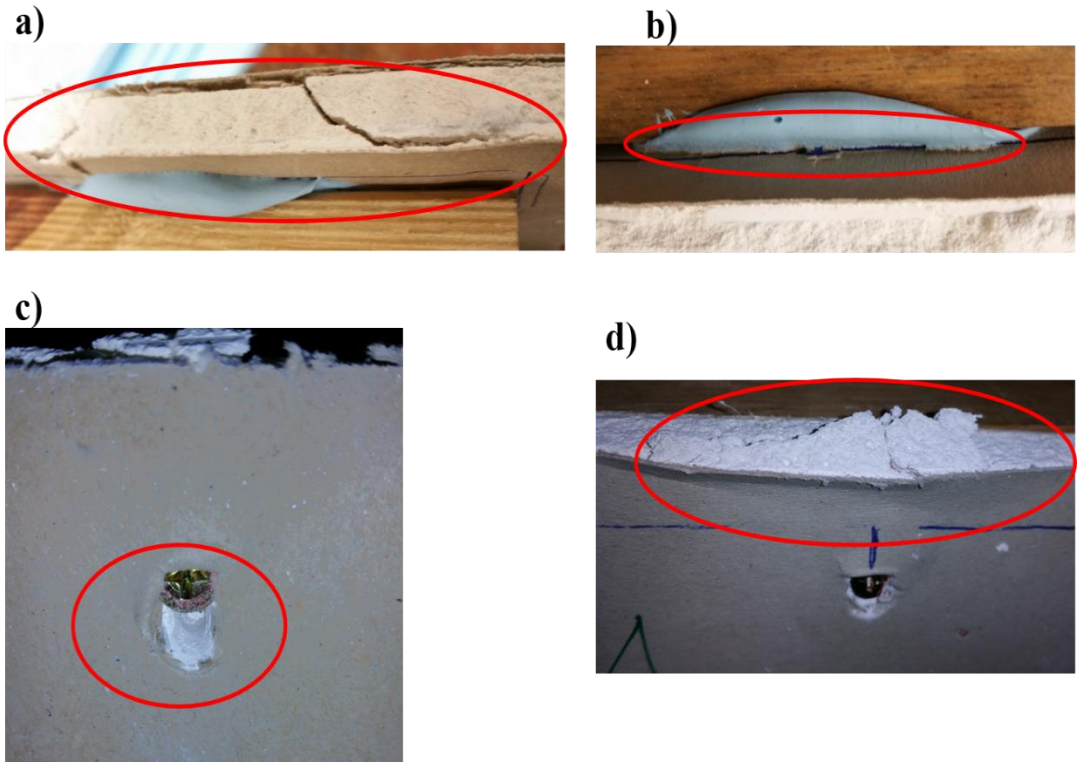

Figure 4.21. Most common failure modes of the shear load test specimens: a) Type S.G, b) Type S.G, c) Type S.S, and d) Type S.S

Figure 4.22 shows the average applied load versus vertical displacement curve for tension load test specimen types T.G and T.S. This figure shows the curve trend was similar in both glue (i.e. Type T.G) and screw (i.e. Type T.S) joints, and they both responded in a ductile manner to tension loads.

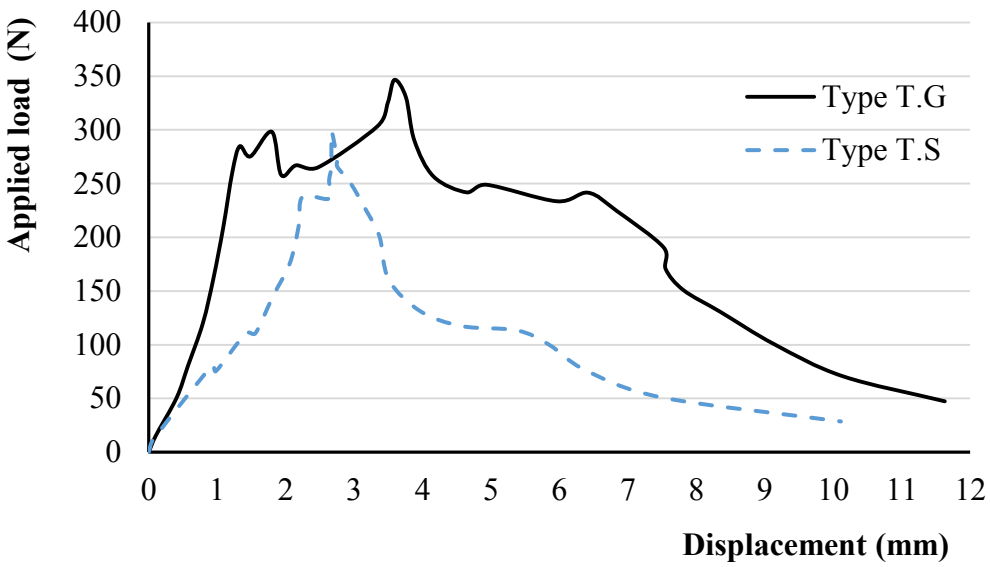

Figure 4.22. Applied load versus vertical displacement for Types T.G and T.S

Figure 4.23 shows the most common failure modes observed in the tension load test for specimens Type T.G and T.S. Figure 4.23a shows that glue separated from the plasterboard by tearing and pulling the paper liner from the plasterboard. Figure 4.23b shows the part of the gypsum from the plasterboard that was pulled out at the glue bonding region. These were the common types of failures observed in the Type T.G test. The common failure modes observed in the Type T.S tests were the screws pulling out and part of the gypsum from the plasterboard separating at the fastener region as shown in Figures 4.23c and 4.23d. These common failure modes indicate a similarity between the glue and screw joints: the glue or screw pulling out and part of the gypsum separating from the plasterboard. This failure similarity was the reason for the tension load test specimens (i.e. Types T.S and T.G) showing ductile behaviour. The common failure modes were found on the plasterboard for both tension load and shear load test specimens. This indicates that strength and stiffness of these connections were mainly dependent on the plasterboard material property (i.e. strength).

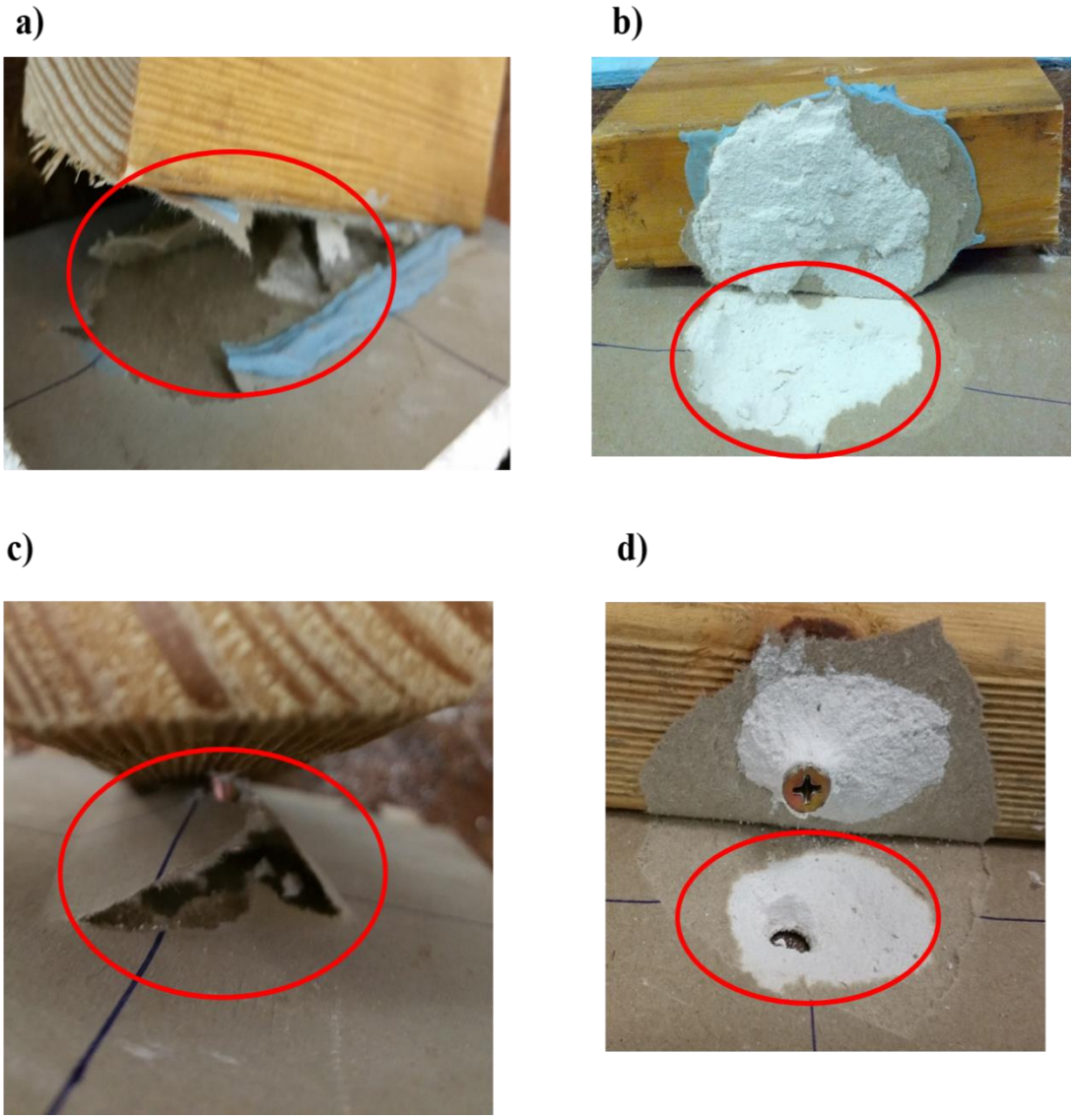

Figure 4.23. Common failure mode of the tension load test specimens: a) Type T.G, b) Type T.G, c) Type T.S, and d) Type T.S

4.5 Summary and discussion

Laboratory tests on the RWC, and the joints between the plasterboard and timber were carried out. The uplift capacity and failure mode of the RWC depends on the number and type of fasteners (nails), timber species, type of framing anchor and the constructions defects. The strength of the RWC was reduced by about 24% when the timber species was changed from radiata pine to spruce pine, and the hand nail changed to gun nail on the triple grip connection. Two missing nails in the hand nailed triple grip connection (i.e.

one nail on the truss and other one on the top-plate) reduced the design uplift capacity by about 40 % of the “Ideal” hand nailed triple grip connection. Results also show that the grouping of nails together on the top-plate in the roof to wall triple grip connection reduced the design uplift capacity by about 20%. This uplift capacity variation in each individual connection will affect the load sharing and load transfer of the timber-framed structure. The weakest connections might fail earlier, and that will change the wind load transfer path during the windstorm.

Wind load transmission paths indicate that the plasterboard to timber joint inherently contributes to the wind load sharing of the timber-framed house. The laboratory tests on the shear and tension load specimens of timber to plasterboard joint showed that the glue joint was stiffer than the screw joint. The response of the glue joint was more brittle, whilst the screw joint behaved as ductile to shear loading. The strength, stiffness and failure modes of the inter-component connections, obtained from the laboratory tests, can be used to evaluate the structural stability of the timber-framed houses to windstorms. These laboratory results can also be used to develop and validate FEMs (Chapters 6).

CHAPTER 5: FULL-SCALE STRUCTURAL TEST

5.1 Introduction

The timber-framed house structure is a complex 3D system, comprising an assembly of several components such as the walls, floors and roof. These components are connected by inter-component connections such as cladding to batten, batten to truss, roof to wall, and wall to foundation connections. Wind loads acting on the roof and walls are transferred to the foundation via these inter-component connections. Therefore, determining the structural response and the load sharing is necessary to assess timber-framed house structural performance.

The structural response of a timber-framed house to wind loading may be investigated by conducting experimental tests or numerical modelling on the individual elements, partial assemblies' components and full-scale testing. The individual and partial assemblies components tests, such as the connections test (i.e. RWC, cladding to batten connection, batten to truss connection, stud to top-plate and bottom plate connection, and ceiling joint, etc.), and tests on the wall and roof structure, will reveal the strength and stiffness of the elements. However, these tests may not provide a proper evaluation of the strength and stiffness of a whole house structure such as gable end roof house. Therefore, full-scale testing and validated numerical model analysis are required to assess the structural response and load sharing of the timber-framed house structure.

In this study, a full-scale test on part of a contemporary representative house is carried out to quantitatively determine the structural response and load sharing. The two main aims of the full-scale test on this test structure were to: (i) determine the load sharing between components through their connections based on the reaction measured at the RWC and the foundation (i.e. bottom plate); (ii) evaluate the contribution of the structural and the lining components (i.e. wall lining, ceiling and ceiling cornice) to the load sharing. In addition, this full-scale test results will be used to develop and validate the full-scale test structure's numerical model.

5.2 Full-scale test structure

The general truss region of the contemporary representative house was constructed for the full-scale experimental study, as shown Figure 5.1. The length and span of the full-

scale test structure were 3.3 x 6.6 m respectively, and the roof pitch was 21.5^{o}, with an overhang of 0.45 m (Figure 5.2).

Figure 5.1. Full-scale test structure

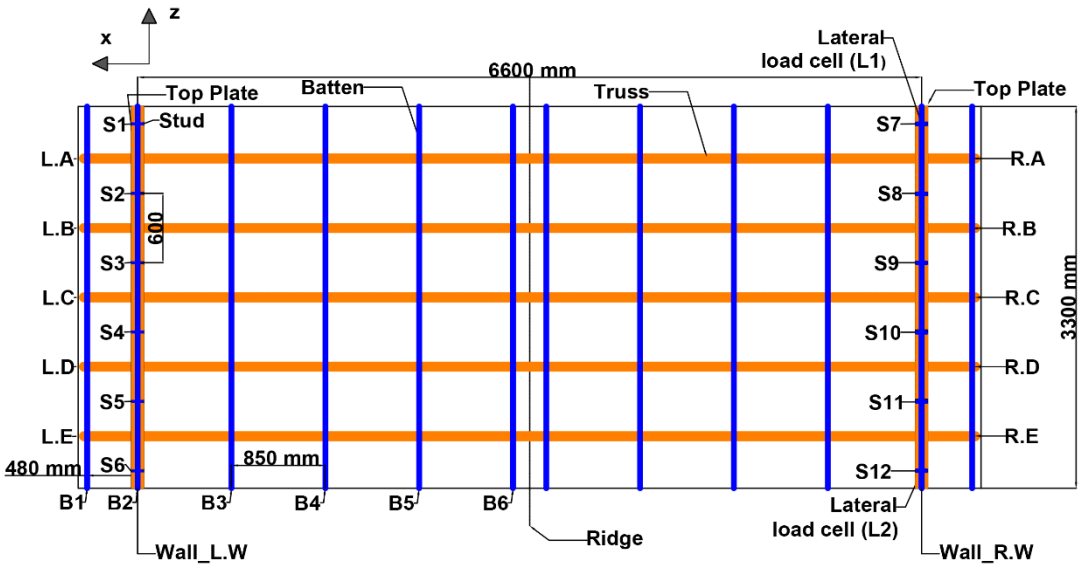

Figure 5.2. Schematic diagram of the plan view and nomenclature of the full-scale test structure

5.2.1 Construction detail of the full-scale test structure

The roof of the full-scale test structure was constructed with five general trusses spaced at 600 mm, and connected to the two ribbon top-plates as shown in Figure 5.3. Each ribbon top-plate consisted of two 90 x 35 mm, MGP10 timber blocks connected by skew nails spaced at 300 mm. Framing anchors (triple grips) with ten, 2.8 mm diameter and 30 mm long hand nails per connection were used to fix the trusses to the ribbon top-plates. Four, 4.5 m Steelbraces were used for the diagonal bracing in the roof structure. Eight, 2.7 x 0.78 x 0.8 mm, 0.42 BMT corrugated metal sheets were used for the roof cladding in the test structure. The metal roof cladding was attached to the metal top-hat battens (40 x 40 x BMT 0.55 mm) with M6-11 x 50 mm Hd/Seal screws (Figure 5.4a), and the fasteners were located based on the cladding manufacturer's specification (Stramit Australia, 2014) (Figure 5.4b). The metal top-hat battens were spaced 480 mm at the edge of roof and 850 mm for other regions, and connected to the trusses with two M5.5 x 40 mm Hex Hd screws per truss (Figure 5.4c).

Two bottom plates and twelve wall studs (i.e. six on each side) spaced at 600 mm were used to construct the wall frame. Plasterboard was used for the ceiling and internal wall lining. The ceiling was attached directly to the bottom chord of the trusses in accordance with findings from the field survey (see Chapter 3, Section 3.2.1). The plasterboard sheets were fastened to the wall frame and bottom chord of the trusses with 8G x 40 mm bugle head power driven screws (Figure 5.4d) and walnuts of Gyprock Acrylic Stud adhesive at regular intervals (Figure 5.5 and 5.6); based on manufacturer's specification (Gyprock Australia 2014). The recessed joints between the plasterboard sheets were paper taped and cemented using Gyprock GB100 along with the screw head dints. Two 90 x 90 x 2600 mm ceiling cornices were installed in the test structure. Gyprock Cornice Cement 45/60 was used for adhesion between the cornice and ceiling and wall lining. Table B1 in Appendix B details the material used in the test structure.

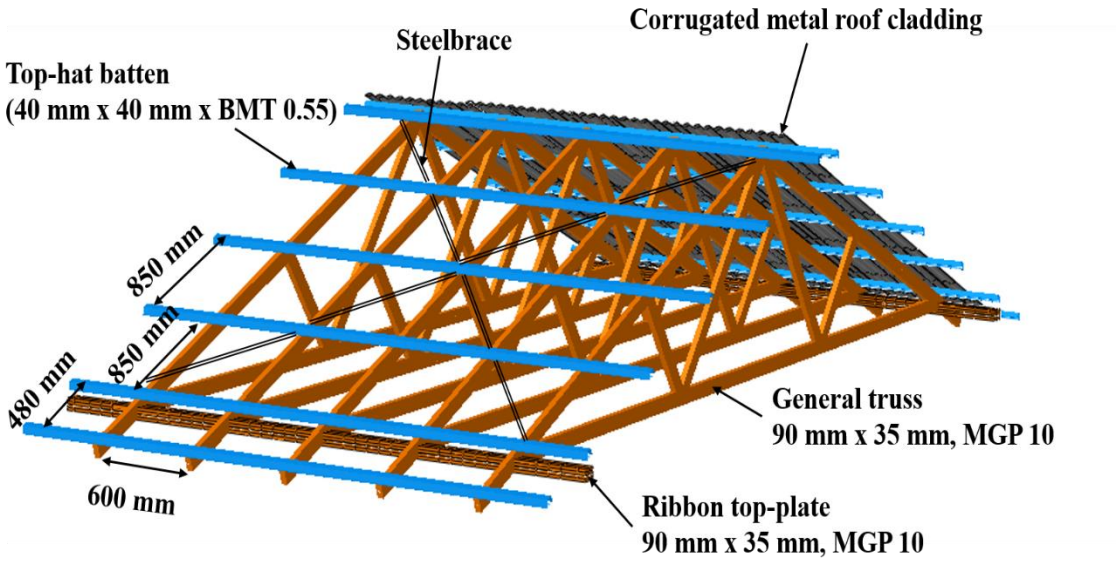

Figure 5.3. Schematic diagram of the roof structure

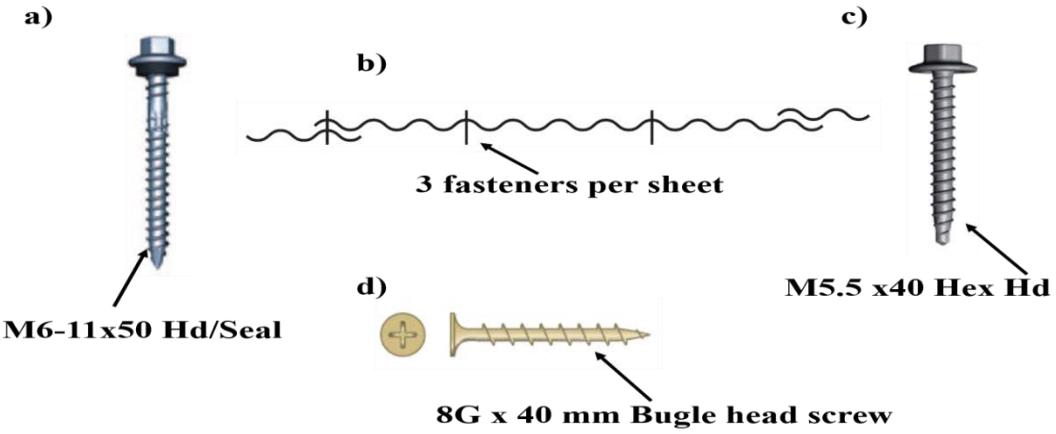

Figure 5.4. Type of fasteners used to construct the wall and roof: a) Batten to cladding fastener, b) batten to cladding fasteners locations, c) batten to truss fastener, and d) plasterboard to timber fastener

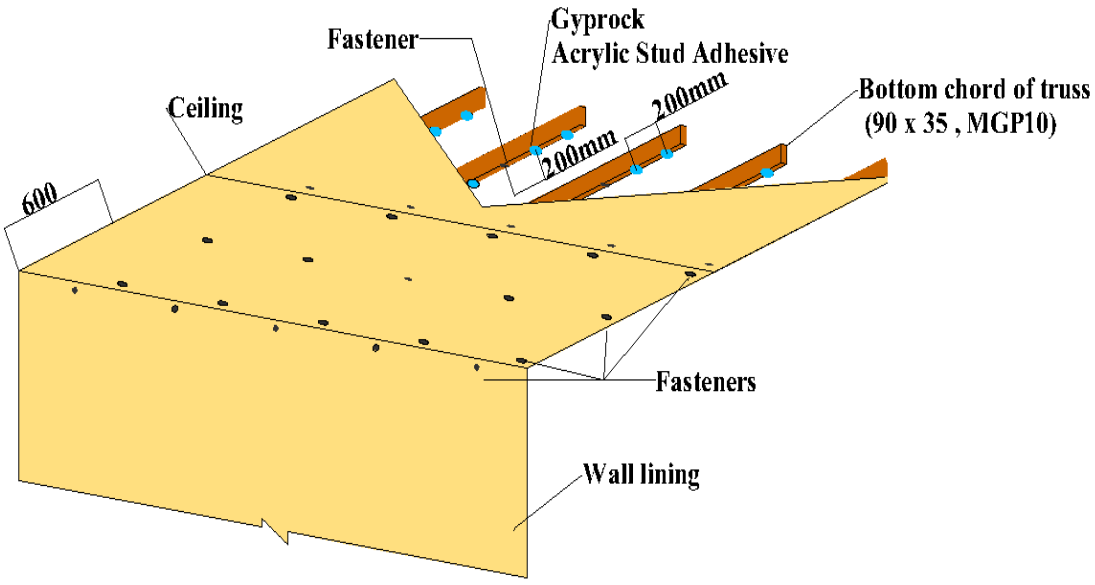

Figure 5.5. Location of fasteners and adhesive in the ceiling

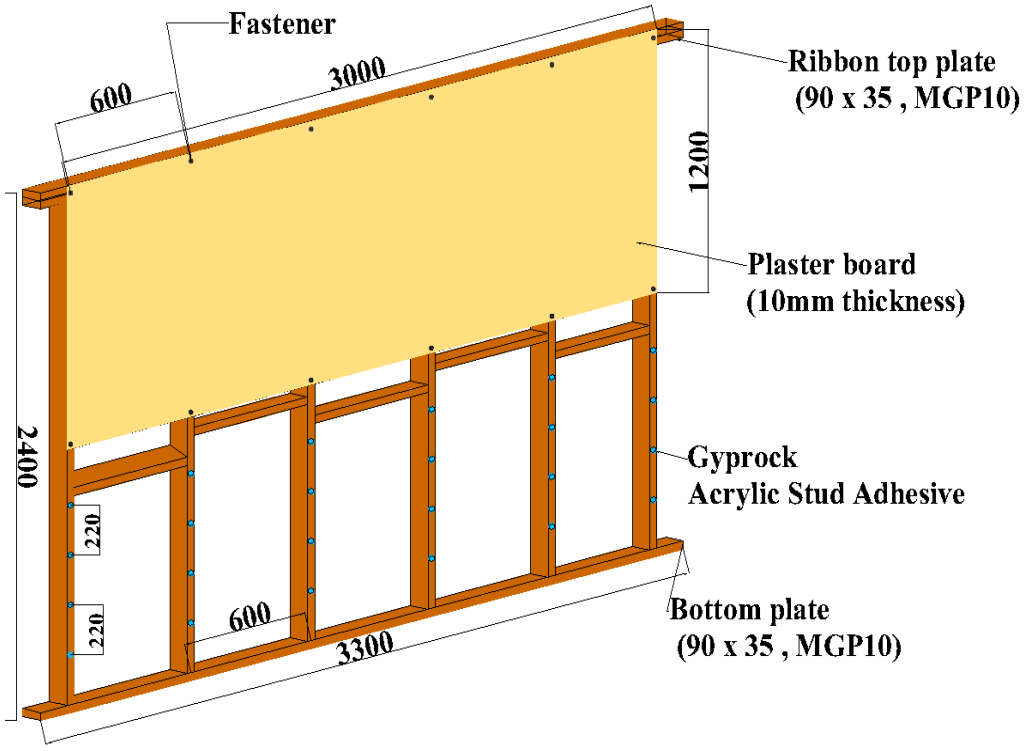

Figure 5.6. Location of fasteners and adhesive in the wall lining

This test structure excluded the exterior brick veneer wall, which generally only transfers the lateral wind loads to the timber frame through the wall ties. The effect of this exterior wall omission is not expected to significantly affect the study of the RWC response and the load sharing from roof to wall when the roof structure is subjected to wind load. This full-scale test structure also did not contain an end wall but shear walls were added as a construction stage in the series of tests. The end wall normally provides resistance to the lateral (i.e. horizontally perpendicular to the ridge) and horizontal (i.e. longitudinally parallel to the ridge) house movement. This could affect the end truss RWC structural response and the load sharing. As the objective of this study was to investigate the behaviour and load sharing of the general truss region of a contemporary representative house, there was no end wall constructed. Thus, exclusion of the end wall should not affect the general truss regions' structural response. In addition, the numerical model replicated the full-scale test structure that consisted of more complex elements (i.e. trusses, battens, roof claddings, wall lining, wall stud, ceiling, etc.).

5.2.2 Loading and measuring systems

The structural system of the full-scale test structure was symmetric; therefore, the loads were only applied to one side of the roof and loading location of the full-scale test, as shown in Figure 5.7. Tests were conducted at eight progressive stages of construction, as described in Table 5.1. The aims of testing at Stages S1 to S4 were to evaluate and quantify the load sharing within the roof structure and obtain the truss' hold-down forces, as well as to evaluate the contribution of the ceiling to the response of the RWC. Testing from Stages S5 to S8 evaluated the response of the whole full-scale test structure and load sharing through the wall structure.

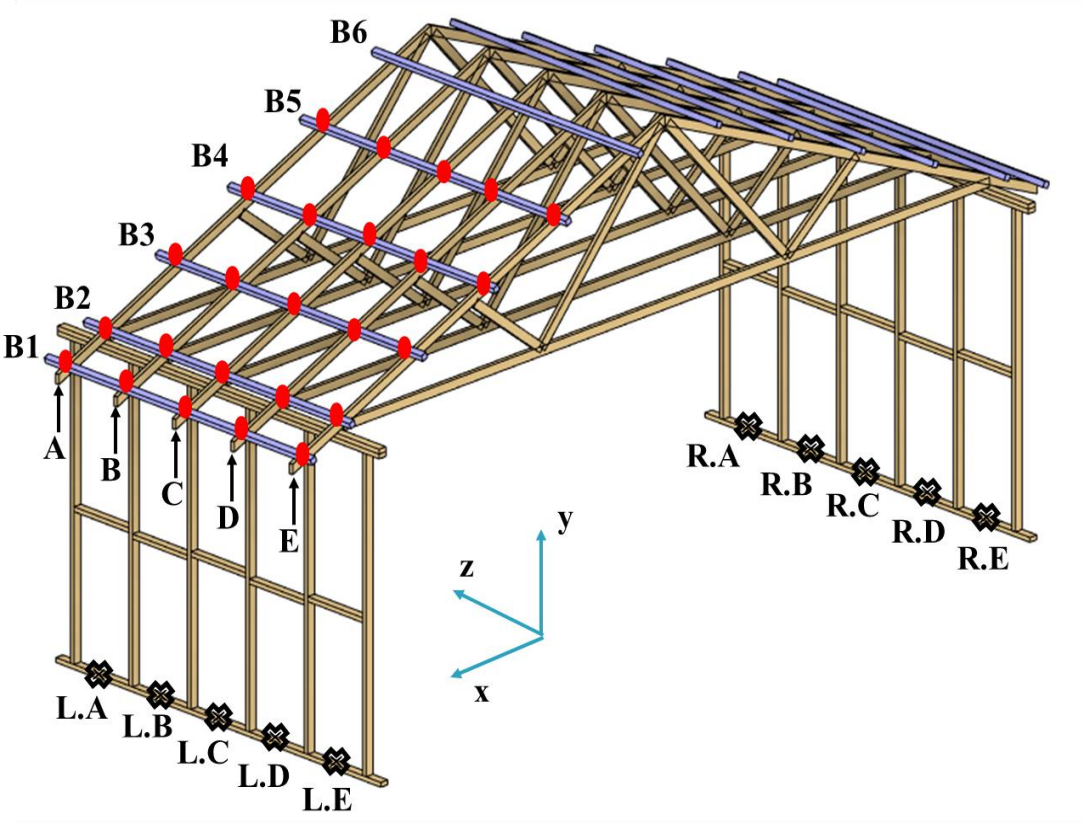

Figure 5.7. Schematic diagram of the structural frame and test loading locations on the roof (•)

Table 5.1. Detail of each stage of the full-scale test

Stage	Construction details	Location of the applied load	Location of the reaction force measurement
	Roof Structure		
1 (S1)	Five trusses, two ribbon top-plates, twelve wall studs and two bottom plates were installed	Loads were applied along the Truss at the batten to truss connection position	At the RWC, on the top-plates' positions, which were connected to load cells (LA, LB, LC, LD, LE, RA, RB, RC, RD and RE) via rods
2 (S2)	Twelve battens were added to construction Stage 1	On the battens at the same positions as for Stage 1	Same as for Stage 1
3 (S3)	Roof cladding was added to construction Stage 2	On the roof cladding at the same positions as for Stage 1	Same as for Stage 1
4 (S4)	Ceiling was added to construction Stage 3	Same as for Stage 3	Same as for Stage 1
	Roof and Wall Structure		
5 (S5)	Steel rod joint between load cells and top-plate were disconnected.	Same as for Stage 3	Reaction forces measured on the bottom plate at the same locations as for Stage 4 (i.e. LA, LB, LC, LD, LE, RA, RB, RC, RD and RE)
6 (S6)	The wall lining was added to Stage 5	Same as for Stage 3	Same as for Stage 5
7 (S7)	Ceiling cornices were added to Stage 6	Same as for Stage 3	Same as for Stage 5
8 (S8)	Shear walls were added to Stage 7	Same as for Stage 3	Same as for Stage 5

Previous studies by Morrison (2010), Henderson et al (2011), and Jayasinghe (2012), showed that the structural response under wind load is well represented by studying its response under static load. Thus, the loads were applied statically and normal to the roof surface at the batten to truss connection locations with a hydraulic ram, which is

connected to a movable loading beam. This loading beam was fixed on to the reaction frame, parallel to battens. Figure 5.8 illustrates the loading systems used in the full-scale test.

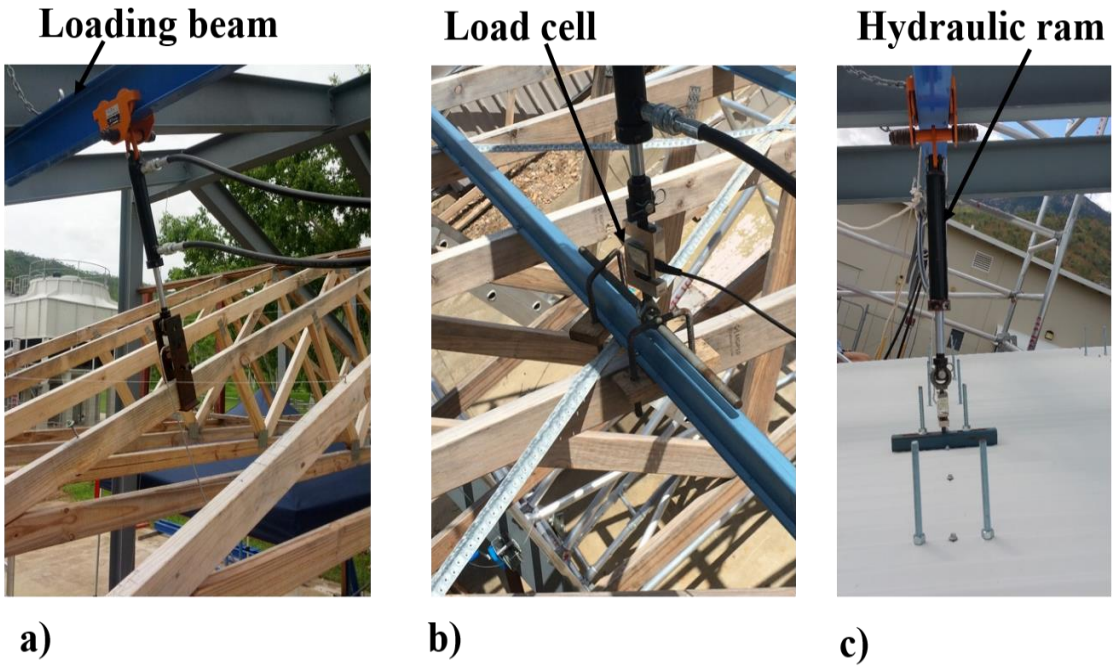

Figure 5.8. Loading systems for: a) Stage S1, b) Stage S2, and c) Stages S3 to S7

The structural system was supported by load cells under the bottom plate; load cells were used to measure the reaction forces (Figure 5.9). Steel rods were connected to the top-plate and load cell (Figure 5.10) to measure the reaction force at the RWC. These steel rods (12 mm diameter) with high stiffness washers pass through oversized holes placed equidistant to the centroid of the RWC (i.e. the rods were located at either side of the truss, Figure 5.10). The oversized holes for the steel rods were drilled in the top-plates, bottom plates and noggings. Ten load cells were located under the bottom plate at the RWCs locations to measure the vertical reactions. In addition, two load cells were located at each end stud of the non-loading side wall. These load cells were used to measure the total lateral direction reaction force, as well as to resist the structural system's lateral movement.

Deflections were measured by linear variable displacement transducers (LVDT) at specific locations on the test structure (Figure 5.9). Thirty LVDTs were used in the tests

and were located at each RWC location. LVDT_1 and LVDT_2 were used to measure the relative (i.e. movement between the truss and top-plate) vertical and lateral displacement of the RWC and LVDT_3 was used to measure the vertical movements of the top-plate. All the load cells and LVDTs were connected via USB cables to the Data Acquisition (DAQ) system from National Instruments. LabView system design software was used to produce code to record the data from these measuring devices. All the LVDT's and load cells were calibrated, and the calibration factors were applied in the LabView code. The detail of the calibration of the measuring devises is detailed in Appendix B.

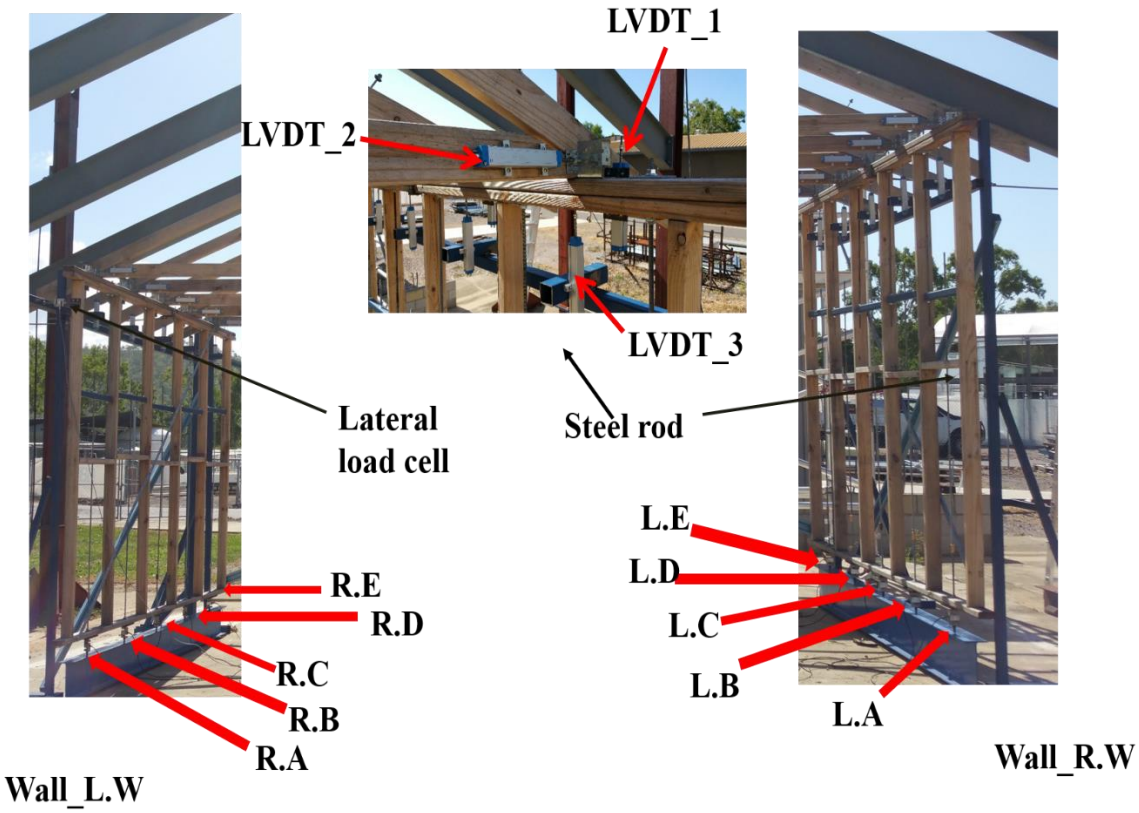

Figure 5.9. Locations of measuring devices

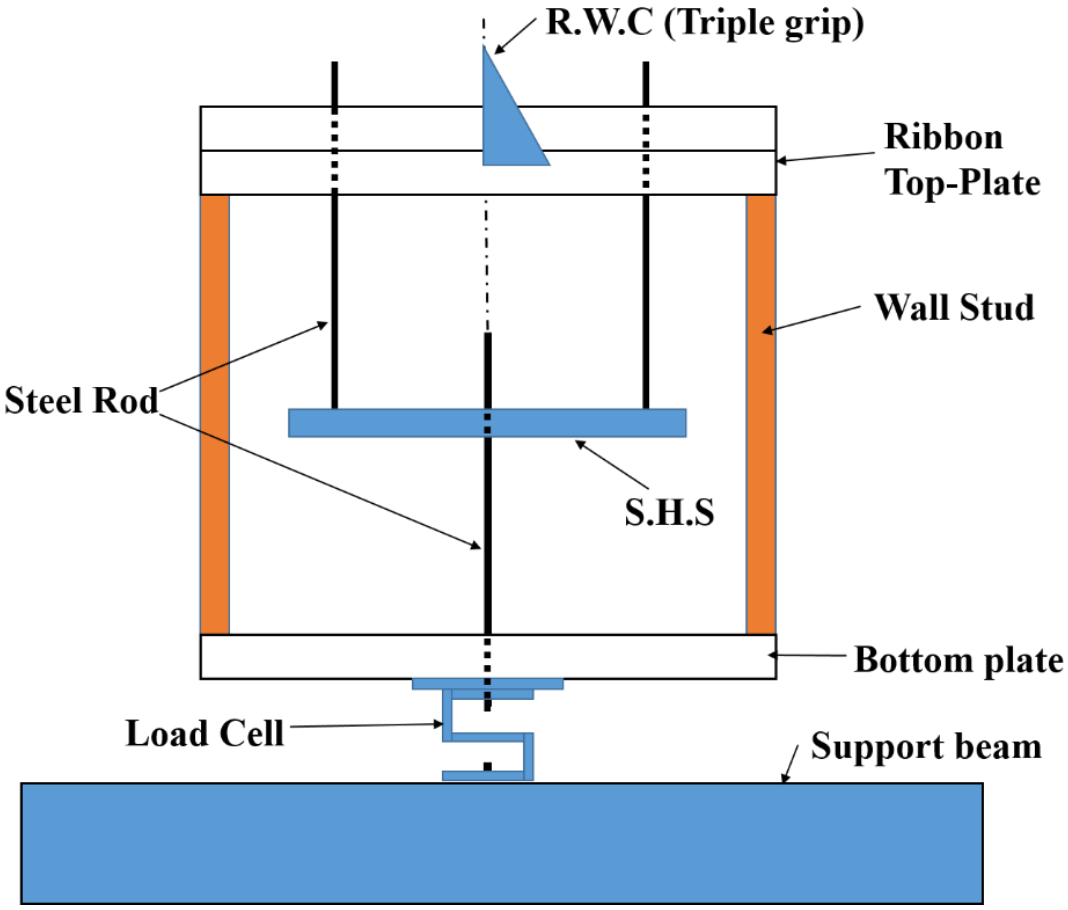

Figure 5.10. Schematic diagram of the steel rod connection from top-plate to load cell

5.3 Test results and analysis

As the tests moved from construction Stage S1 to Stage S8, there might be a gradual deterioration in the stiffness of the inter-component connections (i.e. batten to cladding and truss connection, truss to wall connection, stud to top-plate and bottom plate connection, ceiling to truss connection, etc.) and their individual fasteners as a result of partial nail or screw withdrawal. This gradual deterioration of the stiffness will influence the individual connection structural response. This effect is not considered to be significant when assessing the whole house structural system response and load sharing.

5.3.1 Point loading on roof structure

In these full-scale tests, the loads were applied perpendicular to the roof surface in order to represent wind loading. The applied loads were within the serviceability limit state of the house structure, which did not cause failures of the structural and lining components or the inter-component connections at each stage of testing. The responses (i.e. the measured reaction forces and displacements) to applied loads, ranging between 0.7 kN and 1 kN at batten to truss connections along Trusses A, B and C, are presented in this Chapter with other results detailed in Appendix B. A "reaction coefficient" (i.e. normalized reaction force) is defined as the reaction force divided by the applied load.

5.3.1.1 Structural response of the system to load on the roof

Figures 5.11 to 5.19 show the vertical reaction coefficient (VRC) (i.e. measured vertical reaction divided by the applied load) changes at the RWC support (i.e. L.A, L.B, L.C, L.D, L.E, R.A, R.B, R.C, R.D and R.E) at construction Stages S1, S2, S3, S4, S5, S6 and S7, when the test load was applied along Truss A (i.e. TA), B (i.e. TB) and C (i.e. TC). Figures 5.11, 5.12 and 5.13 show the VRC for all seven construction stages when loaded at Battens B1, B2 and B3 respectively, on Truss A. These figures show that the VRC of the RWC of Truss A at the loading side support (i.e. L.A) was high for Stage S1. This is because in Stage S1, the ribbon top-plate is the only structural element available to distribute the load to the adjacent trusses' supports. About 15% to 25% of applied loads were shared to the adjacent trusses through the wall top-plate and ridge beam (which was used to hold trusses at the same location during Stage S1 testing). The VRC at RWC of Truss A's loaded side support (i.e. L.A) at Stage S1 was reduced by about 10%, when the test load was moved from Batten B1 to B2 (Figures 5.11 and 5.12), whilst the VRC dropped by about 15% when load was moved to Batten B3 from B2 (Figures 5.12 and 5.13). This is due to the location of battens: Batten B1 was located at the eaves and B2 directly above the RWC. Batten B3 was located between the RWC and truss web member. Thus, the distance between the loading (i.e. Battens B1 and B3) and measured (i.e. Batten B2) locations was high when load was applied at Batten B2 compared to Batten B1. This distance variation was the reason for the less VRC reduction obtained when the applied load was move to Batten B1 to B2 compared to Batten B2 from B3.

As Figures 5.11, 5.12 and 5.13 illustrate, the variation of VRCs on the loading side of the adjacent trusses' was negligible at Stage S1, when loads were moved from Batten B1 to B2 and B2 to B3. This indicates that the load was not shared to the adjacent trusses, but transferred to the other end (non-loaded side) support of Truss A (i.e. R.A). The VRC on the loaded side support of Truss A (i.e. L.A) at Stage S1 was reduced by about 10% to 20% at Stages S2 and S3, and about 25% at Stage S4. Figures 5.11, 5.12 and 5.13 show that the VRCs were similar at Stages S6 and S7, indicating that the contribution of ceiling cornice to the vertical load sharing was negligible compared to that of the wall lining. This is because the vertical loads were directly transferred through the wall lining to the bottom plate.

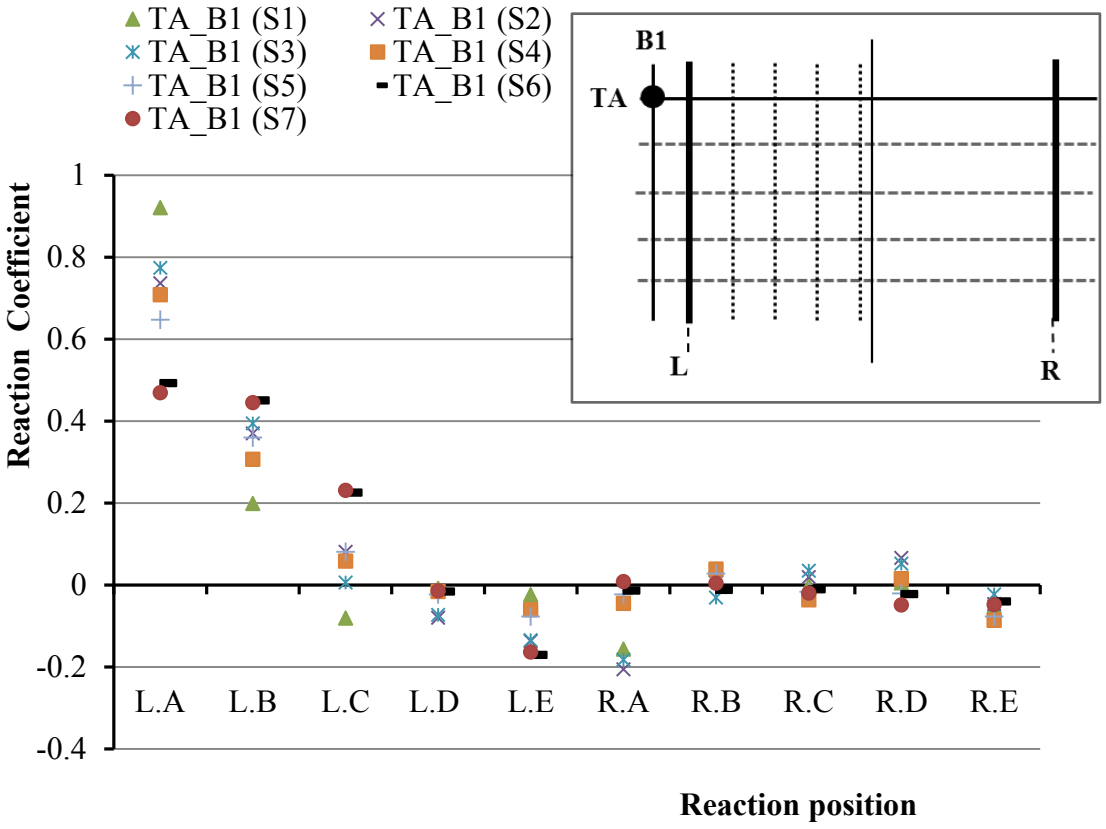

Figure 5.11. VRC, when loading on Battens B1 at Truss A (i.e. TA)

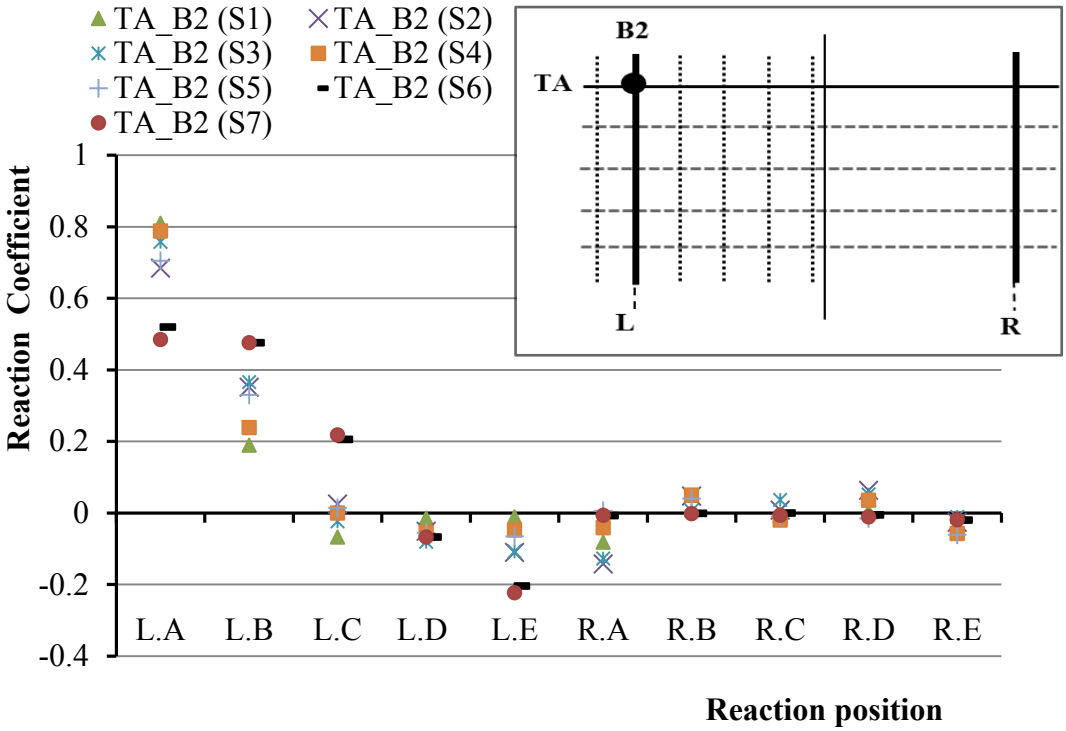

Figure 5.12. VRC, when loading on Battens B2 at Truss A (i.e. TA)

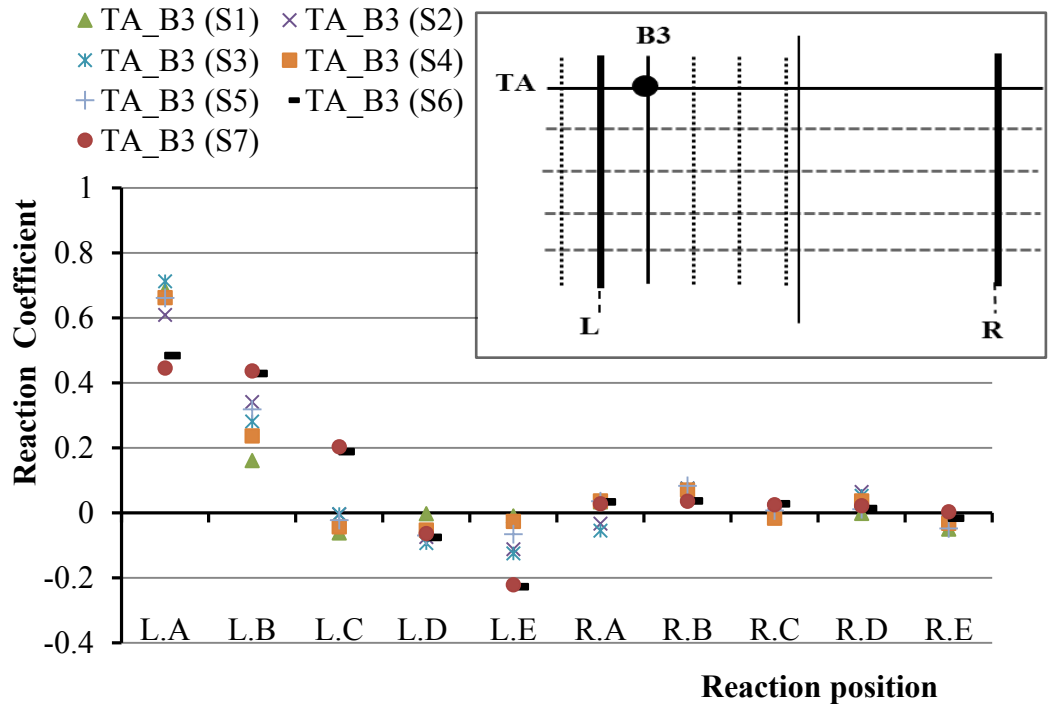

Figure 5.13. VRC, when loading on Battens B3 at Truss A (i.e. TA)

Figure 5.14 gives VRCs when loading on Batten B1 at Truss B, whilst Figures 5.15 and 5.16 show loading on Battens B2 and B3 at Truss B. The VRCs at the Truss B's loaded side support (i.e. L.B) in all the Stages were less than the VRCs obtained at the Truss A loaded side support (i.e. L.A) when loading on these battens (i.e. B1, B2 and B3). This is due to the location of the trusses. Truss A was located at the end of the top-plate and could only share the load to one side of the top-plate, whilst Truss B, located between Trusses A and C, could share more loads between these two truss supports. The VRC at Truss A's loaded side support (i.e. L.A) was generally higher than the VRC of Truss C loaded side support (i.e. L.C) when loading along Truss B (i.e. TB). This was due to the stiffness variation of the roof to wall triple grip connections; the RWC (i.e. included the triple grip, truss, top-plate, etc.) strength and stiffness varies with material non-linearity, construction practices and workmanship. Hence, the stiffness of all the trusses' RWC in the full-scale test structure was not the same. The VRC at the Truss B loaded side support (i.e. L.B) at Stage S3 was higher than that of Stage S2. The corrugated roof cladding was stiffer along the crests (Henderson et al., 2011), thereby promoting the transfer of loads along the crest. As the roof trusses were located parallel to the corrugated crests, a higher percentage of applied load was directly transferred along the loaded truss, with less load distributed along battens.

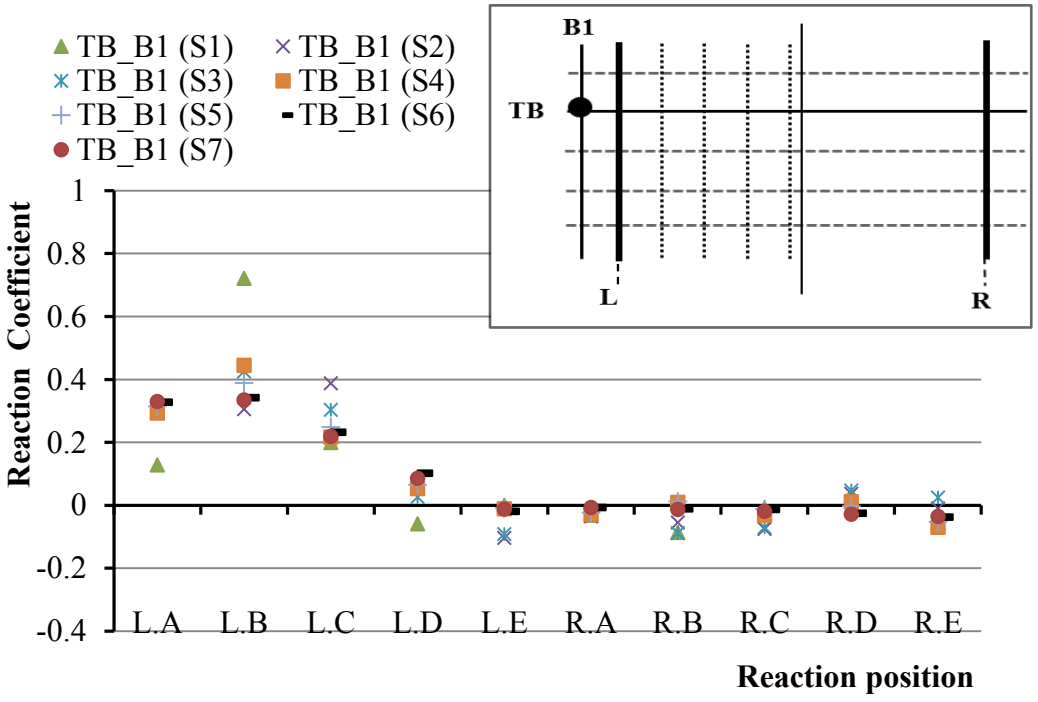

Figure 5.14. VRC, when loading on Battens B1 at Truss B (i.e. TB)

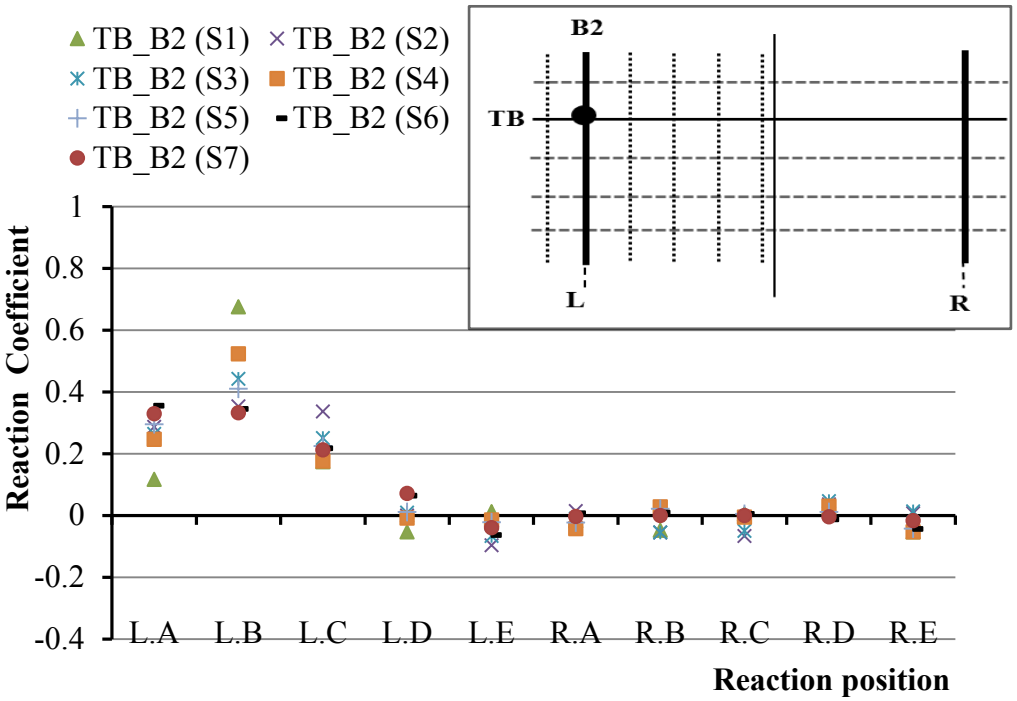

Figure 5.15. VRC, when loading on Battens B2 at Truss B (i.e. TB)

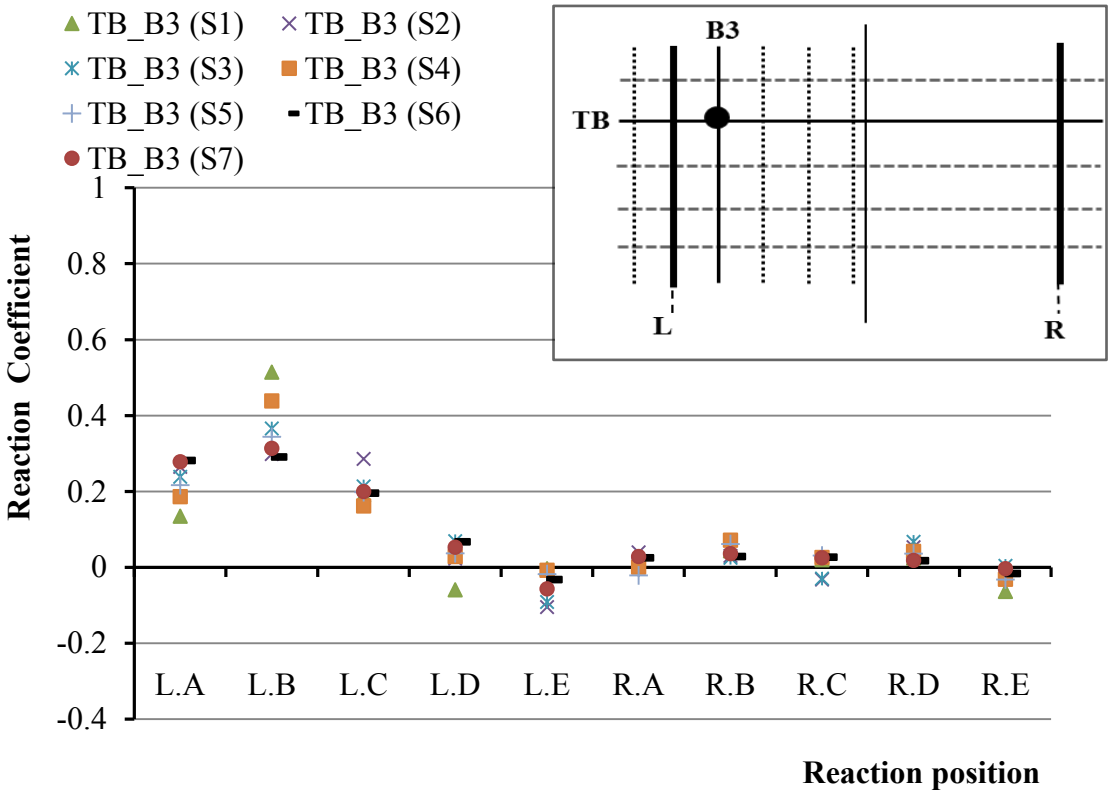

Figure 5.16. VRC, when loading on Battens B3 at Truss B (i.e. TB)

Figure 5.17 presents the VRCs when loading on Batten B1 at Truss C, whilst Figures 5.18 and 5.19 give the VRCs when loading on Battens B2 and B3 at Truss C. The VRC of the Truss C support (i.e. L.C) in all stages was less than that of the VRCs obtained when loading on Battens B1, B2 and B3 at Trusses' A and B supports (i.e. L.A and L.B). Truss C was located in the middle of the test structure and shares more load to the adjacent trusses' supports compared to other trusses. This was the reason for the lower VRC obtained when loading along Truss C. Moreover, the stiffness of the RWC of Truss C was less than the other connections when compared to other trusses' VRC at Stage S1. This lower connection stiffness is also a reason for the less VRC found in all stages when loading along Truss C.

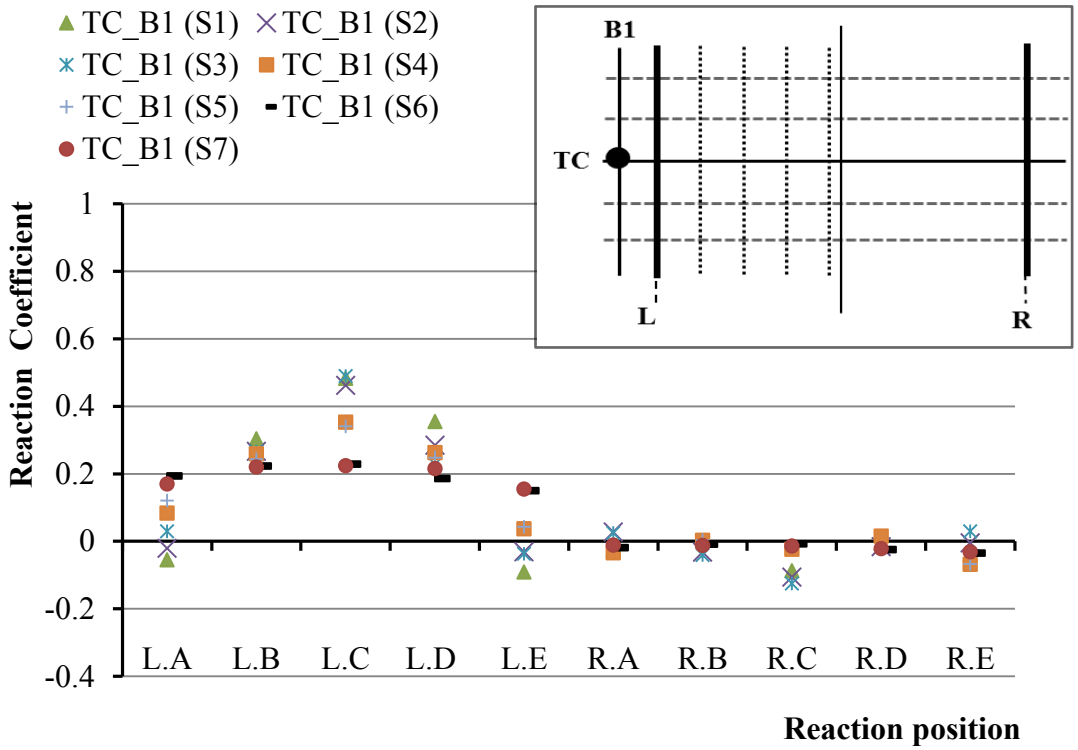

Figure 5.17. VRC, when loading on Battens B1 at Truss C (i.e. TC)

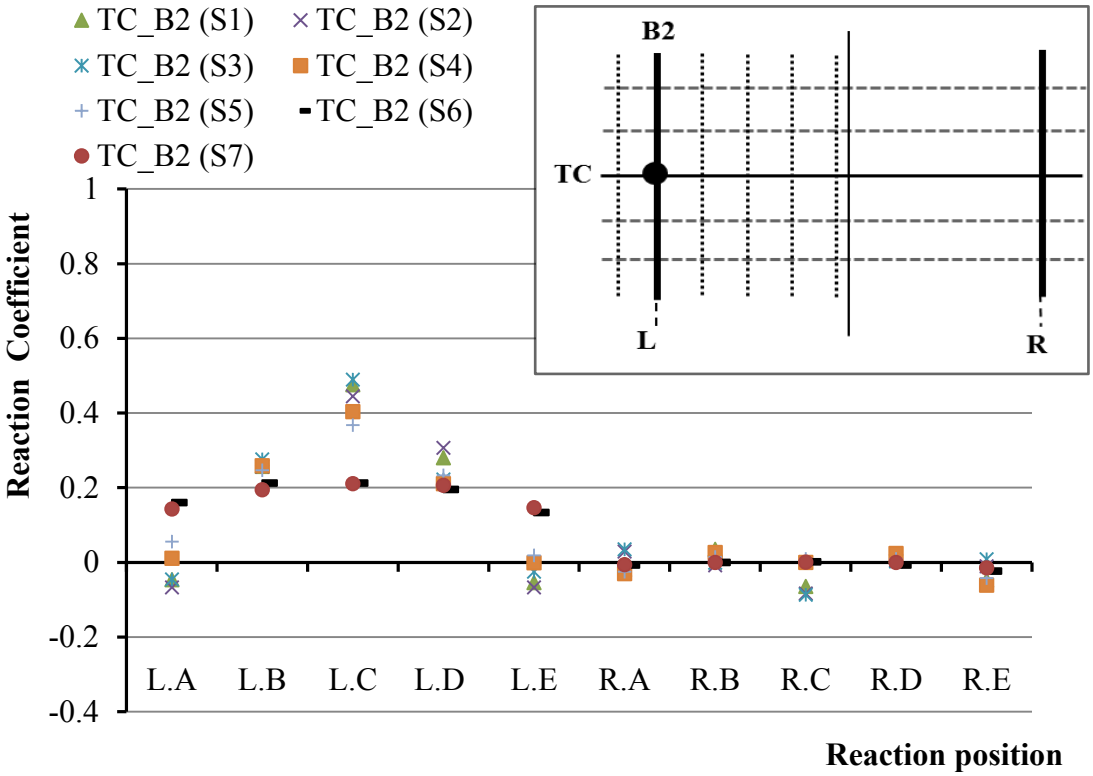

Figure 5.18. VRC, when loading on Battens B2 at Truss C (i.e. TC)

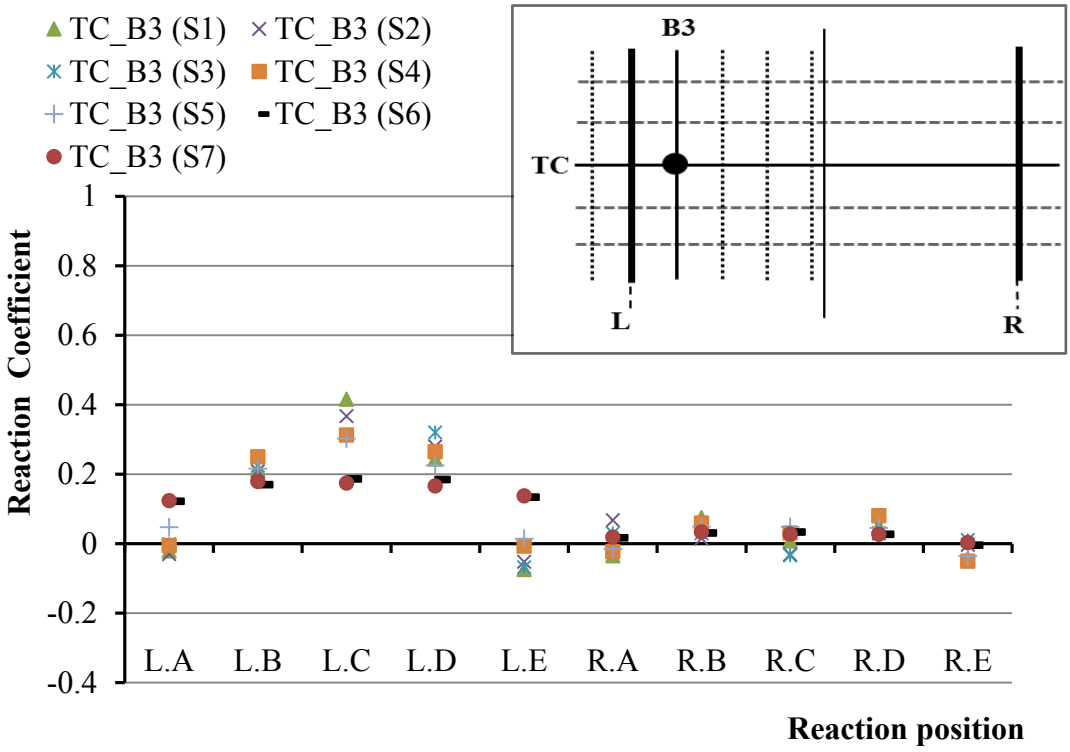

Figure 5.19. VRC, when loading on Battens B3 at Truss C (i.e. TC)

5.3.1.2 RWC flexibility at stages S1 to S7

The measured RWC vertical displacement was divided by the applied load to quantify the flexibility of the connection in mm/kN. Figures 5.20, 5.21 and 5.22 show the flexibility of the RWC on Trusses A and B, and C on the loaded side by considering vertical displacement at each construction stage, and the loading locations on, Battens B1, B2, B3, B4 and B5. These figures show that the maximum displacement was obtained at Stage 1, progressively decreasing when the structural (i.e. S2 and S3) and lining (i.e. S4, S6 and S7) elements were added to the system. This indicates that the vertical movement of the roof structure was reduced by about 80% when lining elements (i.e. wall internal lining, ceiling, cornice) were installed to the timber-framed house. Figures 5.20, 5.21 and 5.22 also show that the vertical displacement was highest when loading along Batten B1 in all stages.

Figure 5.20 shows that the vertical displacements of the RWC of Truss A were high at the Stages S1, S2 and S3 compared to that of Truss B (Figure 5.21). This is because Truss A transferred less load to the adjacent trusses, as shown in Figures 5.11 to 5.13.

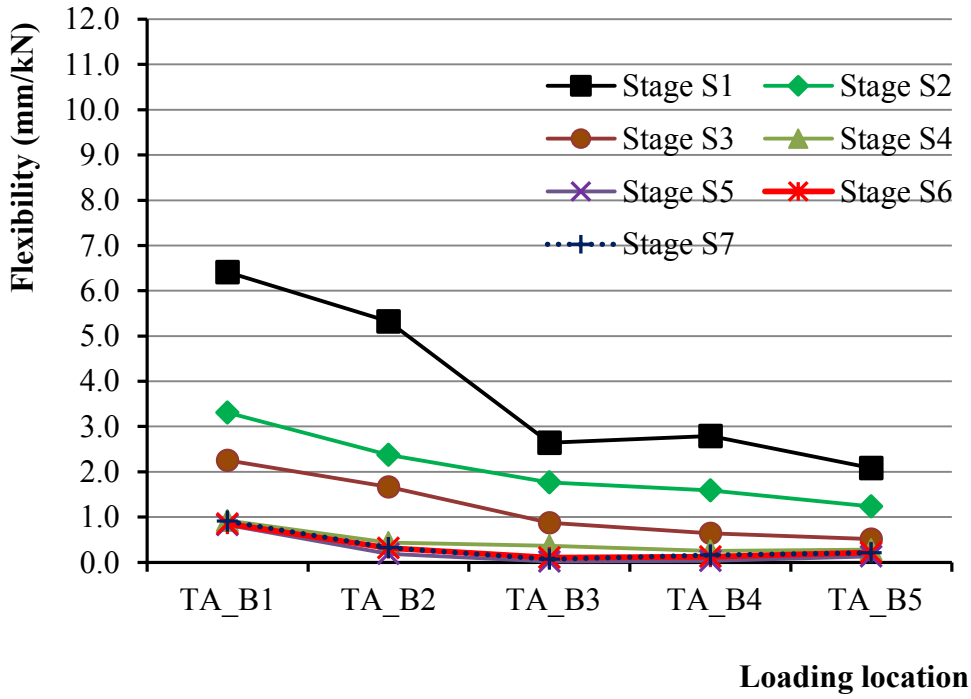

Figure 5.20. RWC vertical displacement variation at Truss A, loaded side support L.A

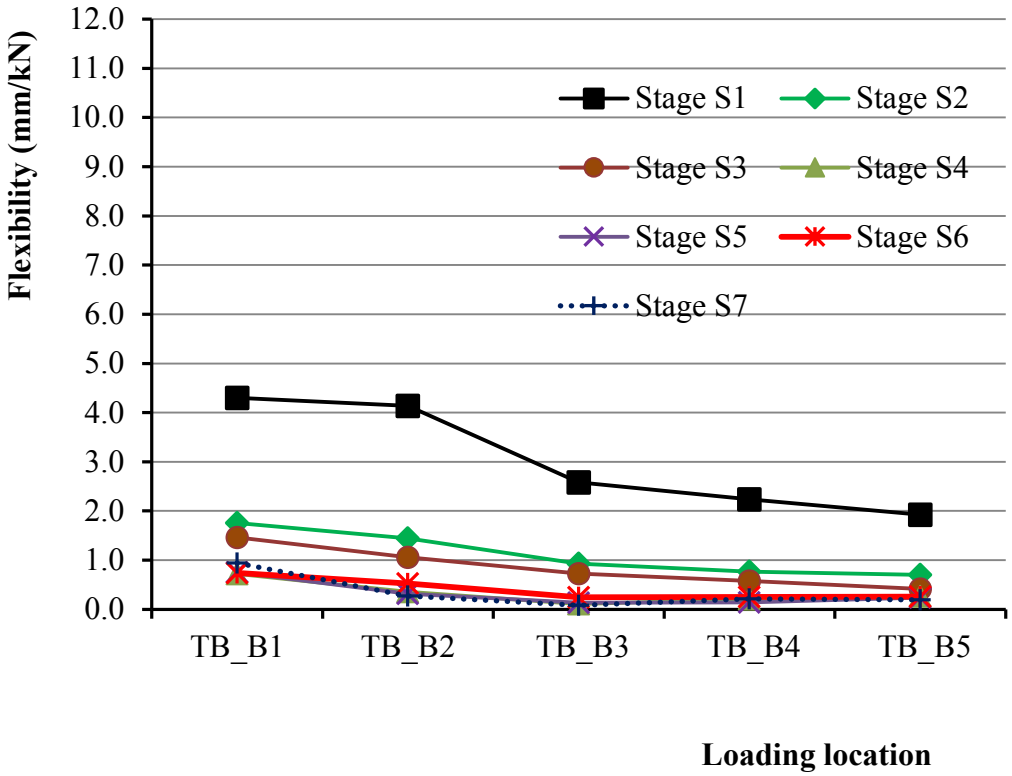

Figure 5.21. RWC vertical displacement variation at Truss B, Loaded side support L.B

The vertical displacements of the RWC of Truss C (Figure 5.22) were high in Stage S1 compared to other trusses (i.e. Truss A and B). This is because the strength of the Truss C roof to wall triple grip connection was lower compared to other trusses (Stage S1 VRC at Batten B2, as shown in Figure 5.18), and Truss C shared more load to the adjacent trusses.

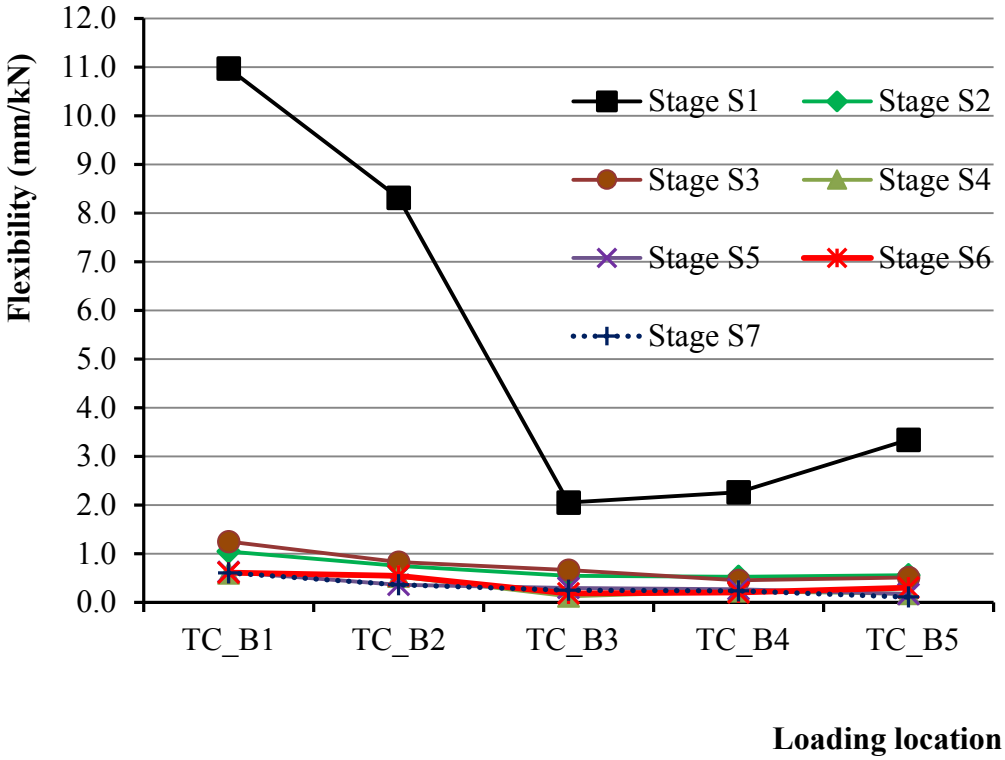

Figure 5.22. RWC vertical displacement variation at Truss C, Loaded side support L.C

5.3.1.3 Stiffness of the RWC when point load was applied to the roof

The resultant loads (i.e. lateral and vertical components of the acting wind loads) on the roof structure are transferred through RWCs to the wall top-plate and surrounding wall structure. Consequently, the RWC must have sufficient capacity to resist and transfer the resultant loads to the wall. In the Stage S1 test, about 90% of the vertical component of the applied load was measured at the loaded truss RWCs, because there was no other element available to share the applied load. Figure 5.23 shows the comparison of the stiffness (i.e. vertical reaction force divided by vertical displacement) variation of the RWC at Trusses A, B and C supports (i.e. L.A, L.B and L.C) when the test load was applied on Battens B1, B2, B3, B4 and B5 of each truss at Stage S1.

Figure 5.23 also shows that the stiffness of the Truss C connection was less than that of the other connections. This was due to the variation of the material (i.e. timber) non-linearity and construction practices and workmanship. This figure also shows the stiffness of the connections were high when loading at Batten B3 on all the trusses. This is because,

the Batten B3 is located between the web member of the truss and the RWC, and this truss web member pushed down on the bottom chord of the truss when load was applied to Batten B3. This action reduced the vertical movement of the RWC, thus the stiffness of the connection was high when loading at Batten B3.

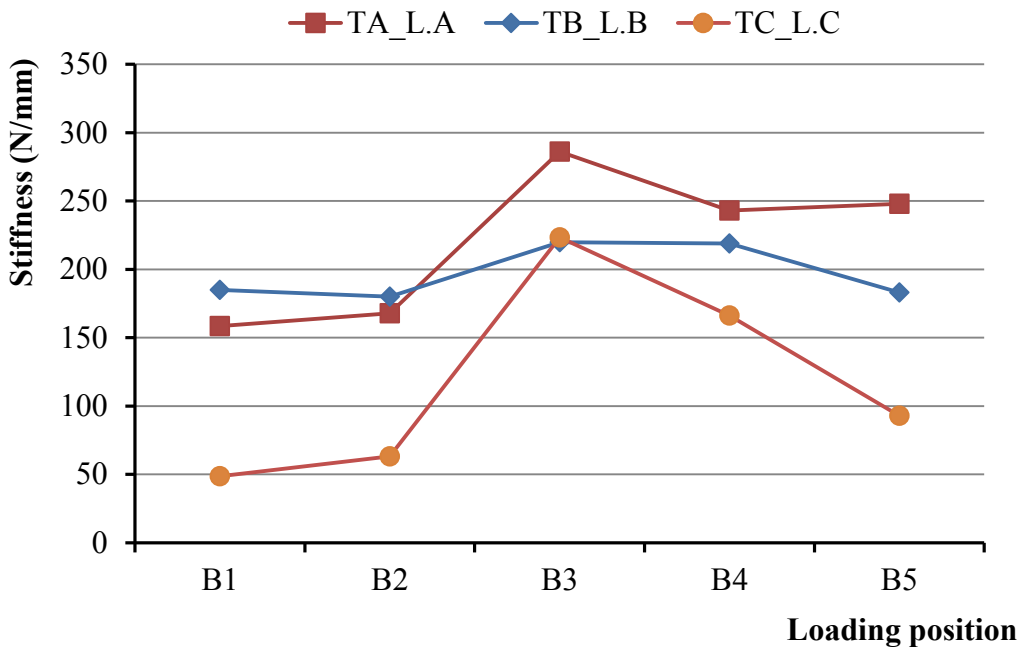

Figure 5.23. RWC stiffness variation at Trusses A (i.e. TA), B (i.e. TB) and C (i.e. TC), supports L.A, L.B and L.C at Stage S1

The vertical reaction force was measured at the top-plates in stages S1, S2, S3 and S4, which represents the RWC reaction force. Yet in stages S5, S6 and S7, the reaction force was measured at the bottom plates, which was not representative of the RWC reaction force. The structural systems were similar in both stages S4 and S5, but the vertical reaction forces were measured at the top-plate in Stage S4 whilst vertical forces were measured at the bottom plate in Stage S5. Moreover, these tests were limited to the elastic limits (i.e. assumed as no significant failure occurred in the structural and lining elements, and their connection). Therefore, to determine the vertical reaction force at the RWC (i.e. at the top-plate) for Stages S6 and S7, the reaction force difference between stages S4 and S5 was added to the measured vertical reaction force of stages S6 and S7.

Based on the vertical reaction force and vertical displacement, the RWC stiffness variation with structural (i.e. S1, S2 and S3) and lining (i.e. S4, S6 and S7) elements was derived and detailed in Table 5.2. This table shows that the lining elements increased the RWC stiffness to twice that of the connection with structural elements only (i.e. battens and roof cladding). This was because in each stage of the full-scale tests, the RWC response behaved differently to loading compared to that of the individual laboratory test. The RWC with lining elements behaved as a more rigid component and resisted the vertical movement and rotation of the connection, and that increased the stiffness of the RWC. Table 5.2 also shows that the ceiling cornice and wall lining did not create any large variation in the RWC stiffness under uplift load. Thus, the contribution of the wall lining and ceiling cornice to the RWC vertical stiffness is negligible.

Table 5.2. RWC stiffness at Trusses A, B and C calculated for the six construction stages (S1, S2, S3, S4, S6, S7)

RWCs stiffness (N/mm)						
Loading position	**Stage S1**	**Stage S2**	**Stage S3**	**Stage S4**	**Stage S6**	**Stage S7**
	Truss A					
Loading at TA_B1	158	246	369	822	771	700
Loading at TA_B2	168	318	490	1944	1933	1775
Loading at TA_B3	286	380	878	1943	5485	13833
	Truss B					
Loading at TB_B1	185	191	313	662	573	446
Loading at TB_B2	180	270	450	1586	941	1759
Loading at TB_B3	220	354	543	4448	1705	5441
	Truss C					
Loading at TC_B1	49	407	503	617	425	420
Loading at TC_B2	63	655	636	767	462	692
Loading at TC_B3	223	742	509	2567	1148	811

5.3.1.4 Load sharing

The point load test results provide a clear indication that the load distribution (Figures 5.11 to 5.19) and hence, the load-sharing characteristics, of a timber-framed structure depends on the inter-component connection stiffness. Figure 5.24 gives the percentages of vertical applied loads that were shared between the adjacent trusses (i.e. Trusses B, C, D and E) when the load was applied at Battens B1, B2, B3, B4 and B5 on Truss A (i.e. TA). This figure shows 10% to 20% of loads were shared to the adjacent trusses at Stage S1, which then increased to 30% to 40% at stages S2, S3, S4 and S5. About 45% to 50% vertical applied loads were shared to the adjacent trusses at stages S6 and S7. This indicates that the lining elements (i.e. ceiling, ceiling cornice and wall lining) increase the load sharing properties (i.e. stiffness, strength, etc.) by about 15% to 20%.

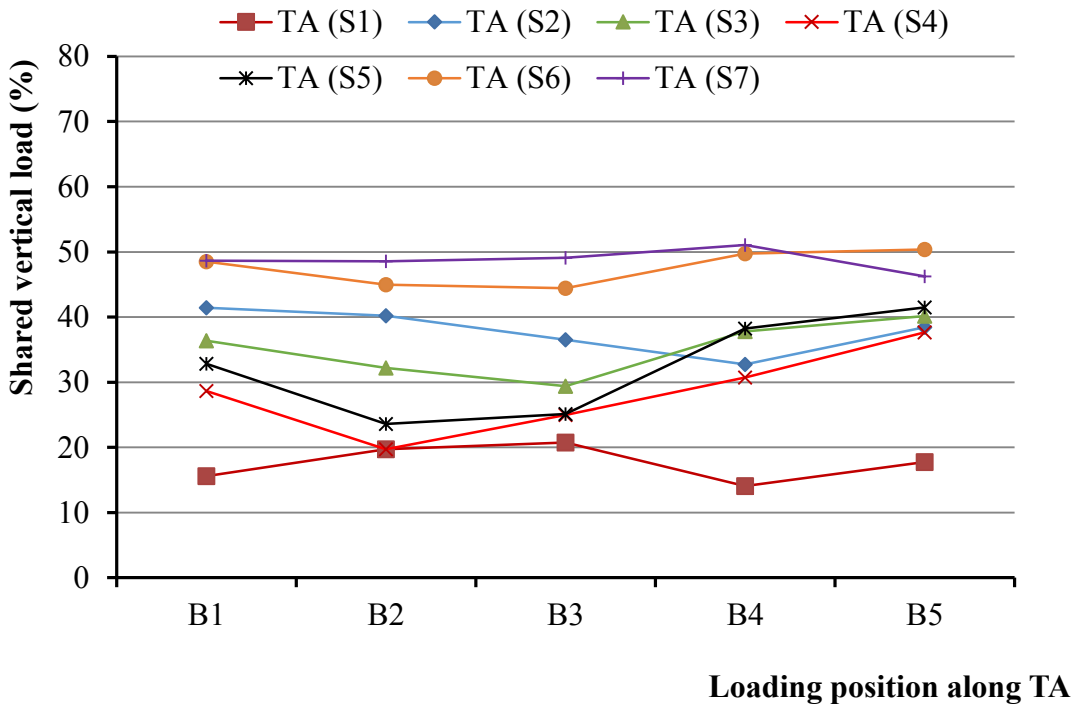

Figure 5.24. Percentage of applied loads were shared to the adjacent trusses when the applied loads were along Truss A (i.e. TA)

Figure 5.25 presents the percentage of applied loads shared by the adjacent Trusses A, C, D and E when loads were applied on Truss B (i.e. TB). About 30% to 45% of the applied vertical loads were shared by the adjacent trusses at Stage S1, which increased to between

55% to 72% at stages S2 and S3. After the ceiling was added to Stage S3 such that the test structure is at Stage S4, the shared load was reduced to between 50% and 55%. The self-weight of the ceiling held down the truss and reduced the vertical displacement of the RWC, eventually increasing the support stiffness; therefore, the percentage of load sharing was reduced at Stage S4. The contribution of lining elements to the load sharing was about 15% to 20% when loading along Truss B, which is similar as when the loads were applied along the Truss A.

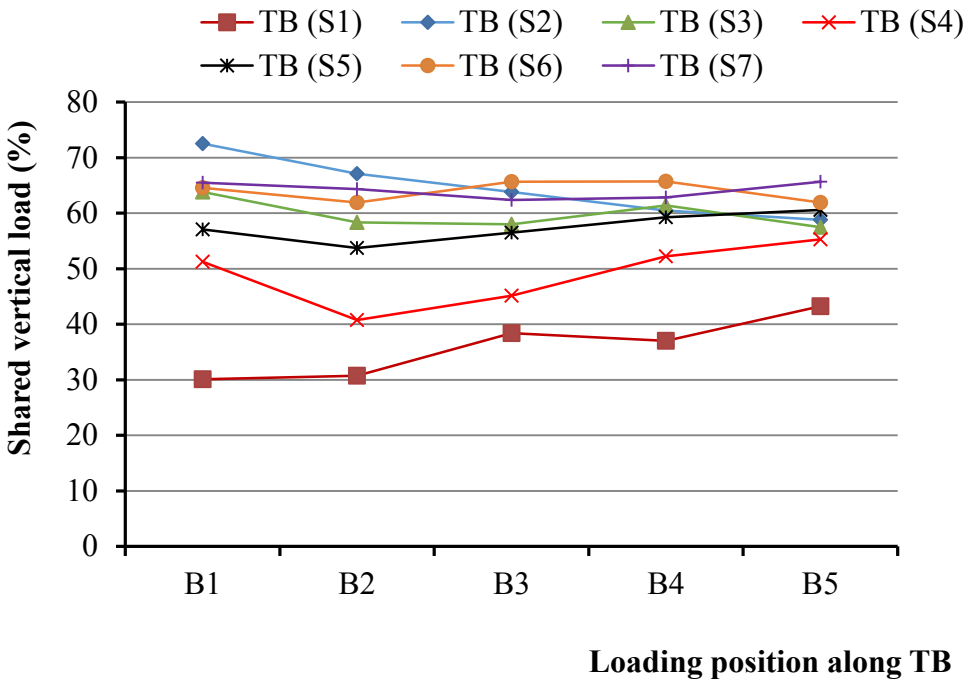

Figure 5.25. Percentage of applied loads were shared to the adjacent trusses when the applied loads were along Truss B (i.e. TB)

Truss C is a middle truss in the full-scale test structure and the applied load was shared in two ways (i.e. shared to Trusses B and A, and Trusses D and E), and also the stiffness of the Truss C, RWC was less than that of the other connections. Therefore, compared to other trusses, a higher percentage of loads were shared to the adjacent trusses in all the stages when loading along Truss C (Figure 5.26).

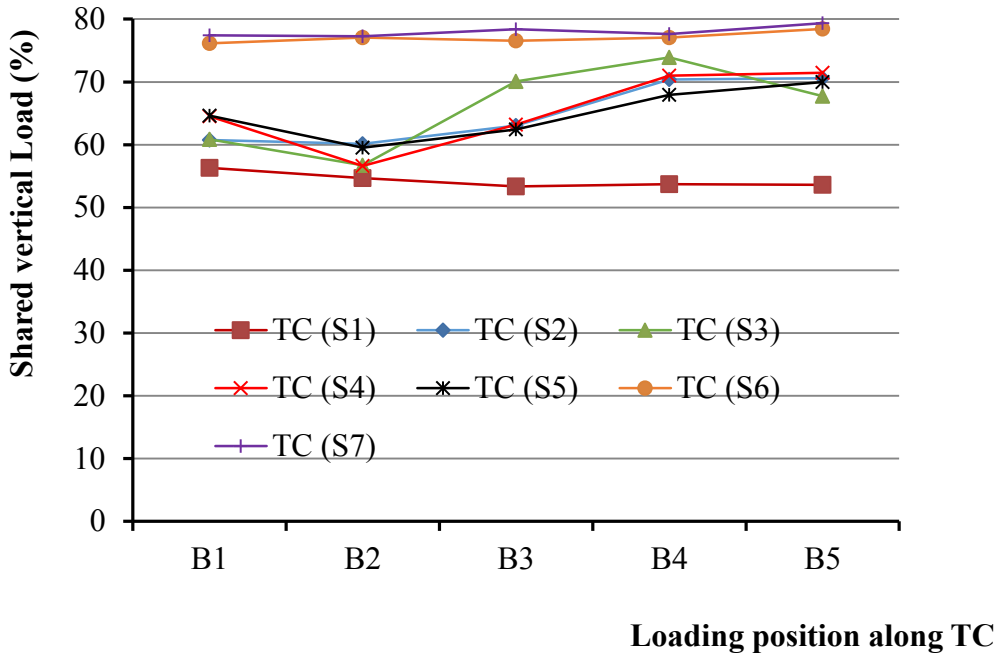

Figure 5.26. Percentage of applied loads were shared to the adjacent trusses when the applied loads were Truss C (i.e. TC)

5.3.2 Influence coefficients

The full-scale test results were used to obtain the influence coefficients that are required to evaluate the wind loads on the roof structural elements (i.e. battens, top-plate, truss and their inter-component connections). Figures 5.27 and 5.28 show the vertical reaction force influence coefficient variation of the Truss B loading side support (i.e. L.B) for all construction stages. Figure 5.27 shows the influence coefficient variation between the construction stages S1 to S4, whilst Figure 5.28 shows the influence coefficient variation between the construction stages S5 to S7. These figures show when compared to other trusses (i.e. Trusses C, D and E), the loading along Truss A significantly influenced the Truss B support reaction. This was because of Truss A's location and the stiffness of the RWC. Truss A was located at the end of the full-scale test structure and its RWC stiffness was less than that of Truss B (Figure 5.23). Thus, a significant portion of load was distributed to the Truss B supports when load was applied along Truss A.

Figures 5.27 and 5.28 also show that the reaction force at the Truss B's supports were influenced by the loading on Trusses C and D, and loading on Truss E had little to no effect on the Truss B support's reaction. This indicates that to evaluate the wind load sharing on a truss supports, the influence of a minimum of two trusses either side of the

targeted truss should be considered, which is similar to the outcome of the Datin et al. (2007) 1/3rd scale model test. However, Datin et al. (2007) study was based on the North American style construction system, wood sheathing was used for the roof and cladding and the load cells were represented as a RWCs. These were the major differences between the full-scale test structure of this study and, Datin et al. (2007)'s study. The stiffness and structural response of the roof to wall triple grip connection are different from that of the load cells (i.e. RWC of the 1/3rd scale model test of Datin et al., 2007), which could generate different influence coefficients. Thus, the influence coefficient obtained in this study can be used to evaluate the wind load sharing and truss hold-down force for the timber-framed house with metal roof cladding.

a) Stage S1: Bare frame

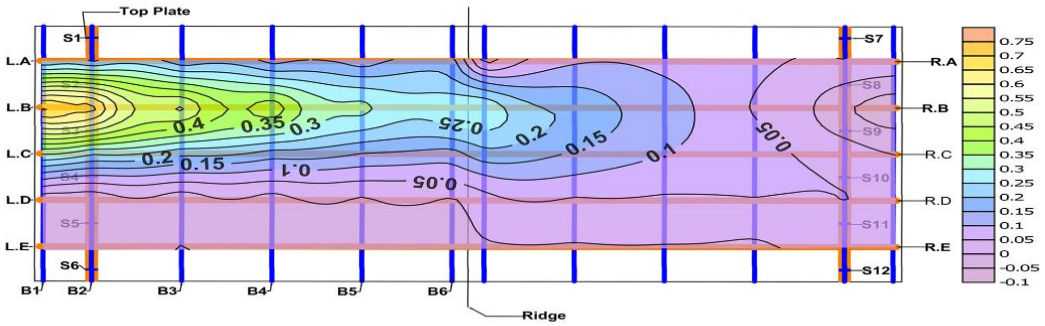

b) Stage S2: Battens installed

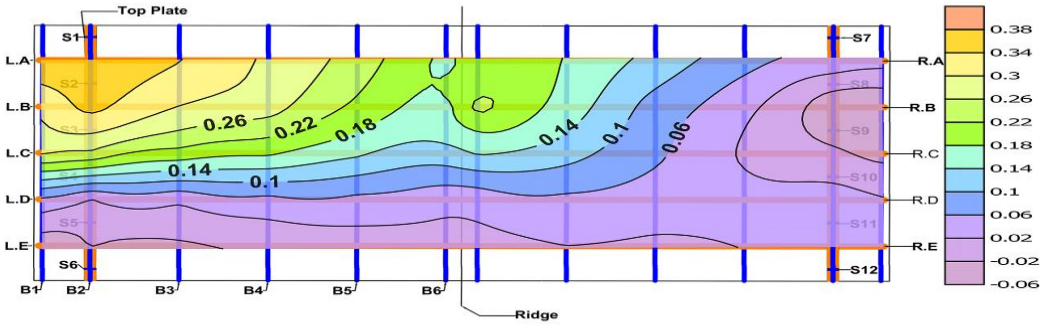

c) Stage S3: Roof cladding installed

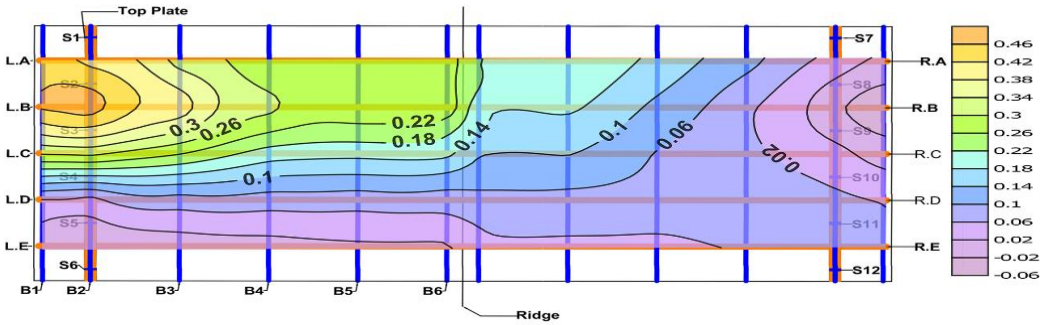

d) Stage S4: Ceiling installed

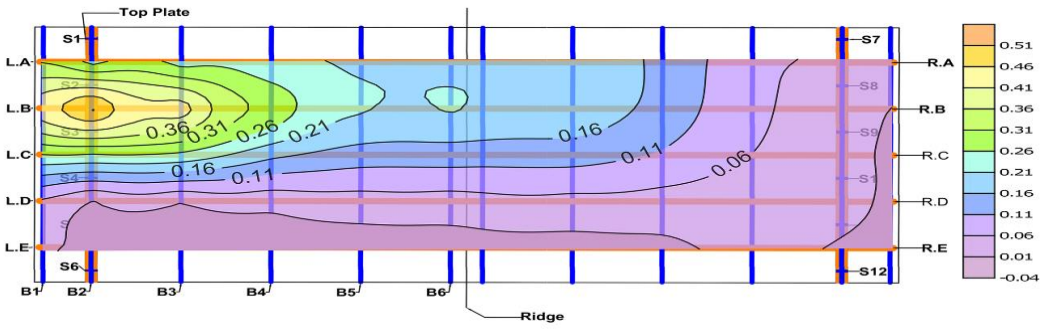

Figure 5.27. Vertical reaction influence coefficient variation of Truss B's loading side support (L.B) between S1 to S4: a) Stage S1; b) Stage S2; c) Stage S3, and d) Stage S4

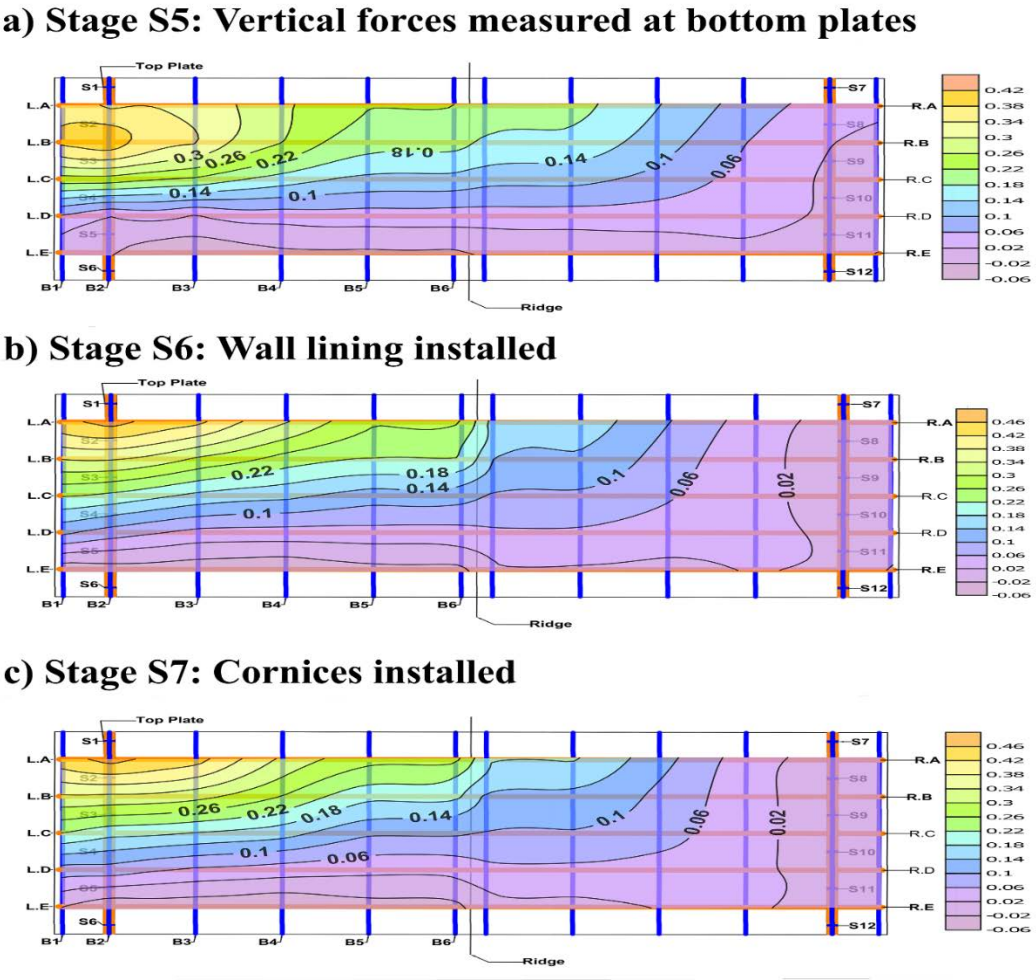

Figure 5.28. Vertical reaction influence coefficient variation of Truss B's loading side support (L.B) between S5 to S7: a) Stage S5; b) Stage S6, and c) Stage S7

5.3.3 Patch-loads on the roof

Patch-loading was applied to the roof at Stage S7, at six different locations P1, P2, P3, P4, P5 and P6, as shown in Figure 5.29. The intention of this test was to compare the structural response with superposition of point load and to validate the numerical model. A load between 2.1 kN to 2.2 kN was applied at the patch-loading locations of the roof using the hydraulic ram (Figure 5.30). The applied load was normal to the roof surface and equally distributed to the four batten to truss connections within the patch.

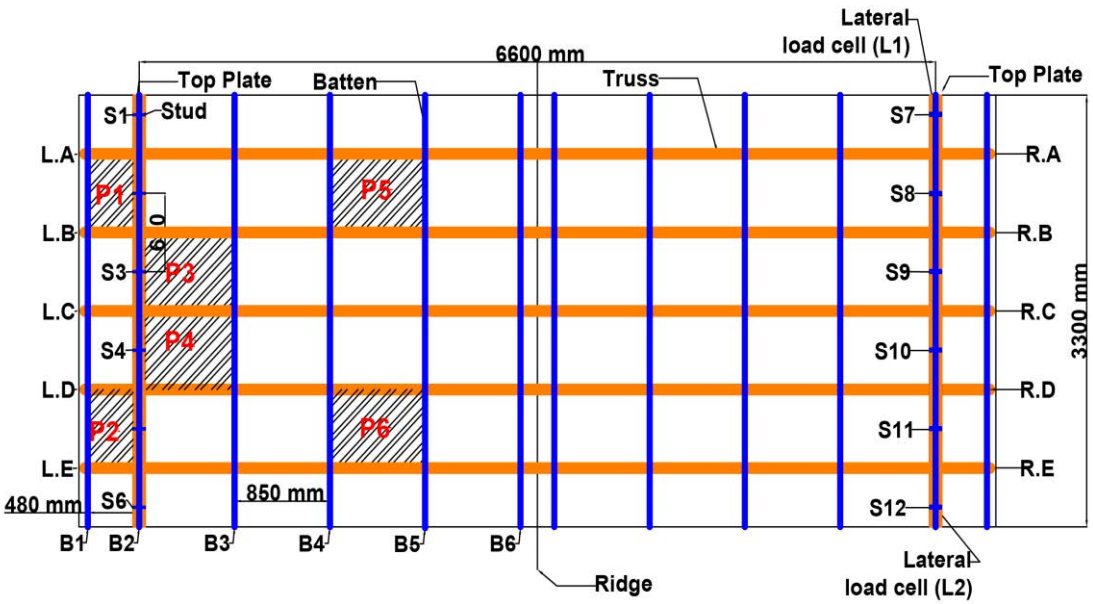

Figure 5.29. Schematic diagram of the patch-load locations

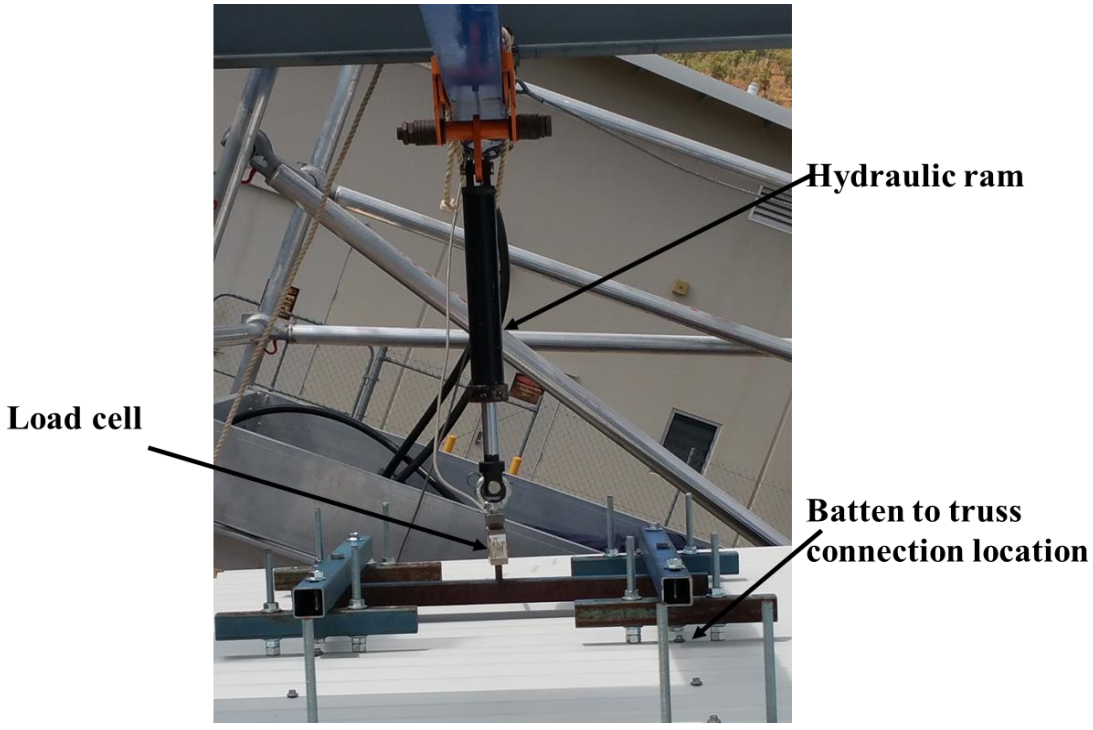

Figure 5.30. Applied loading system for the patch-load test

The vertical reaction forces and displacements were measured and compared with the point load test results of Stage S7. The comparison of the VRCs between the patch-loading test and the reaction coefficients derived using the superposition method of the point load test results are gives in Table 5.3. The comparison of the reaction coefficients showed that the patch-loading test VRCs were about 95% similar to those of the reaction coefficient obtained by using the superposition of point loads. This indicates that the test structural system responded in an elastic range for this applied load (i.e. 2.2 kN). This also indicates that the superposition method can be used to determine the reaction force, if the applied load is in this range.

Table 5.3. Comparison of the VRCs between the patch-load test and calculated from the superposition of point load tests

Test	**Loading locations**	**Reaction coefficients measured locations**									
		L.A	**L.B**	**L.C**	**L.D**	**L.E**	**R.A**	**R.B**	**R.C**	**R.D**	**R.E**
Patch-load	P1	0.4	0.4	0.3	0.0	-0.1	0.0	0.0	0.0	0.0	-0.1
Point load		0.4	0.4	0.2	0.0	-0.1	0.0	0.0	0.0	0.0	0.0
Patch-load	P2	-0.1	0.0	0.2	0.4	0.4	0.0	0.0	0.0	0.0	0.0
Point load		-0.1	0.0	0.2	0.4	0.4	0.0	0.0	0.0	0.0	0.0
Patch-load	P3	0.2	0.3	0.2	0.1	0.0	0.0	0.0	0.0	0.0	0.0
Point load		0.2	0.3	0.2	0.1	0.1	0.0	0.0	0.0	0.0	0.0
Patch-load	P4	0.1	0.1	0.2	0.3	0.2	0.0	0.0	0.0	0.0	0.0
Point load		0.1	0.1	0.2	0.3	0.2	0.0	0.0	0.0	0.0	0.0
Patch-load	P5	0.2	0.3	0.2	0.0	-0.1	0.1	0.1	0.1	0.0	0.0
Point load		0.3	0.3	0.1	0.0	-0.1	0.1	0.1	0.1	0.0	0.0
Patch-load	P6	-0.1	0.0	0.1	0.3	0.3	0.0	0.0	0.1	0.1	0.1
Point load		-0.1	0.0	0.1	0.3	0.3	0.0	0.0	0.1	0.1	0.1

5.3.4 Testing on the full-scale structure with shear walls (Stage S8)

Two, 1.36 m wide shear walls, S.W1 and S.W2, were installed in the Stage S7 test structure at both ends of the wall R.W (Figures 5.31 and 5.32). Point loads were applied on the roof cladding at batten to truss connection locations, as for the Stage S7 test, to evaluate the load sharing and structural response of the structure with shear walls, as well as to assess the contribution of the shear wall to the load sharing. The shear wall stud, top-plate and bottom plate timber member size (i.e. 90 x 35 mm) and grade (MGP10) were the same as for the walls L.W and R.W.

Plasterboard was used as the internal wall lining for the shear walls, and the installation of the plasterboard was the same as for the walls L.W and R.W. In practice, the shear walls are generally connected to the truss, ceiling and ceiling cornice but in this test structure, the shear walls were not connected to the ceiling, ceiling cornice and truss. The omission of this interaction between the shear wall, ceiling, ceiling cornice and truss will affect the load sharing and structural response of the end trusses (i.e. Trusses A and E). However, this test would provide a reasonable prediction of the load sharing and structural response of the other trusses (i.e. Trusses B, C and D).

The shear walls were laterally (i.e. x direction) restrained by the load cells L1 and L2, and vertically (i.e. y direction) supported by the load cells L.V1 and L.V2 at the bottom plate of the shear walls (Figure 5.32). The load cells L1 and L.V1 were located at the bottom plate of shear wall S.W1, whilst load cells L2 and L.V2 were located at the bottom plate of shear wall S.W2. These load cells were used to measure the vertical and lateral reaction at the bottom plates of the shear walls. The vertical reaction forces at the bottom plate of walls L.W and R.W were measured by the same ten vertical load cells located at the walls' bottom plates, as for the previous Stage S7 test. The lateral and vertical displacements of the RWCs and the vertical movement of the top-plates were measured by the same thirty LVDTs located at the same locations as for the Stage S7 test. Additionally, six more LVDTs (i.e. L.X1, L.X2, L.X3, L.X4, L.X5 and L.X6) were used to measure the lateral displacements of the walls' and shear walls' bottom plates and top-plates. The LVDTs L.X1 and L.X2 were located at the shear wall S.W1 top-plate and bottom plate respectively, whilst LVDTs, L.X3 and L.X4 were located at the shear wall S.W2 top-plate and bottom plate respectively. To measure the lateral movements of the wall L.W, the LVDTs L.X5 and L.X6 were located at the top-plate and bottom plate respectively on

the wall L.W. Moreover, two LVDTs, L.Y1 and L.Y2, were located at the bottom plate of the shear walls S.W1 and S.W2 respectively, to measure the shear walls' vertical movement.

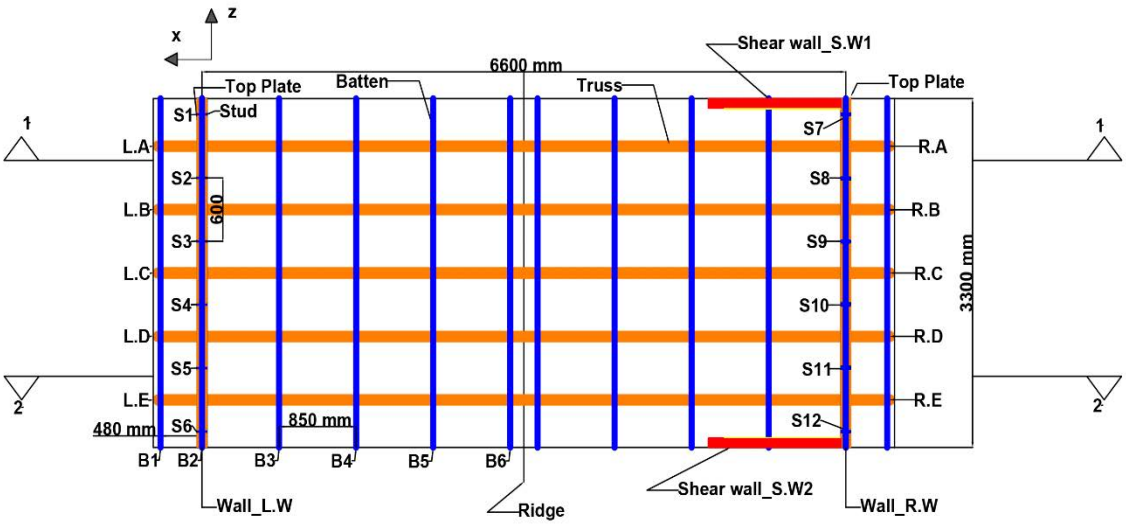

Figure 5.31. Plan view of the test structure after construction of the shear walls (Stage S8)

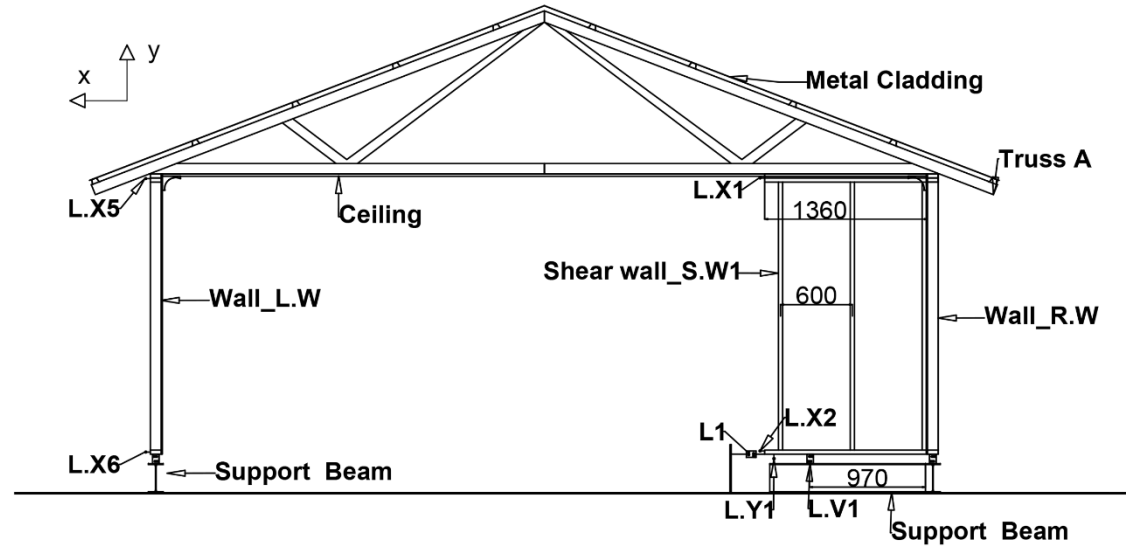

Elevation: Cross section 1-1

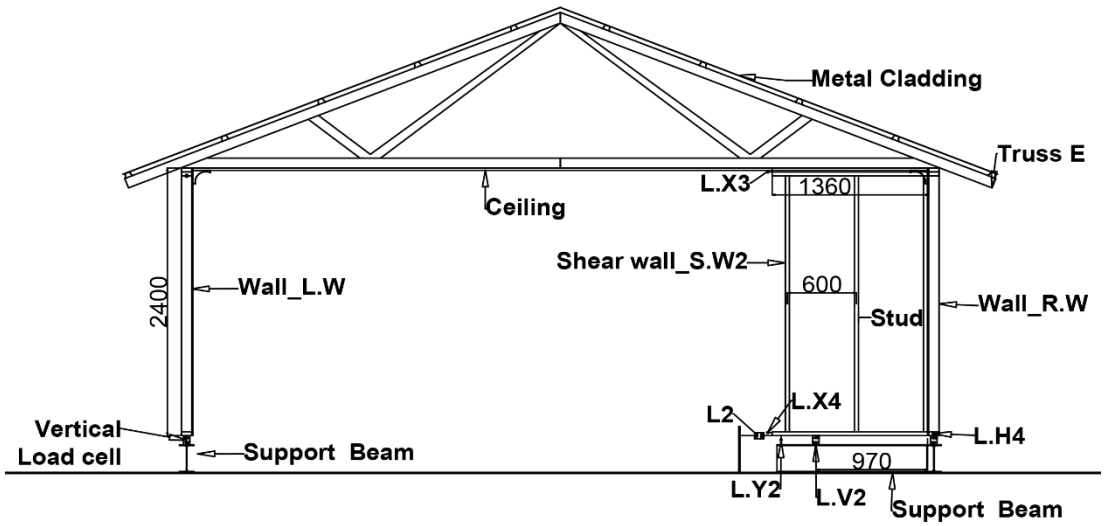

Elevation: Cross section 2-2

Figure 5.32. Elevation of the test structure with shear walls

Two types of tests were carried out with the shear walls in the test structure: (i) Type S.B: the structural system with lateral load cells (i.e. L1 and L2) at the shear wall bottom plate (Figure 5.32); and (ii) Type S.T. In this type, the lateral load cells L1 and L2 were moved to the top-plate of the shear walls S.W1 and S.W2 respectively. The reaction forces and

displacements were compared with Stage S7 test results. Figures 5.33 and 5.34 show the comparisons of the vertical reaction at the bottom plate of the walls and shear walls when load was applied along Batten B1 at Trusses A, B, and C.

Figure 5.33 illustrates the VRCs' changes at the walls' bottom plate supports when load was applied on Batten B1 at Trusses A and B, whilst Figure 5.34 shows the VRCs' variations when load was applied on Batten B1 at Truss C. These figures show that the VRCs of the test Types S.B and S.T at the loaded side wall (i.e. wall L.W) bottom plate supports were similar to Stage S7. The VRCs of test Type S.B at the non-loaded side wall (i.e. wall R.W) bottom plate supports were dissimilar to Stage S7. However, the VRCs of test Type S.T at the non-loaded side wall (i.e. wall R.W) bottom plate supports were similar to Stage S7. In the Type S.B test with the shear wall, the shear wall bottom plate supports (i.e. L.V1 and L.V2) were compressed, creating opposing forces (i.e. tension) at the non-loading side wall bottom plates' supports. This induced action at the non-loaded side bottom plate was the reason for the VRCs variation between the Stage S7 and test Type S.B. Moreover, the total compression force at the shear walls (i.e. S.W1 and S.W2) is equal to the total vertical reaction force variation between the Stage S7 and Type S.B test at the non-loading side wall bottom plate.

The vertical reaction forces at the bottom plates of the shear walls (i.e. S.W1 and S.W2) and wall R.W were reduced by about 75% when the lateral supports of the shear walls moved from the bottom plates (i.e. Type S.B) to the top-plates (i.e. Type S.T). This indicates that if the shear wall was laterally restrained at the top-plate and bottom plates, the vertical resistance at the shear wall will increase by about 75% and the structural stability of the timber framed house will improve.

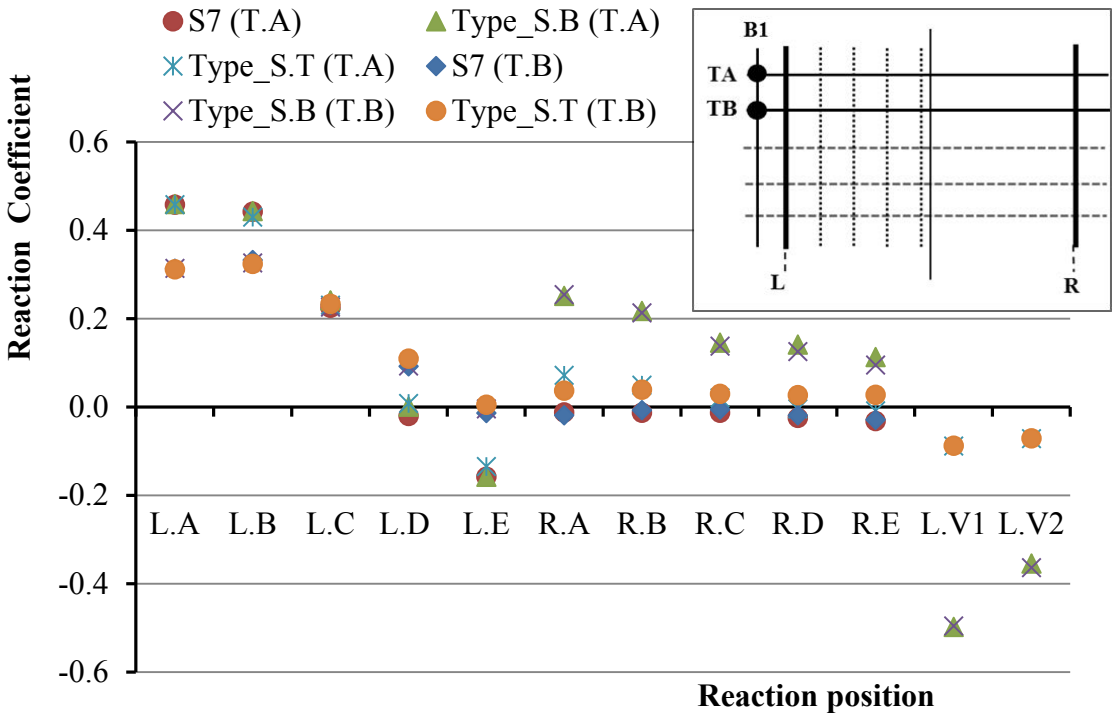

Figure 5.33. VRCs' at the bottom plates of the wall and shear wall when load was applied to Batten B1 at Trusses A (i.e. TA) and B (i.e. TB) at Stage S7 and S8

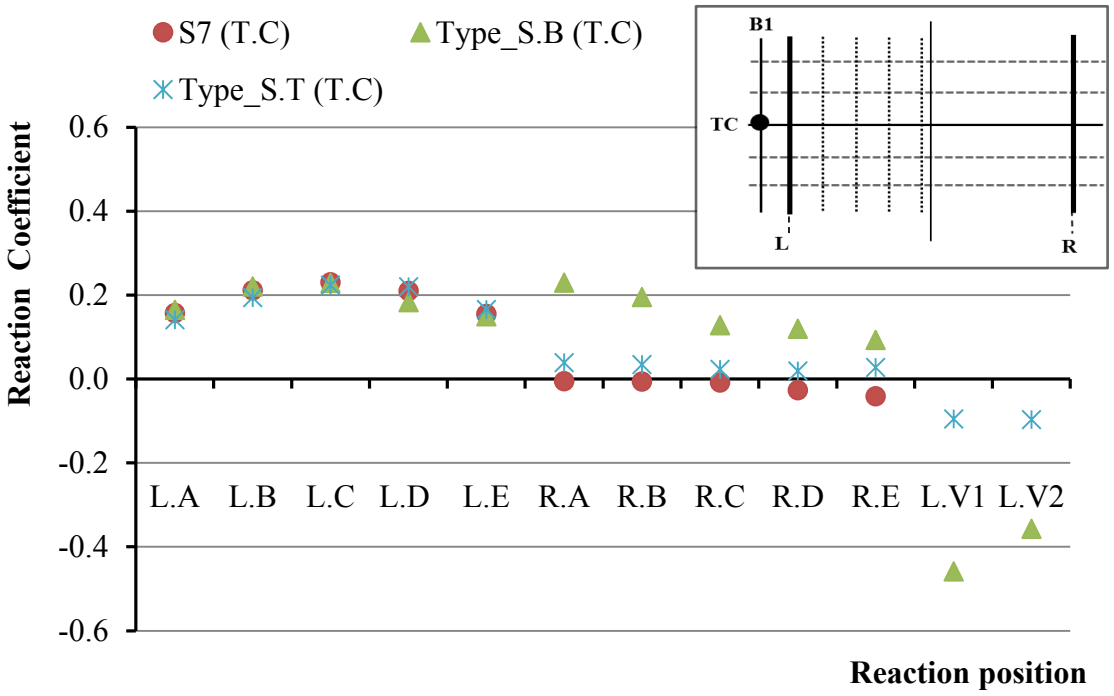

Figure 5.34. VRCs' at the bottom plates of the wall and shear wall when load was applied to Batten B1 at Truss C (i.e. TC) at Stage S7 and S8

Figures 5.35, 5.36 and 5.37 show the comparisons of the flexibility (i.e. displacement divided by the applied load) of the RWCs in the vertical direction between the Stage S7 and Stage S8 tests. Figure 5.35 presents the vertical flexibility of the RWC when load was applied to Batten B1 at Truss A. This figure shows that the vertical displacement of the RWCs was reduced when the shear walls were added to the Stage S7 test structure. The vertical displacement of the loaded truss RWC (i.e. L.A) was reduced by about 25% for the Type S.B test when compared to the Stage S7 test results. When the lateral supports of the shear walls moved from the bottom plate to top-plate (i.e. Type S.T), the vertical RWC displacement at L.A for Type S.B increased by about 10%. This indicates the vertical movement of the RWCs was reduced by about 15% when the shear walls were installed in the timber-framed structure, consequently increasing the vertical stiffness of the RWCs.

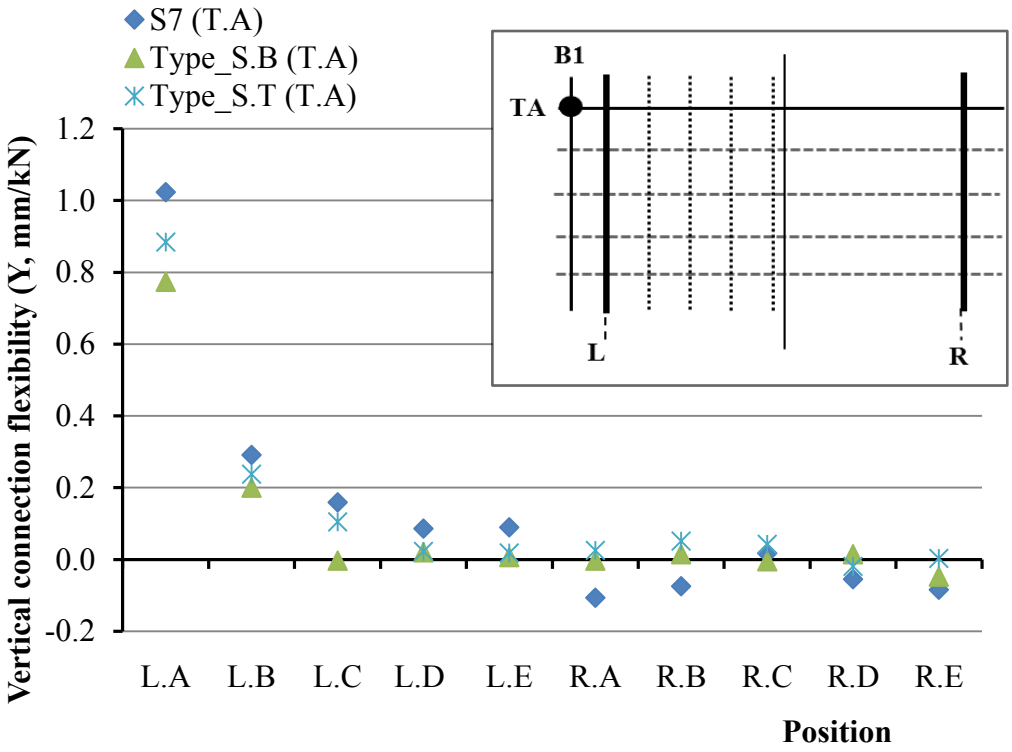

Figure 5.35. Comparison of the vertical flexibility of the RW.C between Stages S7 and S8, when load was applied to Batten B1 at Truss A (i.e. TA)

Figure 5.36 illustrates the vertical flexibility of the RWC when load was applied to Batten B1 at Truss B, whilst Figure 5.37 presents the vertical flexibility of the RWC when load

was applied to Batten B1 at Truss C. These figures show that the vertical displacements of the RWCs were reduced by about 25% when the shear walls were installed in the test structure. This indicates that the shear wall increased the vertical strength and stiffness of the RWC (i.e. includes the ceiling, truss, top-plate and cornice) by reducing the vertical movement of the roof. The increased strength and stiffness will reduce the structural vulnerability of houses to windstorms.

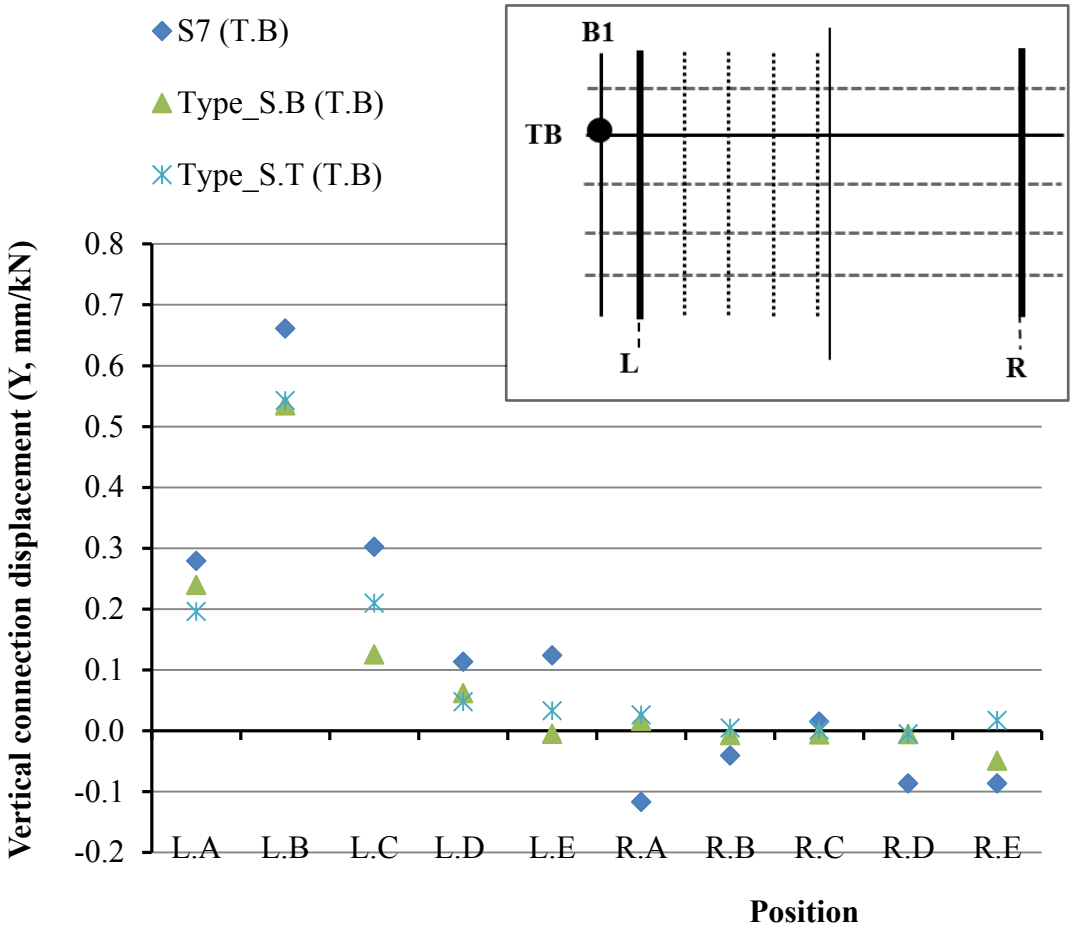

Figure 5.36. Comparison of the vertical flexibility of the RWC between Stages S7 and S8, when load was applied to Batten B1 at Truss B (i.e. TB)

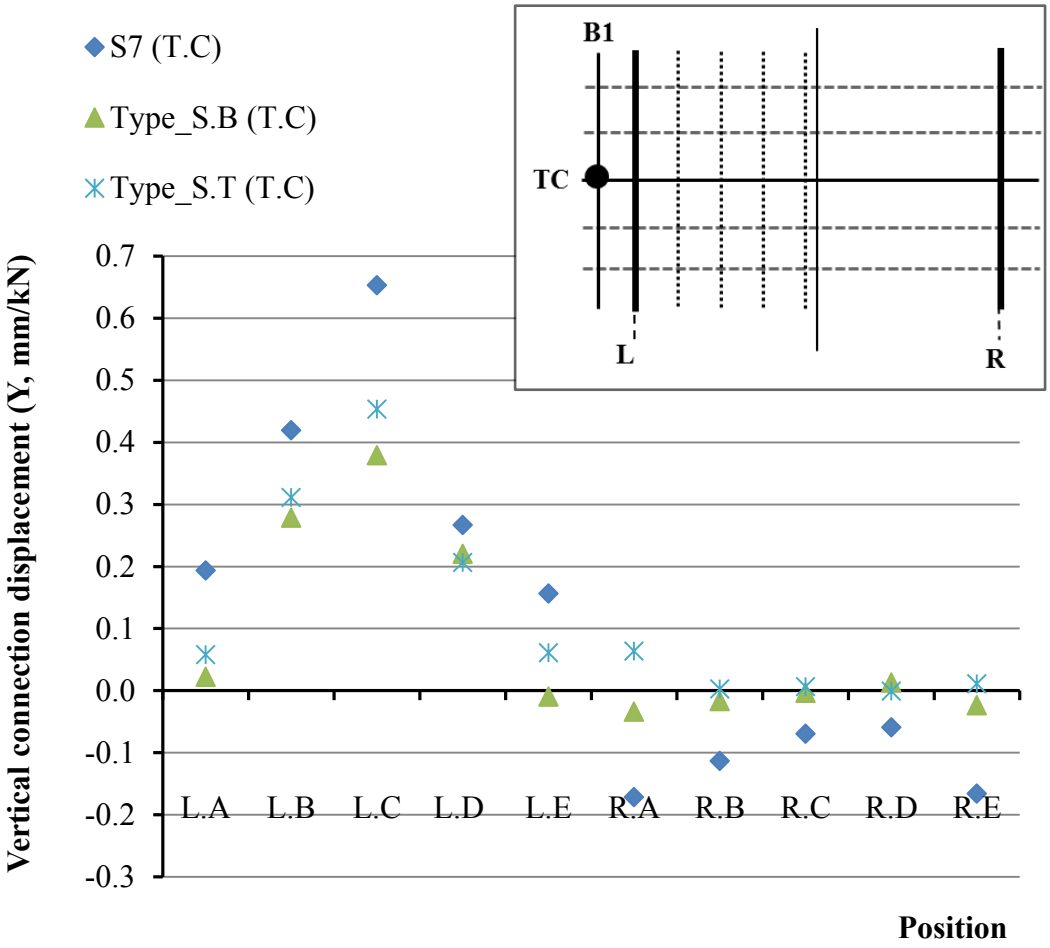

Figure 5.37. Comparison of the vertical flexibility of the RWC between Stages S7 and S8, when load was applied to Batten B1 at Truss C (i.e. TC)

The total lateral load measured by the lateral load cells (i.e. L1 and L2) divided by the applied load is presented as the reaction coefficient in Figure 5.38. This figure shows the comparison of the lateral reaction coefficient variation between Stage S7 and Types S.B and S.T tests when load was applied on Batten B1. Figure 5.38 illustrates that the total lateral load was reduced by about 30% to 35% when shear walls were added to the Stage S7 test structure (i.e. Types S.B and S.T).

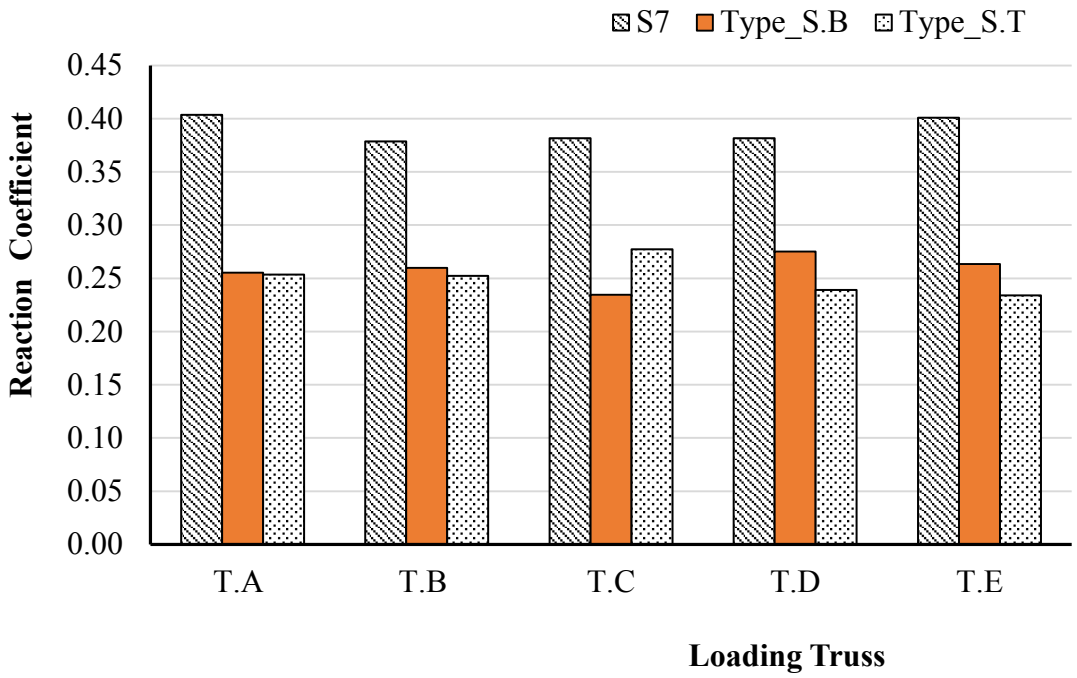

Figure 5.38. Comparison of the total lateral reaction force variation between Stage S7 and Stage S8 Types S.B and S.T tests, when load was applied to Batten B1

The lateral flexibility (i.e. lateral displacement divided by the applied load) of the wall (i.e. wall L.W) and the shear walls' (i.e. S.W1 and S.W2) bottom plates and top-plates was calculated and compared between the Stage S7 and Types S.B and S.T tests. The comparison of the lateral flexibility of the bottom plate and the top-plate of the shear walls and wall, when load was applied along Batten B1 at Trusses A and B is presented in Figure 5.39. This figure shows that the lateral movement of the wall and shear walls' bottom plate was small, varying between 0.05 mm to 0.15 mm. The output signals in the measuring devices and the DAQ system may also be effected by noise, a possible reason for the lateral LVDTs located at the bottom plate showing some movement. Figure 5.39 also shows that the lateral movement of the wall L.W top-plate (i.e. L.X5) at Stage S7 was reduced by about by 75% when the shear walls were added and laterally supported at the bottom plate (i.e. Type S.B). The lateral movement of the wall L.W top-plate was reduced by 85% when the lateral supports moved to the top-plate. This shows that the installation of the shear wall on the house significantly increased the lateral stiffness and strength of the house by about 75%.

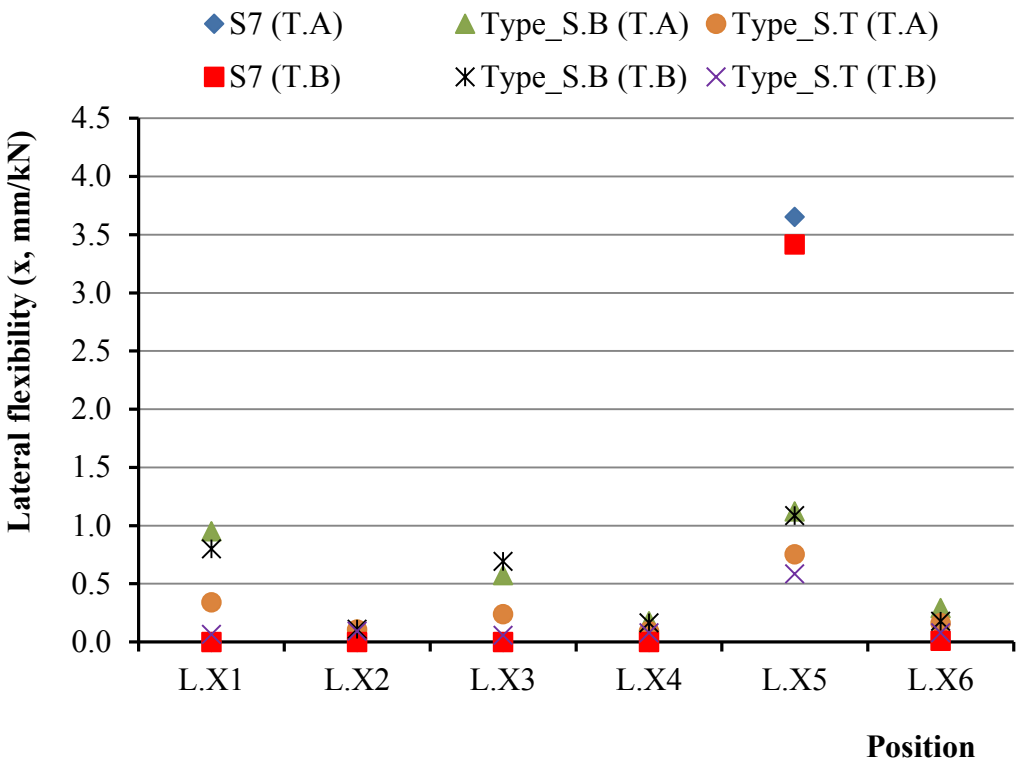

Figure 5.39. Comparison of the lateral flexibility of the wall and shear walls' bottom plate and top-plate between Stage S7 and Stage S8's Types S.B and S.T, when load was applied to Batten B1 at Trusses A (i.e. TA) and B (i.e. TB)

Figure 5.40 shows the comparison of the lateral flexibility of the wall and shear wall bottom plate and top-plate between Stage S7 and Stage S8's Types S.B and S.T, when load was applied to Batten B1 at Truss C. This figure shows when the shear wall's lateral support moved from the bottom plate to the top-plate, the top-plate movements (i.e. L.X1 and L.X3) at Type S.B were reduced by about 80% and the bottom plate movements (i.e. L.X2 and L.X4) were approximately similar for both type (i.e. Types S.B and S.T) tests. This indicates that the lateral movement of the timber-framed structure will significantly reduce, when the shear walls top-plates are laterally restrained.

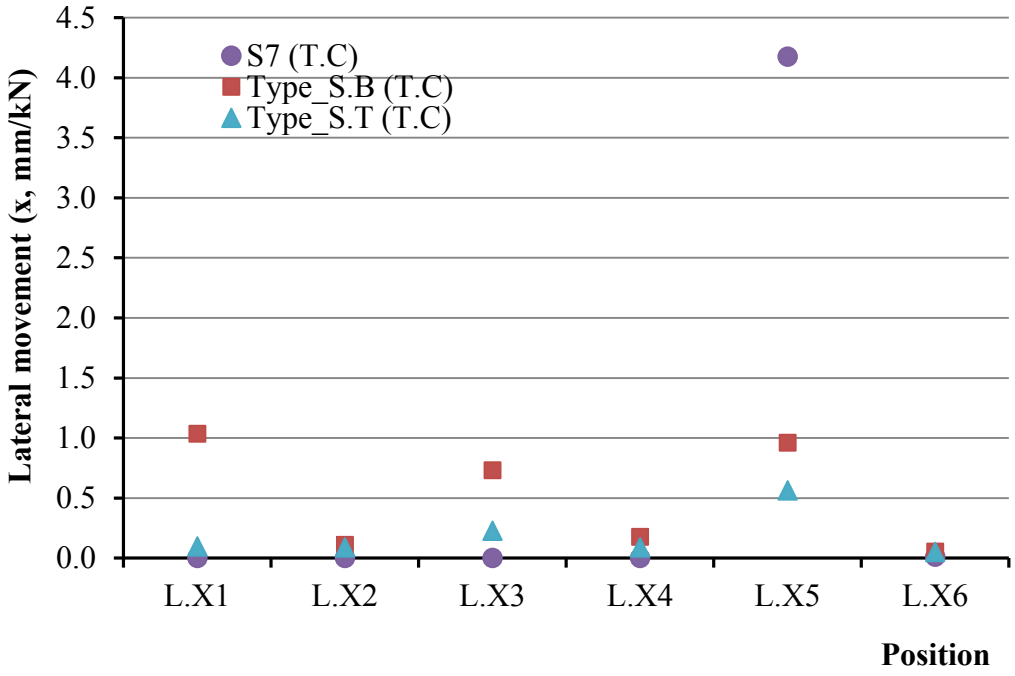

Figure 5.40. Comparison of the lateral flexibility of the wall and shear walls bottom plate and top-plate between Stage S7, and Types S.B and S.T, when load was applied to Batten B1 at Truss C (i.e. TC)

5.3.5 Line loading on the test structure

A line load was applied on the roof at Stage S8's Type S.B test setup. The load was applied on the roof cladding at batten to truss connections along Truss C, normal to the roof surface (Figure 5.41). The objective of this test was to evaluate the behaviour of the structure, where the load was applied to the roof until failure and or beyond the first yielding of connections or members. The results could be used to evaluate the ultimate strength and stiffness of the RWC and structural system, as well as validate the numerical model. The test was stopped before reaching the ultimate load, due to the top of the wall L.W internal lining deflecting close to the LVDTs' stand. Therefore, the test was stopped at applied load 5.9 kN. The reaction forces and the displacements were measured at the same locations as for Type S.B test.

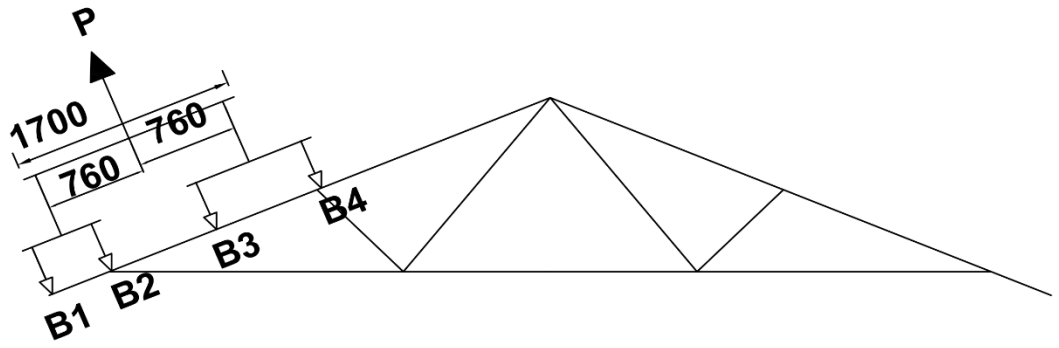

Figure 5.41. Schematic diagram of loading systems for line load test

The vertical reaction forces of Type SB test when load was applied on Battens B1, B2, B3 and B4 along Truss C were used with superposition method (SPM) to compare the vertical reaction forces of line load test. Table 5.4 shows the vertical reaction forces different (i.e. vertical reaction force different between the SPM and line load test divided by the line load test vertical reaction force) between the Type SB and line load tests, and showed that the measured vertical reaction forces and the calculated vertical reaction forces by SPM were approximately similar. However, there was about 8% variation between the measured and calculated vertical reaction forces, until the applied load reached to 2.75 kN, then it increased to 16% when the applied load was 5.93 kN. These VRCs variations could be due to local failures, observed during the line load test. These local failure occurred at the ceiling joint fasteners and adhesive; hair-line crack was observed at the adhesive between the ceiling cornice and wall lining; there was a partial withdraw of nails in the RWC connection, and deformation on the triple grip framing anchor.

Table 5.4. Comparison of vertical reaction force difference between the line load Test and SPM when load was applied along the Truss C at Battens B1, B2, B3 and B4

Applied load (kN)	Vertical reaction force different between SPM and Test (%)									
	L.A	L.B	L.C	L.D	L.E	R.A	R.B	R.C	R.D	R.E
0.75	-2	-2	0	7	3	0	5	8	8	5
1.75	0	-1	0	8	7	-2	1	7	7	8
2.75	-2	1	-1	7	-8	-8	0	7	8	8
3.75	1	1	-2	6	13	-14	0	9	5	10
4.50	8	-4	-4	-3	14	-12	-8	13	2	11
4.75	10	-5	-7	-4	15	-9	-12	11	3	11
5.00	11	-7	-11	0	16	-7	-12	8	0	14
5.25	12	-8	-15	1	15	-8	-13	7	2	15
5.50	13	-8	-15	3	16	-7	-12	5	1	16
5.76	14	-11	-16	6	16	-1	-9	-10	-7	15
5.93	15	-11	-16	7	15	-2	-10	-10	-7	16

The applied load versus vertical and lateral displacement of the loaded and non-loaded side RWCs' of Truss C are shown in Figures 5.42 and 5.43 respectively. The vertical displacement versus applied load of the loading side wall RWC of Truss C (i.e. L.C) shows that the maximum vertical stiffness of the loading side RWC was 2500 N/mm at applied load 1.9 kN (Figure 5.42). The vertical stiffness of the RWC was then reduced to about 1500 N/mm at applied load 3 kN and the trend follows linearly up to applied load 5.93 kN (Figure 5.42). This vertical stiffness reduction of the loading side RWC was due to local failures of the Truss C, RWC and ceiling glue and screw joint failure adjacent to the Truss C loading side support. Figure 5.42 also shows the vertical displacement versus applied load of the non-loading side RWC of Truss C (i.e. R.C), with the vertical stiffness at about 250 kN/mm and the trend linear. This Figure 5.42 also shows that when the applied load reached between 2 kN to 3 kN, the vertical stiffness of the RWC were reduced by about 45% compared to initial stiffness of connections. This indicates when the wind uplift load on a single truss higher than 3 kN, the vulnerability of that RWC will significantly increase.

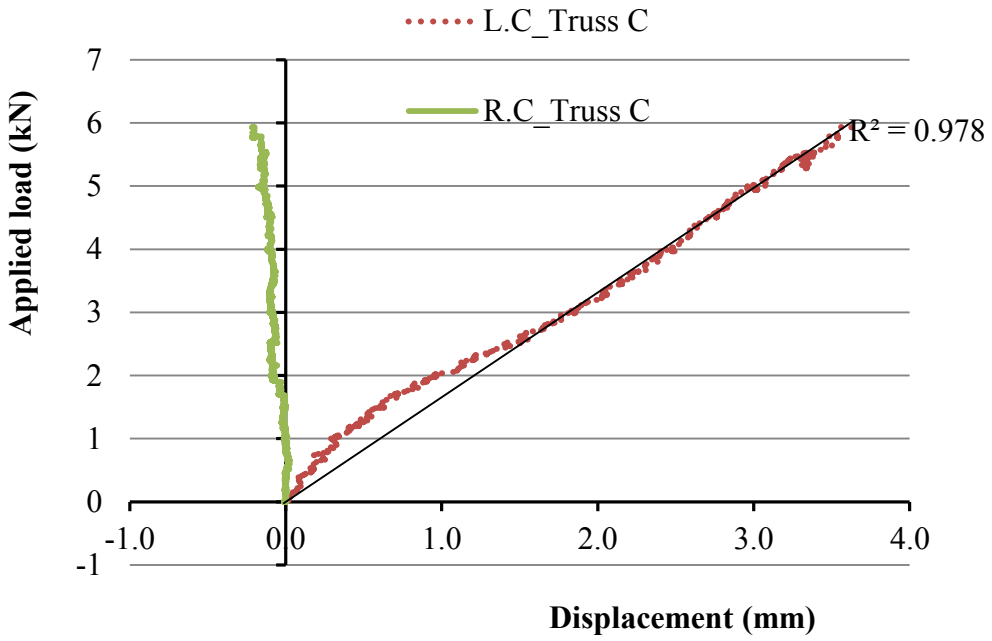

Figure 5.42. Applied load versus vertical displacement of RWCs at Truss C (i.e. L.C and R.C)

Figure 5.43 shows the lateral displacement versus applied load of the loaded and non-loaded side RWCs' of Truss C. This figure shows that the lateral stiffness of the loading and non-loading side RWC of Truss C were similar (13 kN/mm) up to applied load 2.3 kN. The lateral stiffness of the loading side RWC (i.e. L.C) was then reduced to about 4.5 kN/mm, and the trend linear up to 5.93 kN, whilst the non-loading side RWC (i.e. R.C) remained at the same stiffness as applied load 2.3 kN and followed a linear trend. This indicates that the lateral strength and stiffness of the RWC were reduced by about 65% when applied load reached above 3 kN. Figures 5.42 and 5.43 indicate if the wind load on the single truss was above 3 kN, the lateral strength of the RWC will be reduced by about 40% to 60% due to the local failure (i.e. partial withdrawal of fasteners).

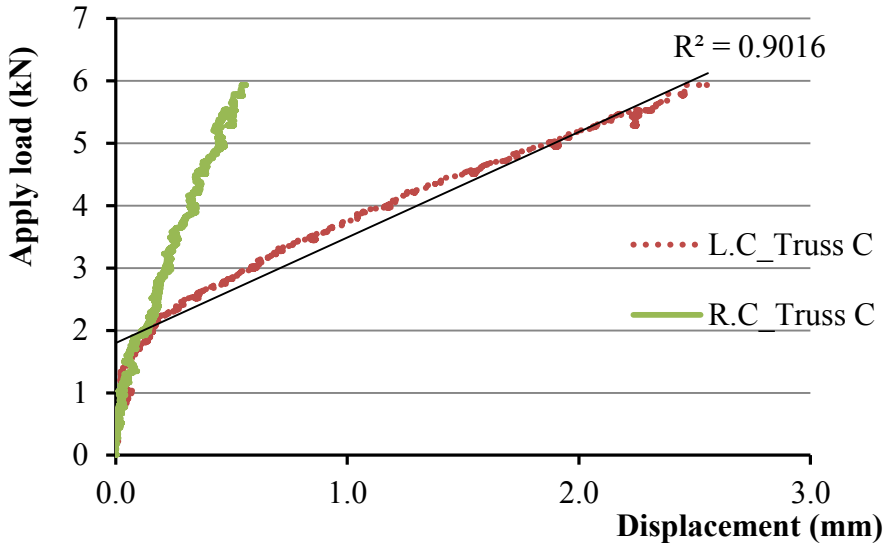

Figure 5.43. Lateral displacement of RWC versus applied load at Truss C (i.e. L.C and R.C)

5.3.5.1 Local failures observed in the line load test

During the line load test, failures at the roof to wall triple grip connections, ceiling glue and screw joints, and hair-line cracks at the cornice were observed. Figures 5.44 and 5.45 show the roof to wall triple grip connection failure of the Truss C loading and non-loading side supports respectively. These figures show that the RWCs on loading and non-loading sides have partial withdrawal of nails, nail bending and triple grip bending. These types of failures were also observed in all other RWCs of the full-scale test structure and individual joint test (Chapter 4). However, the size and shape of the nail and triple grip deformation, and nail pull-out varied at each triple grip connection and it also varied between the loading and non-loading side connections.

A double curvature bending was observed at the nails located on the top-plate side surface at non-loading side RWCs (Figure 5.45), which was not observed in the loading side RWCs. This was because of the combination of the lateral and vertical movement of the roof structure, which causes the roof structure to move towards the loading side. This lateral movement created bending on the triple grip framing anchors located at the loading side towards the loading direction but it does not bend the triple grip at the non-loading

side. This is because the lateral movement of the non-loading side triple grip was resisted by the top-plate. This lateral resistance created prying force on the non-loading side RWC and their fasteners. The combination of the vertical movement and prying force on the non-loading side RWC created the double curvature bending on the nails located at the top-plate side surface. This failure modes of the triple grip connection indicates that this connection does not behave as a pinned joint but it remains a right angle connection and act as a moment resisting connection. A consequence of this is that each truss and supporting walls behave in part like a flexible portal frame. This behaviour creates the secondary moments on the triple grip connection and enabling some of the horizontal component of the applied load to be transmitted directly to the bottom plate.

Partial withdrawal of nails on the top-plate top surface shows that these nails experienced tension load. The nails on the trusses experienced a combination of the shear and tension load as they showed nail bending and partial withdrawal. The failure modes different between the loading and non-loading side RWCs indicates that the structural response of the RWC will be different when the windward side or leeward side wind loads higher than the each other during the windstorm.

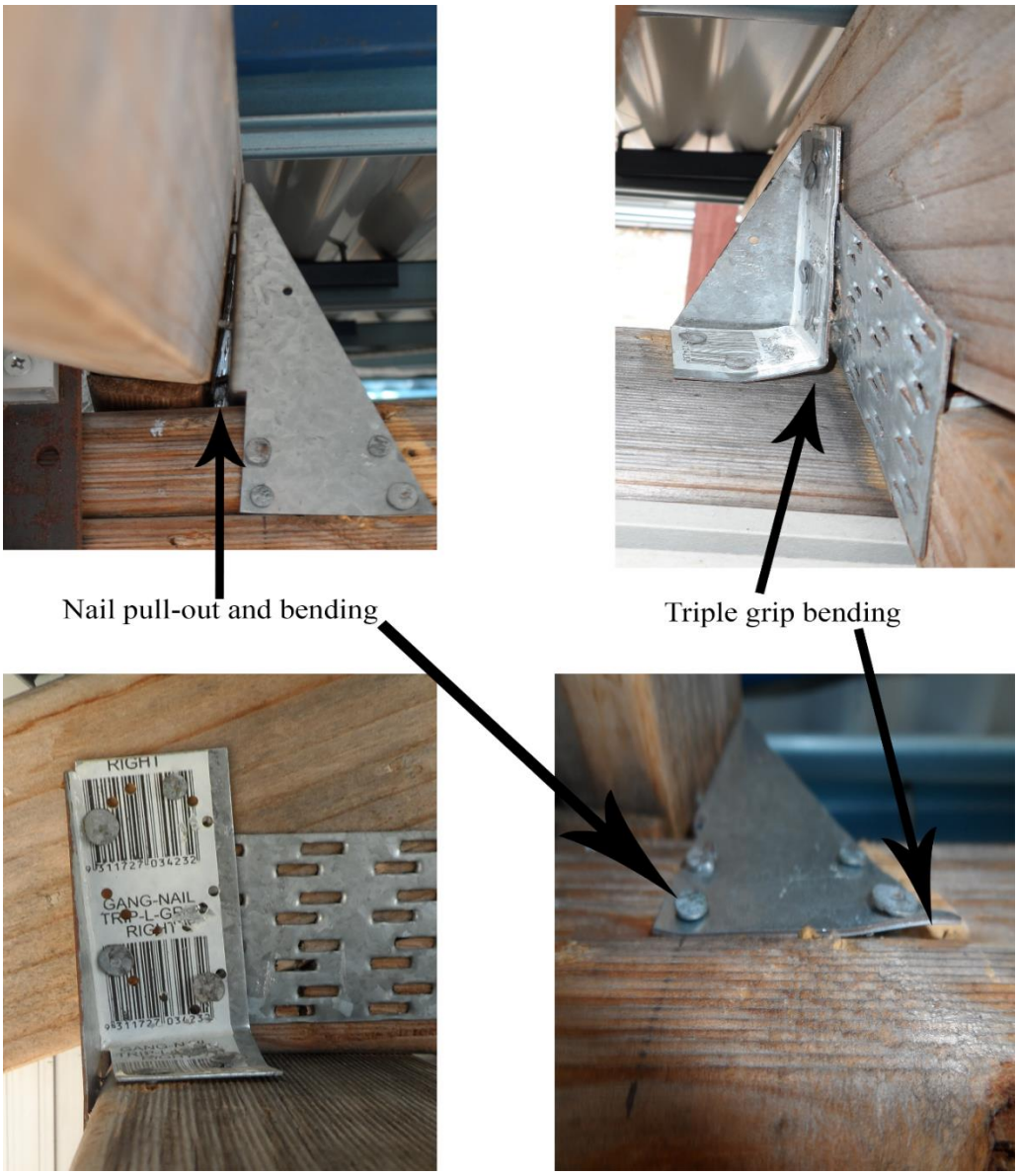

Figure 5.44. The failure modes of the roof to wall triple grip connection of Truss C, at loading side during line load test

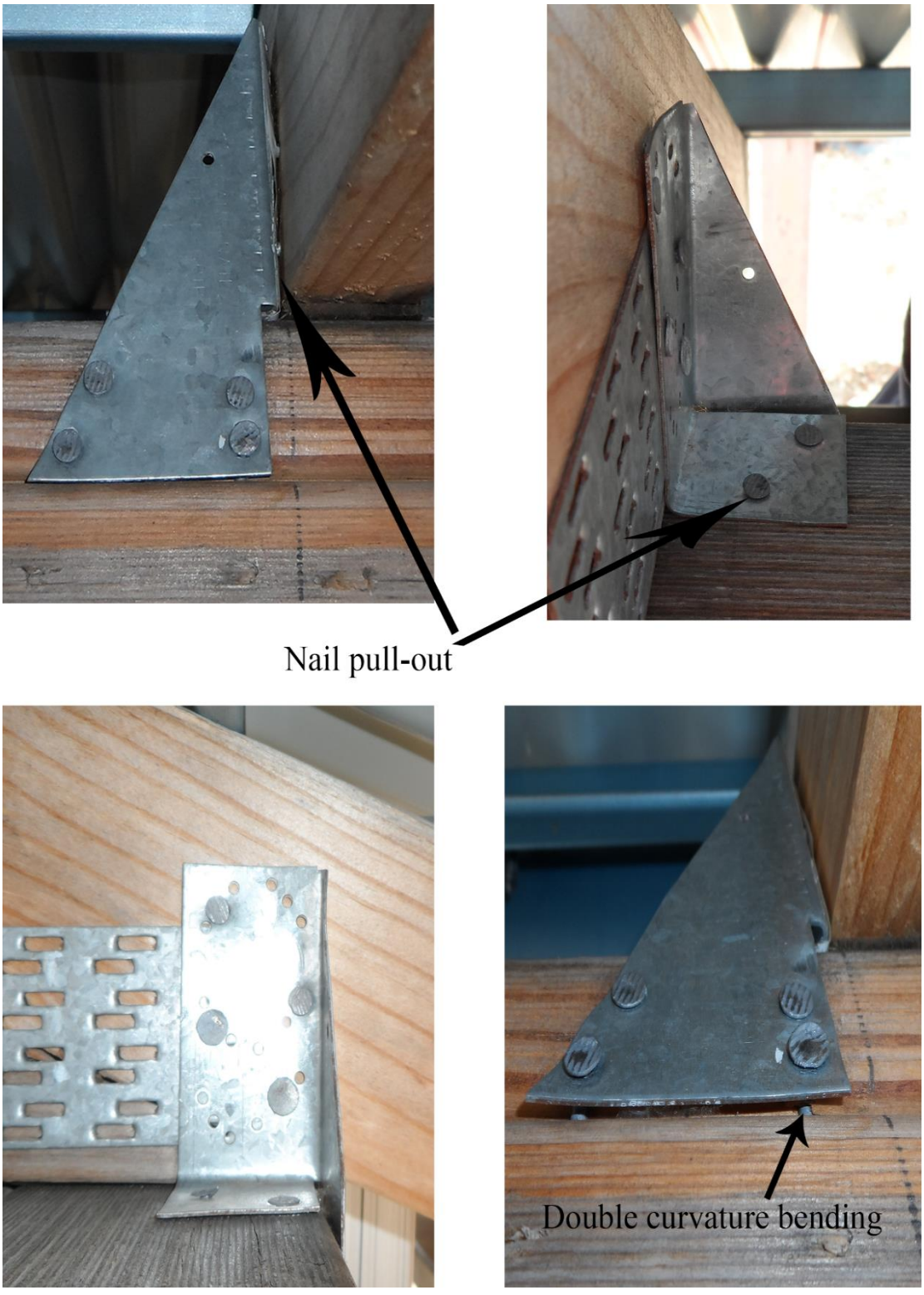

Figure 5.45. The failure modes of the roof to wall triple grip connection of Truss C, at non-loading side during line load test

Figures 5.46 and 5.47 respectively show a hair-line crack on the loading and non-loading side cornice edge, and adhesive between the cornice and ceiling. The hair-line crack on the cornice was mainly due to a combination of the lateral and vertical stress, which was initiated by the lateral and vertical movement of the roof structure. Whilst the hair-line crack occurred on the adhesive between the cornice and ceiling, the crack was highly influenced by the vertical movement of the roof structure.

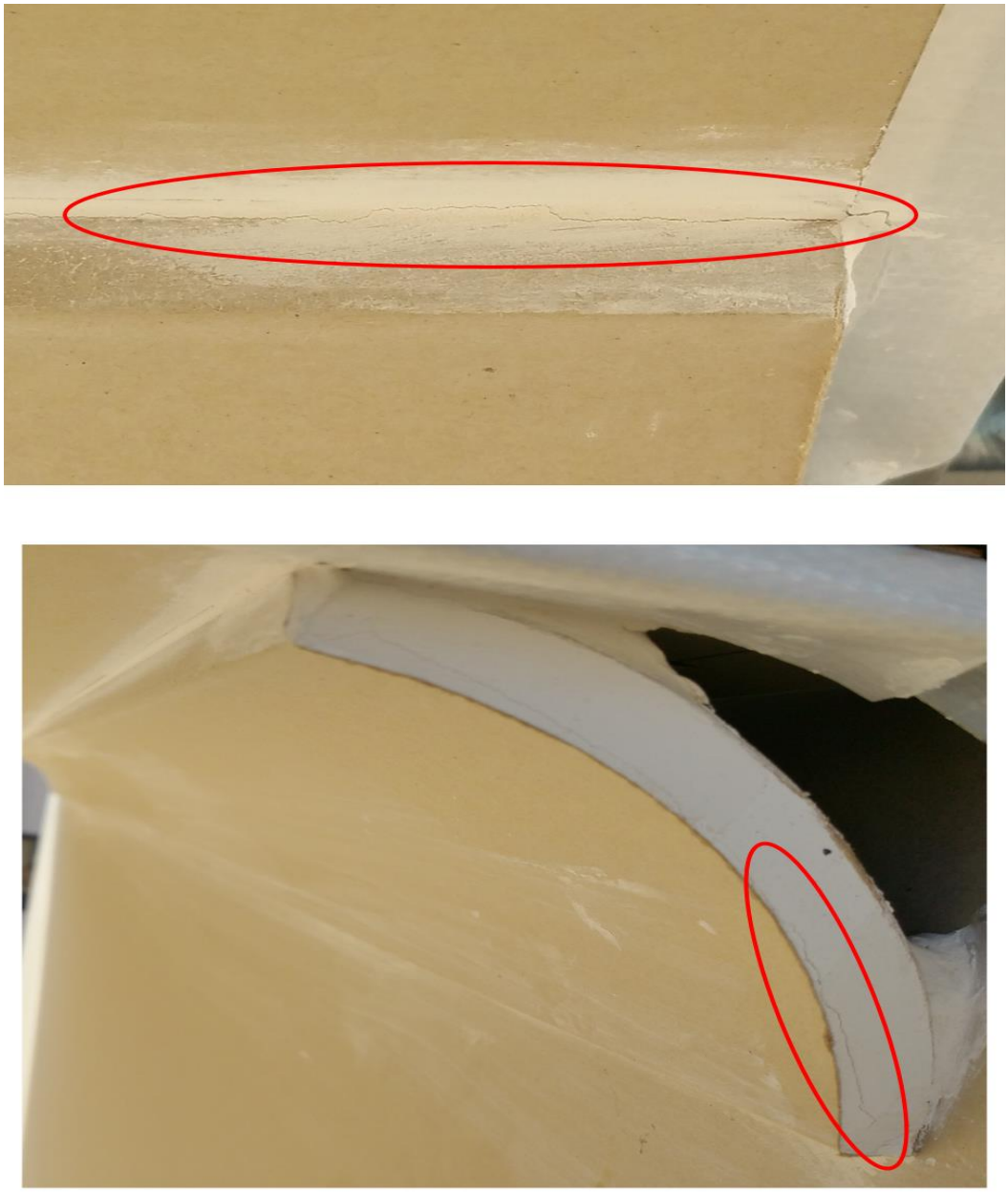

Figure 5.46. Hair-line crack on loading side ceiling cornice

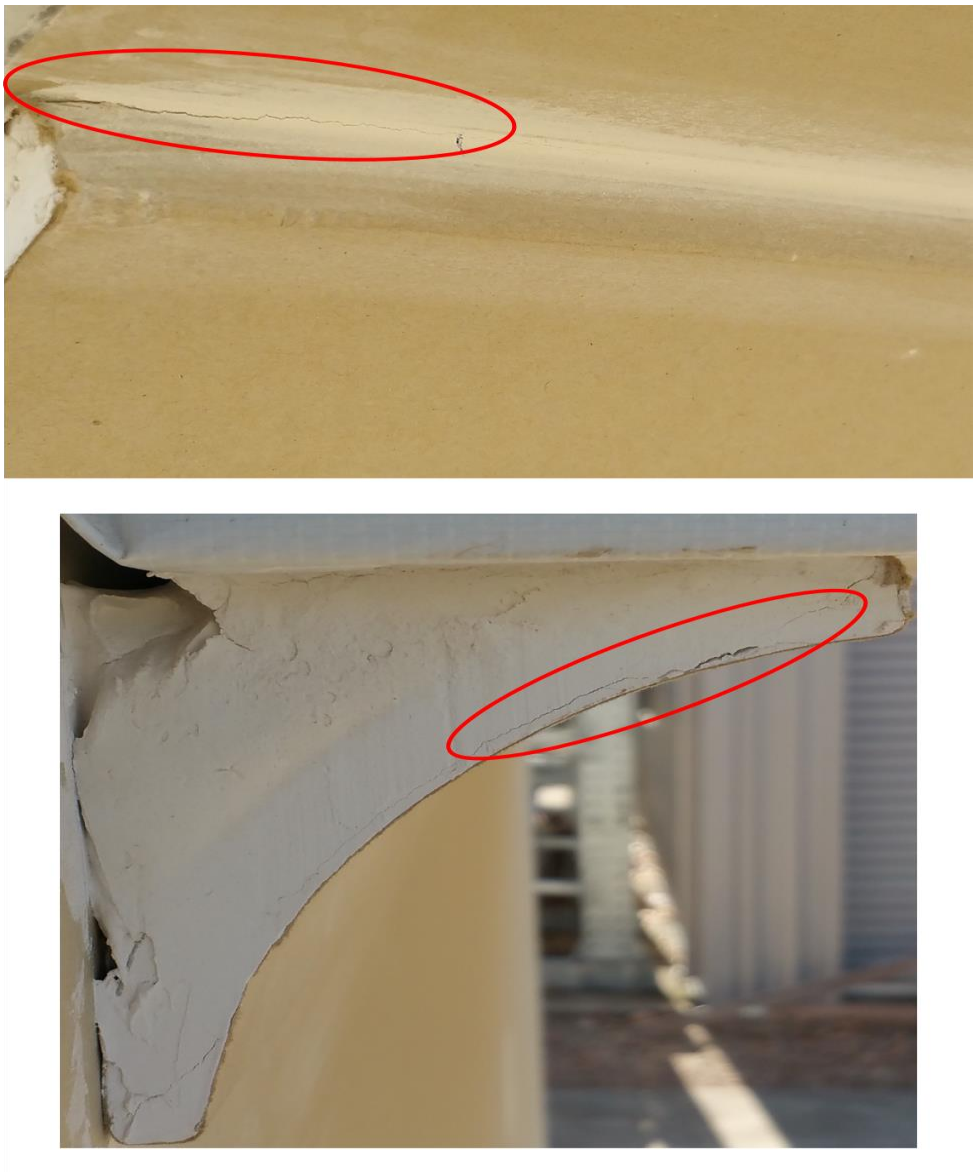

Figure 5.47. Hair-line crack on non-loading side ceiling cornice

The glue joint between the ceiling and bottom chord of the truss was observed to have separated adjacent to the Truss C loading side RWC (Figure 5.48). This failure may have also occurred in other trusses but are hidden from being observed by the naked eye. This failure was also similar to the tension load specimen failure observed in the individual joint test (Figure 5.48b), indicating that the ceiling glue joint suffers more from tension load than lateral load when wind loads acted on the roof. This failure was also the reason for the stiffness reduction observed in Figure 5.43.

a)

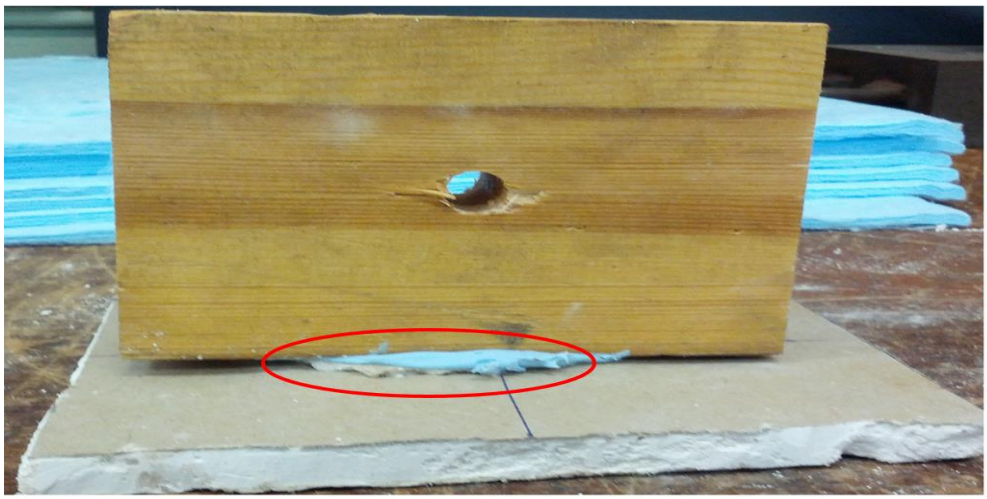

b)

Figure 5.48. Comparison of the ceiling glue joint failure mode between the full-scale test and individual joint test: a) full-scale test, and b) individual joint test

Figure 5.49 shows the ceiling fasteners being pulled out from the bottom chord of Truss C near to the loading side RWC. This failure mode was compared with the individual joint test specimen and was found to be similar to the tension load specimen failure (Figure 5.49). This failure mode comparison indicates that in the full-scale test structure, the tension load dominated the failure of the ceiling fasteners to the bottom chord of the truss. Moreover, partial ceiling joint screw withdrawal was also observed in other connections between the ceiling and truss bottom chord.

a)

b)

Figure 5.49. Comparison of the ceiling screw joint failure mode between the full-scale test and individual joint test: a) full-scale test, and b) individual joint test

5.4 Summary of full-scale tests

Full-scale tests were carried out on a structure that is representative of brick veneer contemporary house general truss region. Loading effects on RWCs and load sharing were assessed. Results of the full-scale test show that the vertical reaction force at the loaded truss support was reduced by about 20% when the lining elements were added to the system with structural elements (i.e. truss, wall frame, batten and roof cladding). The vertical load sharing of the timber-framed house through the RWC depends on the stiffness of the RWC and the truss location (i.e. whether located at the end or middle).

The contribution of the lining elements to the vertical load sharing is about 15% to 20%. The vertical movement of the roof structure was reduced by about 20% when the shear walls were added to the structural system. The loading on a single truss influenced the reaction forces up to two truss supports away from the loaded truss on both sides. The influence coefficient obtained in this study is useful to evaluating the wind load sharing and truss hold-down force for the timber-framed house with metal roof cladding.

Local failures were observed at the roof to wall triple grip connections, ceiling glue and screw joints and ceiling cornice during the line load test. However, when compared to the reaction coefficients obtained in the line load test and point load test, showed there was about 16% variation in the reaction coefficients. This indicates these local failure did not significantly affect the load transmission. The ceiling glue and fastener joint showed tension failure and indicating the vertical loads dominated the structural response of the full-scale test structure.

This full-scale test structure is representative of a middle section of the gable-ended roof house, with results revealing the structural response and load sharing. However, in practice the bottom plates of the house are attached to the floor slab unlike this full-scale test where the bottom plates were supported by the load cells. This could create bending or buckling to the bottom plate and could generate different reaction forces at the bottom plate supports. The objective (i.e. load transfer from roof to wall) requires to evaluating the support reactions at the RWC when wall lining and ceiling cornice were added in the test structure. Moreover, some percentage of the applied load on a truss shares to its adjacent trusses through the top-plates, as they behaved as continuous beams before the lining elements were installed. This load sharing could create different reaction forces at the RWCs. Thus, a numerical model analysis is needed to evaluate the vertical and lateral reaction forces at the RWCs. The overall outcome of this full-scale test can be used to assess the vulnerability of the timber-framed house to windstorm, and develop and validate the FEMs (detailed in the Chapter 6).

CHAPTER 6: FEM OF THE FULL-SCALE TEST STRUCTURE

6.1 Introduction

Full- scale testing is a direct method to evaluate the performance and structural response of timber-framed structures, yet is rarely conducted due to the high cost and time required. This full-scale test is capable of studying the influence of the inter-component connections' parameters (i.e. stiffness, strength, stress, failure mode and etc.), and contribution of the lining elements and the complex loading (i.e. tri axial loads, load and moment, combination of static and dynamic load, and etc.) on the overall structural behaviour. However, it is difficult to obtain all the required data from a full-scale testing, as it requires instrumentation (i.e. LVDTs, Load cells, etc.) to be installed and incorporated into the structure without disturbing the load transfer (i.e. vertical, lateral and horizontal) of the timber-framed structure. Reliable FEM can be used for cost effectively evaluating the structural response of a range of parameters of the timber-framed structure after it is validated with the structural testing results.

Studying the structural response of isolated subassemblies (i.e. part of wall, roof and ceiling) and inter-component connections helps understand the behavior of the subassemblies. However, this is generally not sufficient because the whole-of-structure responds differently (Morrison, 2010; Chapter 5). A few 3D numerical model studies (He et al., 2001; Collins et al., 2005a, 2005b; Gupta et al., 1987; Schmidt et al., 1989; Kasal et al., 1994) have been developed to assess structural response of timber-framed constructions and their constituent components (i.e. cladding, batten, truss, wall, etc.). He et al (2001) numerical model used plate and beam elements to capture the second order P-delta effect in the finite element (FE) technique. Their study also used a nonlinear nail connection with the nail element, based on work by Foschi (2000). This model mainly focused on the effect of a dominant opening in a shear wall to lateral loading. A nonlinear 3D, FEM of light frame buildings capable of static and dynamic analysis was developed by Collins et al (2005a, 2005b). Their model was assembled by replacing individual substructure responses with energetically equivalent and more computationally efficient nonlinear springs. However, these numerical model studies did not account for the vertical load sharing in the entire timber-framed structure and the contribution of the

lining elements (i.e. Ceiling, wall lining and ceiling cornice) to the load sharing and the structural stability to wind loading.

This Chapter describes the development of a 3D, FEM for evaluating the structural response and load sharing in the timber-framed house. This model also has an ability to assess the contribution of the lining elements to the load sharing and structural response. The model is validated by the full-scale test results given in Chapter 5. The aim of this model is to determine the reaction forces at the top-plate of the full-scale test structure, especially after lining elements are added.

6.2 FEM of the test structure

A 3D full-scale test structure model (Figures 6.1 and 6.2) was assembled and subjected to load by using ABAQUS (6.12-3) FE software. The full-scale tests by Boughton and Reardon (1982, 1983, and 1984) Morrison (2010) and Chapter 5 have shown that the inter-component connections are play a major role in the load sharing and load transfer of the timber-framed structure. Therefore, to simplify the model development, material properties within each of the components excluding the inter-component connections were assumed to be isotropic. The aim is to predict the reaction forces at the RWC with additions of elements (i.e. roof cladding, wall cladding, celling, and celling cornice) and determine the load sharing in the timber-framed house.

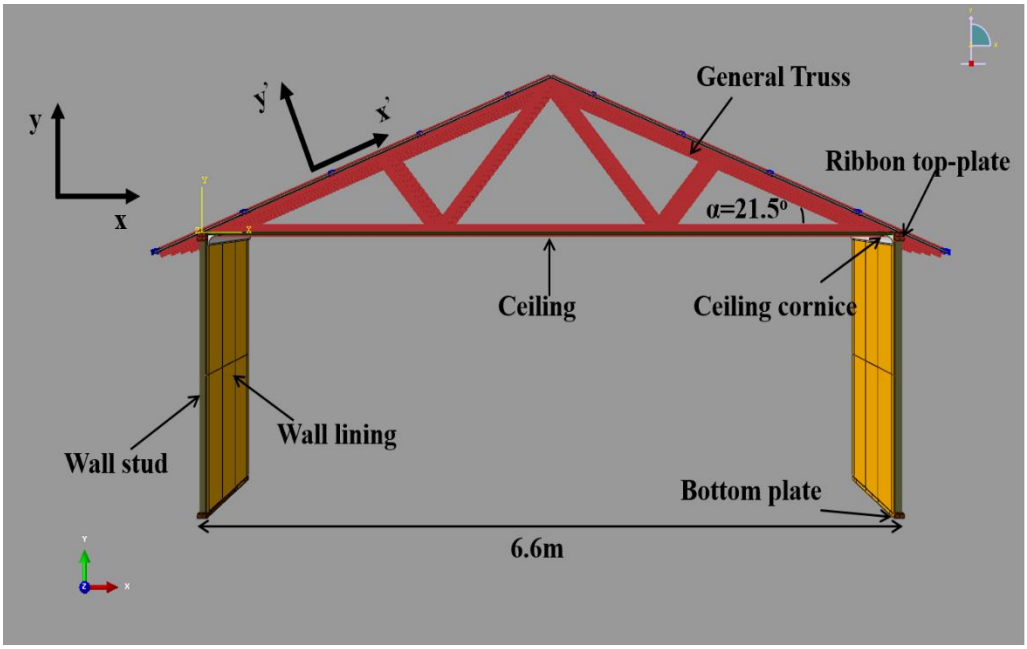

Figure 6.1. Elevation view of the FEM of the full-scale test structure

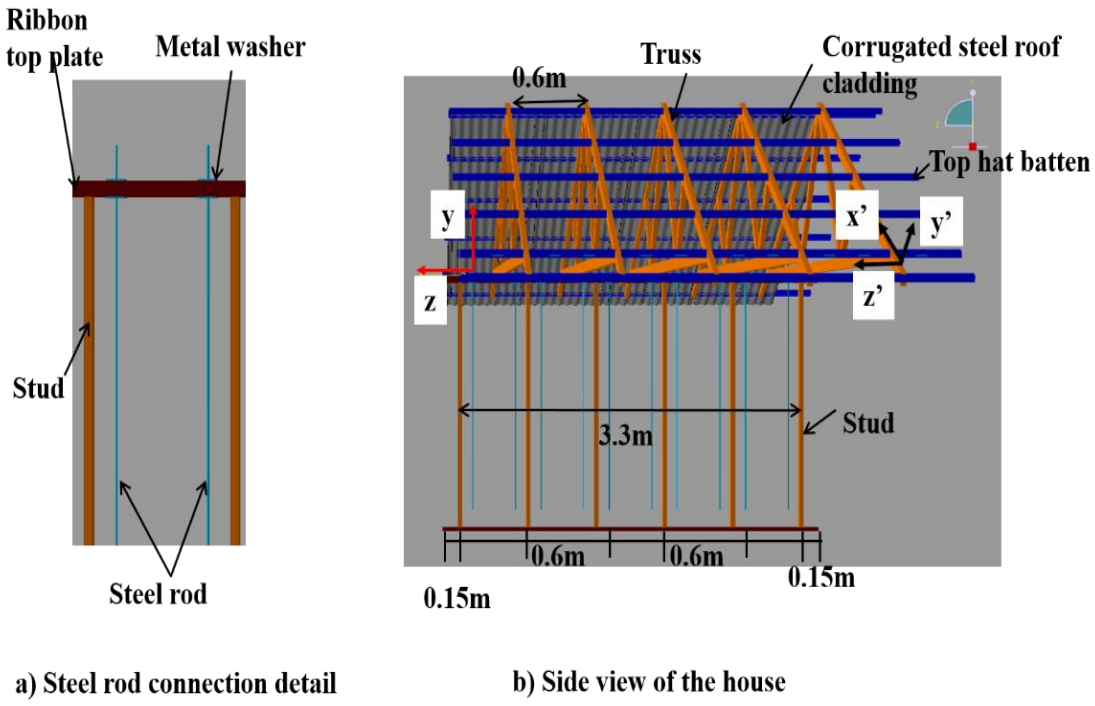

Figure 6.2. Side view of the FEM of the full-scale test structure

The model consisted of eleven types of components: corrugated steel roof cladding, top hat battens, trusses, top-plates, wall studs, bottom plates, wall lining, ceiling, ceiling cornice, steel rods and metal washers. Initially, number of alternative FEMs were assembled with combinations of elements available in ABQUS (6.12-3) such as eight-node brick element (C3D8R), six-node triangular prism element (C3D6), four-node tetrahedron element (C3D4), 20-node quadratic brick element (C3D20R), beam element (B31), two-node truss element (T3D2), four-node shell element (S4R), etc. The computational time of these alternative models was recorded and their analysis results were compared with experimental results. Based on these comparisons, the model assembled with a combination of beam element (B31), brick element (C3D8R) and shell element (S4R) produced reasonable results compared to experimental test with faster model run times compared to other element combinations. (For using a computer of 64-bit operating system with 3.40 GHz processor and 8 GB memory, the computational time for this model was two hours less than that of the alternative FEMs (i.e. minimum 5 hours).

A two-node beam element (B31) was used to assemble the trusses and battens. An eight-node brick element (C3D8R) was used to assemble the top-plate, bottom plate, ceiling cornice, steel rod and metal washer. Roof cladding, wall lining and ceiling were assembled with a four-node shell element (S4R). Applied loads and the boundary conditions of this model were based on the full-scale test. Pinned supports (i.e. replicate the load cells in the full-scale test) were imposed on the bottom surface of bottom plate at RWC locations and bottom of the steel rod in order to obtains the vertical reaction forces. In addition, roller supports were imposed at the lateral load cell locations of the full-scale test structure. These roller supports resisted the lateral movement of the test structure, and were used to measure the lateral reaction.

A surface to surface hard contact was enforced at each contact region between cladding to cladding (i.e. overlap regions), to construct the roof structure. In this model, a surface to surface tie constraint was introduced to connect each contact region between the top-plate to stud, top-plate to metal washer, stud to bottom plate, stud to nogging, metal washer to steel rod, wall lining to ceiling cornice, and ceiling to ceiling cornice. The inter-component connections of the full-scale test structure were represented as linear and non-linear spring elements described in Section 6.3. In addition, the diagonal bracing straps (i.e. Steelbrace) were used in the roof structure of the full-scale test, and were represented as a linear spring element in this model. AS 4440 (2004) specified that the minimum tension capacity for a 2.5 m Steelbrace is 8.4 kN and that it does not contribute more than 3.8 mm to the extension of the bracing. Thus, this model used the stiffness of the diagonal bracing of 2.2 kN/mm (i.e. the minimum tension capacity divided by the 3.8 mm extension). Table 6.1 shows the material parameters and the member sizes used in this model.

Table 6.1. Material parameters and member sizes used in the FEM

Members	Quantity	Sizes (mm)	Material	Young`s Modulus (N/m^2)	Poisson's Ratio	Density (kg/m^3)
Roof cladding	8	760 x 4000 x 0.8	Steel	$2x10^{11}$	0.3	7850
Top-hat battens	12	40 x 40 x BMT 0.55	Steel	$2x10^{11}$	0.3	7850
Truss	5	90 x 35 x 6600	Timber (MGP 10)	$1x10^{10}$	0.37	510
Top-plate	4	90 x 35 x 3300	Timber (MGP 10)	$1x10^{10}$	0.37	510
Stud	12	90 x 35 x 2295	Timber (MGP 10)	$1x10^{10}$	0.37	510
Bottom plate	2	90 x 35 x 3300	Timber (MGP 10)	$1x10^{10}$	0.37	510
Noggings	10	90 x 35 x 565	Timber (MGP 10)	$1x10^{10}$	0.37	510
Wall cladding	4	3000 x 1200 x 10	Gypsum board	$2x10^{9}$	0.2	720
Ceiling	6	2600 x 1200 x 10	Gypsum board	$2x10^{9}$	0.2	720
Ceiling cornice	2	90 x 90 x 2600	Gypsum	$2x10^{9}$	0.2	720
Steel rod	20	1.2 x 2500	Steel	$2x10^{11}$	0.3	7850
Metal washer	40	75 x 75	Steel	$2x10^{11}$	0.3	7850

6.3 Inter-component connections in the FEM

Three nonlinear spring elements were used to represent each roof to wall triple grip connection (i.e. 30 spring elements were used in this model), and were activated in x, y, and z directions (y is the vertical direction, x is lateral direction (i.e. along the span of the truss and z is along the top-plate). A spring element was used to connect a node on the truss and top-plate at the RWC location. In the x, y, and z directions (See Figures 6.1 and 6.2), a force displacement relationship for the non-linear spring elements (Figure 6.3) was obtained from the experiments and FEM analysis of the triple grip connections detailed

in Appendix C, Section C.4. These force displacement relationships were used as the relative displacement (i.e. movement between the node at truss and top-plate) and reaction force of the spring element.

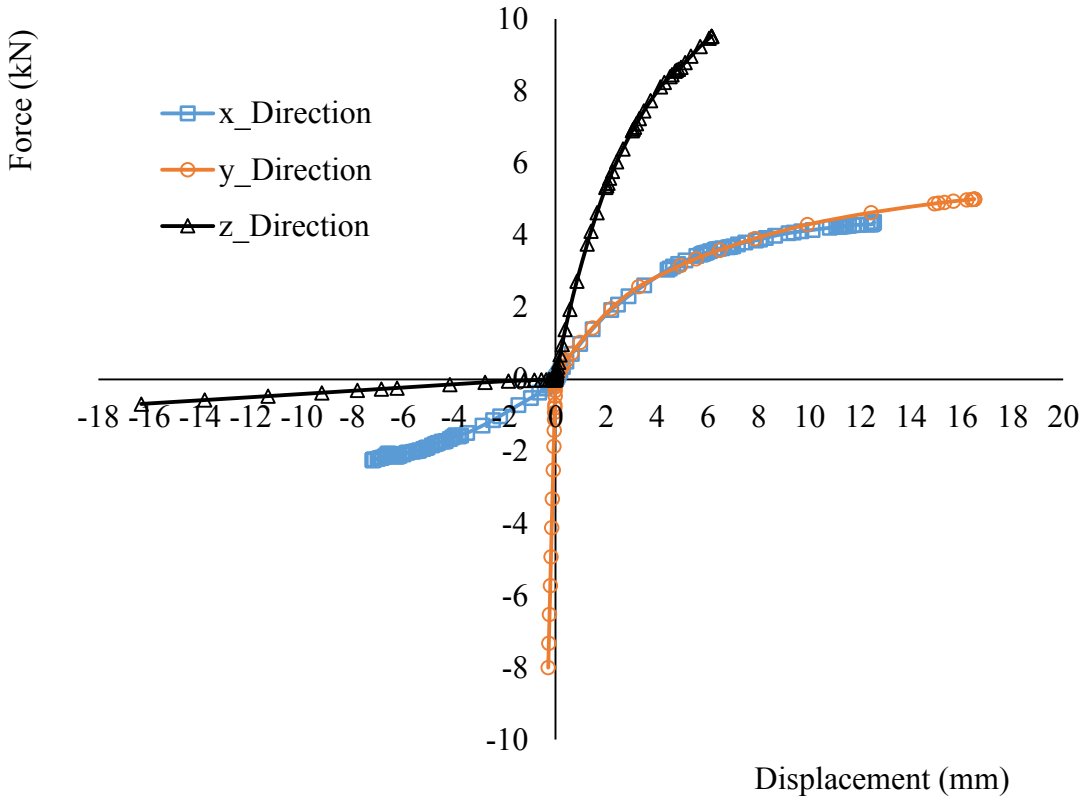

Figure 6.3. Force displacement relationship for the RWC

The batten to truss connection was represented by a non-linear spring element in the y' (i.e. local direction of y) direction and a linear spring element was used in the x', z' directions (See Figures 6.1 and 6.2). The experimental study by Fowler (2003) gives the force displacement relationship of the batten to truss connection when subjected to tension load. A simple FEM was developed to evaluate the compression load response of the batten to truss connection is described in Appendix D, Section D.1. The force displacement relationship for the non-linear spring element in y' direction was obtained from the experimental study of Fowler (2003) and FEM is shown in Figure 6.4. Based on the y' direction force displacement relationship, the maximum linear stiffness of the batten to truss connection in y' direction was 1.8×10^6 N/mm. This linear stiffness was used for x', z' direction stiffness of batten to truss connection to simplify this FEM.

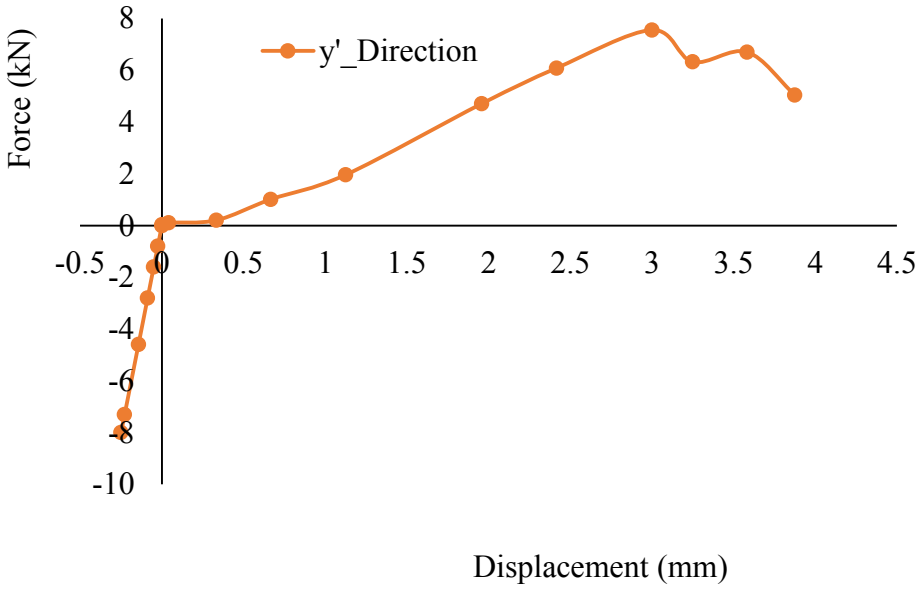

Figure 6.4. Force displacement relationship for the batten to truss connection in y' direction (Fowler, 2003)

Each batten to cladding connection in this model was represented by three linear spring elements, and each spring element stiffness was obtained from previous studies by Henderson (2010) and Dhammika (2003). The maximum y' direction stiffness of the batten to cladding connection obtained from their studies was $3x10^5$ N/mm, and, the x', z' direction was assumed as twice the y' direction stiffness. This is because due to the roofing screws bending to loading, the stiffness in both x', z' was higher than the y' direction stiffness.

The connection between the ceiling and bottom chord of the truss was represented as three non-linear spring elements (i.e. x, y and z direction) at each fastener (i.e. glue and screw) locations. The force displacement relationship of the tension load test of the glue and screw joint given in Chapter 4, Section 4.4 was used for the non-linear spring element property of y direction. However, these experimental result can only be used if the relative displacement is positive. This is because the applied load in the experiment was only tension. This study developed a simple FEM to determine the force displacement relationship of the glue and screw joint when compression load applied, as detailed in Appendix D, Section D.2. The x and z direction non-linear spring element properties were obtained from the shear load test of the glue and screw joint (Chapter 4, Section 4.4).

Figures 6.5 and 6.6 illustrate the non-linear spring element properties that were used for the connection between the ceiling and bottom chord of truss.

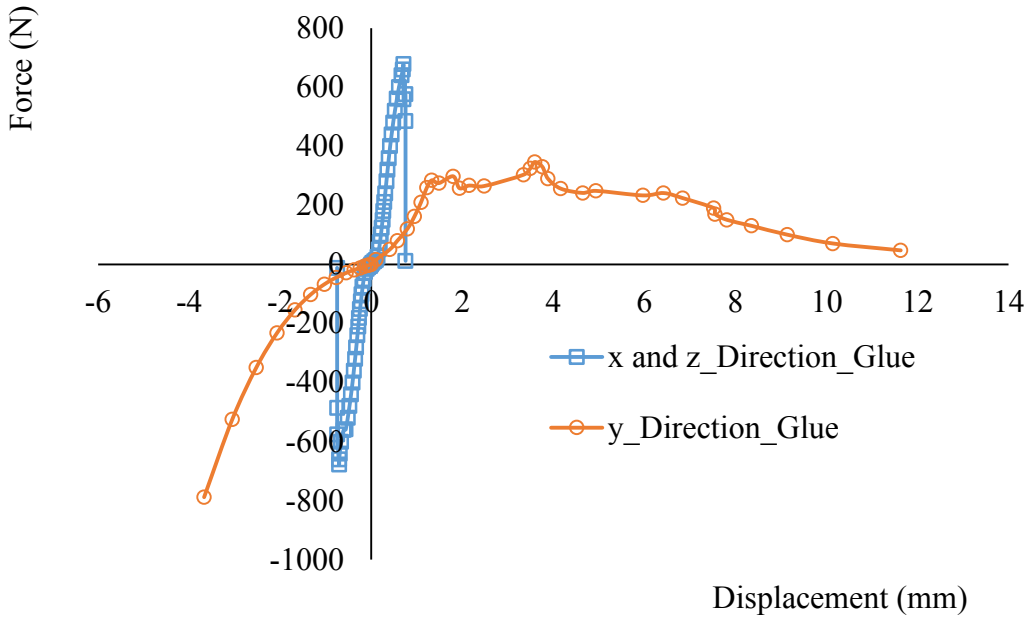

Figure 6.5. Force displacement relationship for the glue joint between the ceiling and bottom chord of the truss

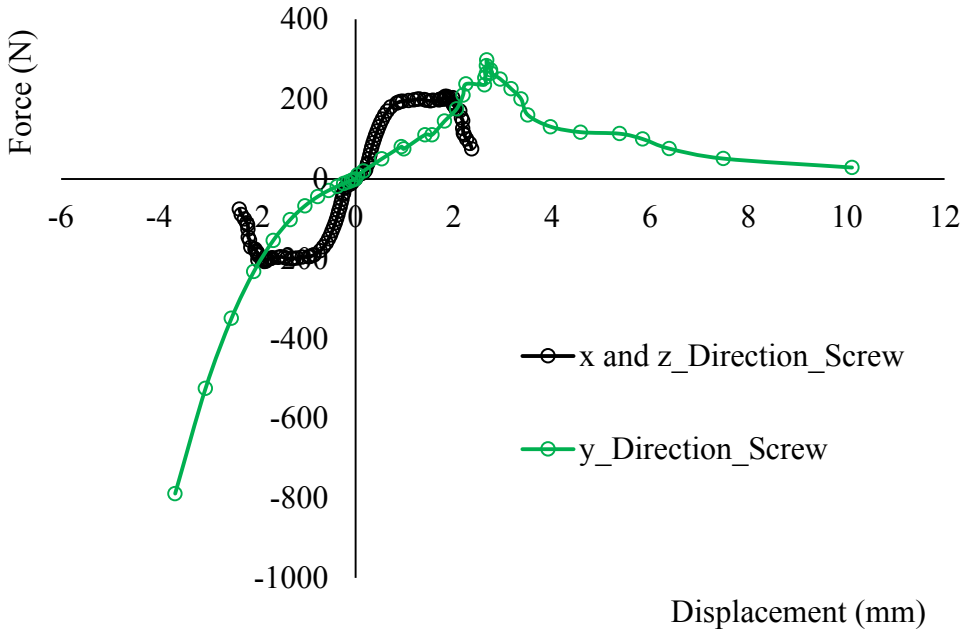

Figure 6.6. Force displacement relationship for the screw joint between the ceiling and bottom chord of the truss

In this model, the wall lining and wall frame were connected by three non-linear spring elements at each fastener (i.e. glue and screw) location of the full-scale test structure. The force displacement relationship of glue and screw joint tests in shear were used for the non-linear spring element properties of y and z direction, whilst the tension load force displacement relationship is used for the x direction non-linear spring element. Figures 6.7 and 6.8 show the force displacement relationship used for the connection between the wall lining and wall frame in this FEM.

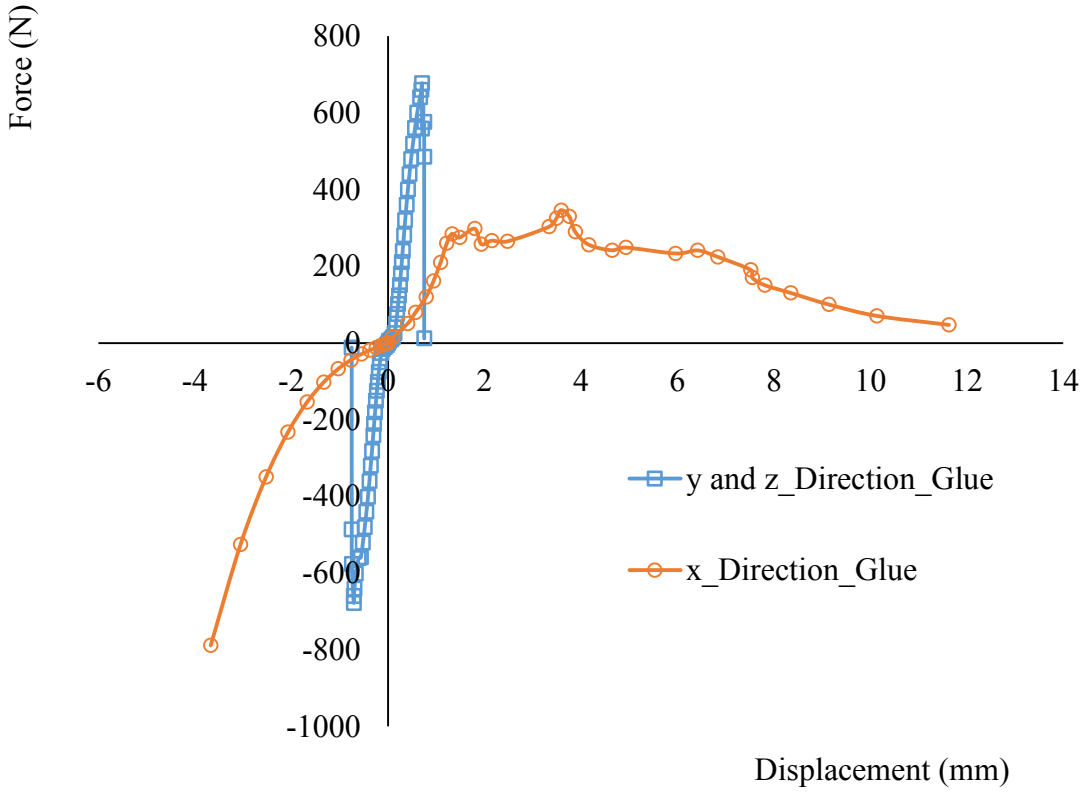

Figure 6.7. Force displacement relationship for the glue joint between the wall lining and wall frame

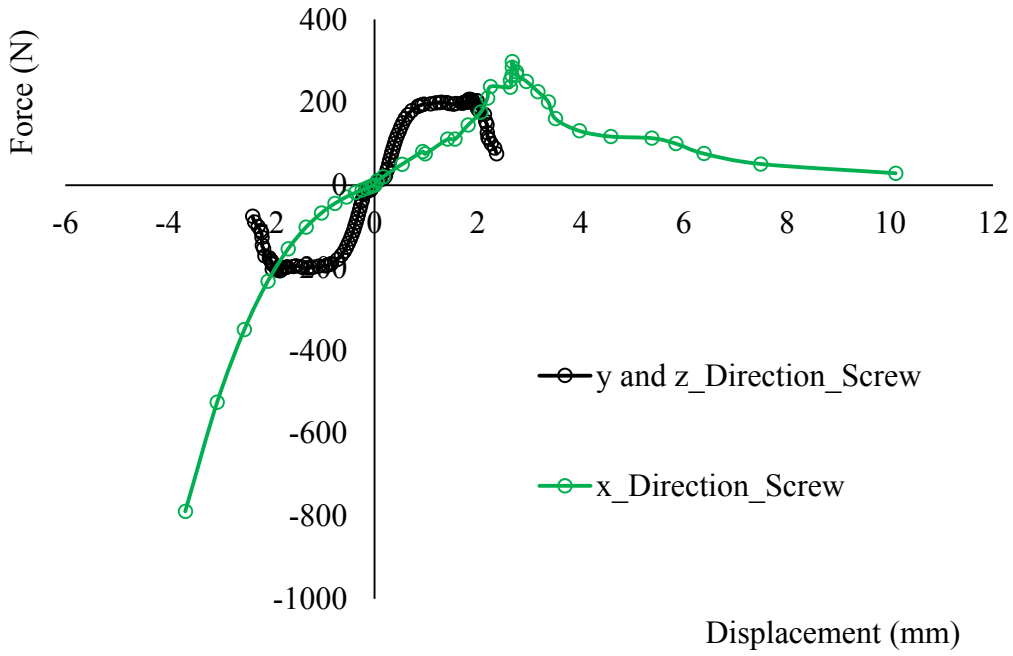

Figure 6.8. Force displacement relationship for the screw joint between the wall lining and wall frame

6.4 Validation of the FEM full-scale test structure

FEM analysis was run in seven construction stages (i.e. Stage S1 to S7), similar to the full-scale tests (Chapter 5, Table 5.1). The applied loads, the measured reaction forces and displacement locations were same as in the full-scale tests. The model was subjected to 1kN uplift load perpendicular to roof surface, representing the wind load. Reaction forces and displacements were obtained and compared with the full-scale test.

The full-scale test results when load was applied at Batten B2 at Stage S1 were used to compare each RWC's initial stiffness between the full-scale test and the FEM. The location of Batten B2 was directly above the RWC and there were no additional elements to share the applied load at Stage S1. The structural system was symmetric and the truss spacing, connection type and number of nails in the connection were same for each truss. Thus, the VRCs should, be same at Stage S1 for Truss A (i.e. L.A) and Truss E (i.e. L.E), and also Truss B's (i.e. L.B) and Truss D's (i.e. L.D) VRC should also be similar, when load is applied to Batten B2. However, Table 6.2 shows these VRCs were not similar in the full-scale test but were similar in the FEM. This is due to the variation in the RWC

stiffness. In the FEM, the y direction (vertical) stiffness of RWC was equal for each connection but it was not equal in the full-scale test due to the material's nonlinearity and construction practice.

The roof to wall triple grip connection loading response detailed in Chapter 4 also showed that the maximum stiffness of each individual connection test specimen varied between about 15% to 20%. In this FEM, an average force displacement relationship was used for the RWC (Figure 6.3). This vertical average force of the RWC was reduced by 8%, 16%, 25%, 20%, 12% on Trusses A, B, C, D and E respectively, in order to introduce similarity to the connection stiffness variation, as in the full-scale test structure's RWCs.

Table 6.2. Comparison between the FEM and full-scale test of the VRCs at loaded side RWCs

Loading locations	**VRCs measured locations**					
		L.A	**L.B**	**L.C**	**L.D**	**L.E**
TA_B2	Full-scale Test	0.81	0.19	-0.07	-0.01	-0.01
	FEM	0.94	0.03	-0.02	0.00	0.00
TB_B2	Full-scale Test	0.12	0.68	0.17	-0.05	0.01
	FEM	0.04	0.88	0.04	-0.02	0.01
TC_B2	Full-scale Test	-0.05	0.26	0.48	0.28	-0.05
	FEM	0.00	0.04	0.88	0.04	0.00
TD_B2	Full-scale Test	0.03	-0.05	0.22	0.56	0.13
	FEM	0.01	-0.02	0.04	0.88	0.04
TE_B2	Full-scale Test	-0.02	0.00	-0.08	0.22	0.75
	FEM	0.00	0.00	-0.02	0.03	0.94

Figure 6.9 shows the VRC comparison between the full-scale test and FEM with and without variations in the RWC' vertical stiffness, when loading at Truss D along Batten B2 at Stage S2. This figure shows that the VRCs of the FEM with variations in the RWC' vertical stiffness are similar to those of the full-scale test. Figure 6.9 also shows when the RWC stiffness was same for each connection (i.e. the model without variations in the RWC' vertical stiffness), the shared applied load to the adjacent trusses was equally distributed to each side near the truss connections (i.e. L.E and L.C) from the loaded truss (i.e. L.D). This also indicates that the load sharing of the timber-framed house structure is influenced by the RWC stiffness.

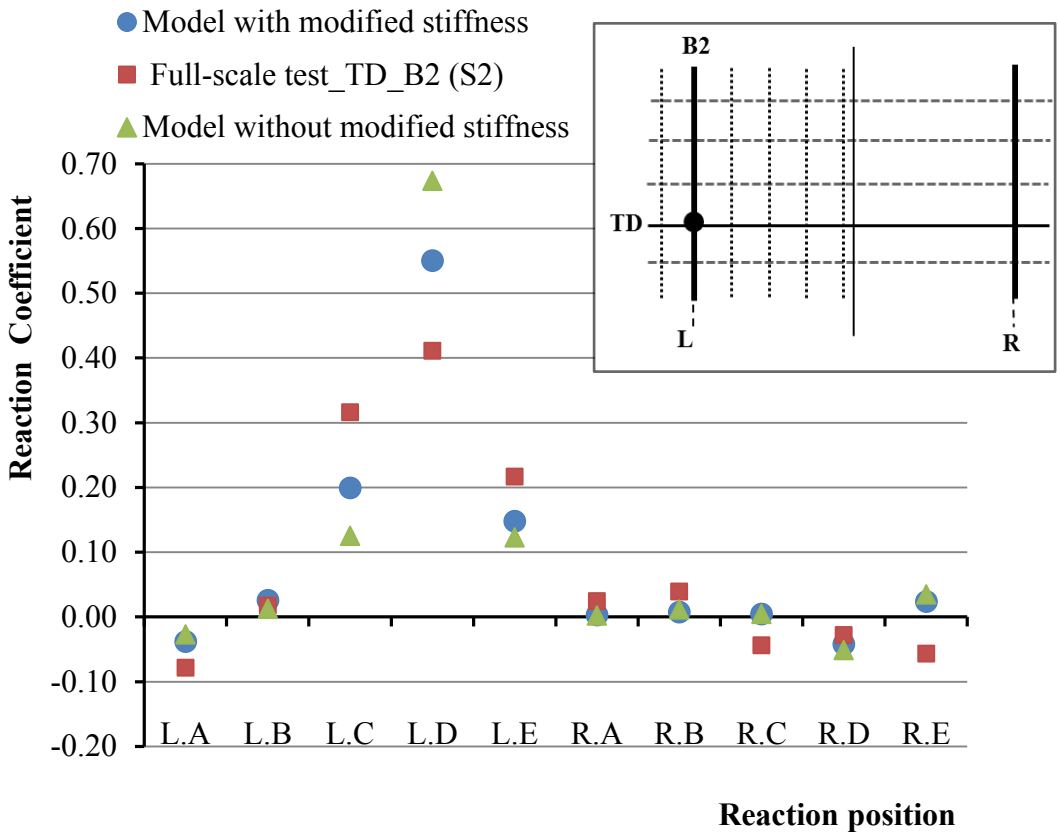

Figure 6.9. Comparison of VRCs between the full-scale test and FEM with and without modified stiffness, when loading at Truss D along Batten B2 at Stage S2.

6.4.1 Structural response when load applied on the roof

Based on the modified (i.e. variation introduced to vertical stiffness of RWC) RWC stiffness, the FEM was developed, and analysed for all construction stages (i.e. S1 to S7). The VRCs at the supports were obtained from the FEM analysis and compared with full-scale test results. Figures 6.10 and 6.11 give the comparison of the VRCs when load was applied at Batten B3 along Truss B (i.e. TB) with the full-scale test and the FEM analysis (more results are detailed in Appendix D, Section D.3). These figures show the full-scale test results and the FEM results were similar. However, the FEM reaction coefficient at the loaded truss support (i.e. LB) was about 5% to 15% higher than that of the experimental test. This difference is due to the RWC stiffness variation between the FEM and full-scale test. In the FEM, the RWC stiffness was same for each connection in x, z

directions and the non-linearity variation in y direction stiffness was constant but it not same in all directions of the full-scale test.

When the experiments moved from Stage S1 to Stage S7, there was a gradual deterioration of the stiffness of the RWCs that resulted from nail withdrawal in the full-scale tests. This gradual deterioration was not accommodated in the FEM as the model assumed a "pristine" structure at the start of each test stage. This also could be a reason for the differences in the reaction coefficients. The load sharing to adjacent trusses in the FEM was less than that of the full-scale tests. This is because the RWC stiffness was same in the both loaded and non-loaded side truss supports, but in the full-scale test, it might not have been similar on both sides. This could the reason for less load sharing to the adjacent trusses obtained in the FEM.

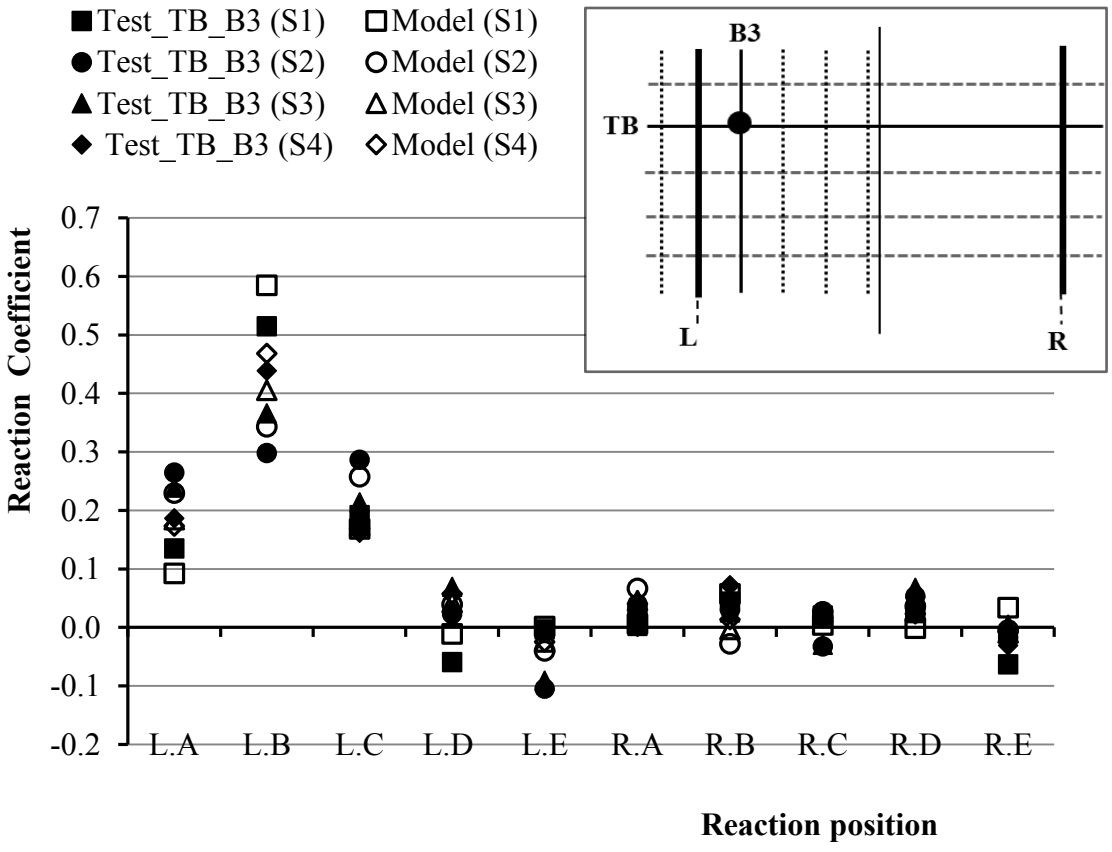

Figure 6.10. Comparison of the VRCs when load was applied at Batten B3 along Truss B at Stage S1, S2, S3 and S4 with full-scale test and the FEM

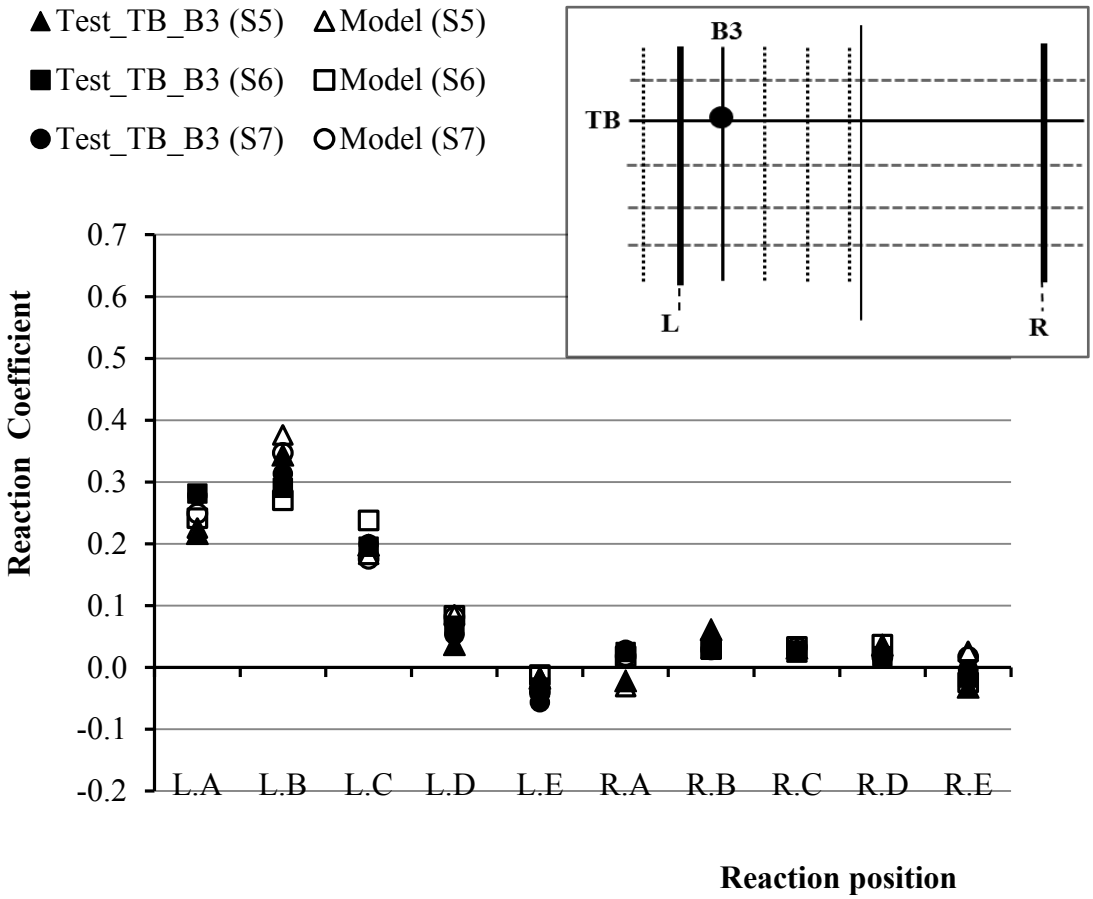

Figure 6.11. Comparison of the VRCs when load was applied at Batten B3 along Truss B at Stage S5, S6 and S7 with full-scale test and the FEM

The total lateral load was measured in the full-scale test by the lateral load cells L1 and L2 (See Figure 5.2, Chapter 5). In the FEM, it was measured at the same location as the full-scale tests. Figure 6.12 shows the comparison of the total lateral reaction coefficients (i.e. total lateral loads measured by L1 and L2, divided by the applied load) when load was applied at Truss C along Battens B1 and B3 with full-scale test and the FEM analysis. This figure shows that the total lateral reaction coefficients obtained from the FEM were higher than that of the full-scale tests. This differences ranged between 2% to 12% and were due to the variation of the RWCs lateral direction (i.e. x direction) stiffness. In the FEM, the lateral direction stiffness of the RWC was the same for all the connections but it was not same in the full-scale test due to the material non linearity and construction practice. However, the FEM analysis gives a reasonable prediction of the full-scale test behaviour, and the model can be used to predict the vertical load sharing and the

contribution of the lining (i.e. ceiling, ceiling cornice and wall lining) to vertical load sharing of the timber-framed house structure.

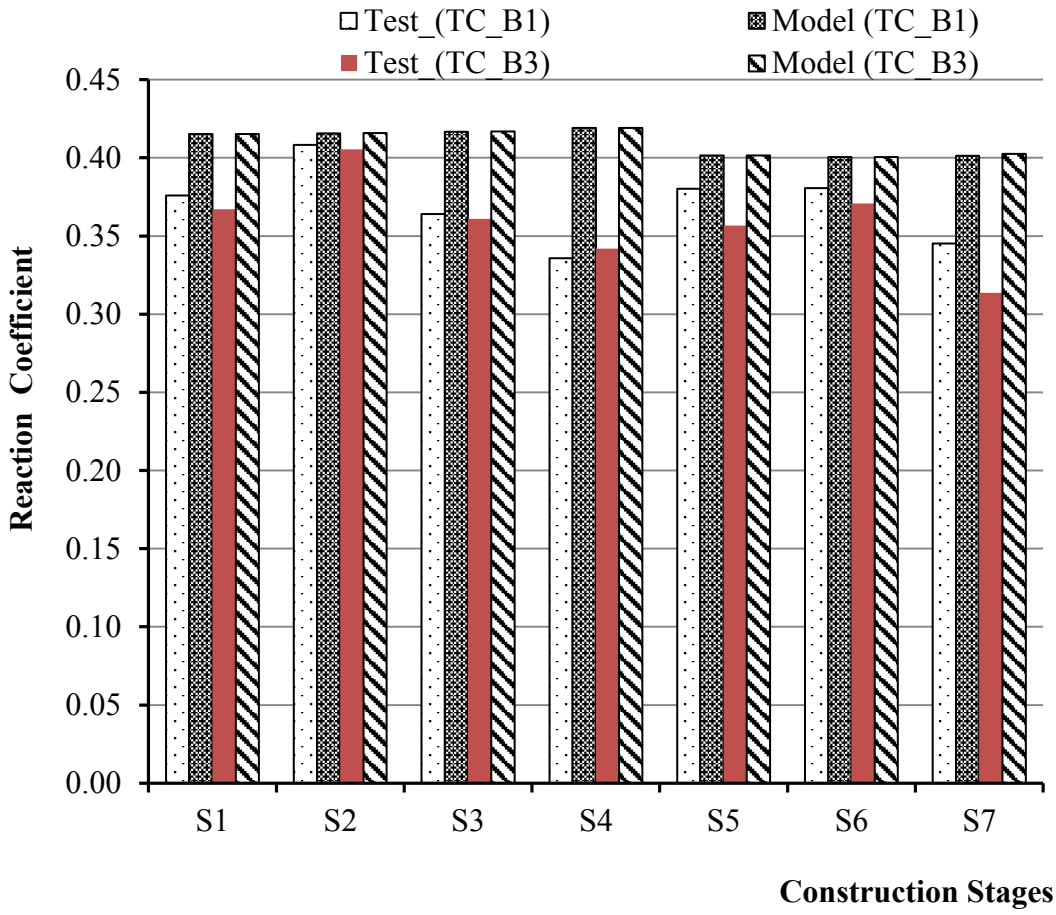

Figure 6.12. Comparison of the total lateral reaction coefficients when load was applied at battens B1and B3 along Truss C (i.e. TC) with full-scale test and the FEM

6.5 Reaction forces at the RWCs

The FEM analysis of a timber-framed structure subjected to vertical (see Section 6.4), lateral (Appendix D, Section D.6) and horizontal (Appendix D, Section D.7) loads agreed favourably with maximum variation of about 15% from the full-scale tests. However, as Figure 6.13 indicates, the Von-mises stress (i.e. equivalent stress as it created by the actual applied load) was high and concentrated at the load cell locations (i.e. vertical supports) when horizontal load was applied to the web members of Truss A. The contact areas of bottom plates to load cells were small, thus the reason the stresses were concentrated and high at those regions. This high and concentrated stress at the load cell location creates

deformation on the bottom plates. In practice, the bottom plate is attached to the concrete slab and the contact surface area is large compared to the full-scale test. This large contact surface will distribute the stress along the bottom plate's bottom surface and consequently, reduces the deformation of the bottom plate. Therefore, pin supports were imposed at the bottom plate's bottom surfaces of the FEM of the full-scale test structure to increase the contact surface between the bottom plates and slab. Based on this FEM analysis, the vertical (i.e. y direction), lateral (i.e. x direction) and horizontal (i.e. z direction) reaction forces at the RWCs of Trusses A, B, C, D and E were obtained.

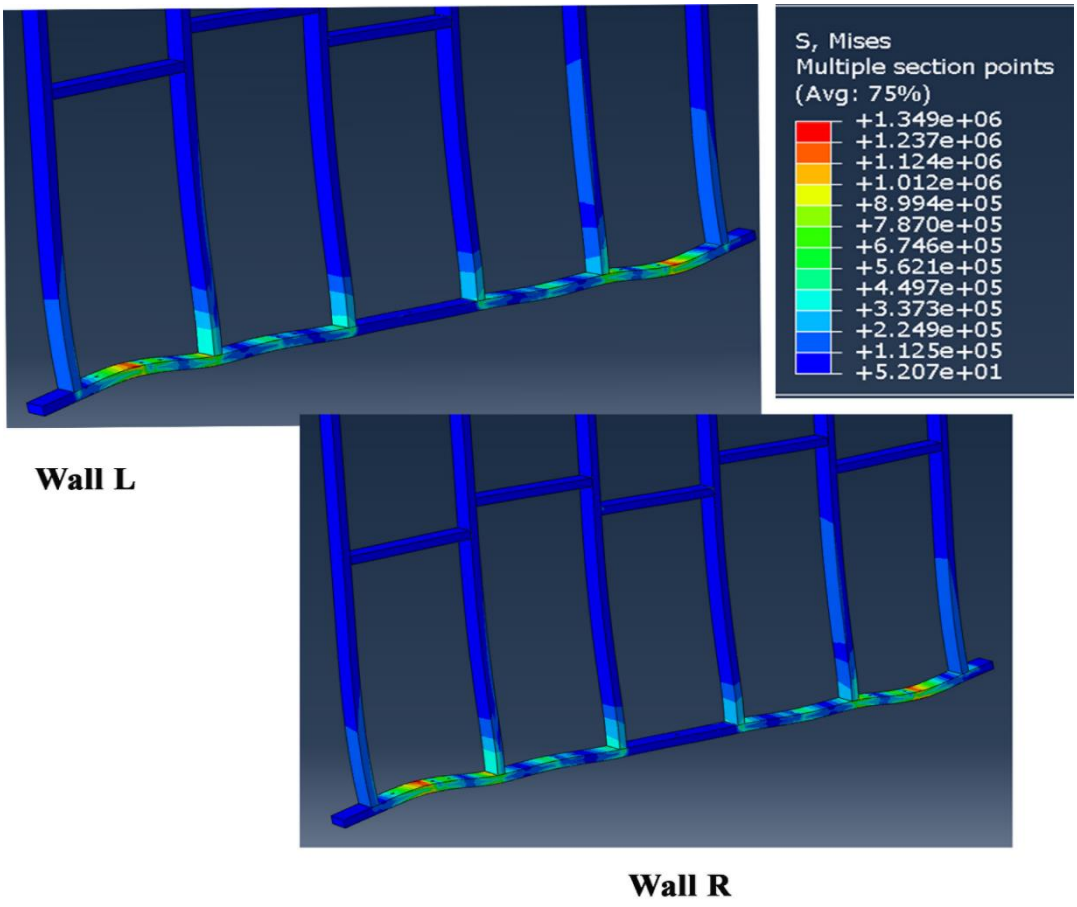

Figure 6.13. Von-mises stress (in Pascal) at the bottom plates of the Wall L and Wall R, when horizontal load was applied to the web members of Truss A

The vertical reaction force influence coefficients at the RWC were derived from the FEM. Figure 6.14 shows the vertical reaction force influence coefficients changes at Truss B's loading side support RWC (i.e. L.B). This figure shows that loading along Trusses A, C and D influences to the vertical reaction force of the Truss B's RWC (i.e. L.B). This figure also shows that the vertical reaction force at the RWC of Truss B (i.e. L.B) was influenced

by the loading on Battens B1, B2, B3, B4, B5, B6, B7 and B8, and loading on Truss E, and Battens B9, B10, B11 and B12 had little to no effect on the vertical reaction of the RWC of Truss B (i.e. LB). This is indicates that the leeward side suction pressure near the ridge region also influenced to the windward side support vertical reaction of the RWCs.

In general design practice, the influence coefficients and wind pressure distribution (i.e. obtained from wind tunnel data) on a single truss's tributary area as described in Ginger et al. (2000), are used to evaluate the wind load effects on the roof structure (i.e. battens, top-plate, truss and their inter component connections). As Figure 6.14 shows the influence coefficients for vertical reaction force on a single truss are affected by the loads that act on adjacent trusses. This indicates that the design load obtained by way of single truss analysis is not an accurate value. Influence coefficients obtained in this FEM can be used to accurately evaluate the wind load sharing and truss hold down force for the timber-framed house with metal roof cladding.

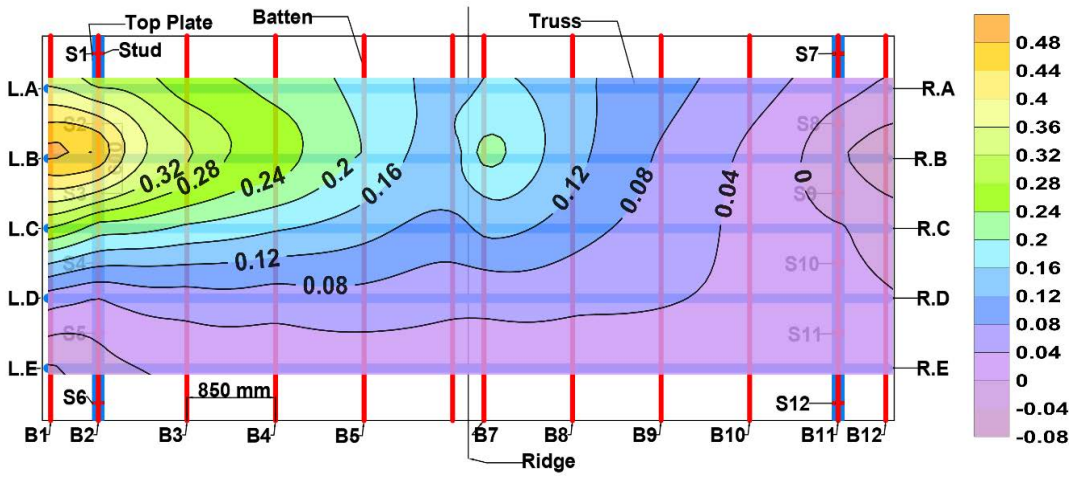

Figure 6.14. Vertical reaction influence coefficient of Truss B's RWC (i.e. LB)

6.6 Summary of the FEM of the test structure

A 3D FEM was developed for part of the contemporary timber framed house by using ABAQUS (6.12-3) FE software. The model assemblage comprised structural (i.e. trusses, battens, metal roof cladding, top plates, bottom plates and the wall studs) and lining

elements (i.e. ceiling, wall lining and ceiling cornice). The inter-components' connection properties were used in the numerical model obtained by previous studies and the individual connection model. Results (i.e. load sharing, contribution of the non-structural elements on the load sharing, roof to wall connection vertical displacement and reaction forces) obtained from the FEM of the test structure were compared with the full scale tests, and showed good agreement.

The FEM analysis of the structural response of a timber-framed structure subjected to vertical, lateral and horizontal loads produced satisfy structural response with maximum variation about 15% with the full-scale test results. Based on this FEM, the vertical reaction force influence coefficients of the RWCs were obtained, showing that the loading at battens, which were located near the ridge line, influenced the vertical reaction forces of both loaded and non-loaded side RWCs. This indicates high suction wind pressure on the ridge will increase the vertical reaction forces of both the windward and leeward side RWCs of the timber-framed house. In addition, the vertical reaction forces influence coefficients' variation with construction defects and the load distribution through the inter-component connection of roof structure are detailed in Chapter 7. This validated model enables confidence in investigation of structural response by changing a structural system such as geometry, materials and construction defects in the timber-framed house. This FEM method can be used for modelling other houses with similar construction systems.

CHAPTER 7: WIND LOAD SHARING ON THE ROOF

Wind tunnel model studies were carried out in the 22.0 m long, 2.0 m high and 2.5 m wide boundary layer wind tunnel by the CTS team at James Cook University to obtain wind loads on the representative contemporary house (Ginger et al., 2015). A complex roof shape, 9.1 x 18.3 x 2.7 m low rise house with 21.5^{o} roof pitch and 0.45 m overhang was constructed at a length scale of 1/50, as shown in Figure 7.1. The fluctuating wind pressures were measured at pressure taps on the roof and walls of the model. One hundred and eight (108) pressure taps were installed under the eaves and three hundred and twenty (320) pressure taps were installed on the external roof surface to measure the spatial and temporal variation pressure on the roof structure. The layout of the pressure taps is given in Figure E.1 (Appendix E). Each tap was connected to a transducer using a tubing system, and a computer-controlled pressure measurement system was used to measure and record pressures. The pressure was recorded at three runs for each approach direction, and the pressure signals were sampled at a frequency of 625Hz for about thirty seconds per run.

Figure 7.1. 1/50 scale wind tunnel model of representative contemporary house

The results are represented as pressure coefficients, which were obtained from Equation 7.1.

$$C_p(t) = {p(t)}\Big/{\left(\frac{1}{2}\rho\overline{U}_h^2\right)} \tag{7.1}$$

Where, $p(t)$ is the pressure varying with time t, ρ is the density of air and $\overline{U}_h$ is the mean wind velocity at mid roof height h. This wind tunnel model study was carried at a length scale (L_r) 1/50 and velocity scale (U_r) 1/2.5, and this velocity scale gives time scale (T_r) as 1/20. The pressures were also recorded as mean ($C_{\bar{p}}(t)$), standard deviation ($C_{\sigma_p}(t)$), maximum ($C_{\hat{p}}(t)$) and minimum ($C_{\check{p}}(t)$) values on a full-scale time equivalent of 10 to 15 minutes.

7.1 Wind loads on the RWC by using loads on tributary area (i.e. traditional design method)

The time varying wind load at the RWCs (i.e. time varying truss hold-down force) are calculated by using spatially and temporally varying wind pressure acting on the roof surface. Equation 7.2 is used to determine the fluctuating reaction forces *X (t)* at the RWC.

$$X(t) = \sum_{i=1}^{N} \beta_i A_i p_i(t) \tag{7.2}$$

Where, *X (t)* is the fluctuating reaction force at RWC, β_i is the influence coefficient for reaction force (*X*), p_i is wind pressure, and A_i is tributary area of patch *i*, and *N* is the total number of battens to truss patches on the tributary area of truss.

The influence coefficient β_i is the reaction force at the truss supports when the unit load (i.e. 1 kN) is applied on the battens to truss connection location on a single truss (Figure 7.2). A single general truss pinned at point A and point B is a roller support, as shown in Figure 7.2. Vertical (R_Ay, R_By) reaction forces at the supports were calculated and those were the β_i for this single truss. Based on the Jayasinghe (2012) study, the pressures (p_i) acting on batten to truss connections were determined by averaging the pressures acting on pressure taps across the tributary area (A_i) of the batten to truss connection (Figure 7.2).

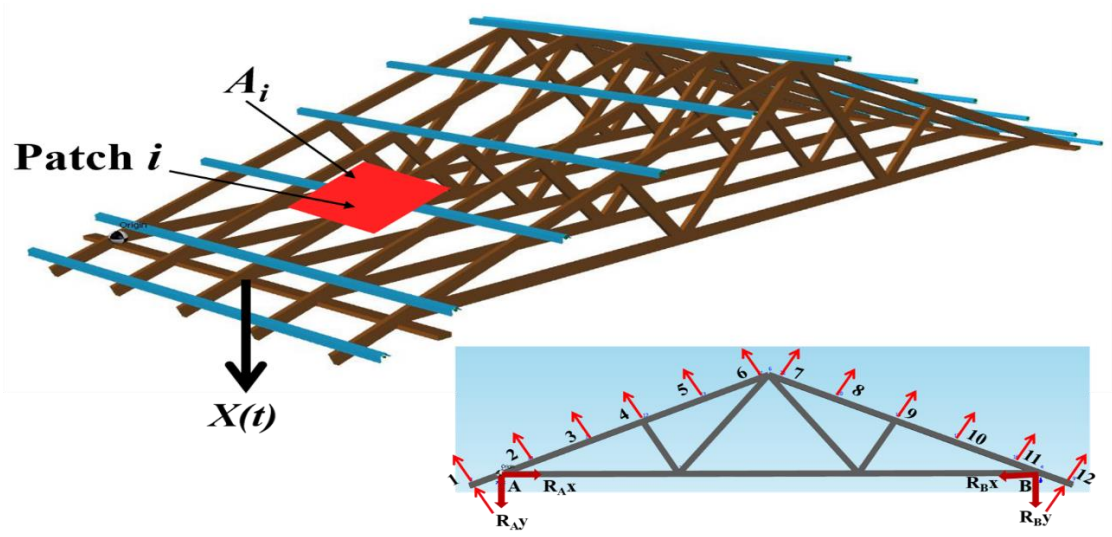

Figure 7.2. Schematic diagram of roof structural system of the representative contemporary house general truss region; showing $\boldsymbol{A_i}$ and vertical reaction forces

Figure 7.3 shows the truss layout and the pressure taps' locations of the contemporary representative house, general truss region. The truss hold-down forces for the general truss region of the representative house were calculated by using wind tunnel data, and obtained β_i from the single truss analysis and tributary area.

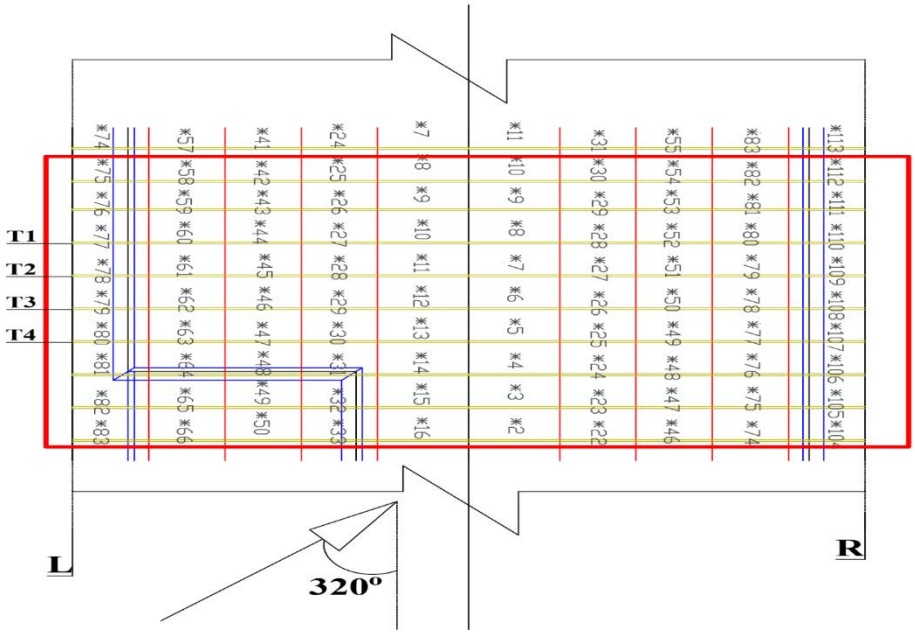

Figure 7.3. Trusses' layout and the pressure taps' location of the representative contemporary house general trusses' region

Table 7.1 shows the maximum dimension-less hold-down force C_N and that obtained from Equation 7.3, where A_N is the total tributary area.

$$C_N(t) = {X(t)}\Big/{\left(\frac{1}{2}\rho\overline{U}_h^2 A_N\right)} \tag{7.3}$$

This C_N is also calculated by using standard AS/NZS 1170.2 (2011) design wind pressure (p) with influence coefficient β_i and tributary area A_i, and compared with C_N obtained from the wind tunnel pressure. The design wind pressure was derived from Equation 7.4, where ρ is the density of air,$V_{des,\theta}$ obtained by Equation 7.5, is the design gust wind speed at mid roof height, C_{dyn} is the dynamic response factor and C_{fig} is the aerodynamic shape factor.

$$p = (0.5\rho)[V_{des,\theta}]^2 C_{fig} C_{dyn} \tag{7.4}$$

$$V_{des,\theta} = V_R M_d M_{z,cat} M_s M_t \tag{7.5}$$

Where, V_R – regional gust wind speed at 10m, M_d – wind directional multiplier (i.e. 0.95), $M_{z,cat}$ – terrain/height multiplier (i.e. 0.83) for terrain category 3, M_s – shielding multiplier, and M_t – topographic multiplier (i.e. 1.0). This C_{fig} is obtained by using Equation 7.6, where C_{pe} is the quasi-steady external pressure coefficient, K_a is the area averaging factor, K_{ce} surface combinations factor, K_l is the local pressure effect factor and K_p is the permeable cladding factor.

$$C_{fig} = C_{pe}(K_a \times K_{ce} \times K_l \times K_p) \tag{7.6}$$

Table 7.1 shows the maximum dimension-less hold-down force (C_N) at general trusses' RWCs (i.e. T1_L, T2_L, T3_L, T4_L, T1_R, T2_R, T3_R and T4_R) and the time stamp of the maximum C_N. The maximum C_N 1.07 was obtained at wind angle 320°. This indicates the 320° wind direction was critical for the general truss region of the contemporary representative house. The C_N from the standard AS/NZS 1170.2 (2011) at wind angle 320° was 1.05 and that was similar to the maximum C_N obtained from the wind tunnel study (i.e. C_N at T1_R). This indicates that the AS/NZS 1170.2 (2011)

provides sufficient design wind pressure to determine the truss hold-down force by using influence coefficient β_i from the single truss analysis.

Table 7.1. Maximum hold-down force at general trusses' T1, T2, T3 and T4 supports

Details	RWCs locations							
	T1_L	**T2_L**	**T3_L**	**T4_L**	**T1_R**	**T2_R**	**T3_R**	**T4_R**
C_N	0.98	0.83	0.89	0.84	1.07	0.77	0.96	0.88
Time Stamp	9208	9205	9207	9207	2704	2704	2711	2702

7.1.1 Wind loads on the RWC by using load sharing

The truss hold-down forces obtained from AS/NZS 1170.2 (2011) and traditional design method (i.e. using wind tunnel data and single truss analysis influence coefficients) were similar. However, the reaction forces at the truss supports will be dependent on the structural system's response and the fluctuating wind loads, which may create different reaction forces. The influence coefficient β_i was obtained from the single truss analysis, which considered pin support at one end and roller support at the other end. In practice, the truss supports in the house did not act as a pure pin or roller support and they may behave as combination of pin and roller. The applied loads on a truss of a roof is shared to the adjacent trusses through the structural elements in the house structural system and this load sharing was not considered when calculating β_i by way of single truss analysis. These load sharing and different supports' boundary conditions behavior may generate a different β_i, which will affect the truss hold-down forces. Therefore, this study used the full-scale tests results to determine β_i for the general truss of the representative house.

The time history of the vertical reaction forces at the bottom plate supports of the general truss region of the contemporary house was obtained by using the influence coefficients of the full-scale test (Chapter 5, Section 5.4), the wind pressure distribution, and tributary area. The pressure coefficient (C_p) obtained from the wind tunnel study needed to be multiplied by the full-scale wind pressure to determine the reaction forces for the full-scale house. The regional gust wind speed needed to be converted to mean velocity by dividing the gust wind speed by the gust factor (G_u) to calculate the full-scale wind

pressure at the roof surface. This gust factor (G_u) was obtained from the turbulent intensity (I_{uu}) measured in the wind tunnel by using Equation 7.7 given by Holmes et al (2014).

$$G_u = 1 + 3.4\, I_{uu} \tag{7.7}$$

The turbulent intensity (I_{uu}) and the gust factor (G_u) at the mid roof height 3.5m was 0.32 and 2.09 respectively. This gust factor (G_u), gust wind speed and pressure coefficient (C_p) were used to determine the truss hold-down forces for the general truss region of the representative house at each approach wind direction.

Wind pressure distributions on the eight general trusses were considered (the region is highlighted in a rectangular box in Figure 7.3) to evaluate the wind load on the batten to truss connection of Trusses T1, T2, T3 and T4. The maximum wind load on the batten to truss connection was again obtained at a wind angle of 320^o.

Figure 7.4 shows the time history of the vertical reaction force at Stage S7, at gust wind speed 57 m/s and wind angle of 320^o, for the windward side bottom plate supports (i.e. T1_L, T2_L, T3_L and T4_L), and were located in-line with the RWC of Trusses T1, T2, T3 and T4 respectively. Figure 7.5 shows the leeward side bottom plate supports (i.e. T1_L, T2_L, T3_L and T4_L) vertical reaction force. Figures 7.4 and 7.5 show the maximum vertical reaction load obtained at a same time for the leeward side bottom plate supports, whilst it was obtained at different times in windward side supports. Figures 7.4 and 7.5 also show the maximum reaction force was similar at both windward and leeward side each trusses' support, and occurred at a different time.

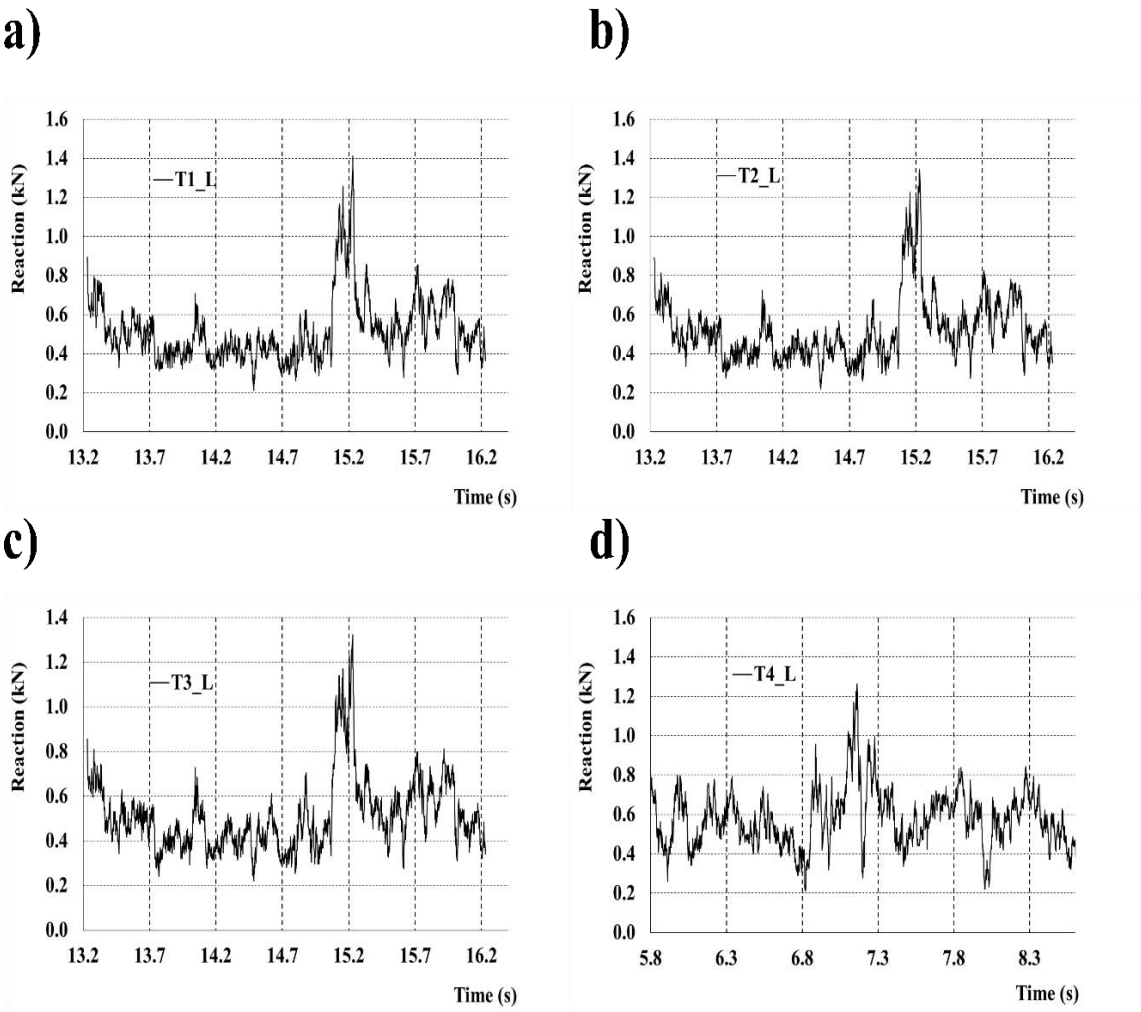

Figure 7.4. Vertical reaction load time history for windward side supports at Stage S7: a) T1_L, b) T2_L, c) T3_L and d) T4_L at a wind speed of 57 m/s and a 320^{o} wind angle

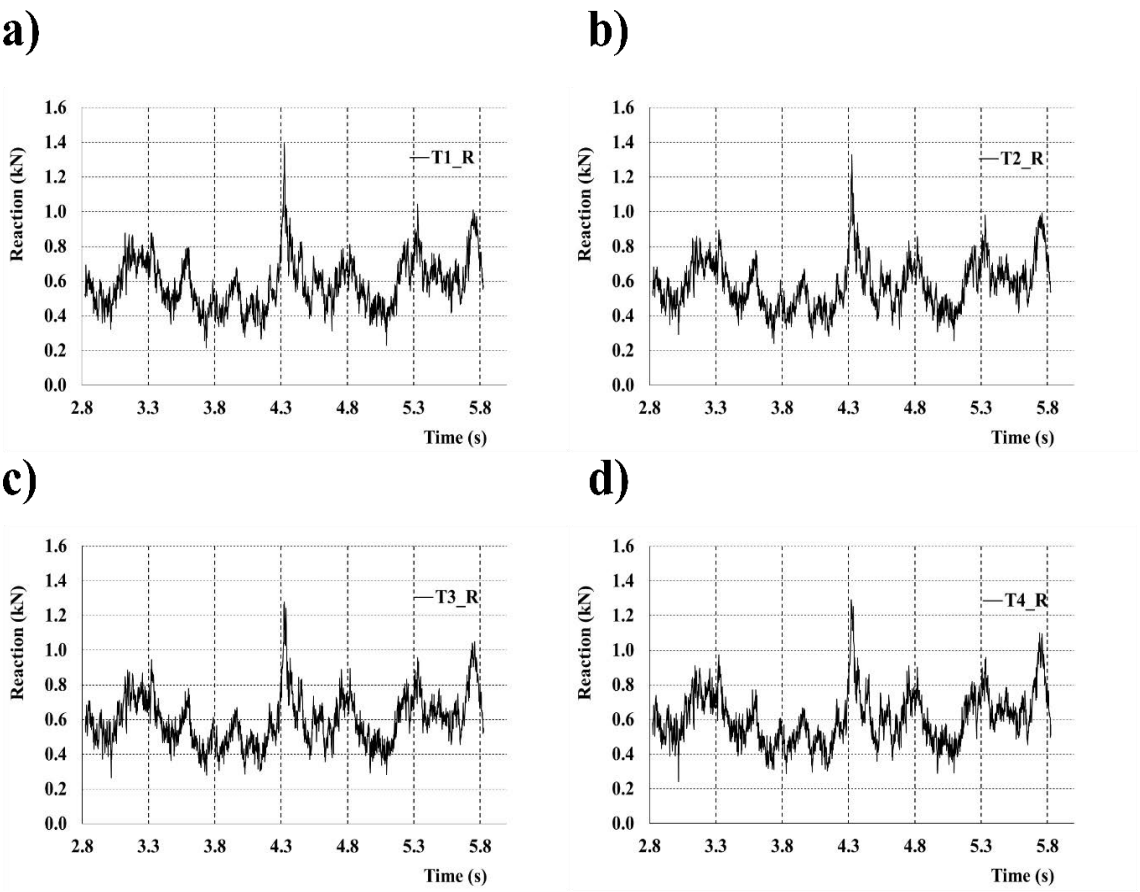

Figure 7.5. Vertical reaction load time history for leeward side supports at Stage S7: a) T1_R, b) T2_R, c) T3_R and d) T4_R at a wind speed of 57 m/s and a 320^{o} wind angle

Table 7.2 shows the time stamp for the maximum C_N occurred at the load cells' (i.e. windward side supports T1_L, T2_L, T3_L, and T4_L, and leeward side supports T1_R, T2_R, T3_R and T4_R) for all construction stage and single truss analysis. This table shows the maximum C_N 1.07 was obtained at leeward side support T1_R from the single truss analysis (i.e. the normal design approach to calculate the reaction forces at the truss support). This maximum C_N of T1_R was less than that of the windward side support T1_L for single truss analysis and similar behaviour was showed at Stage S3. When lining elements are installed to the test structure, the maximum C_Ns obtained for each trusses' were similar in both windward and leeward side supports and occurred at different times. This is indicates that the lining elements reduced the peak load by about 15% at a single support by sharing the load to adjacent trusses. Consequently, these lining elements reduce the peak load at each individual RWC and provides resistance against the failure of the individual RWC and whole house structure to windstorms.

Table 7.2. Maximum reaction load at bottom plate support with a 320^o wind angle

Details		Reaction locations							
		Windward side				Leeward side			
		T1_L	T2_L	T3_L	T4_L	T1_R	T2_R	T3_R	T4_R
C_N	Traditional design method	0.98	0.83	0.89	0.84	1.07	0.77	0.96	-0.9
Time Stamp		9208	9205	9207	9207	2704	2704	2711	2702
C_N	Stage S3	0.99	0.93	0.93	0.89	1.03	0.98	0.93	0.95
Time Stamp		9208	9207	9207	9207	2704	2704	2711	2702
C_N	Stage S4	1.11	1.05	1.05	1.00	1.11	1.05	0.99	1.01
Time Stamp		9208	9207	9207	4477	2704	2704	2702	2702
C_N	Stage S5	0.98	0.94	0.93	0.89	0.99	0.94	0.90	0.91
Time Stamp		9208	9207	9207	4477	2704	2704	2704	2702
C_N	Stage S6	0.92	0.88	0.87	0.83	0.92	0.89	0.86	0.86
Time Stamp		9208	9207	9207	9202	2704	2704	2704	2702
C_N	Stage S7	0.90	0.85	0.84	0.80	0.88	0.84	0.81	0.82
Time Stamp		9208	9207	9207	4477	2704	2704	2704	2702

Figures 7.6 and 7.7 illustrate the pressure coefficients (C_p) for the time stamp 2704 and 9208 (i.e. maximum hold-down force obtained at T1_R) respectively, and the wind angle 320^o. At wind angle 320^o, the leeward side support experiences the high reaction force (i.e. T1_R) due to the high suction pressure at the leeward side and the positive pressure at the leeward side eaves (Figure 7.6). Windward side truss support T1_L experience high uplift load when compared other trusses support at windward side at time stamp 9208. This was due to the high suction pressure occurred at the surrounded region of the T1_L (Figure 7.7)

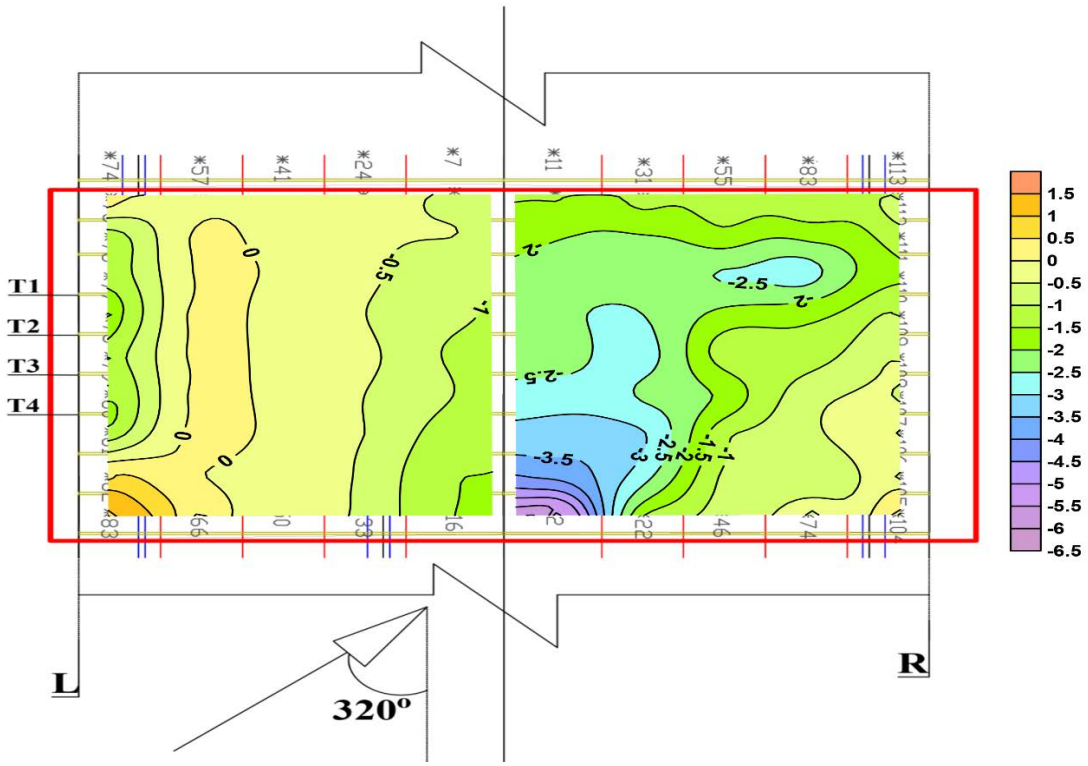

Figure 7.6. C_p variation on the general truss region roof at the time stamp 2704

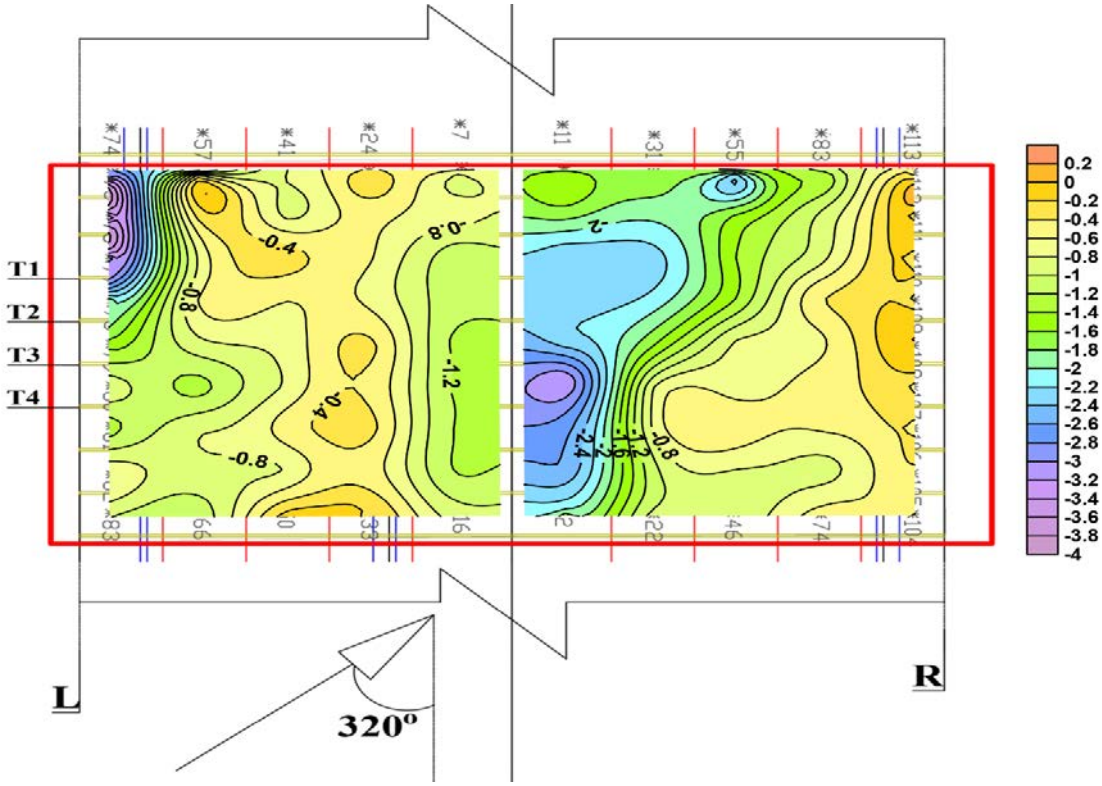

Figure 7.7. C_p variation on the general truss region roof at the time stamp 9208

7.2 Truss hold-down forces

The C_N at the RWCs (i.e. truss hold-down coefficients) of the general truss region of the contemporary representative house were derived from Equation 7.4, with wind tunnel data and influence coefficients obtained from the FEM test structure (Chapter 6, Section 6.5). Table 7.3 shows the maximum C_N for the windward and leeward side RWCs and time stamp for the maximum C_N occurring at wind angles 210^o, 220^o and 320^o. This table also shows the maximum hold-down force obtained at different times, wind directions and truss supports. The maximum C_N 1.21 was obtained at wind angle 220^o on the windward side RWC (T4_R) at time stamp 9652. However, the traditional design method, the maximum C_N (i.e. 1.07) was obtained at wind angle 320^o. This is due to the derived influence coefficients' variation between the single truss analysis and FEM of the test structure. As FEM consider the load sharing to derive the influence coefficients and it was not considered in the single truss analysis, the boundary conditions at the RWCs also different in the FEM compared to the single truss analysis. This will generate different influence coefficients in FEM compared to that of the single truss analysis. The load sharing from large tributary area, differences in the supports' boundary conditions, and fluctuation wind loads, were the reason for the maximum C_N obtained from the influence coefficients of the FEM compared to that of the traditional design method. This indicates that the load sharing of the timber-framed structure changed the critical wind direction (i.e. where maximum truss hold-down force obtained) derived from the traditional method. Table 7.3 also shows that the maximum C_N of windward side RWCs (i.e. at wind angle 210^o and 220^o connections T1_R, T2_R, T3_R and T4_R; at 320^o wind angle connections at T1_L, T2_L, T3_L and T4_L) experiences higher wind loads compared to that of leeward side RWCs.

Table 7.3. Maximum reaction load at the RWC for wind angles 210°, 220° and 320°

Details	C_N measured locations							
	T1_L	**T2_L**	**T3_L**	**T4_L**	**T1_R**	**T2_R**	**T3_R**	**T4_R**
C_N at wind angle 210°	0.98	0.96	0.90	0.86	1.11	1.11	1.13	1.17
Time Stamp	12916	12916	12915	12918	9902	9902	12911	12911
C_N at wind angle 220°	0.86	0.85	0.86	0.88	1.06	1.04	1.12	1.21
Time Stamp	5801	5801	1978	1978	18516	18516	9652	9652
C_N at wind angle 320°	1.03	0.97	0.97	0.93	1.00	0.95	0.91	0.91
Time Stamp	9208	9207	9207	4477	2704	2704	2704	2702

Figure 7.8 illustrates the pressure coefficients (C_p) for the time stamp 9652 (i.e. maximum hold-down force obtained at T4_R, and the wind angle 220°). At wind angle 220°, the windward side support experienced high reaction force (i.e. T4_R) due to the high suction pressure at the windward side and the positive pressure at the windward side eaves. This figure also shows that high suction pressure occurred at the apex region (i.e. location of the Batten B6 in the full-scale test structure and FEM) of the trusses T3, T4 and T2. As Figure 6.14 (Chapter 6) illustrates that the loading along the battens which were located either side of the ridge line closer to apex of truss is influenced to the both loaded and non-loaded side RWCs. Thus, the influence coefficients of non-loaded side trusses' RWCs were higher and/or similar to that of loaded side trusses' RWCs when load was applied along the Batten B7 and B8. This was due to the RWCs stiffness variation between the loaded and non-loaded side RWCs. This higher and/or similar influence coefficients was the reason for the high percentage of load was shared to the windward side supports RWCs (i.e. T1_R, T2_R, T3_R, and T4_R) than that of the leeward side when high suction pressure occurred at the apex region of the contemporary house. This

is also the reason for the high truss hold-down forces obtained at the windward side trusses' RWCs compared to those of the leeward side RWCs.

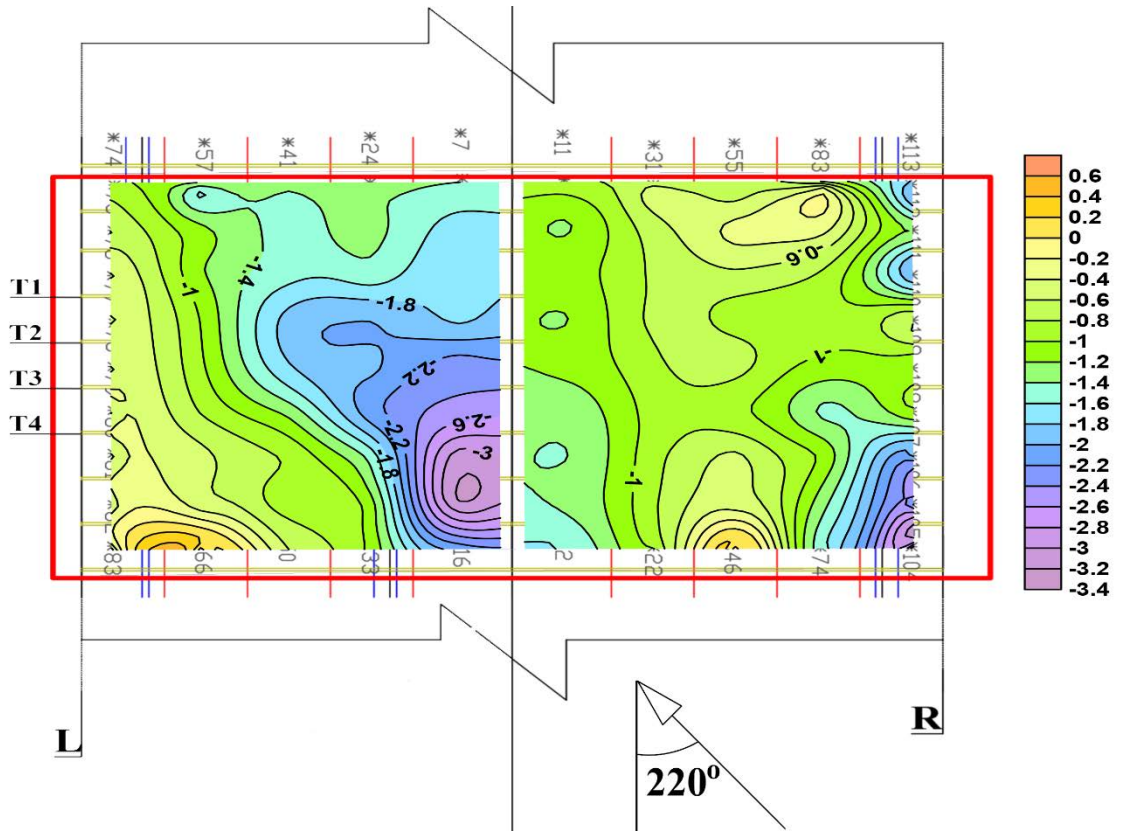

Figure 7.8. C_p variation on the general truss region roof at the time stamp 9652

The maximum truss hold-down forces of the RWCs of the general truss regions were obtained from the influence coefficients of the FEM of the test structure at a wind speed of 57 m/s, with wind angle 220^o and compared with the maximum truss hold-down forces of the traditional design method and AS/NZS 1170.2 (2011). Table 7.4 shows the comparison between the derived maximum truss hold-down forces from the traditional design method, method using influence coefficients of the FEM of test structure and AS/NZS 1170.2 (2011). This table shows that from the method using influence coefficients of the FEM of the test structure, traditional design method and AS/NZS 1170.2 (2011), the maximum truss hold-down force was obtained at wind speed 57 m/s, with a wind angle of 220^o at the windward side RWC (i.e. T4_R). Moreover, the maximum truss hold-down force of RWC, T4_R was similar in both from traditional design method and AS/NZS 1170.2 (2011), whilst it was about 15% less than the method using influence coefficients of the FEM of the test structure. This is because of the variations in the influence coefficients and between the single truss analysis and FEM of

the test structure. Moreover, the loads shared from the large tributary area of adjacent trusses also the reason for high truss hold-down force obtained the method using influence coefficients of the FEM. This indicates that the standard and traditional design methods underestimate the truss hold-down force of the RWCs. The FEM of the individual connection model (detailed in Appendix C) provide the maximum uplift capacity of the roof to wall triple grip connection as 1.50 kN, when the connection subjected to combination loads. This uplift capacity was about 20% less than the truss hold-down force (i.e. 1.91 kN) of the general trusses' RWC of the Brisbane region house at wind speed 57 m/s, with a wind angle of 220°. This indicates that the general truss region of the roof structure was vulnerable at wind angle 220°.

Table 7.4. Comparison of the maximum truss hold-down forces between the FEM of test structure, single truss analysis and AS/NZS 1170.2 (2011)

Wind angle 220°		**Trusses locations**							
		Leeward side				**Windward side**			
		T1_L	**T2_L**	**T3_L**	**T4_L**	**T1_R**	**T2_R**	**T3_R**	**T4_R**
C_N	From β_i of FEM of test structure	0.86	0.85	0.86	0.88	1.06	1.04	1.12	1.21
Hold-down force (kN) at wind speed of 57 m/s		1.35	1.34	1.36	1.39	1.68	1.64	1.77	1.91
C_N	From traditional design method	0.79	0.80	0.79	0.81	0.99	0.91	1.02	1.06
Hold-down force (kN) at wind speed of 57 m/s		1.24	1.27	1.24	1.27	1.57	1.43	1.61	1.68
C_N	From AS/NZS 1170.2 (2011)	0.83	0.83	0.83	0.83	1.06	1.06	1.06	1.06
Hold-down force (kN) at wind speed of 57 m/s		1.32	1.32	1.32	1.32	1.68	1.68	1.68	1.68

Construction defects were introduced on the RWC of the FEM to evaluate the load sharing and truss hold-down forces of the general truss region of the contemporary representative house. Three types of FEMs were developed (details and results are detailed in the Appendix D, section D.5). Based on the FEMs, the vertical influence coefficients were obtained at the RWC for three different cases (Table 7.5). For each case, C_N of the general truss supports of the contemporary house was obtained from vertical influence coefficients and wind tunnel data. Table 7.6 presents the maximum C_N at wind angle 220^o for Truss T3's RWCs and C_N of Trusses T1, T2, T4, T5 at the same time. This table shows that the C_N s of Truss T4's supports were similar in both Cases 2 and 3. This is because the vertical stiffness of the RWC was similar in both single and double nails missing RWC, when the applied load at 1kN (See Figure D.11, Appendix D).

Table 7.6 also shows that when comparing C_N of "Ideal" RWC (i.e. Case 1), both missing single nail (i.e. Case 2) and the combination of missing single and double nails (Case 3) on the RWC increase the hold-down force at the adjacent truss (i.e. T4_R) by about 10%. This is indicates that the peak load at the general truss regions RWC was increased by about 10% when the adjacent truss that has construction defects (i.e. missing a nail and /or nails).

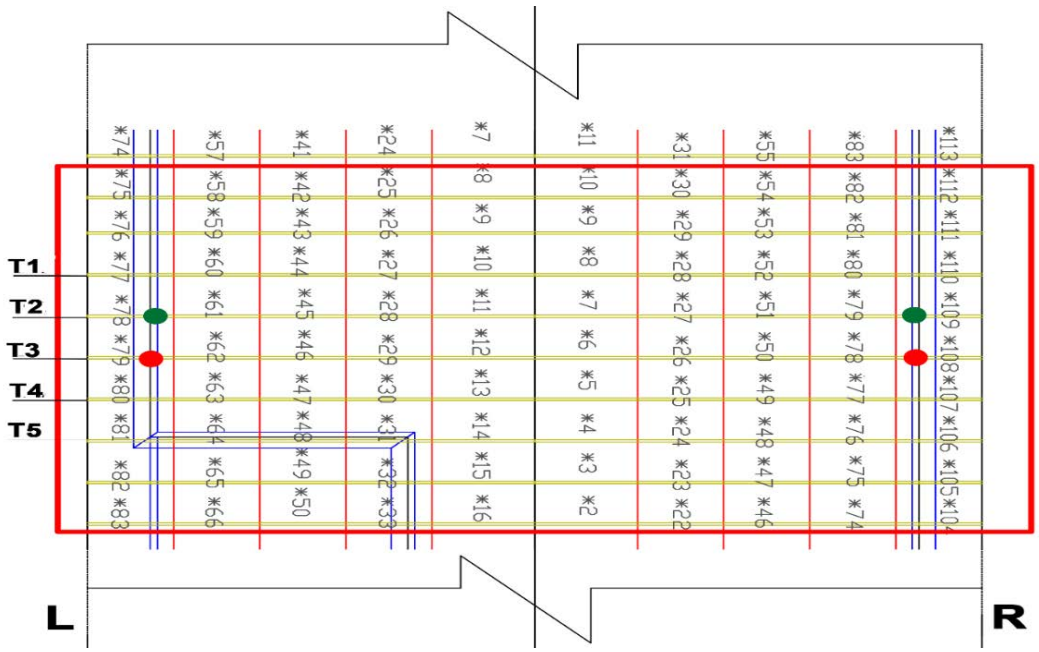

Figure 7.9. General truss region of the contemporary representative house, circles showing the defective RWC locations

Table 7.5. Details of the general truss region with and without construction defects on the RWC

Details	
Case 1	Using "Ideal" roof to wall triple grip connection for all the RWCs
Case 2	Using single nail missing roof to wall triple grip connection for RWCs of Truss T3 (Figure 7.9)
Case 3	Using two nail missing (i.e. one on the top-plate and one on the truss) roof to wall triple grip connection for RWCs of Truss T2 and single nail missing roof to wall triple grip connection for RWCs of Truss T3 (Figure 7.9)

Table 7.6. C_N at the RWCs of the general trusses when the maximum C_N obtained at the Truss T3 at time stamp 9652 from the wind tunnel data

Wind angle 220°	**C_N**									
	Leeward side					**Windward side**				
	T1_L	**T2_L**	**T3_L**	**T4_L**	**T5_L**	**T1_R**	**T2_R**	**T3_R**	**T4_R**	**T5_R**
Case 1 (Ideal)	0.65	0.66	0.63	0.62	0.64	0.24	0.85	0.98	1.16	1.04
Case 2 (Single nail)	0.66	0.73	0.46	0.69	0.66	0.25	0.94	0.74	1.27	1.06
Case 3 (Single $ two nails)	0.77	0.47	0.52	0.72	0.70	0.29	0.63	0.81	1.29	1.15

7.3 Summary of the wind load sharing

This study focuses on the RWC response and load sharing from the roof to foundation of the general truss region of the contemporary house. The reaction forces and truss hold-down forces were obtained using wind tunnel data and influence coefficients. Influence coefficient β_i from the single truss analysis, full-scale tests and the FEM of the test structure were used to calculate the truss hold-down forces. The truss hold-down forces were also derived from the standard AS/NZS 1170.2 (2011). Results show that the

maximum truss hold-down forces obtained from AS/NZS 1170.2 (2011) and traditional design method were similar. However, this maximum truss hold-down force was about 15% less than that derived from the influence coefficients of the FEM of the test structure. This was due to load sharing and the supports' boundary condition differences between the FEM of the test structure and single truss analysis. This indicates that the load sharing from the large tributary area generates higher load effect on the RWCs than the consideration of single truss tributary area (traditional method). The truss hold-down force obtained from the influence coefficients of the FEM of the test structure indicates that the standard AS/NZS 1170.2 (2011) underestimates the truss hold-down forces of the general trusses' RWCs. The general truss region RWC's experienced about 10% high wind load when the adjacent trusses missed a single and/or double nails on the RWC. This will increase the vulnerability of houses to windstorm.

CHAPTER 8: CONCLUSIONS AND RECOMMENDATIONS

The roof of timber-framed houses experience large uplift load resulting from internal and external pressure during wind storms. The roof to wall connection (RWC) is a vulnerable part in the load path of the timber-framed structure, as it experiences lateral and vertical loads from the roof as well as lateral load from the wall. Previous research studies have identified how the loads are transferred from roof to wall, yet they were unable to quantify how much load is transferred from the roof to wall through the RWCs.

This study defines the load sharing between the roof and the wall of contemporary Australian timber-framed houses. Experimental tests and numerical models analysis were used in the investigation of both the individual connections and as part of a complete structural system. This Chapter highlights the key findings, implications and areas of potential further research.

8.1 Key findings

- Full-scale tests were carried out on a structure that is part of a representative brick veneer contemporary house. Tests were carried out at each stage of construction: bare frame followed by the installation of roof battens, cladding, wall lining, ceiling, etc. These construction stages were used to assess the contribution of the structural and lining (i.e. ceiling, ceiling cornice and wall lining) elements to the load sharing and response of the timber-framed house structure to wind loading. Through the full-scale test, the following conclusion are made:

  - Load distribution obtained in the full-scale test was a function of the RWC stiffness and, trusses' and battens' locations within the timber-framed house.
  - High vertical reaction forces were measured at the truss support on the loading side in the initial stage of the test (i.e. bare truss frame only). This reaction force was about 80% of the vertical component of the applied load, which then reduced by about 50% when battens were added to the system and increased by about 10% when the roof cladding was installed.

- The vertical reaction force at the loaded truss support on the loading side with structural elements (i.e. truss, batten and roof cladding) was reduced by about 20% when lining elements (i.e. ceiling, wall lining and ceiling cornice) were added to the system.
- The ceiling contributed significantly to vertical load sharing of the timber-framed house, and it also doubled the vertical stiffness of RWC of the house with structural elements (i.e. truss, battens and roof cladding) only. This is because the self-weight of the ceiling reduced the vertical movement of the connection.
- The RWC experienced high vertical reaction force and displacement due to loads applied near the edge of the roof, thus the RWCs were vulnerable to high uplift wind loads that are applied near the eaves of the roof.
- The loads acting on the roof tributaries supported by two adjoining trusses should be accounted for when assessing the wind loads and response of a RWC of a truss.
- The combination of the vertical and lateral force caused the different failure modes on the roof to wall triple grip connections compared to that of only vertical loading on the individual connection tests. This indicates that this connection does not behave as a pinned joint but it more like a continuous moment resisting connection.

- Triple grips and truss grips are widely used in Australian residential construction. The variation in the strength with a range of construction defects were also studied. From field surveys, missing nails and grouping of nails were the most common construction defects in the roof to wall triple grip connections. The partially driven nail teeth were the common construction defects in the truss grip connections. Laboratory tests on the RWCs and the joints between the plasterboard and timber were carried out. The following conclusions are made from the individual joint tests:

  - Changing nail type from hand nail to gun nail on the "Ideal" connection does change the failure mode location, from truss to top plate. This also causes a reduction in the design uplift capacity by about 20%.
  - Variation in timber species in the connection does effect the structural response and the uplift capacity. About 24% uplift capacity reduction has been observed when the timber material changed from Australian MGP10 radiata pine to spruce pine.

- Defective triple grip connections with a single missing nail, have about 90% of the uplift capacity of the "Ideal" connection.
- Grouping nails together on the top plate in the gun nailed connection will reduce the uplift capacity and stiffness of the connection. This reduces the "Ideal" connection uplift capacity by about 20%.
- If two nails are missing (i.e. one nail on to the truss and other on to the top plate), the uplift capacity and stiffness of the hand nailed triple grip connections are reduced by about 40%. The field survey found that this type of construction defect was a common occurrence.
- The laboratory tests on the shear and tension load specimens of timber to plasterboard joint showed that the glue joint was stiffer than the screw joint.
- The response of the glue joint was more brittle, whilst the screw joint behaved as ductile to shear loading. This indicates that brittle failure on the glue joint will affect the load transfer through the wall lining.

- 3D finite element models (FEMs) were developed for part of the contemporary timber framed house and roof to wall triple grip and truss grip connections by using ABAQUS (6.12-3) FE software. Results (i.e. load sharing, contribution of the non-structural elements on the load sharing, roof to wall connection vertical displacement and reaction forces) obtained from the FEMs were compared with the experimental tests and showed good agreement.

  - The partially driven nail teeth (i.e. 50% of the total length) on the top plate or truss or both truss and top plate reduced the strength, stiffness and design capacity by about 70% of the "Ideal" connection.
  - The RWC was subjected to a combination of the lateral and vertical loads, and the uplift capacity was about 55% less than that of the only vertical loading connection.
  - The vertical reaction force influence coefficients of the RWCs showed that the loading on battens located at near the ridge line significantly affected the vertical reaction forces of the both loaded and non-loaded side RWCs'. This is indicates the high suction pressure on the ridge region will increase the vertical reaction forces of the both windward and leeward side RWCs of timber-framed house.

- The maximum truss hold-down force derived from the traditional method and AS/NZS 1170.2 (2011) was about 15% less than that derived from the influence coefficients of the FEM of the test structure. This was due to load sharing and the supports' boundary condition differences between the FEM of the test structure and single truss analysis. This truss hold-down force variation indicates that the standard AS/NZS 1170.2 (2011) underestimates the truss hold-down forces of the general trusses' RWCs.
- The load sharing from the large tributary area generates the higher wind loads effects on the RWC than just considering a single truss tributary area (i.e. traditional design method).
- Structural response of the RWC obtained in the individual connection FEM and the full-scale test was different. This is because the individual connection model only experienced the vertical load but the full-scale test structure experienced both lateral and vertical loads.
- The construction defects on the RWCs (i.e. missing a single nail and/or double nails) increased the peak load at the adjacent truss roof to wall connection by about 10% and that increased the vulnerability of houses to windstorm.

8.2 Implications and Recommendations for further research

The findings from this research have implications and recommendations for future research into the structural response and performance of timber-framed structure and their inter component connections.

- When the structural and lining elements are added to the system, the influence coefficients for vertical and lateral reaction force on a single truss change due to load sharing. The influence coefficients obtained in this study can be used to evaluate the wind load sharing and truss hold-down force for the timber-framed house with metal roof cladding.
- The quantified load at the top-plates' (i.e. RWCs) and bottom plates' supports, when the structural and lining elements were installed to the test structure, could be used to design and analyse of the timber-framed house to wind loads. This can also be used to validate the experimental test and numerical model results of the individual elements and partial assembled components (i.e. wall, roof, etc.).

- The full-scale test results are a good representation to assess the structural response of gable roof. However, mainly the contemporary houses in Australia are constructed with a combination of gable and hip roofs. Thus, the testing of different roof shapes would be useful to evaluate the vulnerability of the contemporary house to windstorms.
- The wind load at the top-plate generally transfers to the bracing wall by diaphragm action of the ceiling and roof cladding. The effect of this diaphragm action to the vertical load sharing is not considered in this research. Therefore, further research studies are needed to evaluate the influence of diaphragm action of the ceiling and roof cladding to the vertical load sharing of contemporary timber-framed houses.
- The FEM analysis of the full-scale test structure results shows good agreement with that of the full-scale test. This model can be used to predict the roof to wall connection response and truss hold-down force variation with construction defects and different truss bays. The outcomes will provide the effect of the construction defects on the load sharing and reaction forces' influence coefficients of the timber-framed structure.
- In this study, the fatigue effects on the roof to wall triple grip connection were not investigated. During windstorms, the incremental withdrawal of nails in this RWC could create fatigue failure on this connection. However, this is not expected to be significant but further studies are needed to investigate the fatigue effects on the roof to wall triple grip connection.
- The uplift capacities of the roof to wall triple grip connection obtained in the individual connection laboratory test and FEM show good agreement with the AS 1648.2 (2010) specified uplift capacities. However, the study has found that the failure modes of the loaded and non-loaded side roof to wall triple grip connections of the full-scale test structure were different. This is because the RWCs of the full-scale test structure experienced combination loading (i.e. lateral and vertical loads). This combination load reduces the uplift capacity of the roof to wall triple grip connection by about 50% compared to AS 1648.2 (2010) specified uplift capacity. These uplift capacities specified by the standards and the manufacturer were obtained by vertical loading tests. Thus, this study suggests that the standards and the manufacturer should consider the combination load effects on the RWCs to provide more realistic uplift capacity.

- As this study shows that construction defects (i.e. missing nails) cause significant reduction on the uplift capacities and stiffness of RWCs. This stiffness reduction creates variations in load sharing and transmission of the whole structure. These load sharing variations increase the truss hold-down force of adjacent trusses. Therefore, the construction industry, and National Construction Code of Australia need to demonstrate the effect of these construction defects to builders and public through their specifications, trades educations and community awareness programs like Cyclone Sunday, etc.
- Finally, based on the static applied loads, the current study examined the structural response of a timber-framed structure and RWCs. The findings from this study could be used for design and to develop a vulnerability model to windstorms. In addition, testing with dynamic loads on this structure and combination loading on the individual RWC would be useful to contrast the results obtained from this study.

REFERENCES

ABAQUS, FEA Computer software, Version 6.12-3, Product of Dassault Systemes Simulia Corp., Providence, RI, USA.

Ahmed, S., Canino, I., Chowdhury, A., Mirmiran, A., and Suksawang, N. (2011). "*Study of the Capability of Multiple Mechanical Fasteners in Roof-to-Wall Connections of Timber Residential Buildings*." Pract. Period. Struct. Des. Constr., 16(1), 2–9.

Barton, A.D., Duffield, C.D., and Hanks, P.D. (1994). "*Shaking Table Tests on Domestic Steel Structures with Varying Framing Details*." Proceedings of the Australasian Structural Engineering Conference, Sydney, pp. 445 – 449.

BCA (2011). Building Code of Australia, ABCB, Canberra.

Boughton, G.N., Henderson, D.J., Ginger, J.D., Holmes, J.D., Walker, G.R., Leitch, C., Somerville, L.R., Frye, U., Jayasinghe, N.C. and Kim, P. (2011*). "Tropical Cyclone Yasi Structural Damage to Buildings."* Cyclone Testing Station, James Cook University, Townsville ,TR 57.

Boughton, G.N. (1983a). *"Testing of a full-scale house with simulated wind loads."* Journal of Wind Engineering and Industrial Aerodynamics, 14: 103–112.

Boughton, G.N. and Reardon, G.F. (1984). "*Simulated Wind load Test on the Tongan Hurricane House*." Cyclone Testing Station, James Cook University, Townsville. TR 23.

Boughton, G.N. and Reardon, G.F. (1982). "*Simulated Wind Test on a House*." Cyclone Testing Station, James Cook University, Townsville. TR 14.

Boughton, G.N. and Reardon, G.F. (1983b). "*Testing a High Set House Designed for 42m/s Winds*." Cyclone Testing Station, James Cook University, Townsville. TR 19.

Bulleit, W., Rosowsky, D., Fridley, K., and Criswell, M. (1993). "*Reliability of Wood Structural Systems*." Journal of Structural Engineering., 119(9), 2629-2641.

Canino, I., Chowdhury, A., Mirmiran, A., and Suksawang, N. (2011). "*Triaxial Load Testing of Metal and FRP Roof-to-Wall Connectors*." J. Archit. Eng., 17(3), 112–120.

Chen, C.J., Lee, T.L., and Jeng, D.S. (2003). "*Finite element modeling for the mechanical behavior of dowel-type timber joints.*" Computers and Structures 81, 2731–2738.

Cheng, J. (2004), "*Testing and analysis of the toe-nailed connection in the residential roof-to-wall system*", Forest Prod Journal 54(4), 58-65.

Choi, Y. and LaFave, J. (2004). "*Performance of Corrugated Metal Ties for Brick Veneer Wall Systems*." Journal of Materials in Civil Engineering, 16(3), 202–211.

Chui, Y.H. and Ni, C. (2000), "*Performance of wood joints fastened with power-driven nails*." The 6th World Conference on Timber Engineering, Whistler Resort, Canada.

Chui, Y.H., Ni, C., and Jiang, L. (1998). "*Finite-Element Model for Nailed Wood Joints under Reversed Cyclic Load*." Journal of Structural Engineering., 124(1), 96–103.

Chui, Y.H., and Ni, C. (1997). *"Load-embedment response of timber to reversed cyclic load." Wood Fiber Science., 29(2), 148–160.*

Chowdhury, A., Canino, I., Mirmiran, A., Suksawang, N., and Baheru, T. (2013). "*Wind-Loading Effects on Roof-to-Wall Connections of Timber Residential Buildings*." Journal of Engineering Mechanics, 139(3), 386–395.

Collins, M., Kasal, B., Paevere, P., and Foliente, G.C. (2005a). "*Three dimensional model of light frame wood buildings. I: Model formulation*."Journal of Structural Engineering., 131(4), 676–683.

Collins, M., Kasal, B., Paevere, P., and Foliente, G.C. (2005b). "*Three dimensional model of light frame wood buildings. II: Experimental investigation and validation of analytical model*."Journal of Structural Engineering., 131(4), 684–692.

Davenport, A.G. (1961). "*The Application of Statistical Concepts to the Wind Loading Of Structures*." ICE Proceedings, 19 (4), 449 –472. Forest Product Laboratory, Madison, Wis.

Datin, P.L (2010). "*Structural Load Paths in Low-Rise, Wood-Framed Structures*." PhD Thesis, University of Florida, US.

Datin, P.L. and Prevatt, D.O. (2007). "*Wind uplift reaction at roof to wall connections of wood framed gable roof assembly*." 12th International Conference on Wind Engineering, Cairns, Australia.

De Borst, K., Jenkel, C., Montero, C., Colmars, J., Gril, J., Kaliske, M., and Eberhardsteiner, J. (2013). "*Mechanical characterization of wood: An integrative approach ranging from nanoscale to structure*." Computers and Structures., 127, 53-67.

Department of Housing and Urban Development (HUD). (1993). "*Assessment of Damage to Single-Family Homes Caused by Hurricanes Andrew and Iniki*." U.S., Office of Policy and Development and Research, HUD-0006262.

Dhammika, M. (2003). "*Behaviour and design of profiled steel cladding systems subjected to pull-through failures*". PhD thesis, Queensland University of Technology, Australia.

Dorey, D. B., and Schriever, W. R. (1957). ''*Structural test of a house under simulated wind and snow loads*.'' ASTM Special Technical Rep. No. 210, ASTM, Philadelphia

Doudak, G., McClure, G., and Smith, I. (2012). "*Experimental Evaluation of Load Paths in Light-Frame Wood Structure*." Journal of Structural Engineering., 10.1061/(ASCE)ST.1943-541X.0000439, 258-265.

Foschi, R.O, (1974). *"Load-slip characteristics of nails"*. Wood Science 7(1):69-74.

Foschi, R.O. (2000). "*Modeling the hysteretic response of mechanical connections for wood structures*". Proceedings, World Conference on Timber Engineering, Whistler, B.C. Canada.

Fowler, R. (2003). "*Fatigue damage to metal battens subjected to simulated wind loads*". Bachelor of Civil Engineering thesis, James Cook University, Townsville, Australia.

Gad, E.F., Duffield, C.F., Hutchinson, G.L., Mansell, D.S., and Stark, G. (1999). "*Lateral Performance of Cold-Formed Steel-Framed Domestic Structures*." Journal of Engineering Structures, Vol. 21, No. 1, pp. 83 - 95.

Gad, E.F., Duffield, C.F., Stark, G., and Pham, L. (1995). "*Contribution of Non-Structural Components to the Dynamic Performance of Domestic Steel Framed Structures*." Proceedings of the Pacific Conference on Earthquake Engineering, Melbourne, Australia, pp. 177 - 186.

Ginger, J.D. (1997). *"Internal and net pressures on low-rise full scale buildings*." Cyclone Testing Station, James Cook University, Townsville ,TR 45.

Ginger, J., Henderson, D., Humphreys, M., and Parackal, K. (2015). "*Climate Adaptation Engineering for Extreme Events (CAEX)*, *Project 1.1 Progress report #4*." Cyclone testing station, James Cook University, Australia.

Ginger, J.D., Reardon, G.F., and Whitbread, B.J. (2000). "*Wind load effects and equivalent pressures on low-rise house roofs"*. Engineering Structures, 22 (6). pp. 638-646.

Ginger, J.D., Reardon, G.F. and Whitbread, B.J. (1998). *"Wind loads on a typical low-rise house*." Cyclone Testing Station, James Cook University, Townsville ,TR 46.

Guha, T.K. and Alan Kopp, G. (2012). "An Elasto-Plastic Failure Model of Roof-To-Wall-Connections in Residential Wood-Frame Buildings under Realistic Wind Loads." Journal of Wind and Engineering., 9(2), 1-13.

Guha, T.K. and Kopp, G.A. (2013)., "*Storm duration effects on roof-to-wall-connection failures in residential, wood-frame, building roofs*." The 12th Americas Conference on Wind Engineering (12ACWE), Seattle, Washington, USA,

Gupta, A. and Kuo, G. (1985). "*Behavior of Wood-Framed Shear Walls*." Journal of Structural Engineering., 111(8), 1722–1733.

Gupta, A.K., and Kuo, G.P. (1987). ''*Modelling of a wood-framed house*.'' Journal of Structural Engineering., ASCE, 113(2), 260–278.

Gurley, K., Davis, R.H., Ferrera, S.P., Burton, J., Masters, F., Reinhold, T., Abdullah, M., (2006). "*Post 2004 hurricane field survey – an evaluation of the relative performance of the Standard Building Code and the Florida Building Code*." *Proc. 2006 ASCE/SEI Structures Congress*, St. Louis.

Gyprock Australia. (2014). "*Residential installation guide*", [Online]. Available from: http://www.gyprock.com.au/Pages/For-Homeowners.aspx [Accessed 26th November 2014].

Henderson, D.J. (2010). "*Response of pierced fixed metal roof cladding to fluctuating wind loads.*" PhD thesis, James Cook University, Townsville, Australia.

Henderson, D. J. and Ginger, J. D. (2011). "*Response of pierced fixed corrugated steel roofing systems subjected to wind loads*." Engineering Structures., 33, 3290-3298.

Henderson, D.J., and Ginger, J.D. (2005). "*Fatigue failure of roof components subjected to wind loading*." Australian Structural Engineering Conference, Newcastle.

Henderson, D.J., Ginger, J.D., Boughton, G.N., Leitch, C., and Falck, D. (2006*). "Tropical Cyclone Larry Damage to buildings in the Innisfail area*." Cyclone Testing Station, James Cook University, Townsville, TR 51.

Henderson, D.J., and Ginger, J.D. (2008). "*Role of building codes and construction standards in windstorm disaster mitigation"*. Australian Journal of Emergency Management, 23 (2). pp. 40-46.

Henderson, D.J., Ginger, J.D., Kopp, G.A., and Morrison, M.J. (2009). "*Application of simulated cyclonic wind loads on roof cladding*." 11th Americas Conference on Wind Engineering, Puerto Rico.

Henderson, D.J., Kopp, G.A, and Morrison, M.J. (2012) "*Full-scale testing of low-rise, residential buildings with realistic wind loads"*. Journal of Wind Engineering and Industrial Aerodynamics, 104-106, 25-39.

Henderson, D.J., Morrison, M.J., and Kopp, Gregory A. (2013)."*Response of toe-nailed, roof-to-wall connections to extreme wind loads in a full-scale, timber-framed, hip roof*". Journal of Engineering Structures. 56, 1474-1483.

He, M., Lam, F., and Foschi, R. (2001). "*Modeling Three-Dimensional Timber Light-Frame Buildings*." Journal of Structural Engineering., 127(8), 901–913.

Holmes, J.D. (1979), *"Mean and Fluctuating Internal Pressures Induced by Wind"*, Proceedings of the Fifth International Conference on Wind Engineering, Fort Collins, Colorado, USA, pages 435-450, July 1979.

Holmes J.D. (2002)."*Fatigue life under along-wind loading — closed-form solutions*". Engineering Structures, 24. pp. 109–114.

Holmes, J.D., Andrew, C.A., and Ginger, J.D. (2014). "*Gust durations, gust factors and gust response factors in wind codes and standards*." Wind & Structures no. 19:339-352.

Jayasinghe, N.C. (2012). "*The distribution of wind loads and vulnerability of metal clad roof structures in contemporary Australian houses*." PhD thesis, James Cook University, Townsville, Australia.

Kasal, B., Leichti, R. J., and Itani, R. Y. (1994). ‘‘*Nonlinear finite-element model of complete light-frame wood structures.*’’ Journal of Structural Engineering., ASCE, 120(1), 100–119.

Kasal, B., Collins, M., Foliente, G.C., and Paevere, P. (1999). ‘‘*A hybrid deterministic and stochastic approach to inelastic modelling and analysis of light-frame buildings*.’’ Proc., 1st Int. RILEM Symp. on Timber Engineering., L. Bostrom, ed., RILEM, Cachan, Cedex, France, 61–77.

Keith, E. and Rose, J. (1994). "*Hurricane Andrew—Structural Performance of Buildings in South Florida*." *Journal of Performance of Constructed Facilities*, 10.1061/(ASCE)0887-3828(1994)8:3(178), 178-191.

Khan, M. S., and Suaris, W. (1993). "*Design and construction deficiencies and building code adherence*." Hurricanes of 1992, R. A. Cook and M. Soltani, eds, ASCE, Reston, VA.

Khan, M.A. (2012).“*Load-Sharing of Toe-Nailed, Roof-to-Wall Connections under Extreme Wind Loads in Wood-Frame Houses*.” Master of Engineering Science Thesis, Department of Civil and Environmental Engineering, The University of Western Ontario, London, Ontario, Canada

Kopp, G., Oh, J., and Inculet, D. (2008). “*Wind-Induced Internal Pressures in Houses*”. Journal of Structural Engineering., 134(7), 1129–1138.

Leitch, C., Ginger, J.D., Harper, B., Somerville, L.R., Jayasinghe, N.C. and Kim, P. (2009*). “Investigation of performance of housing in Brisbane following storms on 16 and 19 November 2008”* Cyclone Testing Station, James Cook University, Townsville ,TR 55.

Li, M., Foschi, R., and Lam, F. (2012). “*Modeling Hysteretic Behavior of Wood Shear Walls with a Protocol-Independent Nail Connection Algorithm*”. Journal of Structural Engineering., 138(1), 99–108.

Liew,Y.L., Duffield, C.F., and Gad, C.F. (2002). "*The influence of plasterboard clad walls on the structural behaviour of low rise residential buildings*." Electron J Struct Eng, pp. 1–16.

Liu, H., Saffir, H., and Sparks, P. (1989). “*Wind Damage to Wood-Frame Houses: Problems, Solutions, and Research Needs*.” Journal of Aerospace Engineering.,2(2), 57–70.

Lovisa, A.C. (2015). "*Characterising the fatigue response of corrugated roof cladding"*. PhD thesis, James Cook University, Townsville, Australia.

Mahendran, M. (1989). “*Fatigue behaviour of corrugated roofing under cyclic wind loading*.” Cyclone Testing Station, James Cook University, Townsville. TR 35

Mahendran, M. (1995). “*Wind-Resistant Low-Rise Buildings in the Tropics*.” Journal of Performance of Constructed Facilities., 9(4), 330–346.

Mahendran, M. and Tang, R. (1998). "*Pull-Out Strength of Steel Roof and Wall Cladding Systems*." Journal of Structural Engineering., 124(10), 1192–1201.

McCutcheon, W. J. (1985). "*Raking Deformations in Wood Shear Walls*." Journal of Structural Engineer, ASCE, Vol. 111, No. 2, pp. 257 – 269.

McKinnon, R., Bartlett, F.M., Galsworthy, J.K., St. Pierre , L.M. (2003). "*Wind Loads on Houses a wind tunnel study*." Institute for Catastrophic Loss Reduction, Research Paper Series – No. 32.

Meecham, D., Surry, D., Davenport, A.G. (1991), "*The magnitude and distribution of wind-induced pressures on hip and gable roofs*." Journal of Wind Engineering and Industrial Aerodynamics. 38, 257-272.

Mensah, A.F., Datin, P.L., Prevatt, D.O., Gupta, R. and Vand de Lindt, J.W. (2011). "Database-*assisted design methodology to predict wind induced structural behavior of a light-framed wood building*." Engineering Structures 33 (2): 674-684.

Minor, J.E., (1994). "*Windborne debris and the building envelope*". Journal of Wind Engineering and Industrial Aerodynamics 53, 207-227.

MiTek Australia. (2014). MiTek Australia - Building Construction Connectors, [Online]. Available from: http://www.mitek.com.au/Products/Product.aspx?id=209 [Accessed 17th November 2014].

Morrison, M. J. (2010). "*Response of a Two-Story Residential House under Realistic Fluctuating Wind Loads*." PhD Thesis, Department of Engineering, The University of Western Ontario, London, Ontario, Canada

Morrison, M.J., Henderson, D.J., and Kopp, G.A. (2012). "*The response of a wood-frame, gable roof to fluctuating wind loads.*" Journal of Engineering Structures, 41 . pp. 498-509.

Pinelli, J.P., Gurley, K.R., Subramanian, C.S., Hamid, S.S., Pita, G.L. (2008). "*Validation of a probabilistic model for hurricane insurance loss projections in Florida*." Reliability Engineering and System Safety, 93, 1896– 1905.

Prevatt, D.O., Thompson, A., Roueche, D., Ammons, M. and Doreste, J., (2015). " *The 6th May 2015 Great Plains Tornado Outbreak and Flooding*." Wind Hazard Damage Assessment Team, Engineering School of Sustainable Infrastructure and Environment University of Florida.

Reardon, G. F. (1990). "*Simulated Cyclone Wind loading of a Nu-Steel House*." Cyclone Testing Station, James Cook University, Townsville. TR 36.

Reardon, G. F. (1988). "*Effects on Non-Structural Cladding on Timber Framed Construction*." Proceedings of the International Conference on Timber Engineering, Forest Products Research Society, Madison, pp. 276 - 281.

Reardon, G.F. and Mahendran, M (1988). "*Simulated Wind loading of a Melbourne Style Brick Veneer House*." Cyclone Testing Station, James Cook University, Townsville. TR 34.

Reardon, G. F. (1986). "*Simulated Cyclone Wind loading of a Brick Veneer House*." Cyclone Testing Station, James Cook University, Townsville. TR 28.

Reardon, G.F. (1979). "*The Strength of Batten-To-Rafter Joint*." Cyclone Testing Station, James Cook University, Townsville. TR 2.

Reardon, G. F. and Henderson, D.J. (1996). "*Simulated Wind loading of a two storey Test House*." International Wood Engineering Conference, New Orleans, Louisiana, USA.

Reed, T.D., Rosowsky, D.V., Schiff, S.D. (1997), "*Uplift capacity of light-frame rafter to top plate connections*", Journal of Architectural Engineering ASCE 3(4), 156-163.

Rosowsky, D. and Ellingwood, B., (1991). "*System Reliability and Load Sharing Effects in Light Frame Wood Construction.*" Journal of Structural Engineering.,117(4):1096-1114.

Rosowsky, D.V, and Reinhold, T.A., (1999). "*Rate-of-Load and Duration-of-Load Effects for Wood Fasteners.*"Journal of Structural Engineering., 125(7), 719-724.

Rosowsky, D.V., Reed, T.D. and Tyner, K.G. (1998). "*Establishing Design Values for Uplift Connections in Light-Frame Construction*." Journal of Testing and Evaluation, ASTM, 26(4):426-433.

Rosowsky, D.V. Schiff, S.D. Reinhold, T.A. Sparks, P.R. and Sill, B.L., (2000). "*Performance of Low-Rise Structures Subject to High Wind Loads: Experimental and Analytical Program*." Wind Safety and Performance of Wood Buildings, Forest Products Society, pp. 67-83.

Rosowsky, D.V., Yu, G. and Bulleit, W.M., (2005). "*Reliability of Light-Frame Wall Systems Subject to Combined Axial and Transverse Loads*." Journal of Structural Engineering., 130, 1444-1455.

Scruton, C. (1971). "*Steady and unsteady wind loading of buildings and structures*." Phil. Trans. Roy. Soc. London, A 269. pp. 353-383.

Schmidt, R. J., and Moody, R. C. (1989). "*Modeling laterally loaded light-frame buildings*." J. Struct. Eng., 115(1), 201–217.

Shanmugam, B., Nielson, B.G., Prevatt, D.O. (2009), "*Fragility Statistical and analytical models for roof components in existing light-framed wood structures*", Engineering Structures 31, 2607-2616.

Shanmugasundaram, J., Arunachalam, S., Gomathinayagam, S., Lakshmanan, N. and Harikrishna, P. (2000). "*Cyclone damage to buildings and structures—A case study*." Journal of Wind Engineering and Industrial Aerodynamics, 84(3), 369-380.

Shanmugasundaram, J. and Reardon, J. (1995). "*Strong wind damage due to Hurricane Andrew and its implications*." Journal of Structural Engineering., 22 (1), 49-54.

Shivarudrappa, R. and Nielson, B. (2013). "*Sensitivity of Load Distribution in Light-Framed Wood Roof Systems due to Typical Modeling Parameters*." Journal of Performance of Constructed Facilities., 27(3), 222–234.

Smith, D.J., Henderson, D.J., and Ginger, J.D. (2015). "*Insurance loss drivers and mitigation for Australian housing in severe wind events*." 14th International Conference on Wind Engineering, Porto Alegre, Brazil, June 21-26

Surry, D. (1991). *"Pressure measurements on the Texas tech building: Wind tunnel measurements and comparison with full scale*." Journal of Wind Engineering and Industrial Aerodynamics 38(2-3): 235-247.

Standards Australia (2012), "*AS 4055 Wind Loads for Housing*." Standards Australia, Sydney, NSW.

Standards Australia. (2011). "*AS/NZS 1170.2 Structural Design Action Part 2: Wind Action.*" Standard Australia, Sydney, NSW.

Standards Australia. (2002). "*AS/NZS 1170.2 Structural Design Action Part 2: Wind Action.*" Standard Australia, Sydney, NSW.

Standards Australia. (2010). "*AS1720.1 Timber structures Part 1: Design methods*." Standard Australia, Sydney, NSW.

Standards Australia (2010). "*AS 1684.3 Residential Timber-Framed Construction, Cyclonic Areas*". Standards Australia.

Standards Australia (2010). "*AS 1684.2 Residential Timber-Framed Construction, Non-Cyclonic Areas*". Standards Australia.

Standards Australia (2002). "*AS 1684.1 Residential Timber-Framed Construction, Part 1: Design criteria*". Standards Australia.

Standards Australia (2004). "*AS 4440 Installation of Nailplated Timber roof trusses*". Standards Australia.

Standards Australia (2002), "*AS 2050 Installation of roof tiles*", Standards Australia, Sydney, NSW.

Standards Australia (2001). "*AS 1649 Timber-Methods of test for mechanical fasteners and connectors- Basic working loads and characteristic strengths*", Standards Australia.

Stramit Australia (2014), Corrugated roof and wall cladding product technical manual; Available from: <http://www.stramit.com.au/download-files/ product-technical-manuals> [accessed 17th November 2014].

Stathopoulos, T., Surry, D., and Davenport, A.G. (1979). "*Internal pressurecharacteristics of low-rise buildings due to wind action."* Proc.,5th International Conference on Wind Engineering, Fort Collins, Colo., 451–463.

Taly, N. (2003). "*Loads and load paths in buildings: Principles of structural design*", International Code Council, Country Club Hills, IL.

Thampi, H., Dayal, V., and Sarkar, P. (2011). "*Finite element analysis of interaction of tornado with a low-rise timber building*. Journal of Wind Engineering and Industrial Aerodynamics., 99:369–77.

Tieleman, H.W., Surry, D. and Mehta, K.C. (1996), "*Full/model scale comparison of surface pressures on the Texas Tech experimental building*", Journal of Wind Engineering and Industrial Aerodynamics., 61,1-23.

Tuomi, R. L., and McCutcheon, W. J. (1974). "*Testing of a full-scale house under simulated snow and wind loads*." USDA Forest Service Research Paper FPL-234.

Uematsu, Y., and Isyumov, N. (1999). "*Wind pressures acting on low-rise buildings*" Journal of Wind Engineering and Industrial Aerodynamics., 82(1-3),1-25.

Van de Lindt, J., Graettinger, A., Gupta, R., Skaggs, T., Pryor, S., and Fridley, K. (2007). "*Performance of Wood-Frame Structures during Hurricane Katrina."* Journal of Performance of Constructed Facilities, 21(2), 108–116.

Vickery, B. J. (1994). "*Internal pressures and interactions with the building envelope*." Journal of Wind Engineering and Industrial Aerodynamics, 53 (1), 125–144.

Vickery, B. J. (1986). "*Gust factors for internal pressures in low-rise buildings*." Journal of Wind Engineering and Industrial Aerodynamics, 23(1), 259–271.

Vickery, B. J., and Bloxham, C. (1992). "*Internal pressure dynamics with a dominant opening*." Journal of Wind Engineering and Industrial Aerodynamics, 41 (1), 193–204.

Vickery, B. J., and Georgiou, P. N. (1991). "*A simplified approach to the determination of the influence of internal pressures on the dynamics of large span roofs*." Journal of Wind Engineering and Industrial Aerodynamics, 38 (2), 307–369.

Walker, G.R. (2011). "*Modelling the vulnerability of buildings to wind-a review*." Canadian Journal of Civil Engineering 38 (8): 1031-1039.

Walker, G.R. (1975). "*Report on Cyclone Tracy-Effect on buildings-Dec 1974*." Australian Department of Housing and Construction.

Walker, G.R. and Reardon, G.F. (1987). "*A discussion of criteria for the structural design of buildings to resist tropical cyclones*." Cyclone Testing Station, James Cook University, Townsville. TR 29.

Walker, G.R. and Gonano, D. (1983). "*Investigation of Diaphragm Action of Ceiling: Progress Report 3*." Cyclone Testing Station, James Cook University, Townsville. TR 20.

Walker, G.R. and Gonano, D. (1982). "*Investigation of Diaphragm Action of Ceiling: Progress Report 2*." Cyclone Testing Station, James Cook University, Townsville. TR 15.

Walker, G.R. and Gonano, D. (1981). "*Investigation of Diaphragm Action of Ceiling: Progress Report 1*." Cyclone Testing Station, James Cook University, Townsville. TR 10.

Wolfe, R. W. (1982). "*Contribution of Gypsum Wall Board to Racking Resistance of Light Frame Walls*." FPL 439, Forest Products Laboratory, United States Department of Agriculture, Madison, Wisconsin.

Wolfe, R. W. and LaBissoniere, T. (1991). "*Structural Performance of Light-Frame Roof Assemblies II. Conventional Truss Assemblies*." FPL-RP-499, Forest Products Laboratory, Madison, WI.

APPENDIX A: INDIVIDUAL JOINT TESTS DETAILS

A.1 Density and moisture content of the timber

Table A.1 presents the measured moisture content and density of timber species used in the individual joint tests, and the timber species were seasoned. Table 3.2 in the standard AS 1720.1 (2010) specified the timber strength group and joint group for the timber species used in Australian construction. Based on the AS 1720.1 (2010), radiata pine and spruce pine are classified as JD4 and JD5 joint group respectively.

Table A.1. Average density and moisture content, and the joint group of the timber species used in the individual joint tests.

Connection Types	Number of test specimens	Timber types	Average density (kg/m^3)	Average moisture content (%)	Joint group from AS 1720.1
Type A (triple grip and hand nails)	20	Australian radiata pine	530	11	JD4
Type B (universal triple grip and hand nails)	10	Australian radiata pine	525	10	JD4
Type C (triple grip and hand nails)	10	spruce pine	460	12	JD5
Type D (triple grip and gun nails)	10	spruce pine	450	13	JD5
Type E (triple grip and gun nails)	10	Australian radiata pine	510	11	JD4
Type A-N1, (missing nail N1)	10	Australian radiata pine	520	10	JD4
Type A-N6, (missing nail N6)	10	Australian radiata pine	515	11	JD4
Type A-N9, (missing nail N9)	10	Australian radiata pine	512	11	JD4
Type A-(N1-N6), (missing nails N1 and N6)	10	Australian radiata pine	510	10	JD4
Type A-(N1-N8), (missing nails N1 and N8)	10	Australian radiata pine	510	11	JD4
Type E-1, (nails on the truss are in a line along an edge of the triple grip)	10	Australian radiata pine	535	10	JD4
Type E-2, (nails on the truss are grouped)	10	Australian radiata pine	540	11	JD4
Type E-3, (nails on the top-plate are grouped)	10	Australian radiata pine	515	11	JD4
Truss grip connection	10	spruce pine	468	13	JD5

A.2 Probability distribution of the strength of the individual joint test

The RWCs peak load for each type test specimen was derived from statistical analysis by fitting to the data with various distributions (i.e. normal, lognormal, Rayleigh), and the Chi-square test was applied to assess the goodness of fit. The lognormal distribution was the best fit for the all the connection types. Figure A.1 shows the probability distribution curve of the peak load of the "Ideal" roof to wall triple grip connection Types A, B and E. Figure A.1 also shows that there is significant variation in the peak load of the roof to wall triple grip connection Types A, B and E. This is because of the material variability between each of the connections, these connections were constructed with different types of framing anchors (i.e. triple grip and universal triple grip) and nails (i.e. hand and gun nails).

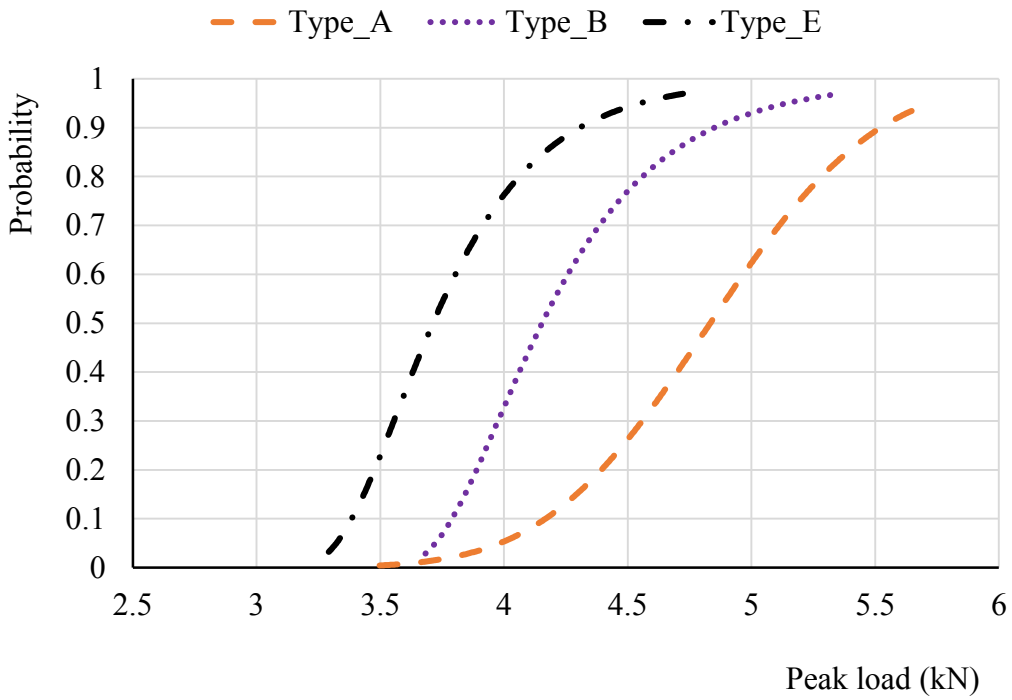

Figure A.1. Probability distribution for the peak load of the triple grip connection Types A, B and E

Figure A.2 shows the probability distribution curve for the peak load of the "Ideal" roof to wall triple grip connection Types C and D. This figure shows that the changing hand nail to gun nail on the roof to wall triple grip connection caused about 15% variation in the peak load of the roof to wall triple grip connection.

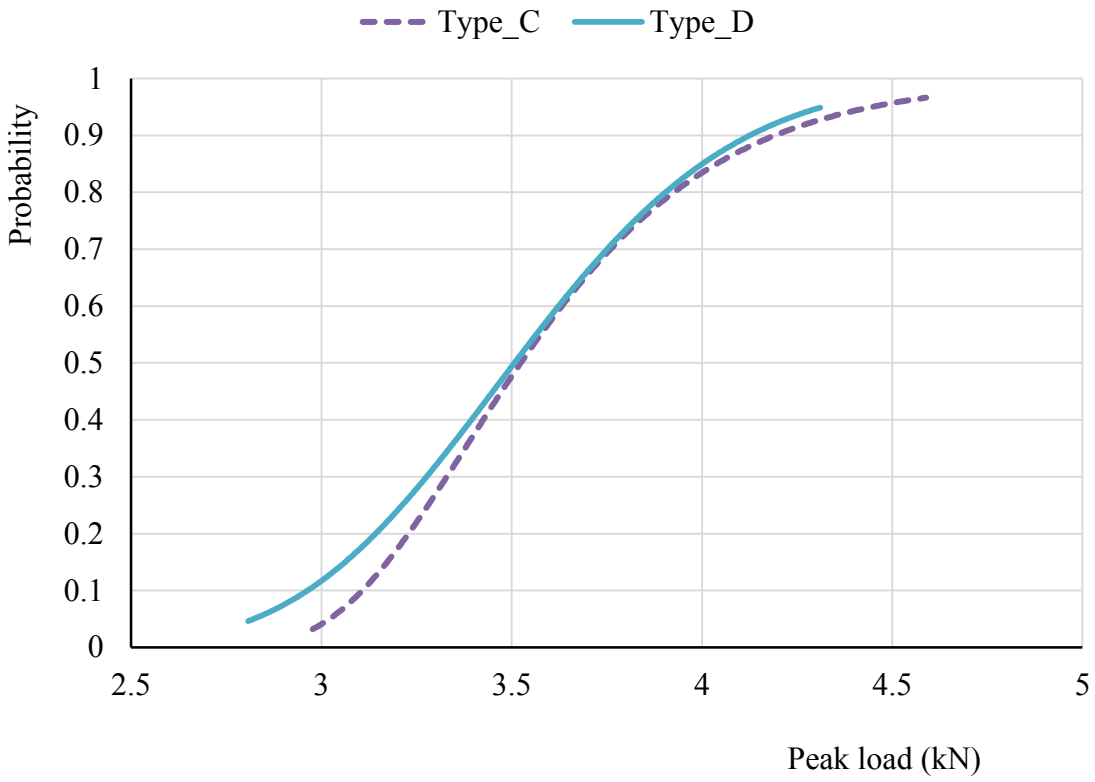

Figure A.2. Probability distribution for the peak load of the triple grip connection Types C and D

Figures A.3 and A.4 show the probability distribution curve for the peak load of the defective roof to wall triple grip hand and gun nailed connections respectively. This figure shows that the construction defects on the roof to wall triple grip connection caused about 20% to 40% variation in the peak load of the roof to wall triple grip connection.

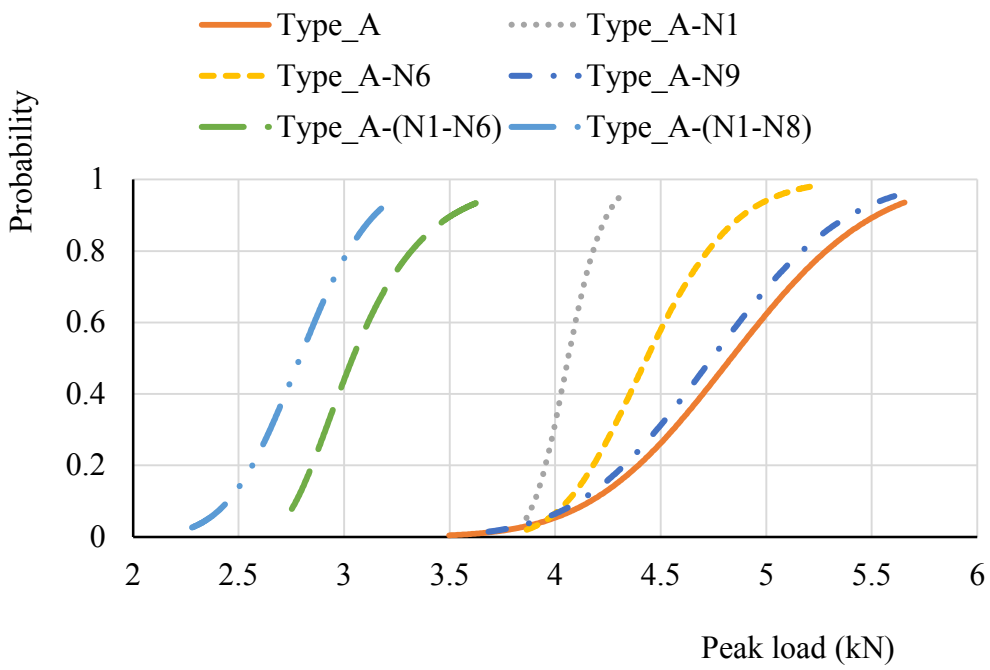

Figure A.3. Probability distribution for the peak load of the defective hand nailed triple grip connections

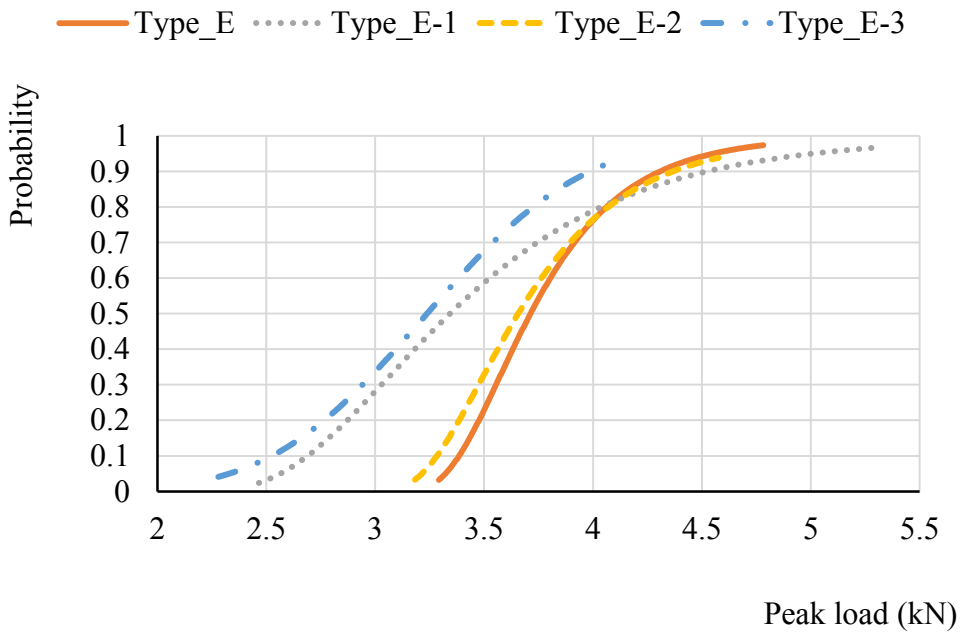

Figure A.4. Probability distribution for the peak load of the defective gun nailed triple grip connections

A.3 Detail of design uplift capacity of the RWCs

The standard AS 1720.1 (2010) specifies the methods to derive the design uplift capacity from the peak load of experimental results. The Equation A.1 is given in the Appendix D of the AS 1720.1 (2010) to determine the uplift capacity.

$$Q^* = \frac{Q_E k_1}{k_2 k_{26} k_{27} k_{28}} \quad \text{A.1}$$

Where, Q_E is the peak load obtained in the experimental tests. Q^* is the critical design load or design uplift capacity. k_1, k_2, k_{26}, k_{27} and k_{28} are strength reduction factors depended on the failure of a constituent element, number of samples and also using the duration of the test.

k_1 is duration of load factor which is 1.0 for the strength of joints.

k_2 is equal to 0.8 for prototype tests for domestic construction when failure occurs at the connectors.

k_{26} is compensation factor which is 1.0 for metal the case of metal fasteners failure in timber that is initially dry.

k_{27} is compensation factor which depends on the time needed to reach peak load. In this study k_{27} = 1.0

k_{28} is sampling factor which depends on the number of tests. In this study k_{28} = 1.5

APPENDIX B: FULL-SCALE STRUCTURAL TEST DETAILS

B.1 Calibration of load cells and LVDTs

Figure B.1 shows the schematic diagram of the load cell calibration test setup. Known weights were loaded and unloaded to the system; input (i.e. applied load) and output data (i.e. measured load by the load cell) were recoded. A similar method was used to calibrate the LVDT, by using scale blocks. Figures B.2 and B.3 show the input data versus output data for the load cell and LVDT respectively. These figures also show the equation for the input-output relationship. Similarly, all the load cells and LVDTs were calibrated and the input-output relationship equations also derived. These equations were applied in the LabView code to measure the actual loads and displacements in the full-scale tests.

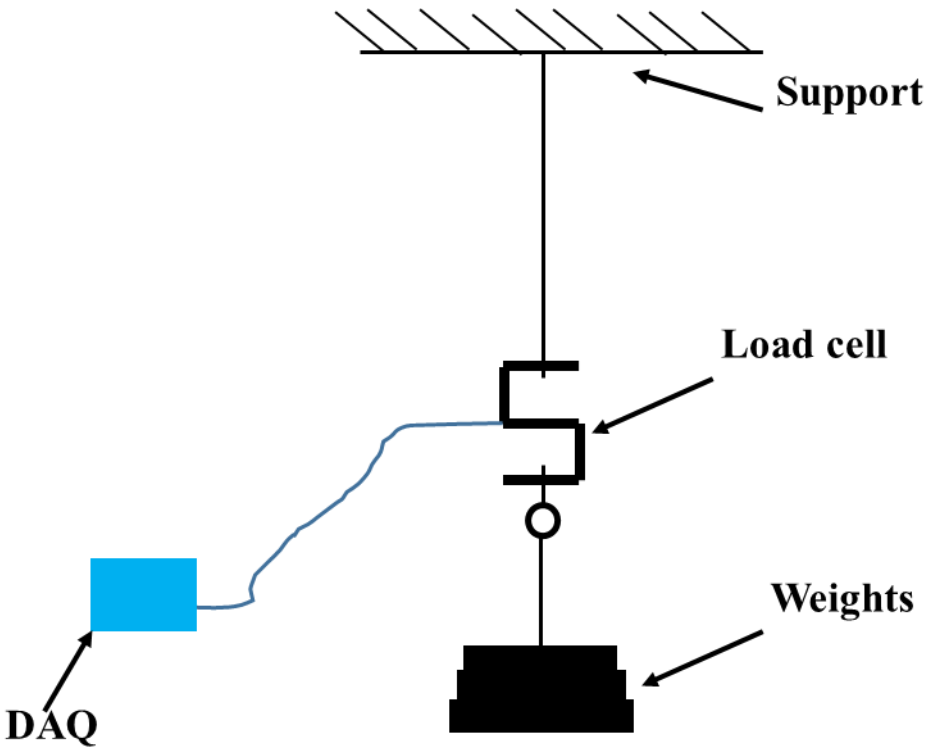

Figure B.1. Schematic diagram of the load cell calibration test setup

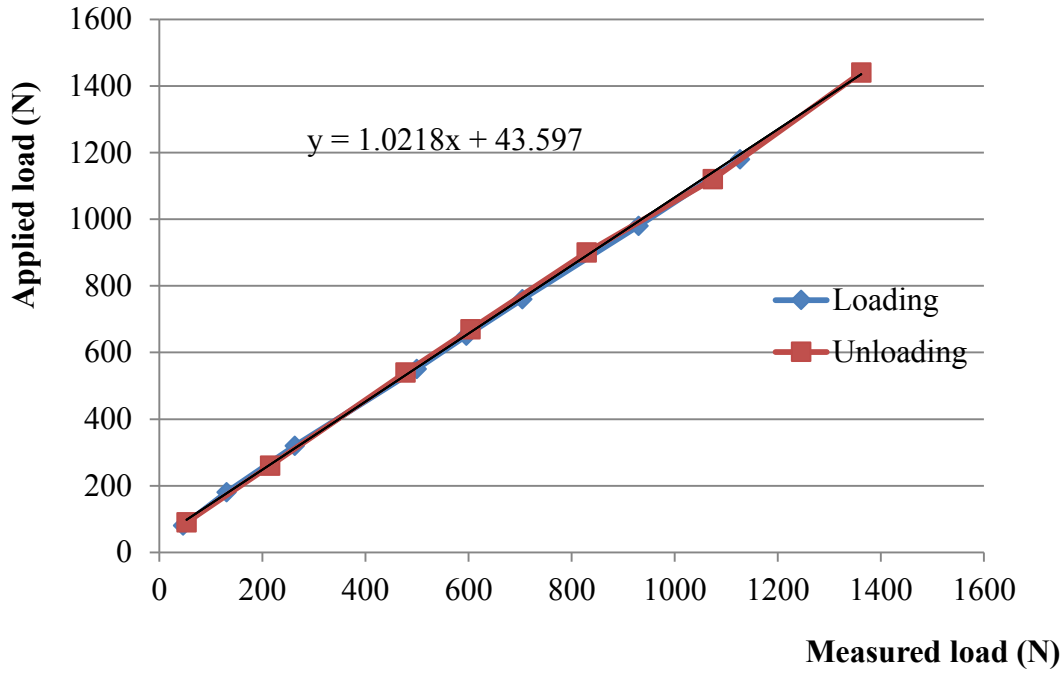

Figure B.2. Applied load versus measured load for load cell

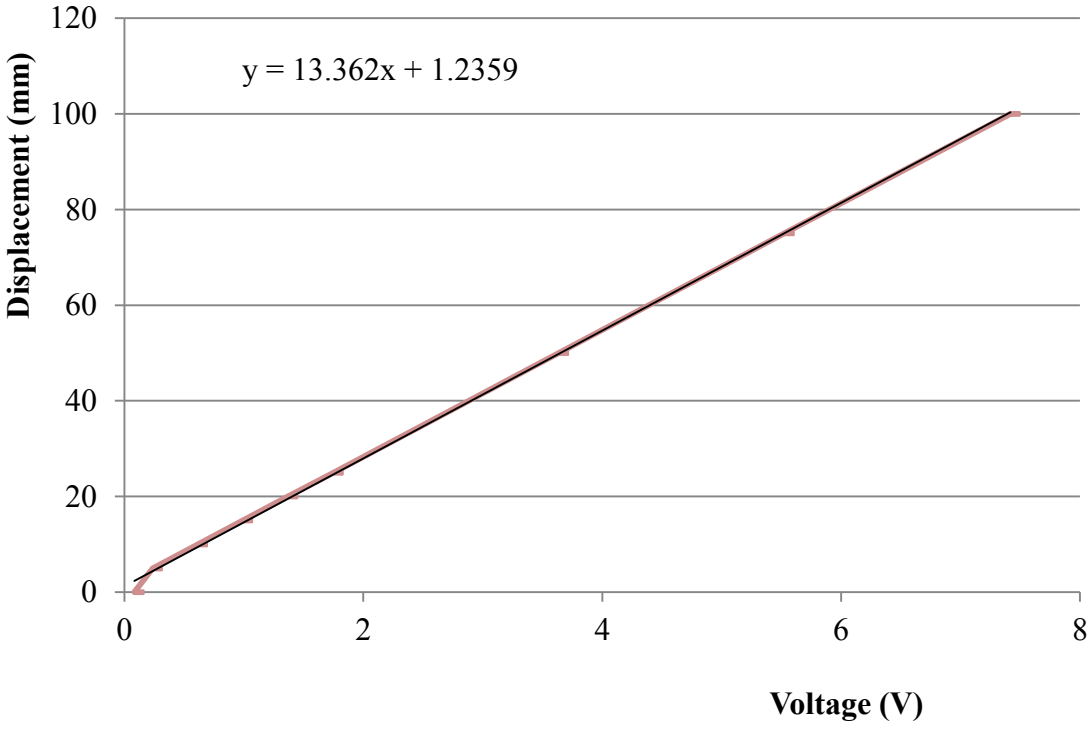

Figure B.3. Applied displacement versus voltage for LVDT

Table B.1. Material parameters and member sizes of the full-scale test structure

Members	Quantity	Sizes (mm)	Material
Roof cladding	8	760 x 4000 x 0.8	Steel
Top-hat battens	12	40 x 40 x BMT 0.55	Steel
Truss	5	90 x 35 x 6600	Timber (MGP 10)
Top-plate	4	90 x 35 x 3300	Timber (MGP 10)
Stud	12	90 x 35 x 2295	Timber (MGP 10)
Bottom plate	2	90 x 35 x 3300	Timber (MGP 10)
Noggings	10	90 x 35 x 565	Timber (MGP 10)
Wall cladding	4	3000 x 1200 x 10	Gypsum board
Ceiling	6	2600 x 1200 x 10	Gypsum board
Ceiling cornice	2	90 x 90 x 2600	Gypsum
Steel rod	20	1.2 x 2500	Steel
Metal washer	40	75 x 75	Steel

B.2 Calibration of full-scale test setup

The load was vertically applied in upward direction to full-scale test structure at Stage S1 to confirm that the applied load was measured by the load cells located at the bottom plates. The vertical load was applied on the trusses at the batten to truss connection locations and apex of the trusses. Table B.2 shows the VRCs of the vertically loaded structural system. This table also shows that the maximum difference between the applied load and measured reactions was about 2.4%. As this test structure used 12 load cells and 33 LVDTs and the input signal from these measuring devises to the DAQ system may be effected by noise. This could be the reason for the differences obtained between the applied load and measured reactions.

Table B.2. VRC of the vertical load test when load was applied at the batten to truss connection locations and apex of the trusses in Stage S1

Stage S1	Loading side L					Non-loading side R					D.F (%)
Loading locations	**L.A**	**L.B**	**L.C**	**L.D**	**L.E**	**R.A**	**R.B**	**R.C**	**R.D**	**R.E**	
TA_B2	0.48	0.26	0.00	-0.01	-0.04	0.21	0.10	0.04	0.00	-0.04	-0.91
TA_B3	0.18	0.17	0.02	-0.01	-0.04	0.54	0.17	0.03	-0.02	-0.05	0.01
TB_B2	0.16	0.39	0.15	0.02	-0.02	0.12	0.10	0.06	0.04	-0.01	-2.36
TV_B3	0.13	0.30	0.12	0.02	-0.01	0.16	0.18	0.09	0.05	-0.01	-1.85
TC_B2	0.04	0.19	0.29	0.14	0.03	0.06	0.07	0.06	0.09	0.03	-0.99
TC_B3	0.04	0.15	0.20	0.11	0.03	0.05	0.12	0.12	0.15	0.02	-0.68
TD_B2	-0.01	0.01	0.21	0.28	0.19	0.00	0.02	0.06	0.12	0.11	0.78
TD_B3	0.00	0.02	0.09	0.09	0.11	0.00	0.04	0.14	0.34	0.17	-0.32
TE_B2	-0.04	-0.04	0.04	0.23	0.50	-0.04	-0.01	0.04	0.13	0.19	0.22
TE_B3	-0.04	-0.02	0.06	0.11	0.21	-0.04	-0.02	0.04	0.20	0.51	-0.38
TA_Apex	0.34	0.21	0.05	-0.03	-0.07	0.36	0.20	0.02	-0.02	-0.06	-0.54
TB_Apex	0.14	0.18	0.14	0.06	-0.02	0.13	0.24	0.09	0.05	0.00	-0.05
TC_Apex	0.04	0.12	0.15	0.16	0.03	0.03	0.14	0.16	0.15	0.03	-0.53
TD_Apex	0.01	0.02	0.11	0.25	0.11	0.02	0.04	0.08	0.25	0.11	0.55
TE_Apex	-0.06	-0.01	0.02	0.24	0.32	-0.06	-0.02	0.04	0.23	0.30	0.56

Note: D.F is the percentage of different between the applied load and total measured reaction forces

B.3 Additional VRC

VRC obtained in each stage when load was applied perpendicular to the roof surface at all batten to truss connection locations are presented in Tables B.3, B.4, B.5, B.6, B.7, B.8 and B.9.

Table B.3. VRC when load was applied perpendicular to the roof surface at the batten to truss connection locations in Stage S1

Stage S1	**Loading side L**					**Non-loading side R**				
Loading locations	**L.A**	**L.B**	**L.C**	**L.D**	**L.E**	**R.A**	**R.B**	**R.C**	**R.D**	**R.E**
TA_B1	0.92	0.20	-0.08	-0.01	-0.02	-0.16	0.04	0.00	0.01	-0.05
TA_B2	0.81	0.19	-0.07	-0.01	-0.01	-0.08	0.05	-0.01	0.00	-0.05
TA_B3	0.69	0.16	-0.06	0.00	-0.01	0.03	0.06	-0.01	0.00	-0.05
TA_B4	0.62	0.13	-0.05	-0.01	0.00	0.16	0.08	-0.02	-0.01	-0.06
TA_B5	0.47	0.12	-0.04	-0.01	-0.01	0.28	0.09	-0.02	-0.01	-0.04
TB_B1	0.13	0.72	0.20	-0.06	0.00	-0.03	-0.09	-0.01	0.03	-0.06
TB_B2	0.12	0.68	0.17	-0.05	0.01	-0.02	-0.05	0.01	0.03	-0.05
TB_B3	0.13	0.51	0.19	-0.06	0.00	0.02	0.04	0.02	0.02	-0.06
TB_B4	0.10	0.44	0.17	-0.03	0.00	0.02	0.13	0.05	0.03	-0.04
TB_B5	0.09	0.32	0.10	-0.03	-0.01	0.03	0.19	0.07	0.01	-0.04
TC_B1	-0.05	0.30	0.48	0.36	-0.09	-0.03	0.00	-0.09	-0.01	-0.04
TC_B2	-0.05	0.26	0.48	0.28	-0.05	-0.02	0.04	-0.06	0.02	-0.05
TC_B3	-0.02	0.21	0.42	0.24	-0.07	-0.04	0.07	0.01	0.05	-0.04
TC_B4	0.00	0.17	0.34	0.20	-0.05	-0.02	0.10	0.08	0.07	-0.03
TC_B5	0.00	0.14	0.28	0.16	-0.04	-0.03	0.14	0.14	0.12	-0.05
TD_B1	0.00	-0.04	0.22	0.69	0.12	-0.03	0.05	-0.03	-0.10	-0.03
TD_B2	0.03	-0.05	0.22	0.56	0.13	-0.03	0.05	-0.01	-0.06	-0.03
TD_B3	-0.03	-0.04	0.18	0.60	0.10	-0.03	0.05	0.02	0.02	0.01
TD_B4	0.00	-0.03	0.13	0.48	0.08	-0.03	0.04	0.05	0.10	0.04
TD_B5	-0.01	-0.01	0.10	0.39	0.05	-0.05	0.04	0.08	0.20	0.03
TE_B1	0.00	0.00	-0.10	0.23	0.85	-0.02	0.01	0.01	0.01	-0.15
TE_B2	-0.02	0.00	-0.08	0.22	0.75	-0.03	0.02	0.00	0.04	-0.12
TE_B3	-0.02	0.00	-0.08	0.22	0.66	-0.02	-0.01	0.02	0.06	0.00
TE_B4	-0.01	0.00	-0.08	0.24	0.49	-0.01	0.00	0.00	0.10	0.10
TE_B5	0.01	0.00	-0.07	0.19	0.38	-0.02	0.00	0.00	0.13	0.21

Table B.4. VRC when load was applied perpendicular to the roof surface at the batten to truss connection locations in Stage S2

Stage S2	Loading side L					Non-loading side R				
Loading locations	**L.A**	**L.B**	**L.C**	**L.D**	**L.E**	**R.A**	**R.B**	**R.C**	**R.D**	**R.E**
TA_B1	0.74	0.37	0.08	-0.08	-0.14	-0.21	0.03	0.02	0.07	-0.05
TA_B2	0.68	0.35	0.02	-0.05	-0.11	-0.14	0.05	0.01	0.06	-0.03
TA_B3	0.61	0.34	0.00	-0.08	-0.11	-0.03	0.07	-0.01	0.06	-0.03
TA_B4	0.54	0.29	0.03	-0.07	-0.14	0.07	0.13	0.00	0.05	-0.03
TA_B5	0.40	0.24	0.05	-0.06	-0.14	0.15	0.18	0.00	0.04	-0.04
TB_B1	0.30	0.30	0.39	0.07	-0.10	-0.04	-0.06	-0.08	0.04	-0.01
TB_B2	0.29	0.35	0.34	0.00	-0.10	0.01	-0.05	-0.07	0.04	0.01
TB_B3	0.26	0.30	0.29	0.02	-0.10	0.04	0.03	-0.03	0.05	-0.02
TB_B4	0.18	0.28	0.21	0.05	-0.08	0.04	0.08	0.00	0.07	0.02
TB_B5	0.19	0.21	0.17	0.03	-0.09	0.08	0.16	0.03	0.08	-0.01
TC_B1	-0.02	0.27	0.46	0.28	-0.03	0.03	-0.03	-0.11	-0.02	0.00
TC_B2	-0.07	0.26	0.45	0.31	-0.07	0.03	-0.01	-0.08	0.00	-0.01
TC_B3	-0.03	0.21	0.37	0.28	-0.05	0.07	0.01	-0.03	0.03	0.00
TC_B4	-0.06	0.18	0.27	0.24	-0.01	0.02	0.07	0.00	0.10	0.03
TC_B5	-0.01	0.15	0.21	0.18	-0.03	0.03	0.12	0.06	0.14	0.00
TD_B1	-0.10	0.05	0.35	0.39	0.27	0.03	0.02	-0.06	-0.06	-0.06
TD_B2	-0.08	0.02	0.32	0.41	0.22	0.02	0.04	-0.04	-0.03	-0.06
TD_B3	-0.11	0.03	0.26	0.37	0.22	0.02	0.03	-0.02	0.04	-0.01
TD_B4	-0.10	0.05	0.18	0.34	0.16	0.01	0.04	0.02	0.10	0.05
TD_B5	-0.10	0.05	0.14	0.29	0.12	0.02	0.05	0.05	0.16	0.05
TE_B1	-0.13	-0.04	0.01	0.40	0.71	0.02	0.03	0.04	0.00	-0.22
TE_B2	-0.09	-0.02	-0.04	0.36	0.68	0.02	0.03	0.02	0.02	-0.16
TE_B3	-0.13	-0.02	-0.02	0.35	0.61	0.02	0.02	0.02	0.06	-0.05
TE_B4	-0.16	-0.01	-0.01	0.32	0.48	0.00	0.01	0.04	0.11	0.05
TE_B5	-0.15	0.00	0.04	0.23	0.38	0.01	0.02	0.04	0.15	0.12

Table B.5. VRC when load was applied perpendicular to the roof surface at the batten to truss connection locations in Stage S3

Stage S3	**Loading side L**					**Non-loading side R**				
Loading locations	**L.A**	**L.B**	**L.C**	**L.D**	**L.E**	**R.A**	**R.B**	**R.C**	**R.D**	**R.E**
TA_B1	0.77	0.39	0.01	-0.07	-0.13	-0.18	-0.03	0.03	0.05	-0.02
TA_B2	0.76	0.37	-0.02	-0.08	-0.11	-0.13	0.01	0.04	0.05	-0.01
TA_B3	0.71	0.28	0.00	-0.09	-0.12	-0.06	0.07	0.01	0.05	-0.03
TA_B4	0.54	0.22	0.05	-0.04	-0.12	0.03	0.13	0.02	0.04	-0.03
TA_B5	0.41	0.24	0.05	-0.05	-0.12	0.14	0.18	0.01	0.04	-0.02
TB_B1	0.31	0.43	0.30	0.03	-0.09	-0.03	-0.09	-0.07	0.05	0.02
TB_B2	0.26	0.44	0.25	0.01	-0.07	-0.01	-0.05	-0.05	0.05	0.01
TB_B3	0.24	0.37	0.21	0.07	-0.09	0.00	0.03	-0.03	0.07	0.00
TB_B4	0.26	0.27	0.18	0.04	-0.09	0.06	0.09	0.01	0.06	0.00
TB_B5	0.20	0.25	0.15	0.01	-0.07	0.11	0.15	0.04	0.06	0.01
TC_B1	0.03	0.27	0.49	0.23	-0.04	0.03	-0.04	-0.12	0.00	0.03
TC_B2	-0.05	0.28	0.49	0.22	-0.02	0.03	0.00	-0.09	0.00	0.01
TC_B3	0.00	0.22	0.31	0.32	-0.07	0.03	0.03	-0.03	0.05	0.01
TC_B4	0.03	0.16	0.24	0.26	-0.02	0.03	0.06	0.00	0.09	0.03
TC_B5	0.01	0.15	0.24	0.12	0.02	0.06	0.10	0.06	0.09	0.05
TD_B1	-0.04	0.02	0.33	0.47	0.22	0.02	0.02	-0.07	-0.04	-0.03
TD_B2	-0.09	0.00	0.32	0.48	0.20	0.04	0.03	-0.05	-0.03	-0.03
TD_B3	-0.08	0.04	0.20	0.50	0.18	0.03	0.04	0.00	0.04	0.01
TD_B4	-0.05	0.04	0.15	0.39	0.12	0.02	0.05	0.03	0.08	0.03
TD_B5	-0.11	0.04	0.19	0.24	0.17	0.01	0.05	0.08	0.11	0.11
TE_B1	-0.11	-0.05	0.03	0.39	0.73	-0.01	0.03	0.05	-0.02	-0.16
TE_B2	-0.15	-0.04	0.01	0.38	0.70	0.01	0.04	0.05	-0.01	-0.13
TE_B3	-0.14	-0.04	-0.02	0.42	0.57	0.01	0.02	0.03	0.05	-0.03
TE_B4	-0.14	-0.03	0.00	0.38	0.46	-0.02	0.01	0.06	0.13	0.03
TE_B5	-0.19	-0.03	0.08	0.23	0.41	-0.02	0.01	0.08	0.12	0.16

Table B.6. VRC when load was applied perpendicular to the roof surface at the batten to truss connection locations in Stage S4

Stage S4	Loading side L					Non-loading side R				
Loading locations	**L.A**	**L.B**	**L.C**	**L.D**	**L.E**	**R.A**	**R.B**	**R.C**	**R.D**	**R.E**
TA_B1	0.71	0.31	0.06	-0.02	-0.06	-0.04	0.04	-0.04	0.02	-0.09
TA_B2	0.79	0.24	0.00	-0.05	-0.05	-0.04	0.05	-0.02	0.04	-0.06
TA_B3	0.66	0.24	-0.04	-0.05	-0.03	0.04	0.07	-0.02	0.04	-0.03
TA_B4	0.52	0.22	0.04	-0.04	-0.06	0.12	0.15	-0.01	0.04	-0.07
TA_B5	0.37	0.20	0.07	-0.02	-0.07	0.21	0.20	0.00	0.03	-0.09
TB_B1	0.29	0.44	0.22	0.05	-0.01	-0.03	0.01	-0.03	0.01	-0.07
TB_B2	0.25	0.52	0.18	-0.01	-0.01	-0.04	0.03	-0.01	0.03	-0.05
TB_B3	0.19	0.44	0.16	0.03	-0.01	0.00	0.07	0.03	0.04	-0.03
TB_B4	0.22	0.30	0.14	0.03	-0.02	0.04	0.14	0.04	0.06	-0.06
TB_B5	0.17	0.22	0.12	0.05	0.00	0.07	0.20	0.06	0.08	-0.06
TC_B1	0.08	0.26	0.35	0.26	0.04	-0.03	0.00	-0.02	0.02	-0.07
TC_B2	0.01	0.26	0.40	0.21	0.00	-0.03	0.03	0.00	0.02	-0.06
TC_B3	-0.01	0.25	0.31	0.26	-0.01	-0.02	0.06	0.03	0.08	-0.05
TC_B4	0.03	0.17	0.19	0.24	0.04	-0.02	0.10	0.08	0.11	-0.05
TC_B5	0.02	0.14	0.16	0.16	0.05	0.00	0.13	0.11	0.15	-0.04
TD_B1	-0.03	0.05	0.21	0.53	0.21	-0.02	0.00	-0.01	-0.01	-0.07
TD_B2	-0.03	0.01	0.20	0.61	0.13	-0.02	0.03	0.00	0.03	-0.08
TD_B3	-0.06	0.01	0.17	0.52	0.17	-0.01	0.03	0.04	0.08	-0.05
TD_B4	-0.06	0.03	0.15	0.38	0.18	-0.02	0.04	0.06	0.15	-0.01
TD_B5	-0.08	0.04	0.12	0.28	0.17	-0.05	0.04	0.09	0.23	0.03
TE_B1	-0.08	0.02	0.04	0.36	0.65	-0.04	-0.01	0.00	0.00	-0.08
TE_B2	-0.09	0.01	-0.01	0.31	0.70	0.00	0.00	0.01	0.02	-0.08
TE_B3	-0.08	-0.04	-0.04	0.31	0.65	0.01	0.03	0.02	0.07	-0.03
TE_B4	-0.10	-0.02	0.03	0.28	0.49	-0.01	0.00	0.03	0.15	0.06
TE_B5	-0.11	-0.01	0.07	0.28	0.33	-0.05	-0.01	0.05	0.21	0.14

Table B.7. VRC when load was applied perpendicular to the roof surface at the batten to truss connection locations in Stage S5

Stage S5	**Loading side L**					**Non-loading side R**				
Loading locations	**L.A**	**L.B**	**L.C**	**L.D**	**L.E**	**R.A**	**R.B**	**R.C**	**R.D**	**R.E**
TA_B1	0.65	0.36	0.08	-0.02	-0.08	-0.02	0.03	-0.02	-0.02	-0.08
TA_B2	0.71	0.33	0.01	-0.06	-0.07	0.01	0.04	-0.01	-0.01	-0.06
TA_B3	0.66	0.32	-0.02	-0.07	-0.07	0.03	0.08	0.01	0.01	-0.05
TA_B4	0.46	0.27	0.04	-0.05	-0.07	0.12	0.14	0.02	0.01	-0.07
TA_B5	0.35	0.22	0.08	-0.03	-0.08	0.20	0.19	0.02	0.01	-0.07
TB_B1	0.31	0.39	0.25	0.07	-0.01	-0.02	0.01	-0.01	0.00	-0.05
TB_B2	0.29	0.41	0.22	0.01	-0.02	-0.02	0.02	0.00	0.01	-0.04
TB_B3	0.22	0.34	0.20	0.04	-0.02	-0.02	0.06	0.03	0.04	-0.03
TB_B4	0.20	0.26	0.16	0.05	-0.01	0.03	0.12	0.06	0.05	-0.04
TB_B5	0.17	0.22	0.12	0.05	0.00	0.07	0.20	0.06	0.08	-0.06
TC_B1	0.12	0.24	0.34	0.25	0.04	-0.01	0.00	-0.01	-0.02	-0.07
TC_B2	0.06	0.25	0.37	0.23	0.02	-0.03	0.01	0.01	0.01	-0.04
TC_B3	0.05	0.21	0.30	0.22	0.01	-0.02	0.05	0.05	0.04	-0.04
TC_B4	0.06	0.16	0.21	0.19	0.05	0.00	0.09	0.09	0.08	-0.03
TC_B5	0.07	0.13	0.16	0.13	0.04	0.02	0.11	0.12	0.11	-0.02
TD_B1	-0.01	0.05	0.25	0.45	0.25	-0.01	0.01	0.00	-0.02	-0.06
TD_B2	-0.02	0.02	0.25	0.47	0.20	-0.01	0.02	0.01	0.00	-0.05
TD_B3	-0.06	0.01	0.21	0.41	0.22	-0.01	0.03	0.04	0.05	-0.02
TD_B4	-0.03	0.04	0.17	0.31	0.18	-0.02	0.04	0.08	0.11	0.01
TD_B5	-0.03	0.04	0.13	0.22	0.16	-0.02	0.04	0.11	0.16	0.05
TE_B1	-0.07	0.00	0.08	0.39	0.60	-0.04	-0.02	0.00	0.00	-0.05
TE_B2	-0.07	-0.02	0.02	0.35	0.64	-0.01	0.00	0.02	0.01	-0.04
TE_B3	-0.10	-0.04	0.00	0.35	0.59	-0.01	0.01	0.03	0.06	0.00
TE_B4	-0.12	-0.03	0.05	0.31	0.45	-0.03	-0.01	0.05	0.11	0.08
TE_B5	-0.11	-0.03	0.07	0.26	0.33	-0.05	-0.01	0.07	0.18	0.16

Table B.8. VRC when load was applied perpendicular to the roof surface at the batten to truss connection locations in Stage S6

Stage S6	Loading side L					Non-loading side R				
Loading locations	**L.A**	**L.B**	**L.C**	**L.D**	**L.E**	**R.A**	**R.B**	**R.C**	**R.D**	**R.E**
TA_B1	0.49	0.45	0.23	-0.02	-0.17	-0.01	-0.01	-0.01	-0.02	-0.04
TA_B2	0.52	0.48	0.21	-0.07	-0.20	-0.01	0.00	0.00	-0.01	-0.02
TA_B3	0.48	0.43	0.19	-0.08	-0.23	0.03	0.04	0.03	0.01	-0.02
TA_B4	0.36	0.34	0.16	-0.04	-0.16	0.11	0.10	0.05	0.00	-0.04
TA_B5	0.28	0.26	0.13	-0.02	-0.11	0.19	0.16	0.07	0.00	-0.06
TB_B1	0.33	0.34	0.23	0.10	-0.02	-0.01	-0.01	-0.01	-0.03	-0.04
TB_B2	0.35	0.34	0.22	0.06	-0.06	0.01	0.01	0.01	-0.01	-0.04
TB_B3	0.28	0.29	0.20	0.07	-0.03	0.02	0.03	0.03	0.02	-0.02
TB_B4	0.23	0.24	0.16	0.06	-0.02	0.07	0.08	0.06	0.03	-0.01
TB_B5	0.20	0.22	0.14	0.04	-0.04	0.14	0.14	0.08	0.04	-0.01
TC_B1	0.19	0.22	0.23	0.19	0.15	-0.02	-0.01	-0.01	-0.02	-0.03
TC_B2	0.16	0.21	0.21	0.20	0.13	-0.01	0.00	0.00	-0.01	-0.02
TC_B3	0.12	0.17	0.19	0.18	0.13	0.02	0.03	0.03	0.03	-0.01
TC_B4	0.11	0.15	0.15	0.15	0.12	0.04	0.06	0.06	0.06	0.02
TC_B5	0.08	0.12	0.12	0.12	0.09	0.07	0.09	0.08	0.08	0.03
TD_B1	0.00	0.11	0.22	0.33	0.32	0.00	0.00	-0.01	-0.03	-0.06
TD_B2	-0.02	0.08	0.21	0.34	0.33	0.01	0.01	0.01	-0.01	-0.04
TD_B3	-0.06	0.05	0.18	0.31	0.32	0.01	0.03	0.03	0.03	0.00
TD_B4	-0.04	0.04	0.14	0.25	0.26	0.01	0.04	0.06	0.08	0.05
TD_B5	-0.02	0.05	0.12	0.20	0.20	0.01	0.05	0.08	0.12	0.09
TE_B1	-0.16	-0.04	0.24	0.47	0.49	-0.03	-0.02	-0.01	-0.01	-0.02
TE_B2	-0.18	-0.04	0.20	0.44	0.48	0.01	0.01	0.00	-0.02	-0.04
TE_B3	-0.18	-0.04	0.17	0.40	0.45	0.01	0.02	0.03	0.03	0.00
TE_B4	-0.18	-0.05	0.14	0.35	0.40	-0.03	0.01	0.05	0.10	0.08
TE_B5	-0.13	-0.03	0.11	0.28	0.31	-0.04	0.02	0.08	0.16	0.15

Table B.9. VRC when load was applied perpendicular to the roof surface at the batten to truss connection locations in Stage S7

Stage S7	Loading side L					Non-loading side R				
Loading locations	**L.A**	**L.B**	**L.C**	**L.D**	**L.E**	**R.A**	**R.B**	**R.C**	**R.D**	**R.E**
TA_B1	0.47	0.44	0.23	-0.01	-0.16	0.01	0.00	-0.02	-0.05	-0.05
TA_B2	0.48	0.48	0.22	-0.07	-0.22	-0.01	0.00	-0.01	-0.01	-0.02
TA_B3	0.45	0.44	0.20	-0.06	-0.22	0.03	0.04	0.02	0.02	0.00
TA_B4	0.33	0.33	0.15	-0.03	-0.13	0.13	0.11	0.06	-0.01	-0.05
TA_B5	0.28	0.27	0.13	-0.03	-0.12	0.22	0.18	0.08	-0.02	-0.08
TB_B1	0.33	0.33	0.22	0.09	-0.01	-0.01	-0.01	-0.02	-0.03	-0.04
TB_B2	0.33	0.33	0.21	0.07	-0.04	0.00	0.00	0.00	0.00	-0.02
TB_B3	0.28	0.31	0.20	0.05	-0.06	0.03	0.04	0.03	0.02	0.00
TB_B4	0.24	0.26	0.15	0.05	-0.02	0.10	0.09	0.06	0.03	-0.01
TB_B5	0.18	0.19	0.12	0.05	-0.01	0.12	0.13	0.08	0.04	0.00
TC_B1	0.17	0.22	0.22	0.22	0.15	-0.01	-0.01	-0.01	-0.02	-0.03
TC_B2	0.14	0.19	0.21	0.21	0.15	-0.01	0.00	0.00	0.00	-0.02
TC_B3	0.12	0.18	0.17	0.17	0.14	0.02	0.03	0.03	0.03	0.00
TC_B4	0.09	0.16	0.15	0.15	0.10	0.04	0.08	0.06	0.05	0.02
TC_B5	0.08	0.11	0.11	0.12	0.10	0.08	0.10	0.08	0.08	0.04
TD_B1	-0.02	0.08	0.22	0.36	0.34	0.00	-0.01	-0.01	-0.03	-0.04
TD_B2	-0.01	0.08	0.21	0.34	0.31	0.02	0.02	0.00	-0.02	-0.04
TD_B3	-0.04	0.05	0.17	0.30	0.30	0.01	0.02	0.03	0.03	0.01
TD_B4	-0.05	0.04	0.16	0.27	0.23	0.01	0.04	0.05	0.08	0.06
TD_B5	-0.03	0.03	0.11	0.20	0.21	0.04	0.05	0.06	0.13	0.10
TE_B1	-0.16	-0.02	0.21	0.47	0.48	-0.02	-0.02	-0.01	-0.02	-0.03
TE_B2	-0.19	-0.05	0.19	0.46	0.49	0.02	0.01	0.00	-0.02	-0.04
TE_B3	-0.18	-0.04	0.15	0.41	0.45	0.01	0.03	0.03	0.03	0.00
TE_B4	-0.15	-0.05	0.14	0.36	0.35	0.00	0.02	0.05	0.09	0.08
TE_B5	-0.13	-0.03	0.12	0.28	0.31	-0.03	0.01	0.08	0.16	0.15

B.4 Lateral (i.e. horizontally perpendicular to ridge line) loading on the wall

A lateral load (i.e. horizontally perpendicular to ridge line) was applied to the wall in order to assess the lateral load distribution to the non-loading side wall through the roof structure, ceiling and ceiling cornice. Nine LVDTs were used to measure the lateral displacements and the reaction loads were measured by lateral load cells L1 and L2,

located at the studs S7 and S12 respectively (Figure B.4). The wall geometry was symmetric, thus the loads were only applied to the three wall studs (i.e. S1, S2 and S3) at three different locations (i.e. P1, P2 and P3). The LVDTs locations (i.e. LD1 to LD9) used to measure the lateral displacement of the wall structure, as shown in Figure B.5. This figure also shows the loading locations (i.e. S1_P1, S1_P2, S1_P3, S2_P1, S2_P2, S2_P3, S3_P1, S3_P2 and S3_P3) of the lateral load test.

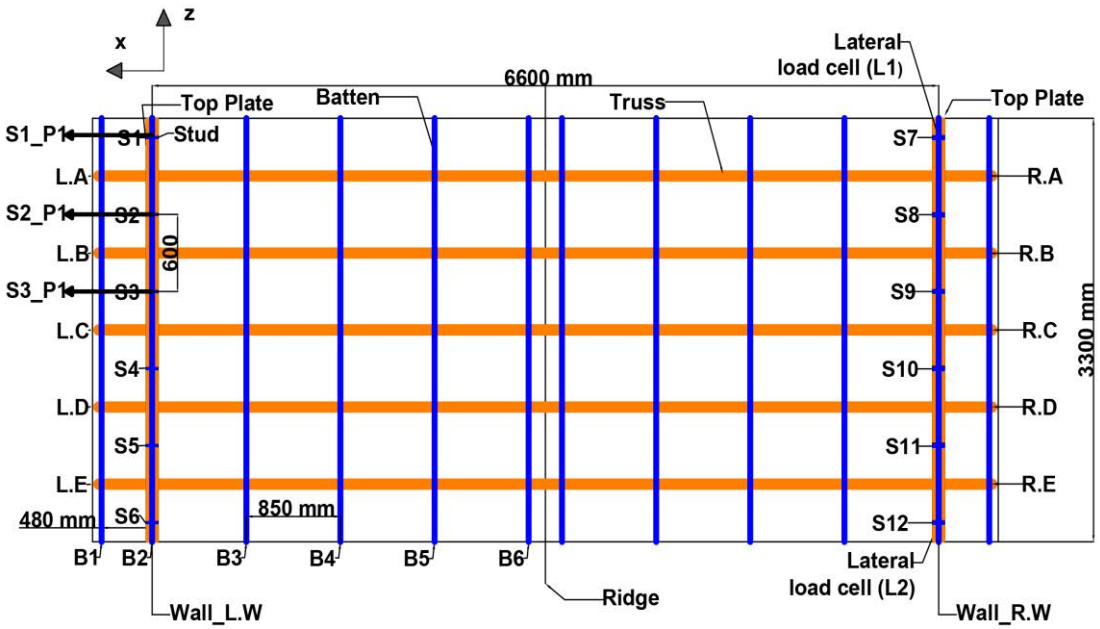

Figure B.4. Plan view of the lateral loading locations and direction

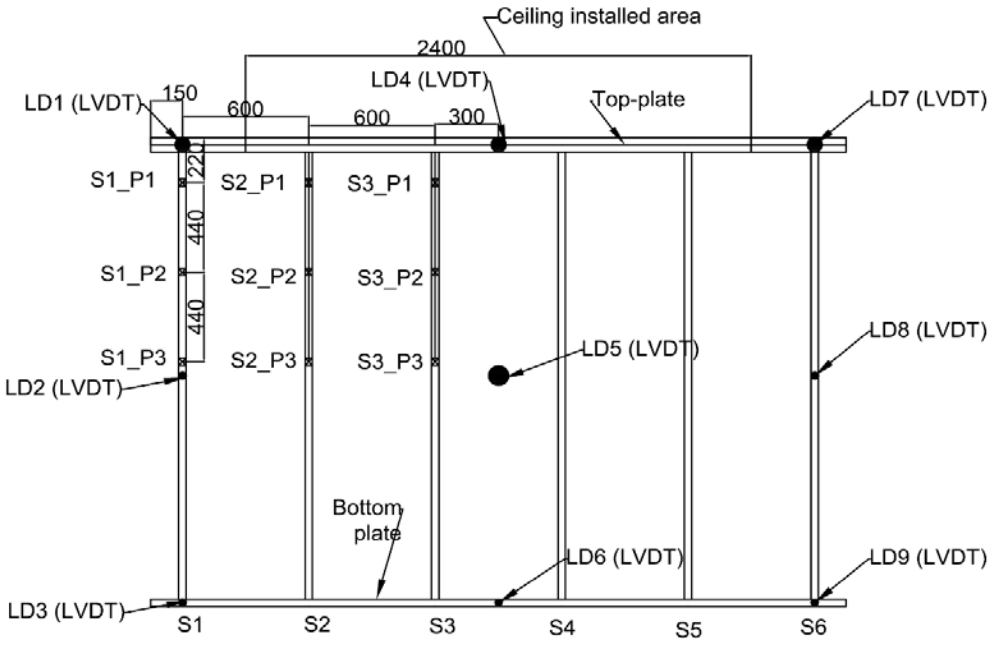

Figure B.5. Loading and LVDTs locations of the lateral load test

The wall studs were pulled by the hydraulic ram at each of the positions separately, and the pulling loads varied between 0.6 kN to 1.4 kN. A load between 0.6 kN and 0.65 kN was applied at loading position P1, whilst the P2 position was subjected to a load between 0.9 kN and 0.95 kN. Location P3 was pulled by a load between 1.15 kN and 1.35 kN.

Figures B.6, B.7 and B.8 show the lateral reaction coefficient (i.e. the lateral reaction force measured by the lateral load cells (i.e. L1 and L2)) divided by the applied load. Figure B.6 presents the lateral reaction coefficient when load was applied to the studs at S1_P1, S2_P1 and S3_P1, whilst Figures B.7 and B.8 show the lateral reaction coefficient variation when load was applied at positions S1_P2, S2_P2, S3_P2, and S1_P3, S2_P3 and S3_P3 respectively. These figures show that the lateral reaction coefficients at studs S7 (i.e. load cell location L1) and S12 (i.e. load cell location L2) were approximately similar with maximum 5% variation at all loading positions. Thus, this test results indicate that the applied lateral load was equally distributed to the non-loading side wall through the ceiling and ceiling cornice, trusses and top-plates.

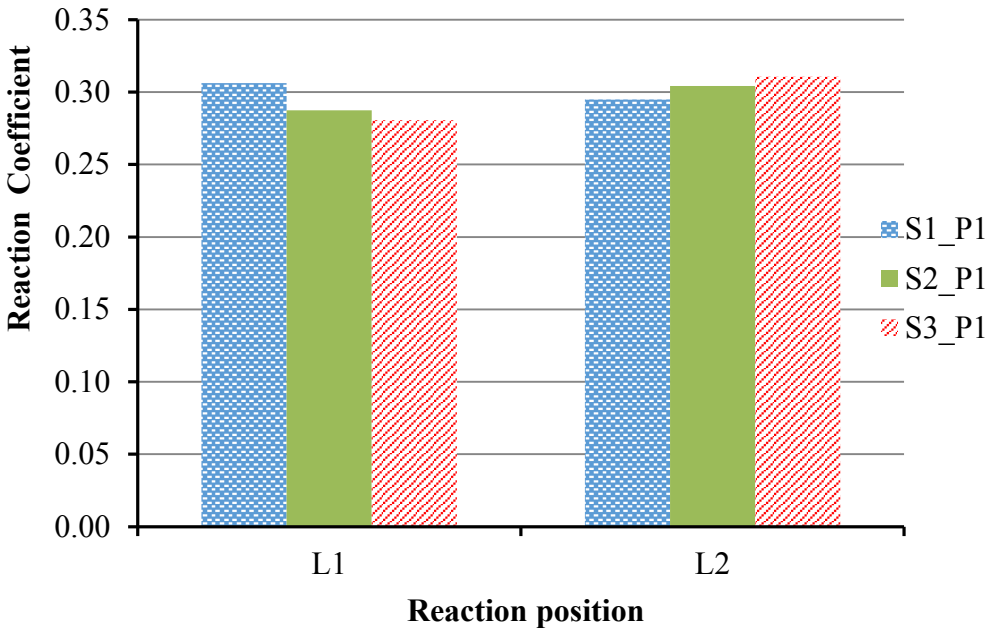

Figure B.6. Lateral load reaction coefficients when load was applied to the studs S1, S2, and S3 at P1

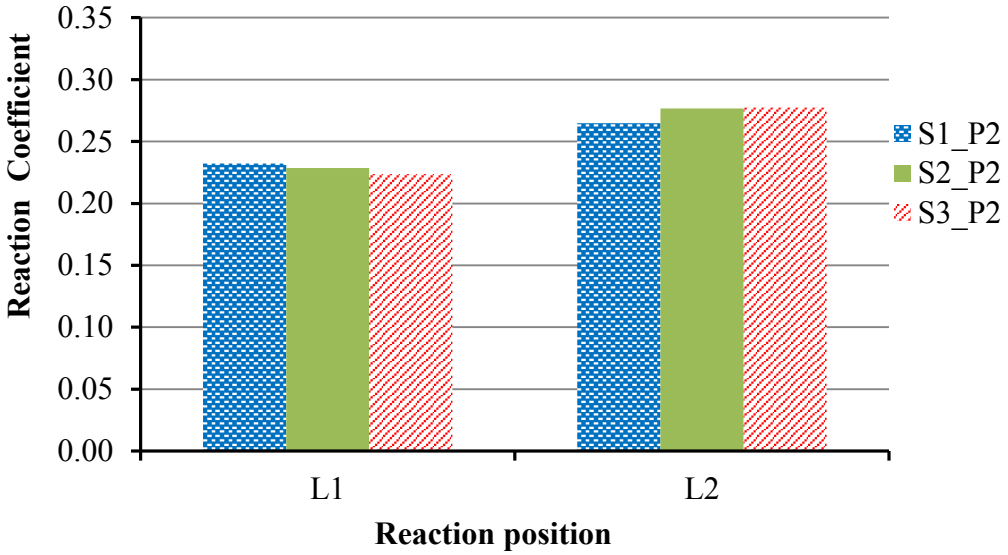

Figure B.7. Lateral load reaction coefficients when load was applied to the studs S1, S2, and S3 at P2

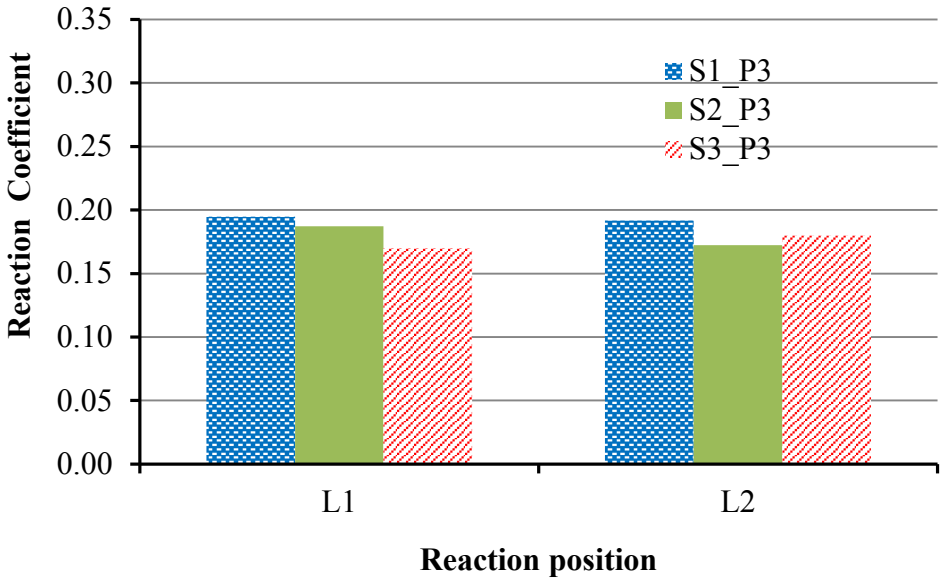

Figure B.8. Lateral load reaction coefficients when load was applied to the studs S1, S2, and S3 at P3

In this experimental tests, some percentage of the applied load was transferred to the loading and non-loading side walls bottom plate. This did not accounted by the lateral load cells (i.e. L1 and L2). Therefore, the total load at loaded side top-plate was calculated by using simple beam theory to assess the load sharing through the ceiling from loaded side to non-loaded side. The measured reaction forces at non-loaded side wall supports divided by the total distributed load at top-plate were normalized as reaction coefficients in Table B.10. This table shows minimal variation between the lateral reaction coefficient of the non-loaded side wall support and the applied loading locations (i.e. P1, P2, and P3). This lateral load reaction coefficients could use to assess the wind load sharing from the windward wall to leeward wall through roof, ceiling and cornice.

Table B.10. Lateral reaction coefficients at non-loaded side wall supports

Loading locations	Load at loading side top-plate (kN)	Reaction coefficients at lateral supports	
		L1	L2
S1_P1	0.55	0.34	0.33
S2_P1	0.58	0.32	0.34
S3_P1	0.56	0.31	0.34
S1_P2	0.64	0.33	0.37
S2_P2	0.64	0.32	0.39
S3_P2	0.64	0.31	0.39
S1_P3	0.60	0.37	0.37
S2_P3	0.60	0.36	0.33
S3_P3	0.73	0.34	0.34

Figures B.9, B.10 and B.11 show the flexibility of the loaded side wall; flexibility is the measured wall lateral displacement divided by the applied load (i.e.mm/kN). Figure B.9 presents the variation of the lateral displacement of the loaded side wall when load was applied to the studs S1, S2 and S3 at position P1, whilst Figures B.10 and B.11 show the lateral displacement of the wall when the load was at P2 and P3 respectively. These figures show there was negligible movement at the bottom plate (i.e. LD3, LD6 and LD9). This is because the full-scale test structure was supported at the bottom plate. The top-plate movement was high in all loading location (i.e. LD1, LD4 and LD7), which indicates that the wall was swaying in the direction of the applied load. Figure 5.38 shows that the top-plate displacement was high at LD1, this was because the celling and celling cornice were not installed above the stud S1 region on the top-plate. This could have increased the flexibility of the top-plate at location LD1. This indicates that the lateral movement of top-plate will reduced when installed the ceiling with ceiling cornice in the timber-framed house.

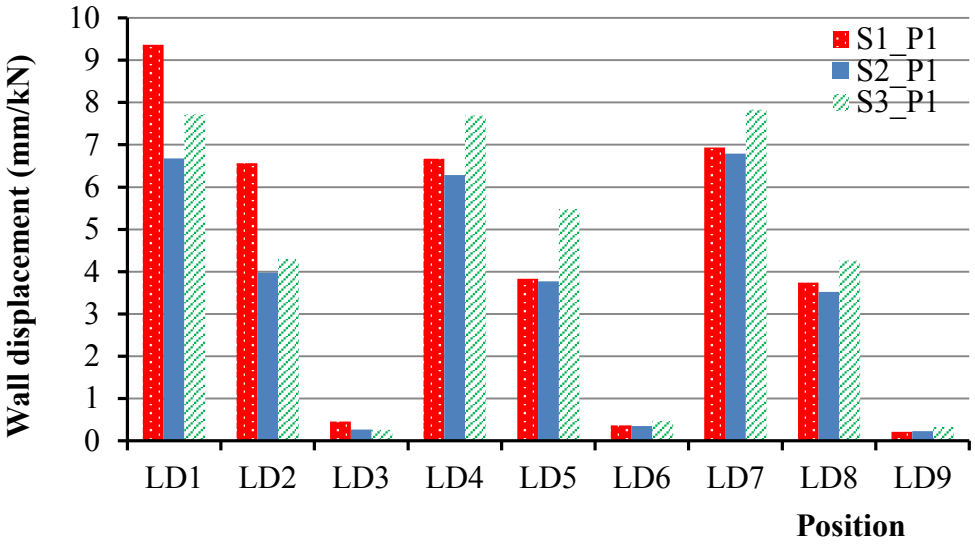

Figure B.9. Wall lateral displacement variation when load applied at P1

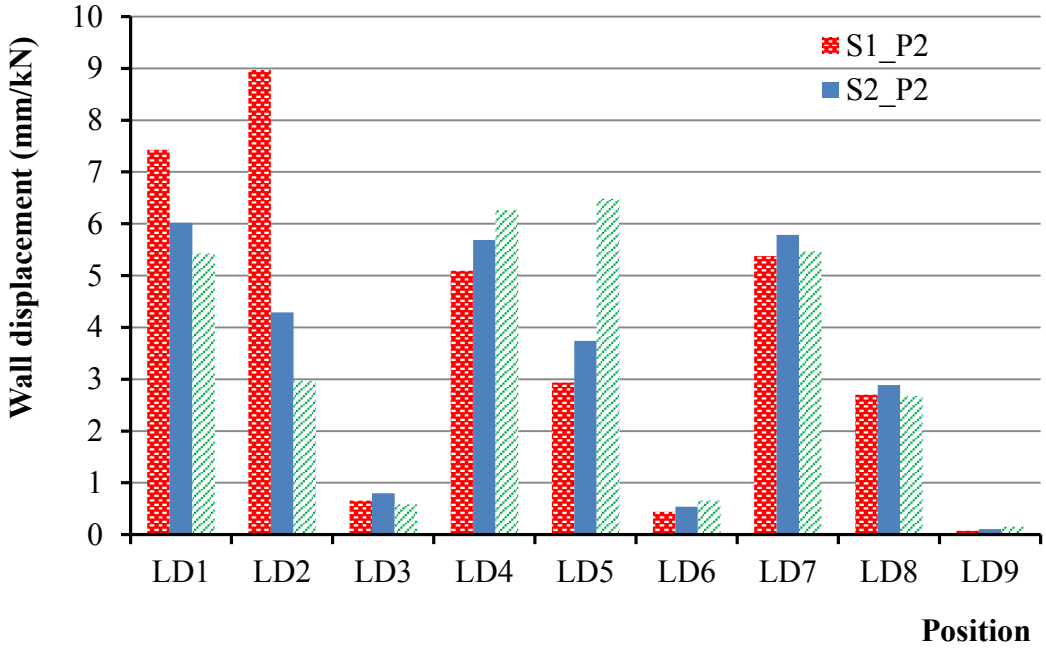

Figure B.10. Wall lateral displacement variation when load applied at P2

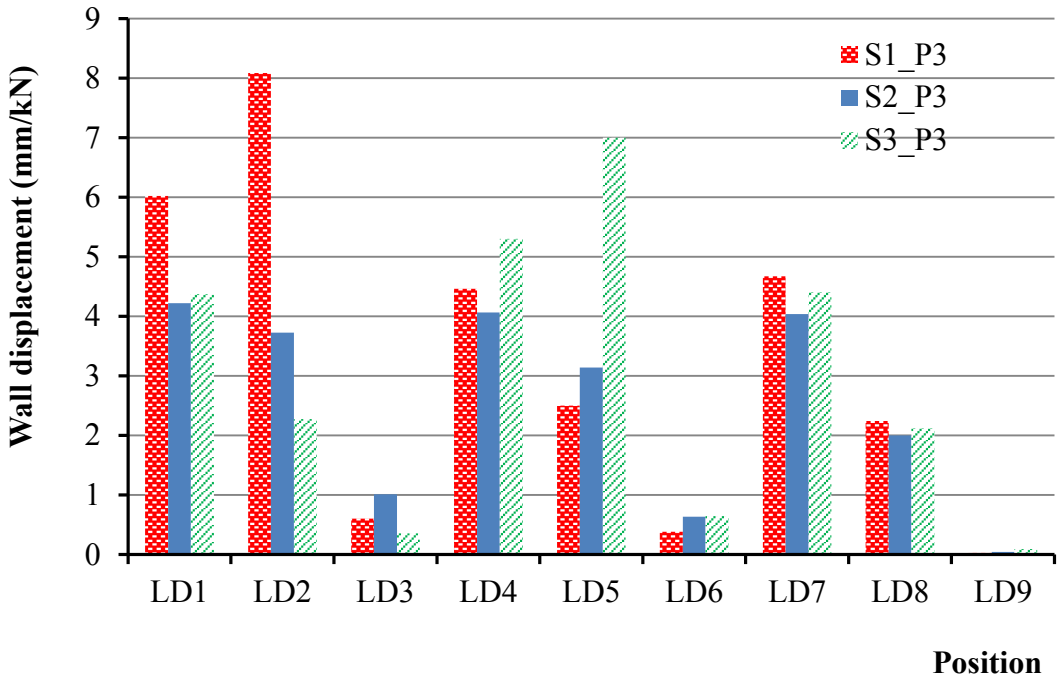

Figure B.11. Wall lateral displacement variation when load applied at P3

B.5 Horizontal loading on the truss (i.e. horizontally perpendicular to ridge line)

The aim of this test was to assess the horizontal load sharing and the horizontal stiffness of the structural system, and represented the case of wind loads acting on the end wall of the house. Horizontal load was applied to the web members of Truss A (Figures B.12 and B.13) to evaluate the horizontal load sharing through the roof, wall, ceiling and ceiling cornice. The location of the loading was 0.4 m above the bottom chord, which is the centroid of the triangle of Truss A. Seven LVDTs (i.e. L.D1, L.D2, L.D3, L.D4, L.D5, L.D6 and L.D7) were used to measure the horizontal displacements. The structural system was horizontally supported by the horizontal load cells (i.e. L.H1, L.H2, L.H3 and L.H4), which were used to measure the horizontal reactions. The load cells L.H1 and L.H2 were connected to the wall L.W top-plate and the bottom plate respectively, whilst L.H3 and L.H4 were connected to the wall R.W top-plate and the bottom plate respectively (Figures B.12 and B.13).

Figure B.13 also shows the locations of the horizontal LVDTs and the load cells used in this test; the LVDTs, L.D1 and L.D5 were located at the top-plate, whilst LVDTs, L.D2 and L.D4 were located at the ceiling. The LVDT L.D3 was located at the bottom chord of Truss A, to measure the relative movement between the ceiling and bottom chord of

the truss. LVDT, L.D6 was located at the bottom chord of Truss E, whilst LVDT, L.D7 was located at the apex of Truss A, and was used to measure the relative movement between the apex and bottom chord. Moreover, the vertical reaction at the bottom plate, lateral reaction at the lateral supports and the vertical movement of the top-plate were measured at the same locations as for the Stage S7 test.

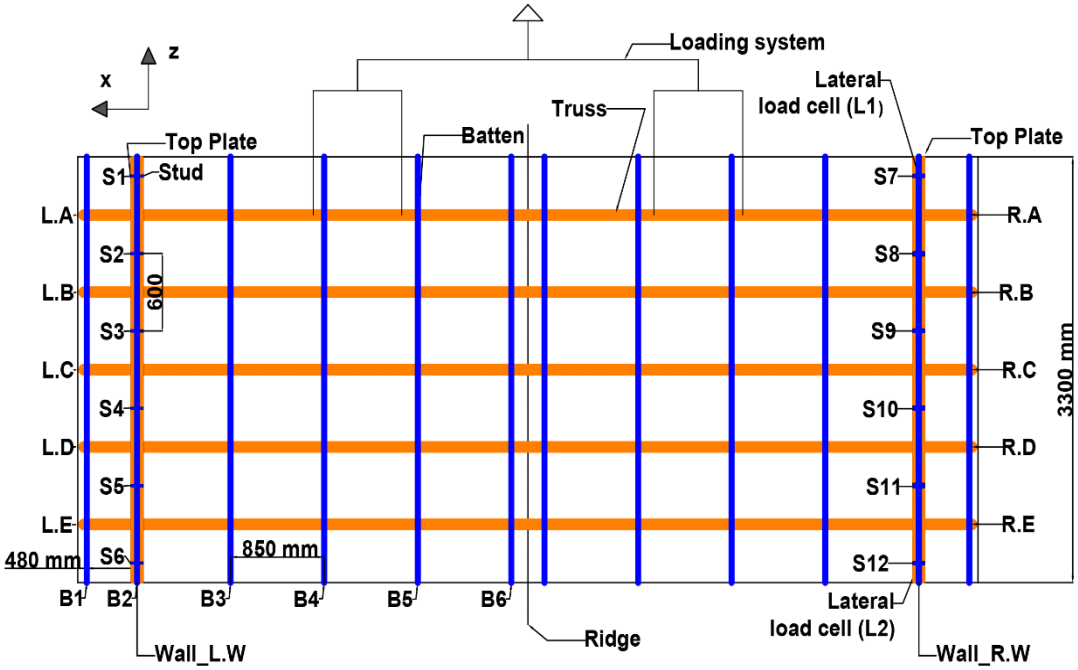

Figure B.12. Plan view of the horizontal loading test structure

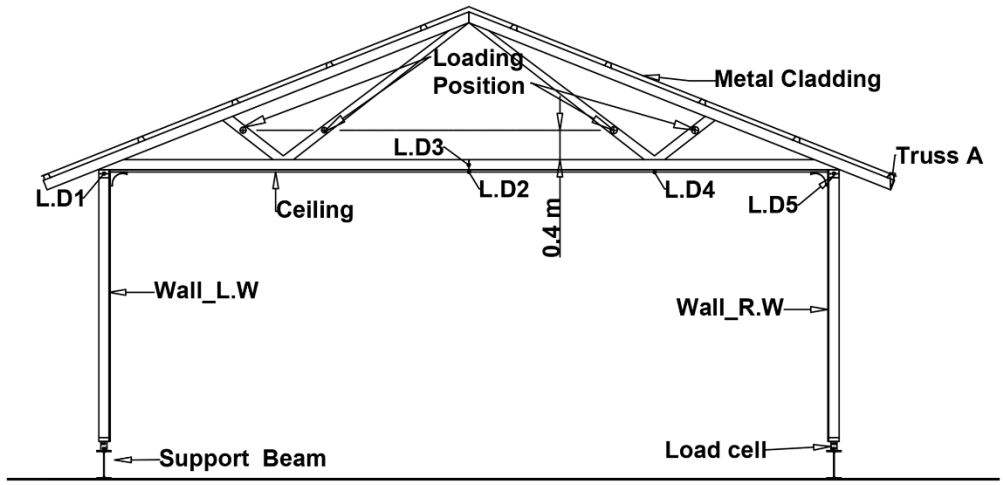

Elevation: View from Truss A

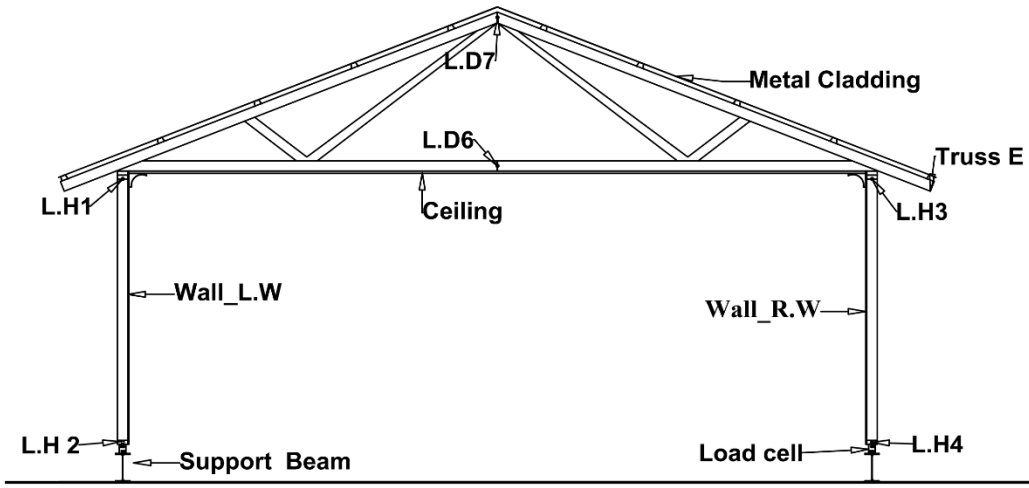

Elevation: View from Truss E

Figure B.13. Elevation view of the horizontal loading test structure

Truss A was pulled by a hydraulic ram with a pulling load of 1.54 kN, and the horizontal, vertical and lateral reaction forces and displacements were measured. The horizontal reaction forces measured at the top-plate and bottom plate by load cells (i.e. L.H1, L.H2, L.H3 and L.H4) were divided by the total applied load, represented as a reaction coefficient in Figure B.14. This figure shows that the horizontal reaction forces measured at each wall top-plate were similar (i.e. L.H1 and L.H3). The horizontal reaction forces at each wall bottom plate (i.e. L.H2 and L.H4) were different; this is because the wall

bottom plates were also supported with the vertical load cells. Thus, some of the horizontal loads were conveyed through the wall bottom plates' vertical supports (i.e. vertical load cells) to the foundation. Figure B.14 also indicates that 42% of the applied load was equally distributed to the top-plate horizontal supports through the roof, wall, ceiling and ceiling cornice. About 28% and 30% of the applied load was transferred to the bottom plates' horizontal (i.e. load cells L.H2 and L.H3) and vertical (i.e. vertical load cells) supports respectively.

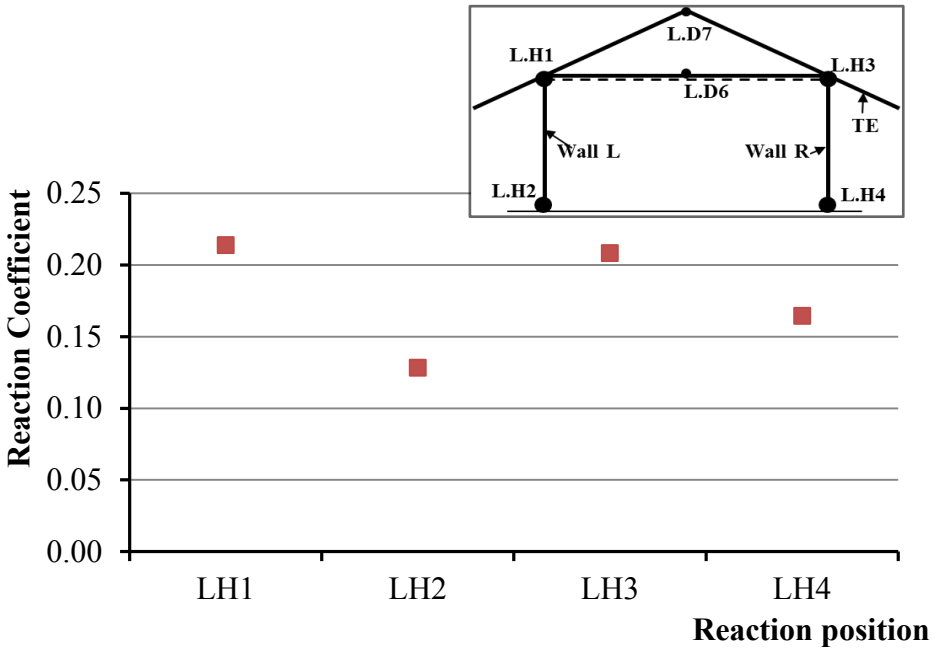

Figure B.14. Horizontal reaction coefficients at the top-plate and the bottom plate horizontal supports

Figure B.15 shows the maximum horizontal displacement measured by the horizontal LVDTs. This figure shows that the maximum horizontal displacement at the wall L.W top-plate (i.e. L.D1) was 50% higher than that of the wall R.W top-plate (i.e. L.D5). This indicates that the stiffness of the wall R.W was higher than the wall L.W, and could be the reason for the high reactions force measured at the wall R.W bottom plate (i.e. L.H4) than that of the wall L.W (i.e. L.H2). Due to the locations of the LVDTs, the horizontal displacement of the ceiling at L.D2 was twice that of the displacement at L.D4. The LVDT, L.D2 was located mid ceiling span, whilst LVDT, L.D4 was located approximately one-fourth the length of the ceiling span from the wall R.W and also closer

to the ceiling cornice. This was the reason for LVDT, L.D2 measured higher displacement than LVDT, L.D4. The horizontal displacement of bottom chord of Truss A (i.e. L.D3) was twice that of the ceiling (i.e. L.D2). This is due to the bottom chord's rotation about centroid of the bottom chord, towards the loading direction. The LVDT L.D3 is located at mid height of the bottom chord (i.e. centroid of the bottom chord). Thus, the LVDT, L.D3 measured a higher displacement than the LVDT, L.D2.

The bottom chord of Truss E's horizontal displacement (i.e. L.D6) was higher than that of Truss A (i.e. L.D3). This was due to Truss E bottom chord's rotation about mid height of the bottom chord, higher than that of Truss A. This indicates that the horizontal stiffness of the Truss A roof to wall triple grip connections was higher than that of the Truss E's roof to wall triple grip connections. The apex of the Truss E horizontal displacement (i.e. L.D7) was 75% higher than the Truss E bottom chord horizontal displacement. This illustrates that the roof structure was moving horizontally about the ridge line toward the loading direction.

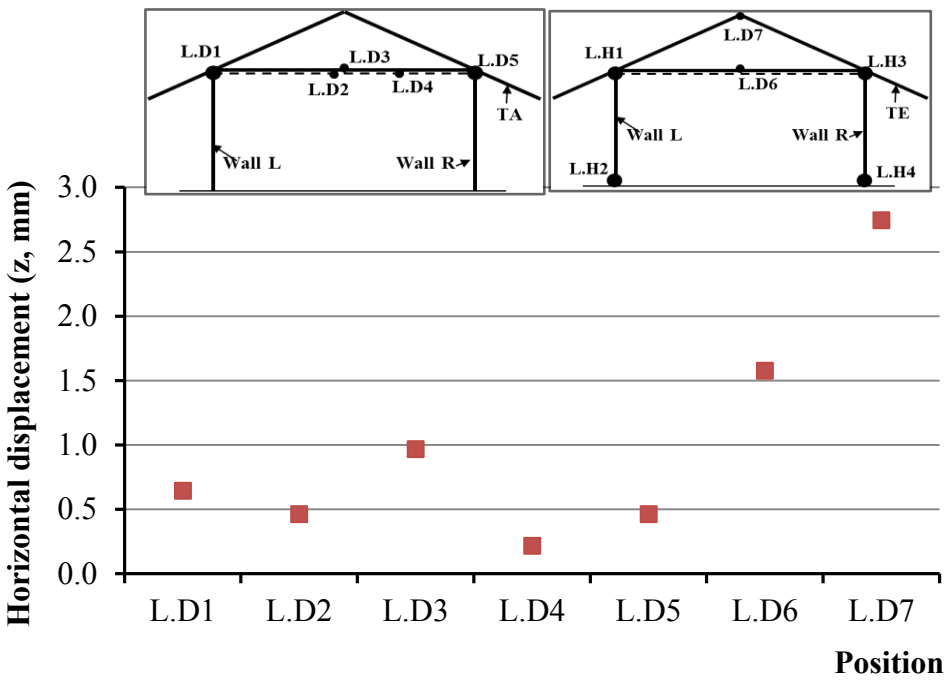

Figure B.15. Horizontal displacement at the top-plate, truss and the ceiling

Figure B.16 shows the applied load versus horizontal displacement at the ceiling (i.e. L.D2), Truss E apex (i.e. L.D7), and the bottom chord of Truss A (i.e. L.D3) and Truss E (i.e. L.D6). This figure shows that the applied load displacement relationship of the Truss E apex was almost linear and it was not linear at the bottom chord of Trusses' A and B. This could be due to the rotation of the Trusses' A and B bottom chord, nail slip in the RWC and hidden failure at the ceiling joint (i.e. partial failure in the glue and screw). This figure also shows the variations between the applied load displacement relationship at the ceiling (i.e. L.D2) and bottom chord of the Truss A (i.e. L.D3). This was due to the flexibility in the glue joint between the bottom chord of the truss and ceiling.

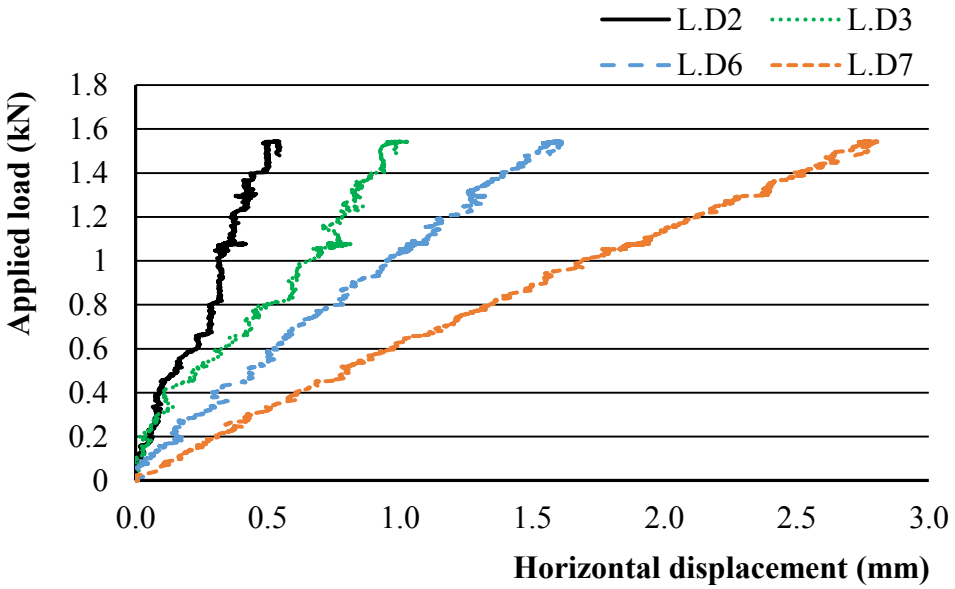

Figure B.16. The horizontal applied load versus displacements at the ceiling and truss bottom chord and apex

The vertical reaction forces at the wall bottom plates are presented in Figure B.17. This shows the vertical reaction force variation at each wall bottom plate were symmetric. This figure also shows the supports L.A, R.A, L.B, and R.B experienced compression forces, whilst supports L.D, R.D, L.E, and R.E were subjected to tension forces. This indicates that the wall bottom plate moves up and down about (i.e. rotated) mid support (i.e. L.C and R.C). Digital Dial Gauges were used to measure the lateral movement of the wall top-plate and bottom plate; measurements showed the lateral movement of the wall was negligible (i.e. maximum 0.08 mm). The maximum lateral reaction force measured by the

lateral load cell was about 6 N and negligible. These lateral movements and reaction forces indicate that the horizontal load applied to the truss was not affect the lateral load sharing and lateral response of the house structural system.

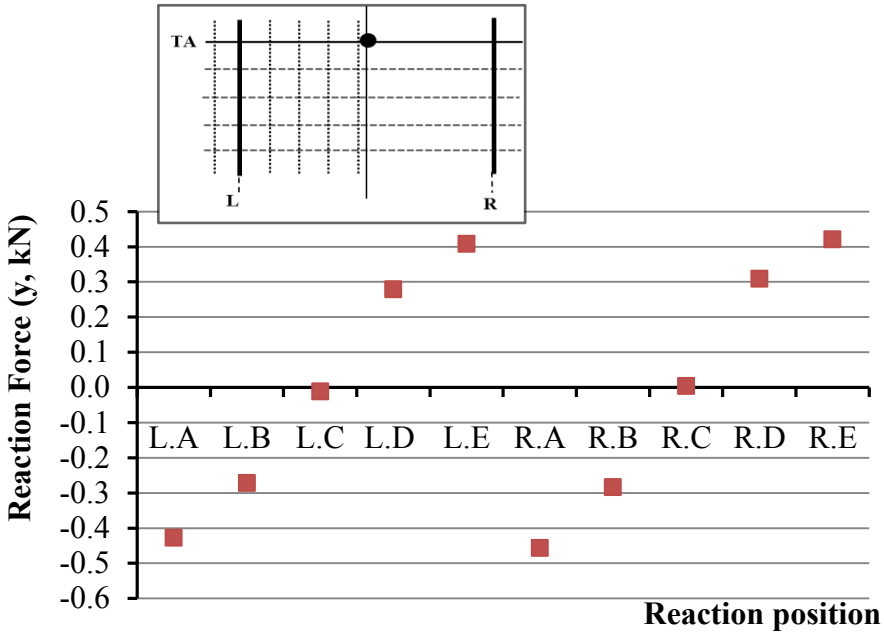

Figure B.16. The vertical reaction at the wall bottom plate, when horizontal load of 1.54 kN was applied to the bottom chord of the Truss A

B.6 Photographs of full-scale test structure

Figure B.17. Full-scale test structure at Stage S1

Figure B.18. Full-scale test structure at Stage S3

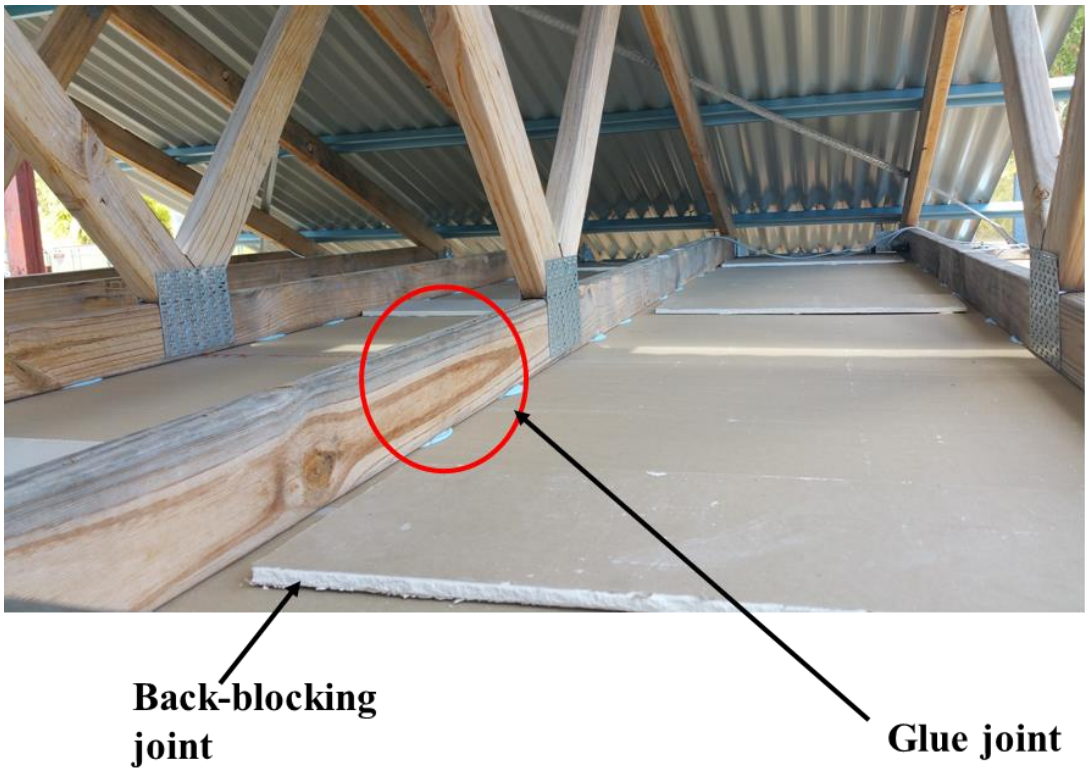

Figure B.19. Back-blocking joint of the ceiling and glue joint between the bottom chord of truss and ceiling

Figure B.20. Full-scale test structure at Stage S7

Figure B.21. Full-scale test structure with shear walls at Stage S8

APPENDIX C: NUMERICAL MODEL OF THE RWC

C.1 Introduction

Connections between the structural elements of a timber-framed structure are critical for ensuring stability and transferring forces from the roof to the foundation. Consequently, for a house structure to survive under extreme wind loading, it is crucial for these connections to have sufficient strength to resist these induced actions. The experimental study (Chapter 4) has shown that the strength and uplift capacity of the RWC depends strongly on each nail's structural response to loading and the stiffness of the surrounding structure (i.e. framing anchor, timber species). Test results also shows that construction defects in the RWC will reduce the strength of the connection, and identifies the critical nails and their locations that may cause reduction in the uplift capacity.

Post windstorm investigations by Boughton et al (2011), Walker (1975), and Shanmugasundaram et al (1995) etc., have shown that the failure of connections between structural components is mainly responsible for major damage to timber-framed houses. This indicates that evaluation of structural stability of the timber-framed house to windstorms is required to assess the strength, stiffness and the structural response of the inter-component connection. Thus, the analysis of the response of timber-framed house structures to windstorms needs reliable prediction methods. These methods should focus on connection stiffness as well as resistance strength, to provide a reliable and safe connection design and to mitigate failure of houses from windstorms. Development of the individual connection model is essential to develop a full-house numerical model. Therefore, this study developed a FEM to evaluate the strength, stiffness and structural response of the RWC.

This chapter analyses the response of typical RWCs (i.e. triple grip and truss grip connections), subject to loading by using the FEM analysis. This FEM provides an insight into important issues such as connection strength capacity, stiffness and failure modes. The FEM also able to provides a wide-ranging parametric study (i.e. the effect of construction error and tri axial loading of the connections, deformed shape and size of nails and framing anchors) that would be difficult to achieve in laboratory tests. The formation of a dependable FEM validated by existing test results was an aim in this chapter to allow: economic simulation of the various triple grip and truss grip

connections, including their many fastener location combinations with the aim of developing probabilistic distributions of strength capacity. FEM results are used to predict the design uplift capacity of the connection with and without construction defects. Being able to make these predictions would greatly assist experimental tests and result in significant savings in time and cost.

C.2 Single nail joint

Nailed connections are widely used in timber-framed structures as they enable prefabricated structural elements (i.e. Truss, top-plate, wall, stud, battens, etc.) to be erected quickly on site. Observations in isolated connection tests and wind damaged buildings show that the behavior of single nail joint is extremely important in maintaining structural integrity. Mechanically fastened joints are the only elements in a timber structure capable of absorbing a large amount of loading energy through plastic deformation in the metal fasteners as described by Chui et al (1997 and 1998). Thus the behaviour and response of mechanically fastened joints is important for timber-framed structures' responses to wind loading.

The response of a single nail joint under loading provides a basis for understanding the response of the RWCs. The action of the nail or timber bond transfers forces in a complex way between the metal nail and the surrounding embedded timber. Several research studies have focused on this single nail joint response under monotonic loading or reversed cyclic loading (Foschi, 1974, 2000; Chui, 1997; Li et al., 2012). Foschi (1974, 2000) investigated the behavior of a connector and the embedment characteristics of the surrounding timber medium by using experimental and empirical models. A single mechanical connector described in Figure C.1 was used in his study. Foschi (2000) found when the connector joint is subjected to load F, there will be a reaction force P from the timber medium. Correspondingly, the connector will deform and adopt a shape $w(u)$, where u is the axial displacement of the cross-sectional centroid of the nail, and w is the lateral displacement of the nail.

The reaction from the timber medium per unit length is assumed to be a function $p(w)$ of the displacement w (i.e. timber deformation). $p(w)$ is named as the "embedment" property of the surrounding timber medium. A recent study by Li et al (2012) further developed the embedment function $p(w)$ derived by Foschi (2000) and also derived a curve for the response $p(w)$, as shown in Figure C.2. This embedment function $p(w)$ takes into account

the lateral nail deformation, which was not considered in previous studies by Foschi (2000).

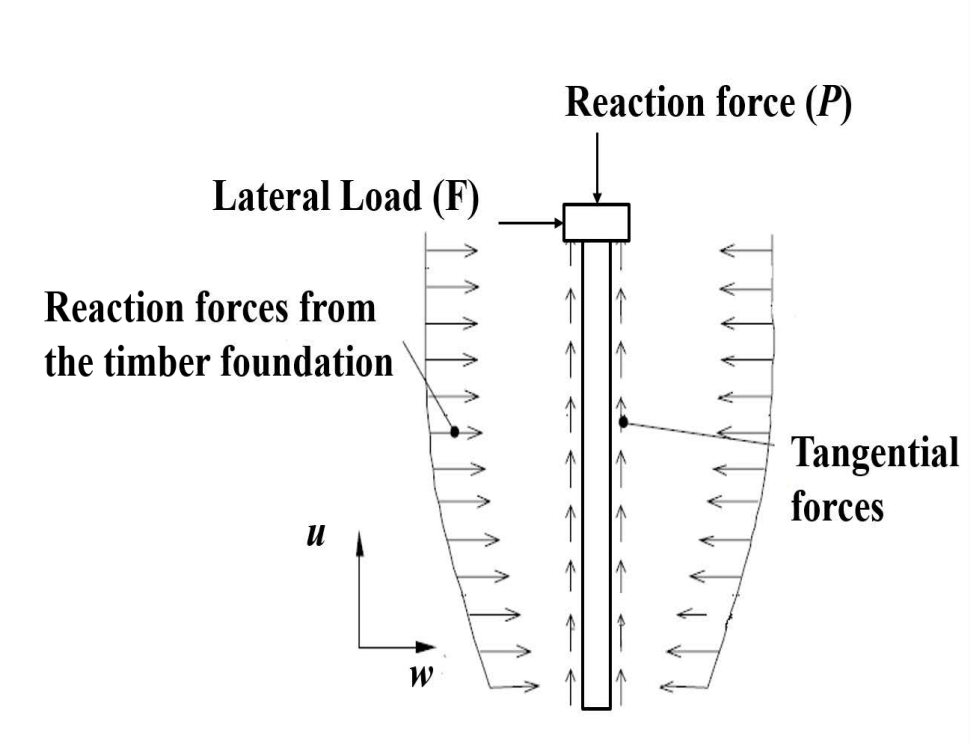

Figure C.1. Schematic diagram of reaction forces of single nail embedded in timber

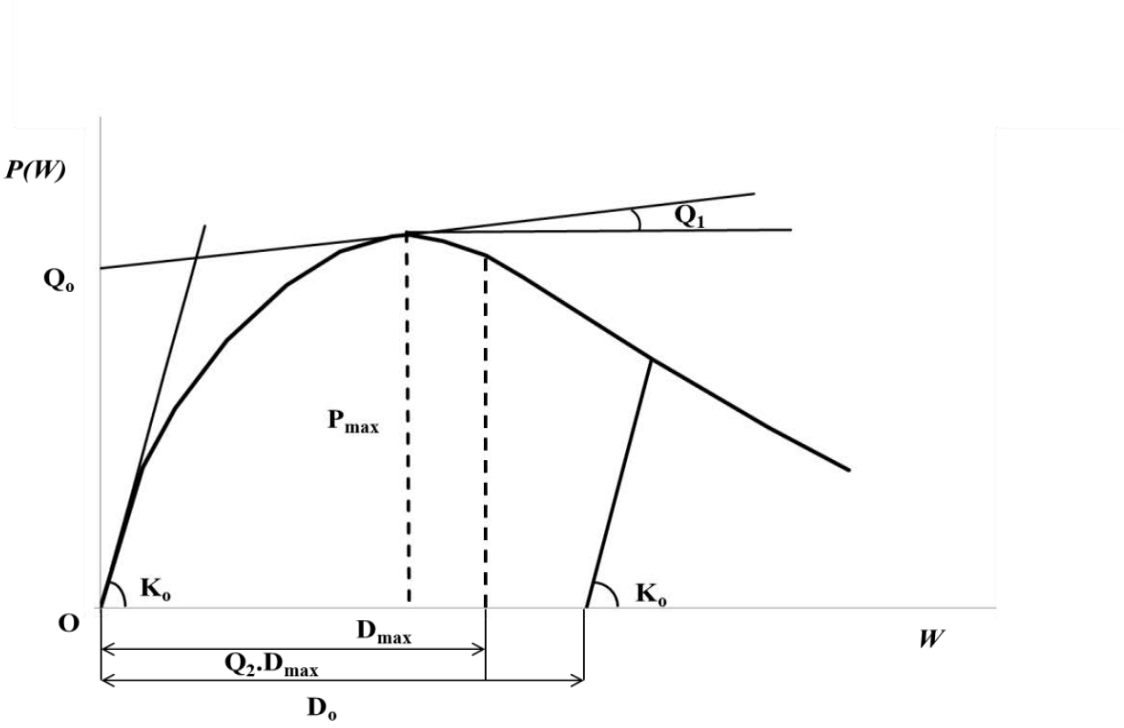

Figure C.2. Embedment function *p*(w) for single nail joint

$p(w)$ is expressed as follows,

If $w \leq D_{max}$

$$p(w) = (Q_0 + Q_1 w)\left(1 + e^{[-Kw/Q_o]}\right) \quad \text{C.1}$$

If $w > D_{max}$ then;

$$p(w) = P_{max} e^{\{Q_3 (w - D_{max})^2\}} \quad \text{C.2}$$

Figure C.2 shows that the initial stiffness is K_0, Q_0 and Q_1 are the intercept and the slope of the asymptote approached as the deformation w tends to infinity. K_0, Q_0, Q_1, Q_3, and D_{max} are independent parameters and Q_2 gives the fraction of D_{max} *at* which the pressure drops to 0.8 P_{max} during the softening phase (Li *et al*., 2012), These independent parameters are calibrated using test results for monotonically increasing w; P_{max}, Q_3 are defined by:

$$P_{max} = (Q_0 + Q_1 D_{max})\left(1 - e^{[-K_0 D_{max}/Q_o]}\right) \quad \text{C.3}$$

$$Q_3 = \log\{0.8\} / [D_{max}(Q_2 - 1)]^2 \quad \text{C.4}$$

The current study estimated the values of embedment parameters (K_0, Q_0, Q_1, Q_2, Q_3, and D_{max}) from single nail joint tests. They were used in the FEM development.

C.2.1 Experimental Tests and Results

The embedment parameters (K_0, Q_0, Q_1, Q_2, Q_3, and D_{max}) were determined by testing the joints of 30 mm x 2.8ϕ hardened head galvanized hand nail embedded in timber of Australian MGP10 radiata pine (Figure C.3). The tests were carried out at the crosshead movement rate of 2.5 mm/min based on the Australian standard AS 1649 (2001) in an Instron testing machine; the test set-up is shown in Figure C.4. The test joints were stored at 25ºC and 65% relative humidity for 24-hours prior to testing. Ten joints were tested for reaction forces and vertical displacements (i.e. the relative displacement of the crosshead of Intron machine).

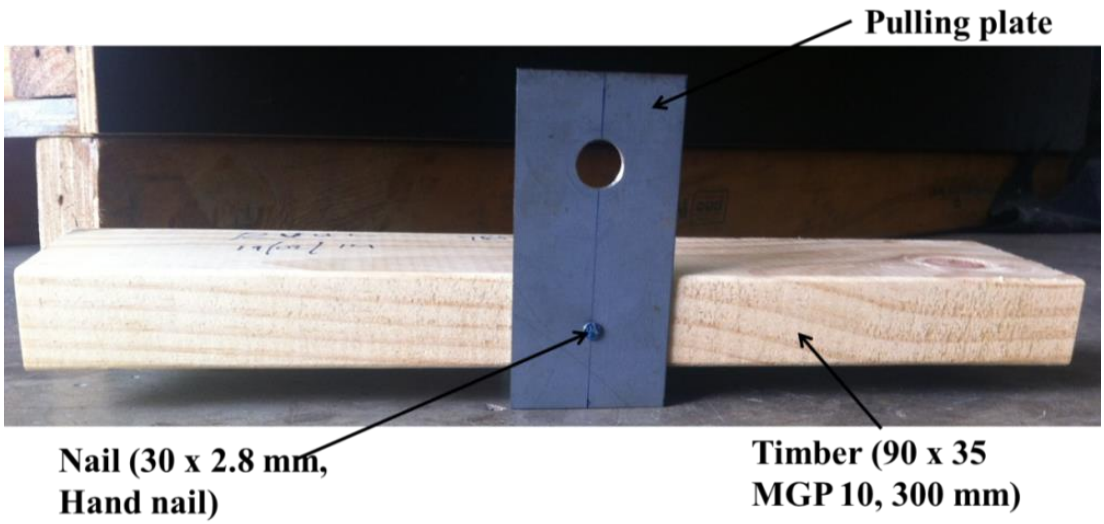

Figure C.3. Single nail joint test specimen

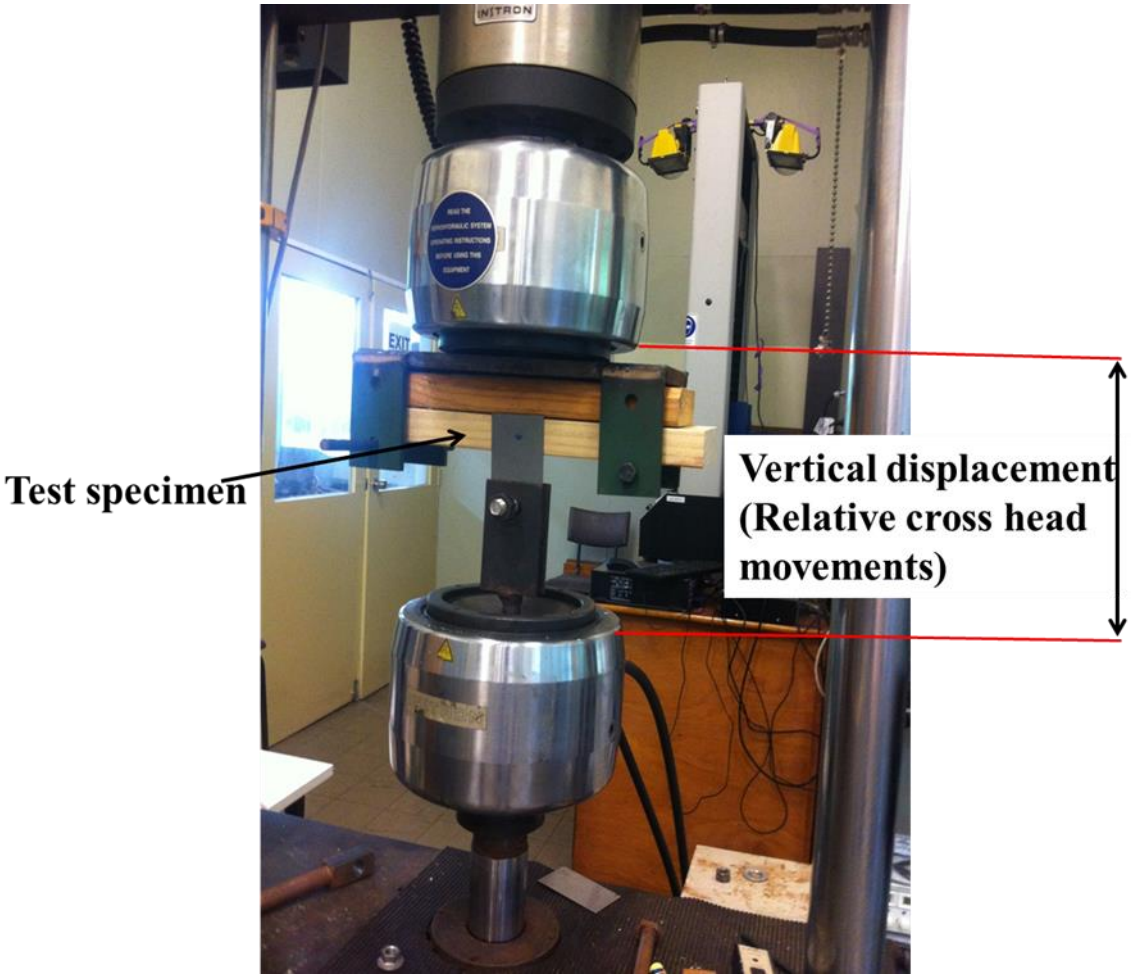

Figure C.4. Load test setup

Figure C.5 shows the maximum, average and minimum force versus vertical displacement relationships of the single nail joint tests. Figure C.5 also shows that the maximum average force is 2 kN at a vertical displacement of 8.1mm. The results are used to develop the FEMs of roof to wall triple grip and truss grip connections.

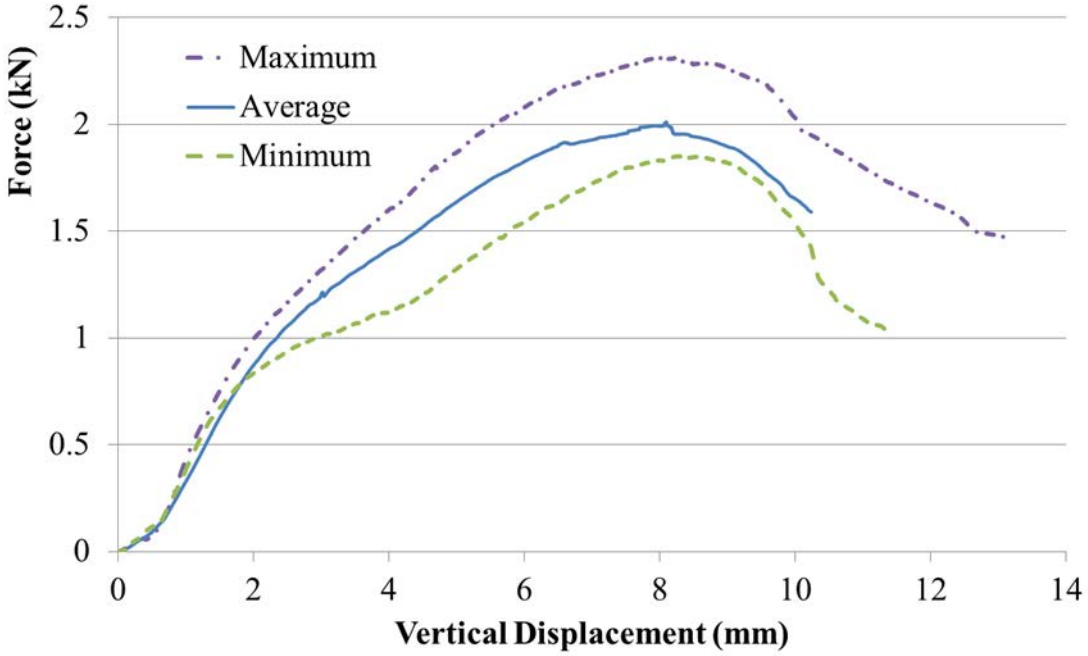

Figure C.5. Force-displacement relationship-determined from single nail joint tests

C.3 FEM development

The FE software package ABAQUS (6.12-3) was used to develop the numerical model of the roof to wall triple grip and truss grip connections for prediction of uplift capacity and failure modes. The starting point for the FEM was a single nail joint model and the results of this model used for validation of the embedment property.

To simplify the model development, three assumptions were made to achieve the objectives (i.e. determine the strength and stiffness of the RWC): i) the variability of material properties are neglected, which means that timber, nails and triple grip are treated as isotropic materials; ii) *p(w)* is assumed to be a deterministic function; and iii) based on (i), the splitting failure of timber is not considered.

However, the FEM assumed that the timber and nail are isotropic materials while in nature the timber and nail are anisotropic materials (De Borst et al., 2013). Therefore, this model used a 0.5 mm thickness nail shape membrane between the nail and timber interaction area, which was also able to represent sufficient embedment contact pressure and material non-linearity in the interaction regions between the nail and timber. The modulus of elasticity of the membrane, E_m is expressed as;

$$E_m = p(w)_{max} \times L/A \qquad \text{C.5}$$

where, $p(w)_{max}$ is the maximum reaction from the timber medium per unit length, A is the interaction surface area between the nail and timber and L is the interaction surface length. Poisson`s ratio of membrane is taken as 0.34, which is the average Poisson's ratios of nail and timber. The material properties detailed in Table C.1 were used in the FEM.

Table C.1. Material properties for the FEMs

Material	Modulus of Elasticity, E (GPa)	Poisson's Ratio, v	Density, ρ (kg/m^3)
Timber (MGP10)	10	0.37	510
Steel (Nail, Triple grip and Truss grip, Yield strength 340 MPa)	210	0.3	7850
Membrane	0.85	0.34	-

C.3.1 Embedment property of single nail joint

The embedment property of a single nail joint is essential to develop the FEM of the RWC. Accurate estimations of the parameters of $p(w)$ are difficult as estimation can only be achieved by pure compression tests without some bending of the nails (Foschi, 2000; Li et al., 2012). Thus, this study used the NEURAL NETWORK coding of MATLAB to determine the embedment parameters K_0, Q_0, Q_1, Q_2, Q_3, and D_{max} from the single nail joint tests. The force displacement relationship and the embedment parameters of Li et al (2012) have been used as input data for the NEURAL NETWORK coding to calibrate the embedment parameters. Table C.2 shows the obtained timber embedment parameters of a single timber nail joint. The embedment relationship ($p(w)$) of the single timber nail

joint was derived from Equations C.1 and C.2, and the resulting embedment relationship of the single timber nail joint is shown in Figure C.6.

Table C.2. Embedment parameters of a single timber nail joint

Embedment parameters	30 x 2.8 mm hardened head galvanized hand nails MGP 10 (E=10 GPa and density 510 kg/m^3)
Q_o (kN/mm)	0.5
Q_1(kN/mm^2)	0.05
Q_2	1.6
K_o(kN/mm^2)	0.8
D_{max}(mm)	5

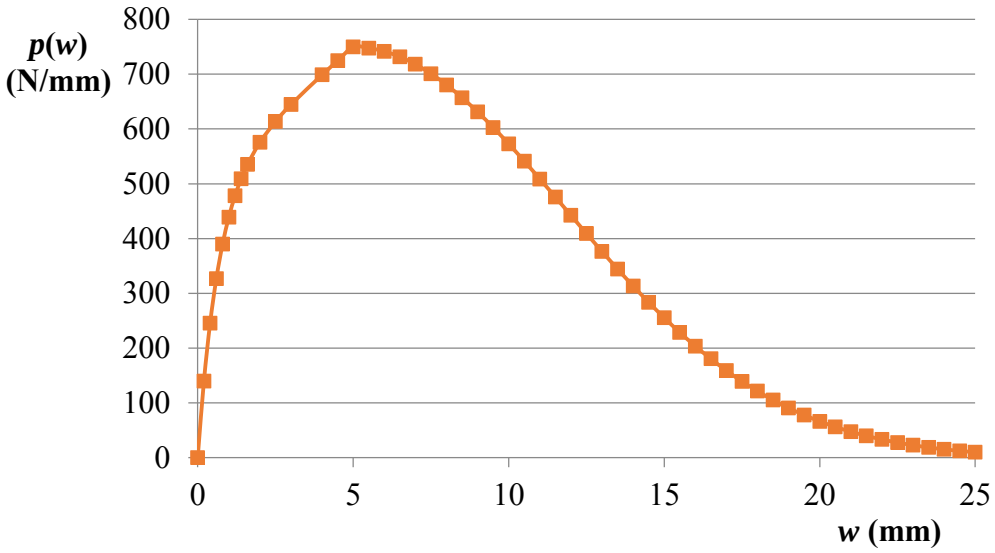

Figure C.6. Embedment function *p(w)* determined by the single timber nail joint tests

C.3.2 Validation of embedment property

A 3D single nail joint model was developed using ABAQUS (6.12-3) to validate the embedment property, as shown in Figure C.7. This model was initiated with the formation of individual components such as nail, membrane and truss, then assembled from these components.

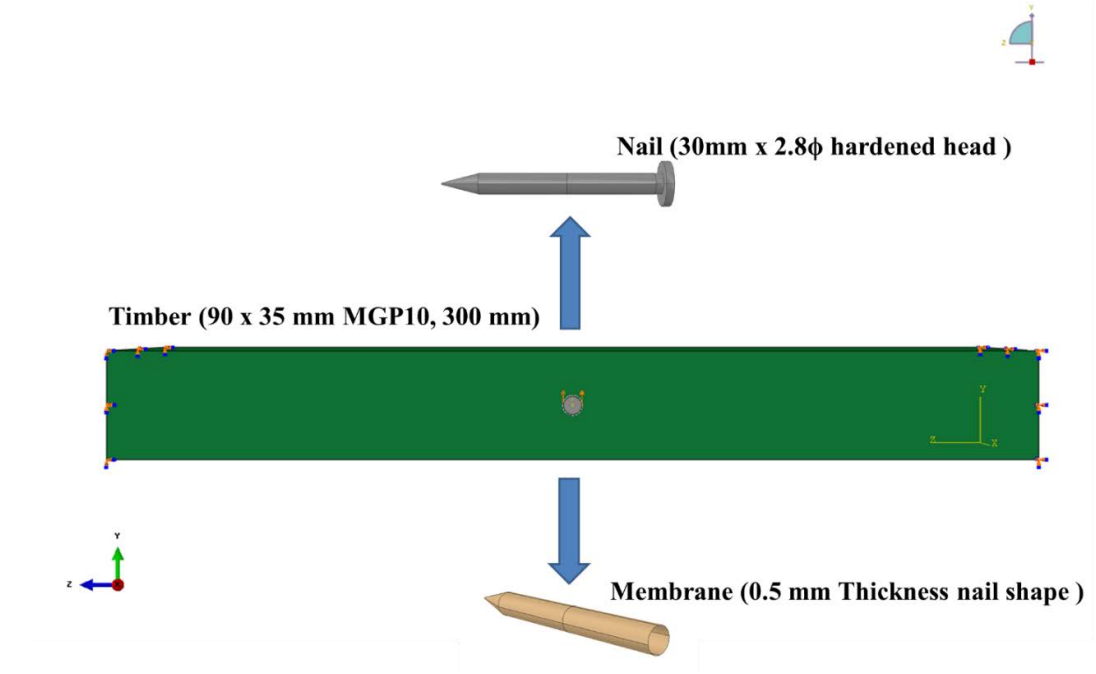

Figure C.7. FEM of single nail joint

All of the joint components were modelled using fifteen-node quadratic triangular prism elements (C3D15). The quadratic triangular prism element is capable of representing large deformation, geometric and material nonlinearity. The applied boundary condition of this model is based on the single nail experimental test as described in Section C.2.1. At the head of the nail surface, a displacement boundary condition was imposed (i.e. where the nail head moves upwards). A fixed boundary condition was also assigned at the edge surface of the timber (Figure C.7). A tie constraint was introduced between the membrane and timber surface. In addition, a nonlinear spring element available in ABAQUS was used to connect the nodes at the interface between the membrane and nail along the length of the nail (Figure C.8). The spring was activated in the nail pull out direction. A hard contact was employed in the other direction's interface, replicating a master-slave relationship. The input force-displacement relationship of the spring was obtained using the relationships in Equations C.6, C.7 and C.8.

$$F_s = p(w) \times w/(e * n) \qquad \text{C.6}$$

$$D = w + S_i \qquad (\text{If } w>0) \qquad \text{C.7}$$

$$D = w \qquad (\text{If } w=0) \qquad \text{C.8}$$

Where, F_s represents the force in each spring, n is the number of springs connected along the nail (in this model, 16 spring elements were used) and e is the approximate global seed size of nail (in this model the global seed size is 1.5). The initial nail slip found in the single nail joint test represents as S_i, and D is the relative distance between the two nodes connected by a single spring. The input force-displacement relationship for each spring is shown in Figure C.9.

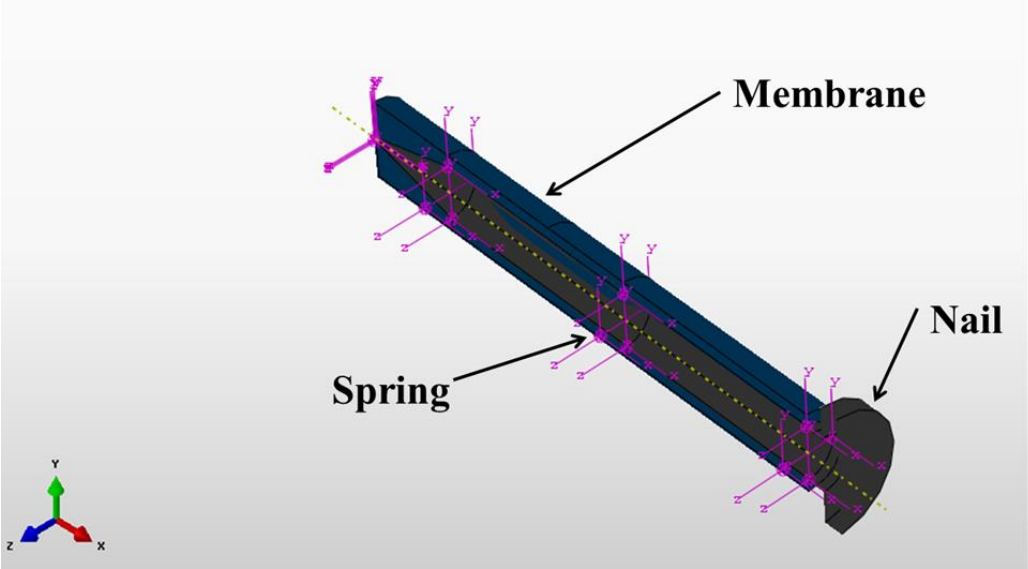

Figure C.8. Nonlinear spring location in the single nail joint model

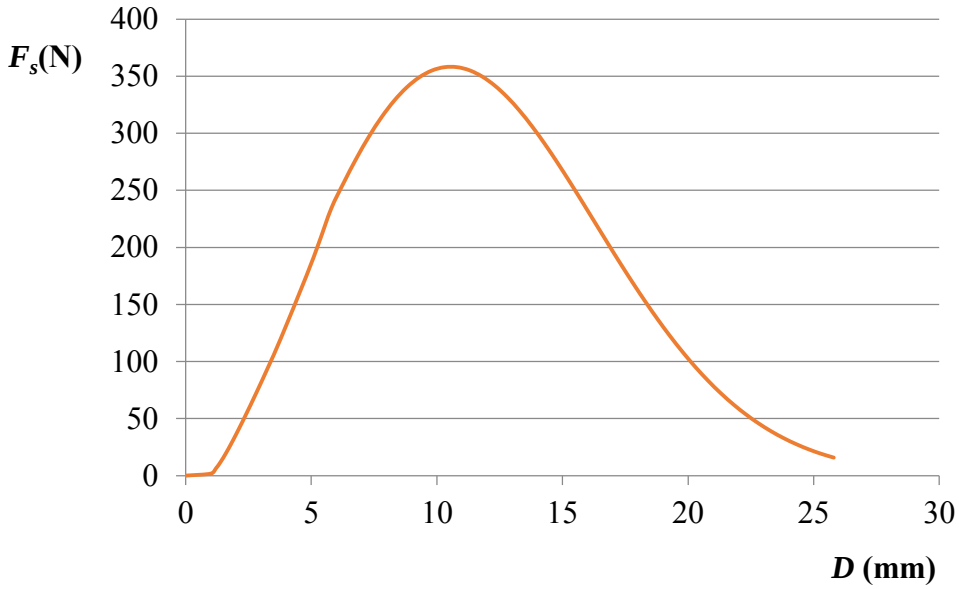

Figure C.9. Input force-displacement relationship for each spring

The experimental test and FEM comparisons of the force versus vertical displacement relationship of the single nail joint are shown in Figure C.10. The maximum reaction force was reached at a vertical displacement of 8.1 mm in both the experiment and FEM. However, the maximum reaction force determined by the FEM was 2.1 kN, higher than the experimental test result of 2 kN. The FEM also gives an initial stiffness value higher than the experimental results. This difference could be due to the nail slip observed at the beginning of the experiment (Figure C.10). Nail pull-out and nail bending failure modes were observed in this model, which was similar to the experimental test. Figure C.11 illustrates the deformed nails observed in the experiments and the FEM. This shows that the deformation at the head of the nail observed in the experiments is slightly different to the FEM. This difference is due to the applied load location, in the experiments the displacement was applied to the nail by the steel plate (1 mm thickness), whereas in the FEM it was directly applied to the nail head. That is, the restraint from the steel plate in the experimental test results in a different deformed shape at the head of the nail compared to that in the FEM. The contact area between the nail and steel plate was smaller than that of the nail and timber. Therefore, in order to simplify the single nail model development, the model did not consider the effect of the steel plate. In summary, for a single nail joint model loaded in shear, the FEM analysis gives a reasonable comparison to the experimental test behaviour.

The FEM analysis results of peak load and maximum stiffness (i.e. peak load divided by the displacement at peak load) shows approximately 5% difference with that of the load tests. Therefore, the largely empirical embedment property parameter (K_0, Q_0, Q_1, Q_2, Q_3, and D_{max}) values obtained from the single nail joint test results along with NEURAL NETWORK is optimised for the FE single nail model. These parameters form the basis of the multiple connections for the triple grip model discussed in Section C.4.

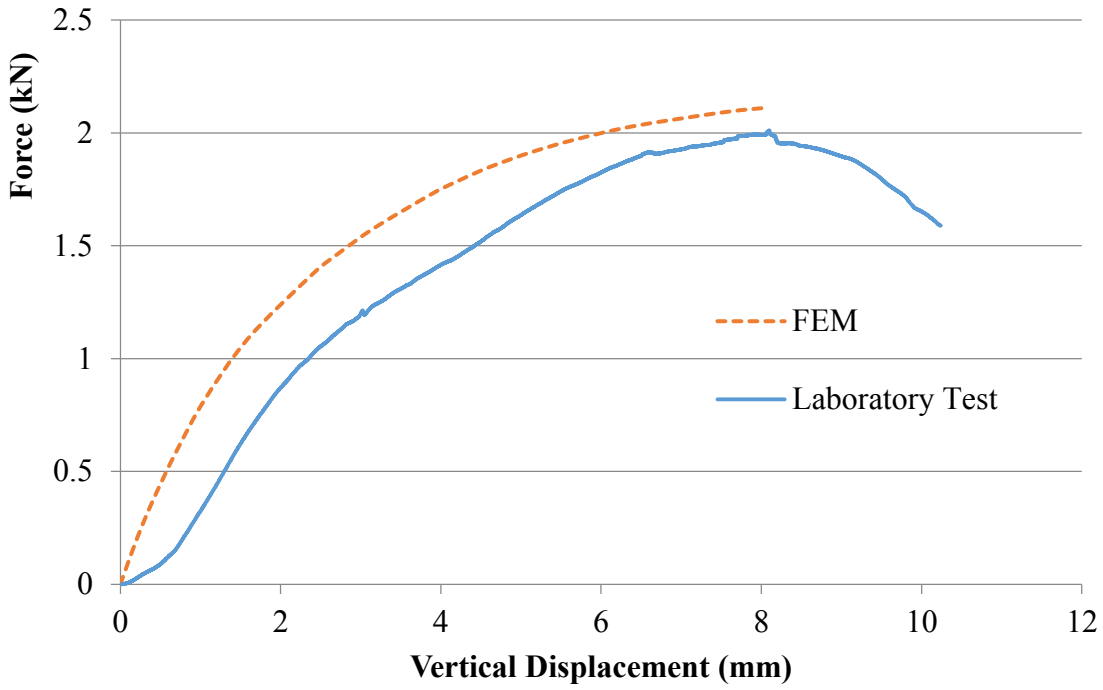

Figure C.10. Comparison of force-displacement relationship for a single nail joint model and experimental test

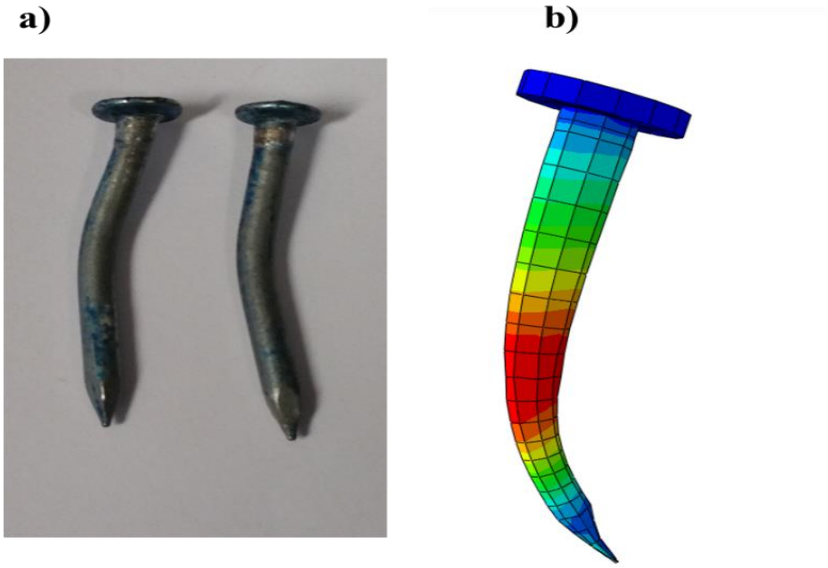

Figure C.11. Deformed shape of nails observed in the laboratory test and the FEM: a) laboratory test; b) FEM analysis

C.4 Numerical model analysis of roof to wall triple grip connections

A three-dimensional (3D) triple grip connection FEM was assembled and subjected to load (Figure C.12). The model consisted of five separate parts: triple grip (1 mm thickness), nail, membrane, truss and top-plate. A fifteen-node quadratic triangular prism element (C3D15) was used to assemble the truss, top-plate and membrane. An eight-node linear brick element (C3D8R) was used to assemble the triple grip and nail. In addition, a non-linear spring element was used to represent the embedment property of the timber nail joint, as described in Section C.3.2. A "surface-to-surface" contact interaction was developed for this model to interact with the triple grip, truss and top-plate. In the tangential direction of the contact surface between triple grip to truss and top plate, a penalty friction contact was introduced and in other directions of those regions, a hard contact was employed. A friction coefficient of 0.3 was used between the triple grip and top-plate or truss contact surface. To connect the nail and the triple grip in this model, a tie constraint was introduced between the nail and triple grip surface.

Boundary conditions and applied loads for this model were based on the experimental tests detailed in Chapter 4; the applied loading consisted of an axial displacement imposed at the top-plate in the pull-out direction, which generated a force used to pull the top-plate to a certain distance. Table C.3 illustrates the boundary conditions assigned to this model.

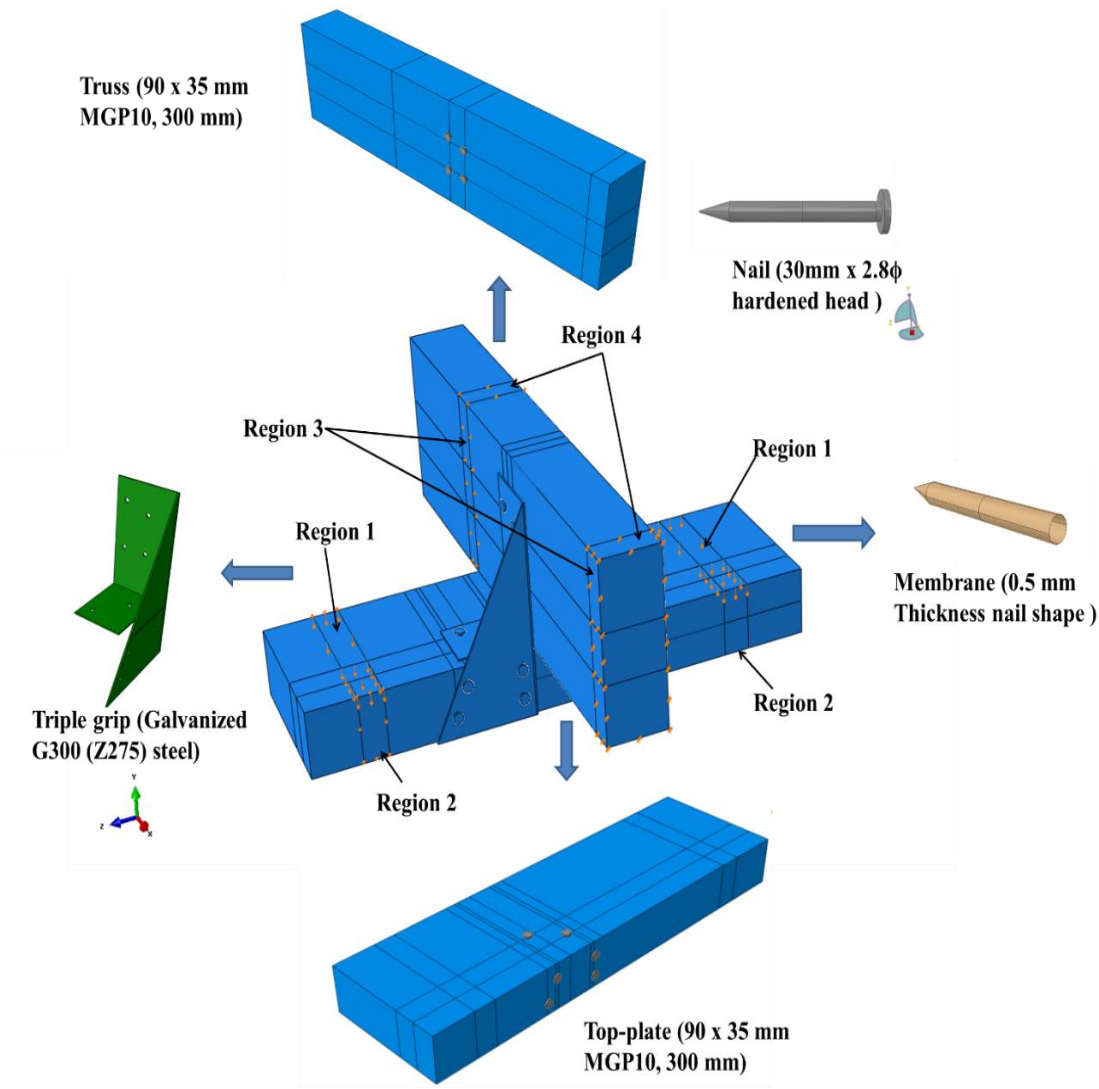

Figure C.12. FEM of triple grip connection

Table C.3. Applied boundary condition based on the laboratory test.

Region	Boundary condition
1	U1=U3=0
2	U1=U3=0
3	U1=U3=0
4	U1=U2=U3=0
Note: U1, U2, U3 are the displacements in x, y and z directions of this model	

Six different types of hand nailed triple grip connections were assembled and analysed in this study. These are representative of the experimental test of hand nailed connections described in Chapter 4 and details of these connections are given in Table C.4.

Table C.4. Detail of the triple grip connections with and without construction defects

Connection types	Detail
Type A	Ideal (Figure 4.4)
Type A-N1,	Missing nail N1
Type A-N6	Missing nail N6
Type A-N9	Missing nail N9
Type A-(N1-N6)	Missing nail N1and N6
Type A-(N1-N8)	Missing nail N1and N8

C.4.1 Verification against test results

The reaction force versus vertical displacement and the peak loads were obtained from the FEM analysis and compared with laboratory test results presented in Chapter 4 (Section 4.2.3). Figure C.13 depicts the comparison of the reaction force versus vertical displacement relationship for the "Ideal" triple grip connection Type A with the experimental test results and the numerical model. The experimental tests were conducted on twenty specimens and Figure C.13 shows the average of the reaction forces and the vertical displacement of the twenty test results. The FEM analysis gives a peak load of 5.15 kN at a vertical displacement of 19mm. This peak load and displacement were higher than the average peak load and displacement of the experimental test. Nail slip behaviour was found in the experimental test but it did not show in the FEM. This nail slip behaviour could be the reason for the peak load variation between the FEM and the laboratory test.

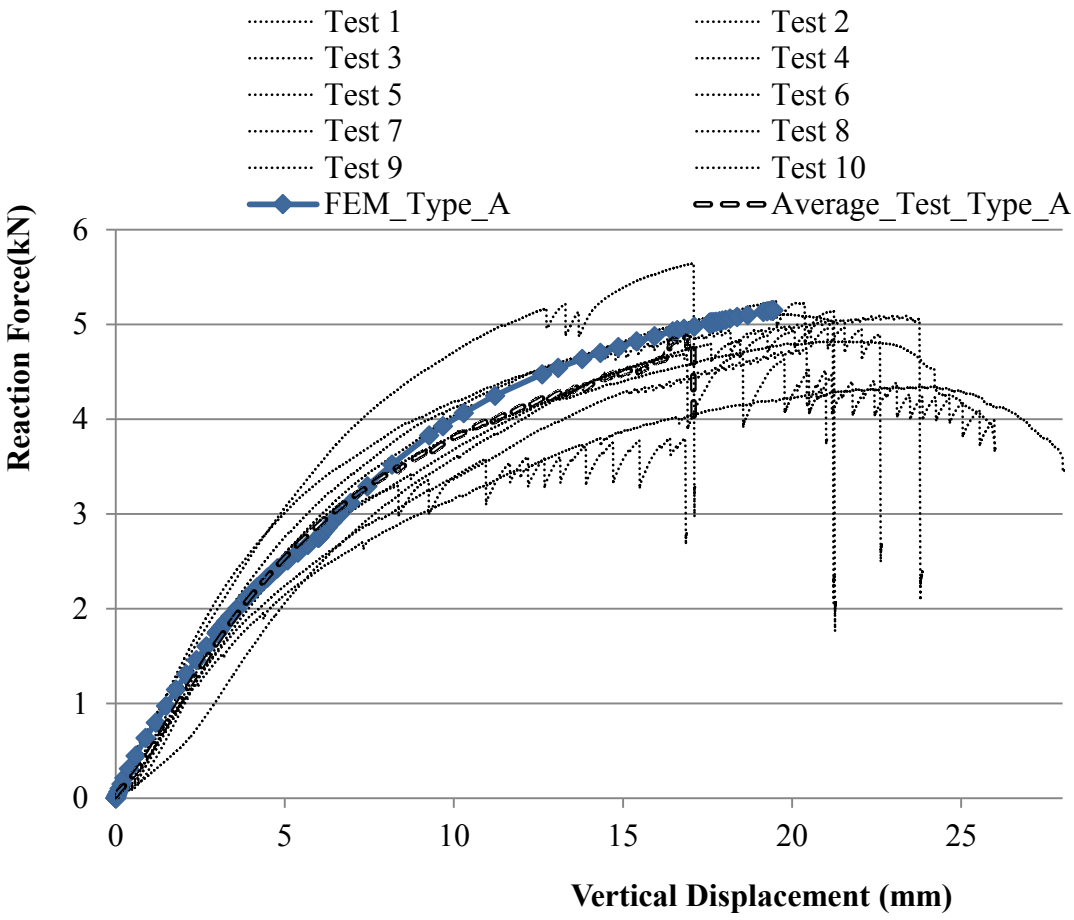

Figure C.13. Comparison of the FEM analysis and the laboratory test force-displacement relationships for the triple grip connections Type A

Figures C.14 and C.15 show the comparison of the reaction force displacement curves of the defective hand nailed connections numerical model (Types A-N1, A-N6, A-N9, A-(N1-N6) and A-(N1-N8)) with the reaction force displacement curve of the experiments. Figure C.14 shows that the peak loads and the maximum displacements of the FEM of the connection Types A-N1, A-N6 and A-N9 were less than those of the experimental results. Material non-linearity between the experiments and FEM might be the reason for the peak load variation between the experiments and FEM. In the experiments, the nail slip was observed from the beginning (Figure C.14), but was not observed in the FEM of those connections. This could be one reason for the variation in the displacements and peak loads of the experiments and the FEM. However, the stiffness of those connections in the FEM was similar to the experiments.

The peak load obtained in the FEM analysis of the connection Type A-(N1-N6) was less than the experimental test results, whilst the peak load of connection Type A-(N1-N8) was higher than the experimental test results (Figure C.15). High nail slip was found in the experimental test of connection Type A-(N1-N6) compared to Type A-(N1-N8) connections, as described in Figure C.15. This is the reason for connection Type A-(N1-N6) having high peak load. Based on the FEM and experiments, the failure load and stiffness of each hand nailed triple grip connection shows the FEM analysis gives about 90% of the peak loads and the stiffness (i.e. peak loads divided by the displacement at peak load) obtained in the experimental tests (Table C.5). Further, the lowest stiffness obtained in the FEM was with connection Type A-(N1-N8) compared to other connections (Table C.5). This is due to the missing nail N8, because this nail was located very close to the centre line of the loading actions.

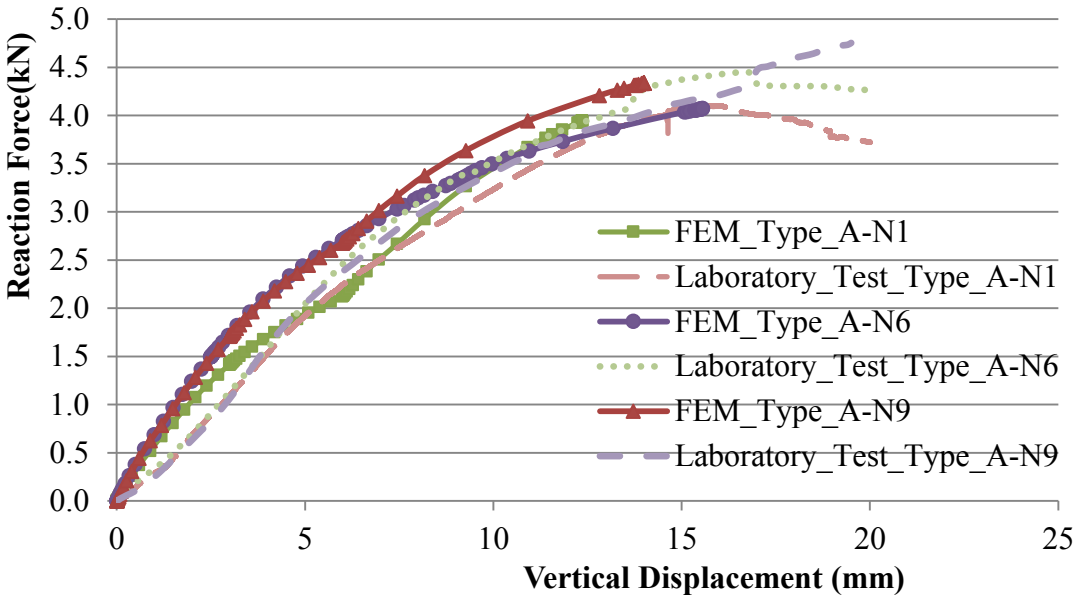

Figure C.14. Comparison of the FEM analysis and laboratory test force- displacement relationships for the triple grip connections Type A-N1, A-N6 and A-N9

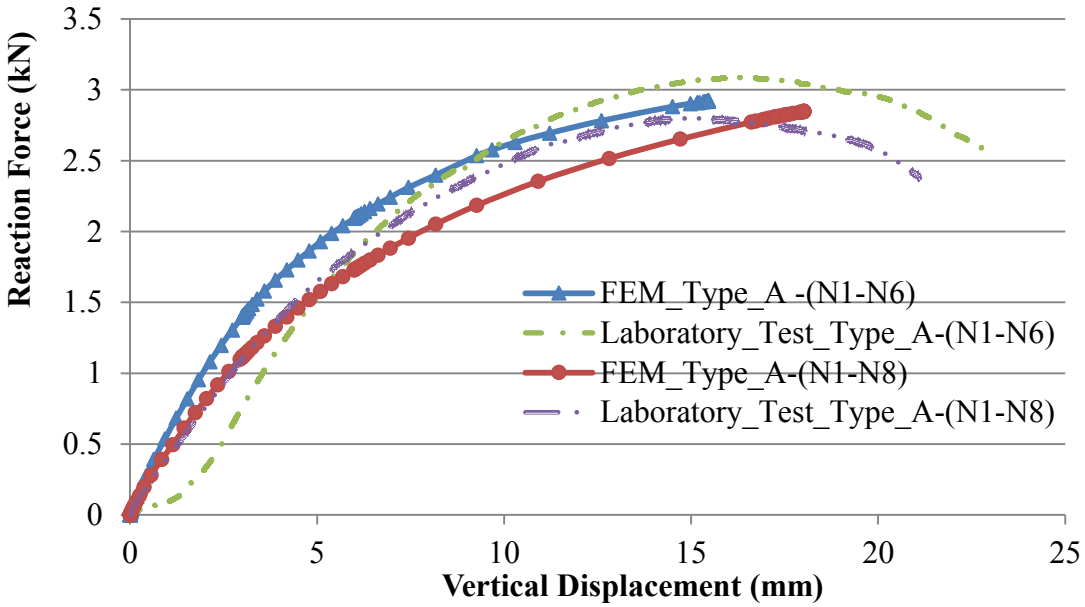

Figure C.15. Comparison of the FEM analysis and laboratory test force- displacement relationships for the triple grip connections Type A-(N1-N6) & A-(N1-N8)

Table C.5. Comparison of the peak load and stiffness of the connections between the laboratory and numerical model results

Detail	Peak Load (kN)		Stiffness (N/mm)	
	Laboratory Test	FEM	Laboratory Test	FEM
Type A (Ideal)	4.85	5.15	273.22	273.12
Type A-N1, (missing nail N1)	4.07	3.92	275.34	278.26
Type A-N6, (missing nail N6)	4.45	4.1	264.18	264
Type A-N9, (missing nail N9)	4.75	4.35	260.13	293.3
Type A-(N1-N6), (missing nail N1& N6)	3.1	2.93	194.69	194.31
Type A-(N1-N8), (missing nail N1&N8)	2.78	2.86	198.46	164.74

Figure C.16 illustrates the un-deformed and deformed shapes of the triple grips and nails obtained from the FEM analysis. The nails N1, N2, N3, N7 and N8 deformed significantly compared to the other nails. This is because these nails are located closer to the centre line of loading action. This indicates these nails N1, N2, N3, N7 and N8 have a significant influence on the response of the triple grip connection to loading. This behaviour is similar to the experimental test failures detailed in Chapter 4. Nails N1, N2, N3 and N4 on the truss indicate pull out failure and bending failure while the nails on the top-plate (i.e. N5, N6, N9 and N10) show the pull-out failure with minimal bending. Figure C.16 also shows the bending failure of nails N7 and N8 but this failure was not observed in all types of hand nailed triple grip connections in the experimental tests. This could be the reason for differences in the peak load and stiffness between the FEM and experiments, as listed in Table C.5. Figure C.17shows the comparison between the deformed shapes of the FEM analysis and the experimental test for the triple grips. The deformed shape of the triple grips in the FEM is indistinguishable with deformation in the experimental tests. Thus, the FEMs have given an acceptable prediction of the test behavior.

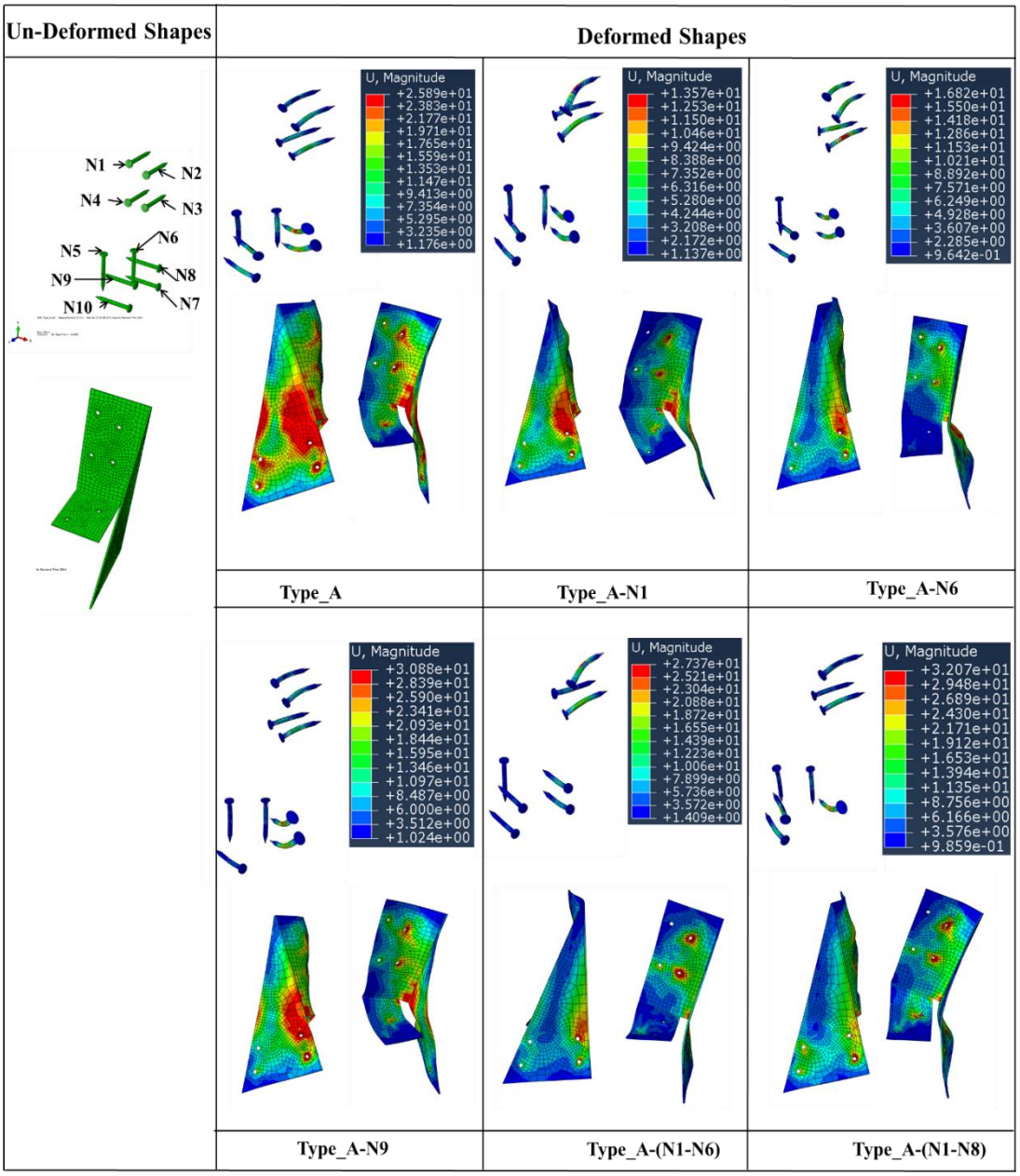

Figure C.16. FEM of triple grip connections: deformed and un-deformed shapes of triple grip and nails

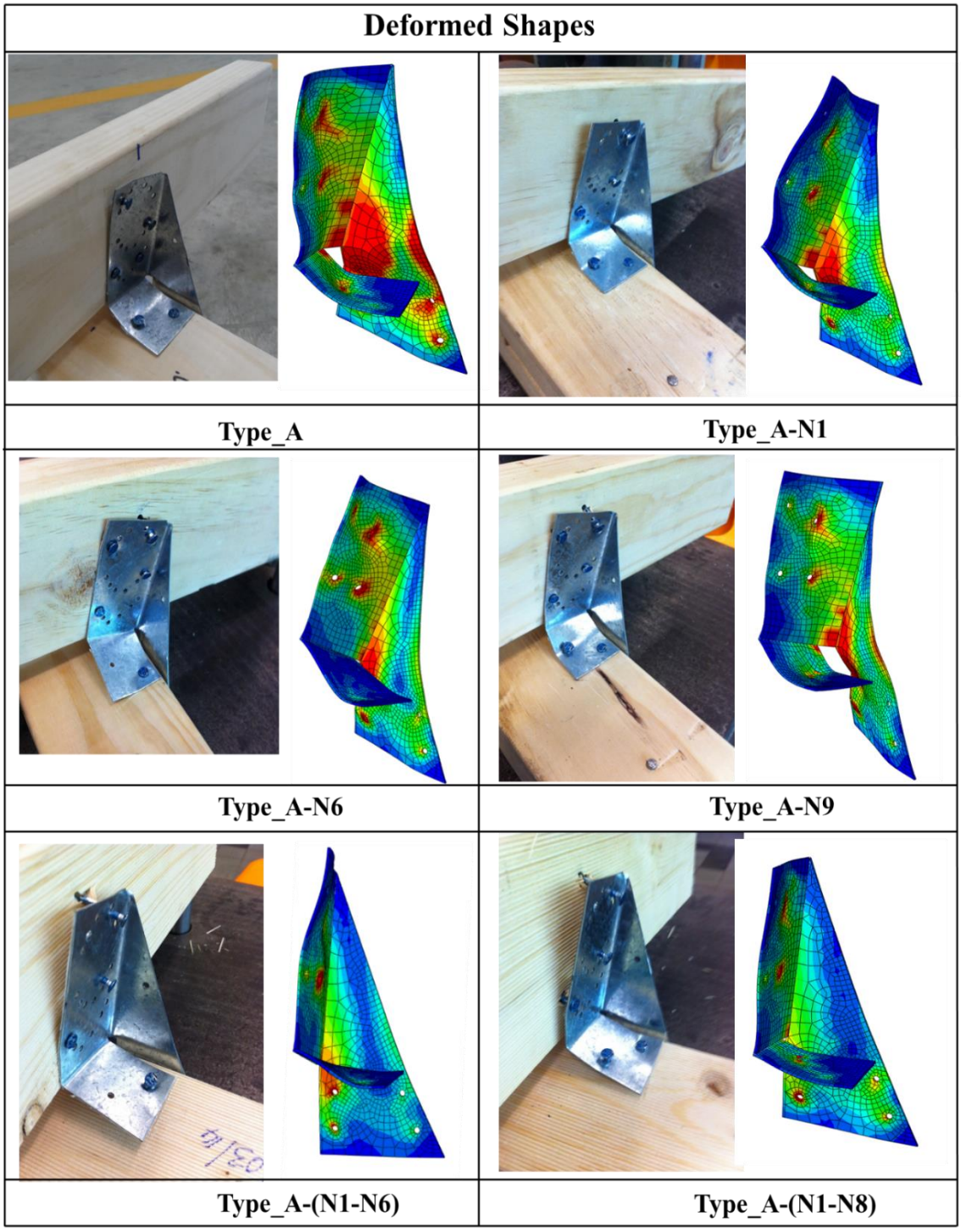

Figure C.17. Comparison of the FEM analysis and laboratory test deformed shape for the triple grip

C.4.2 Combination loading effect on the roof to wall triple grip connection

Australian houses are constructed with a pitched roof (i.e. generally 20^{o} to 22.5^{o}); therefore, when the timber-framed house is subjected to wind loading, the RWCs

experience tri axial loading (i.e. vertical, lateral and horizontal). When load were applied perpendicular to the roof surface, the RWCs experienced vertical (i.e. y direction) and lateral (i.e. x direction) forces (Figure C.18a), but in the individual tests and FEM, the load was applied in only the vertical direction. This indicates that the structural response and design uplift capacity of the roof to wall triple grip connection needs to be analysed with a combination of vertical and lateral direction loads.

A 68.5^{o} angle (i.e. toward to vertical axis y) loading (P= 6 kN) was subjected to the "Ideal" roof to wall triple grip connection FEM (Figure C.18b) to evaluate the combination loading effect on the RWC structural response. The RWCs of windward side (i.e. Support A) experiences high lateral direction force (i.e. –x direction) compared to that of leeward side (i.e. Support B) when wind loads on the windward side is higher than leeward side. Therefore, two types of angle loading were subjected to the model, one with +x direction load (i.e. Type_A(+x)) and other one with –x direction load (i.e. Type_A(-x)). In reality, the horizontal movement (i.e. z direction) of the truss was resisted by the battens, cladding and roof cross bracing. Thus, in this model the boundary condition of U3 was equal to zero (i.e. there is no horizontal movement) at Region 2, and pin boundary condition was imposed at the top-plate Region 1 (Figure C.18b).

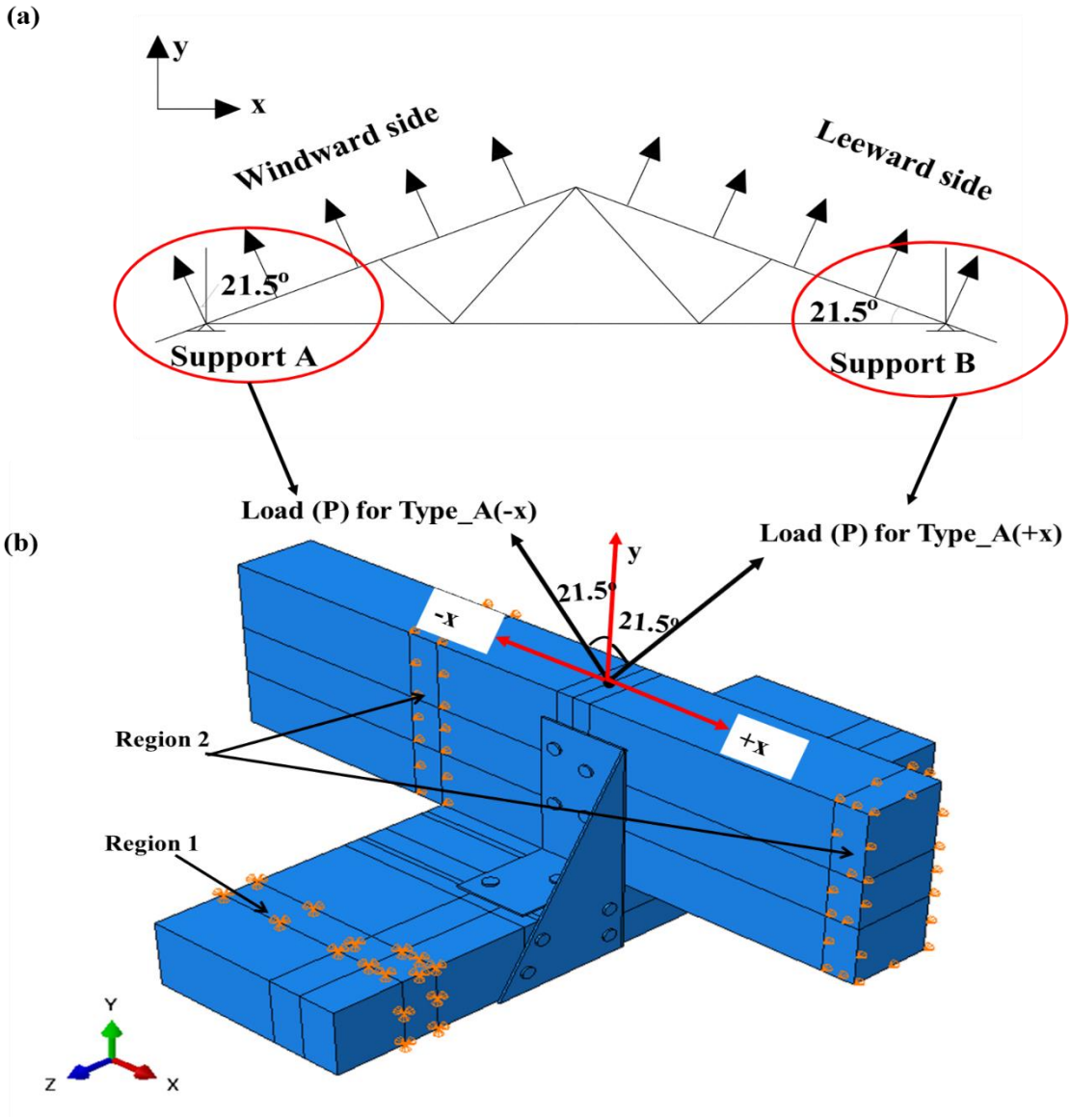

Figure C.18. "Ideal" roof to wall triple grip connection model subjected to angle load; a) schematic diagram of wind load on a single truss, and b) angle loading FEM

Figure C.19 shows the comparison of the vertical reaction force versus displacement between the combination loading FEMs (i.e. Type_A(+x) and Type_A(-x)) and vertical loading FEM (i.e. Type_A). This figure shows the maximum vertical reaction force 1.9 kN was obtained at 12.5 mm vertical displacement in the Type_A(+x) FEM, whilst maximum vertical reaction force 1.8 kN was obtained at vertical displacement 13.5 mm in the Type_A(-x) FEM. These maximum vertical reaction forces were about 65% less than that of the Type_A FEM (i.e. 5.15 kN). This was due to the combination loading,

which created different failure modes and structural response compared to that of the Type_A model. This reaction force difference indicates that the uplift capacity of the roof to wall triple grip connection is reduced by about 65%, when the roof structure experiences wind load.

Figure C.19 also shows that the maximum vertical stiffness of the Type_A(+x) FEM was about 10% higher than that of the Type_A(-x). This indicates the vertical stiffness of the loading side connection was higher than that of the non-loading side connection in the full-scale test structure. This stiffness variation of the RWCs indicates that the roof to wall triple grip connection stiffness and failure modes depend on the loading type and the direction based on the connection configuration.

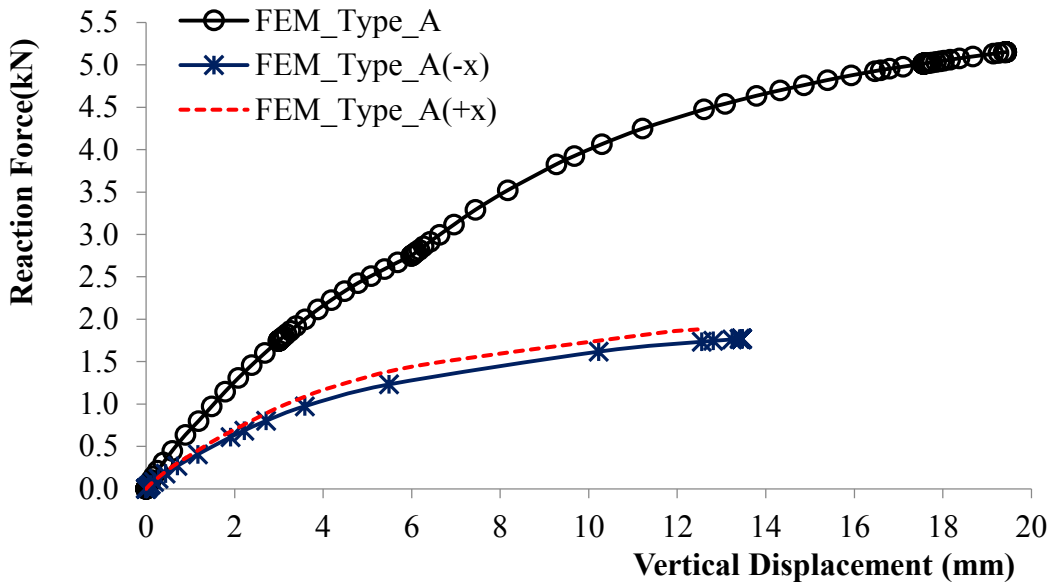

Figure C.19. Comparison of the vertical reaction force displacement relationship for RWCs subjected to vertical and angle loading

The vertical reaction force-displacement relationship of Type_A(+x) FEM was compared with that of the loaded side trusses' RWCs obtained from the full-scale test results at Stage S3 when loading along the Batten B2 (Figure C.20). The Batten B2 was located in-line with RWCs in the full-scale test structure thus the reason for the reaction force-displacement relationship obtained when loading along this Batten B2 was compared with

FEM. In addition, at Stage S3, the reaction forces were measured at top-plate before installed the ceiling this also the reason for the results compared at this construction stage.

Figure C.20 shows the vertical reaction force-displacement relationship of the each RWC in the full-scale test structure was not similar. This indicate that the stiffness of the RWC was different in each individual connection due to their location, material non-linearity and construction practice. This type of similar behaviour was showed in the individual joint test results (Chapter 4). Moreover, the FEM analysis gives an average reaction force-displacement relationship and this also the reason for the reaction force-displacement relationship variation between the FEM and each individual connection. However, Figure C.20 also shows the average reaction force-displacement relationship of the loaded side RWCs of the full-scale test structure (i.e. reaction forces and displacements are divided by the number of connections). This average reaction force-displacement relationship shows the initial stiffness (i.e. vertical displacement up to 0.75 mm) of the RWC in the FEM was about 10% less than that of the full-scale test.

In the full-scale test, the vertical movement of the trusses were partially resisted by the battens and their connections but in the FEM, there was no restriction on the vertical movement. This was the reason for less stiffness obtained in the RWC of FEM. When compared the RWC stiffness differences between the FEM and full-scale test, the RWC of Trusses T.A and T.E showed less differences than other trusses' RWC (i.e. T.B, T.C and T.D). This was due to the location of the trusses in the test structure. Truss T.A and T.E were located at the end of the test structure and the vertical movement of these trusses' was resisted by battens is about 50% less than other trusses.

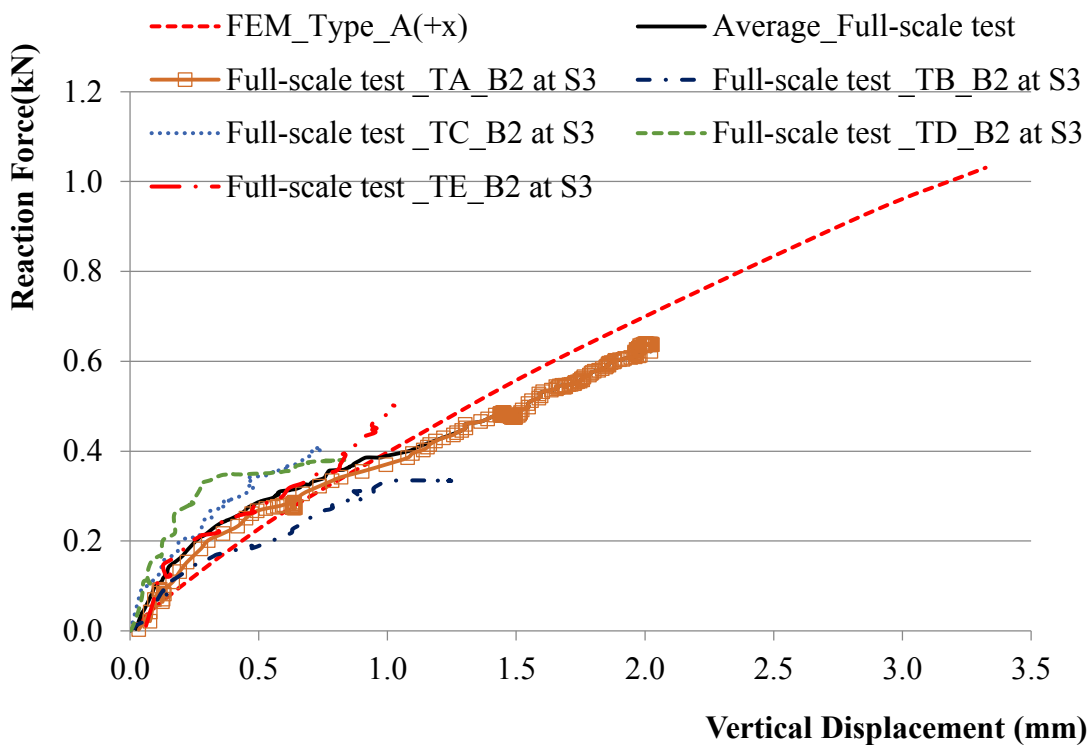

Figure C.20. Comparison of the RWCs vertical reaction force displacement with FEMs and the full-scale test at Stage S3

The deformed shape and nail withdrawal obtained in the "Ideal" connection model subjected to angle loading were compared with that of the full-scale test Truss B connection after Stage 3, as shown in the Figure C.21. Figure C.21a shows the loaded side truss RWCs comparison with Type_A(-x) FEM, whilst Figure C.21b presents non-loaded side connection comparison with Type_A(+x) FEM. This Figure C.21 shows that the deformed shape of triple grip and the nail obtained in the FEMs were similar as the full-scale test. Type_A(-x) FEM showed that the deformation of triple grip was higher than that of the Type_A(+x) FEM. Partial nail withdrawal was observed in the Type_A(-x) FEM but it was minimal or negligible in the Type_A(+x) FEM. This failure mode deference between the loaded side and non-loaded side is due to the prying force created at the non-loaded side RWCs by the lateral load.

The deformed shape and nail withdrawal observed in the Type_A(-x) FEM was higher than that of the full-scale test. This is because, the numerical model was subjected load was three times higher than that of the full-scale tests. However, the RWC behaviour is similar in both FEM and the full-scale tests. The stiffness variations and the failure modes

of the RWCs indicate that the roof to wall triple grip connection stiffness and failure modes are depends on the loading type and the direction based on the connection configuration. The reaction force-displacement relationship (Figure C.20) and the failure modes (Figure C.21) comparison between the FEMs and the full-scale test indicates that the FEM model of the individual connection shows the similar experimental behavior. Therefore, this model can be used as alternative to laboratory test to predict and asses the RWC strength and structural response.

a)

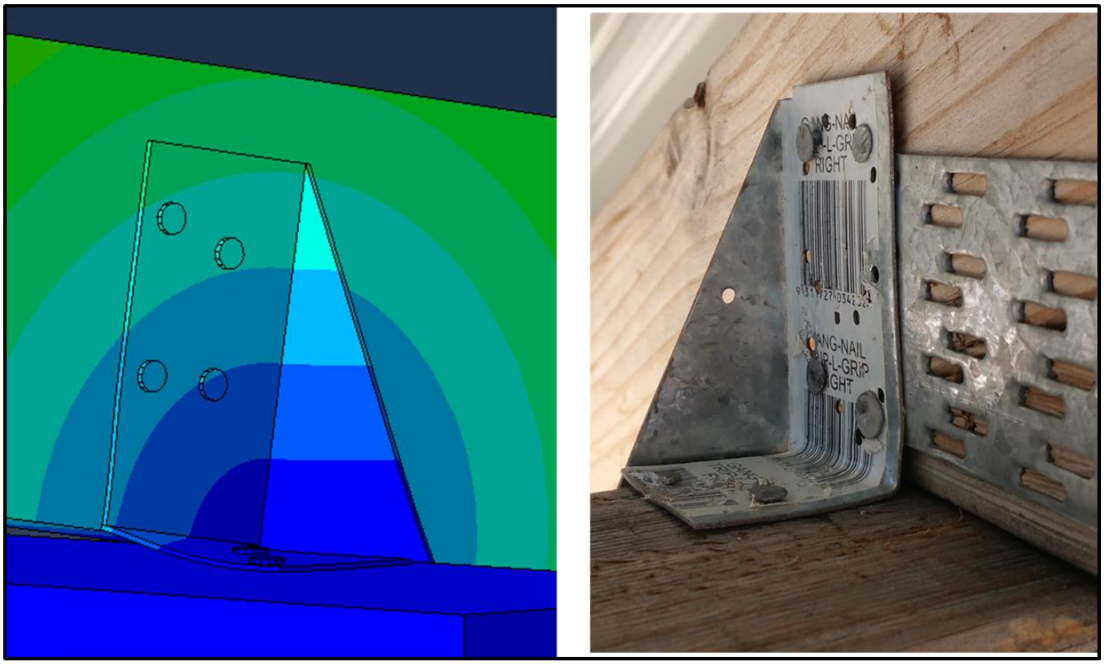

b)

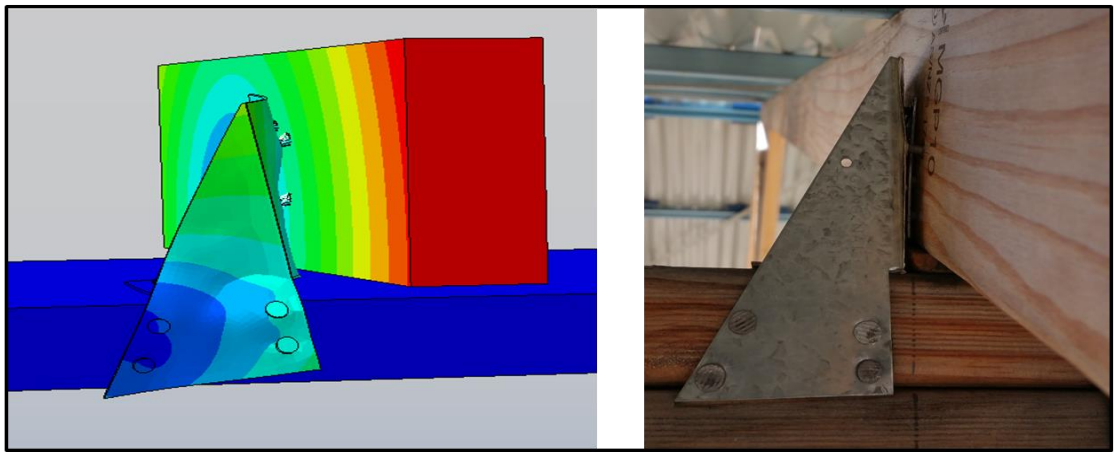

Figure C.21. Comparison of the RWCs deformed shape with FEMs and the full-scale test after Stage S3: a) loading side support and Type_A(+x), and b) non-loading side support and Type_A(-x)

C.5 FEM analysis of roof to wall truss grip connection

A FEM of a truss grip connection was developed in order to analyse and understand the behaviour and response of such a connection to loading. The four main parts of the truss grip connection as shown Figure C.22 are; the truss, the top-plate, and membrane were modelled using fifteen-node quadratic triangular prism elements (C3D15) and the truss grip modelled using eight-node linear brick elements (C3D8R). The assembling method and applying boundary condition and contact interaction were similar to the FEM of the triple grip connection described in Section C.4. The geometry of nail teeth in the truss grip was modelled as rectangular shape to simplify the development of this model.

Conducting the experimental tests of the truss grip connection with construction defect is burdensome. Because the most common construction defects of this connection are partially driven nail teeth as described in Chapter 3. The construction of this defective connection for the experiments is excessively difficult as per the length of nail teeth (10 mm) in the truss grip. Consequently, the FEM would be the main source to assess the defective connection response to loading. Thus, this study developed a FEM of the defective truss grip connection. Three different types of defective truss grip connections were developed and the details of these connections are described in Table C.6.

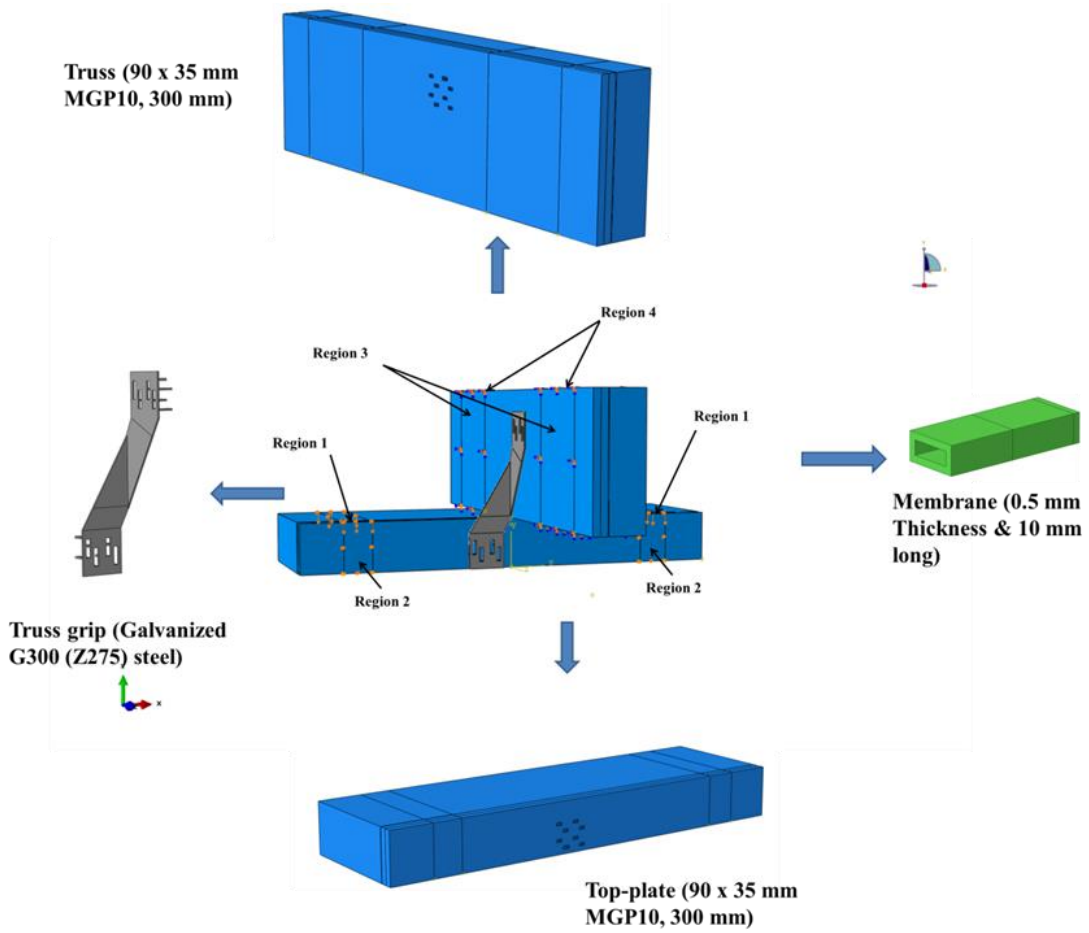

Figure C.22. FEM of truss grip connection

Table C.6. Detail of the truss grip connections with and without construction defects

Connection types	**Details**
Type B	"Ideal" connection
Type B-TR50	Partially driven (50%) nail teeth on the truss
Type B-TP50	Partially driven (50%) nail teeth on the top-plate
Type B- (TR-TP) 50	Partially driven (50%) nail teeth on the top-plate and truss

C.5.1 Validation of the truss grip connection FEM

For the "Ideal" truss grip connection (Type B), Figure C.23 shows the comparison of the reaction force versus vertical displacement relationship derived from the FEM with that

of experimental test results (Chapter 4). The peak load was achieved at a vertical displacement of 4.95 mm in both the experiment and FEM. However, the peak load obtained in this model was 1.16 kN, higher than the experimental test result of 1.12 kN. This difference could be due to the differences in nail teeth shape between the FEM and the experiments. Figure C.24 illustrates the failure modes observed in the experiments and the FEM analysis. Nail teeth pull-out, nail teeth bending and truss grip bending failure modes were observed in this model. These failure modes were similar to the experimental test. However, some nail teeth were bent up and some were bent down in the experiments while in the FEM they were bent down only. Nail teeth on the top-plate showed the pull-out failure in the model but it was not observed in the experiments. These variations in the failure modes were due to the nail teeth shape difference and material non-linearity between the experiments and FEM. The FEM analysis gives a reasonable experimental test behavior of the truss grip connections, with a 5% differences in the peak load and maximum stiffness.

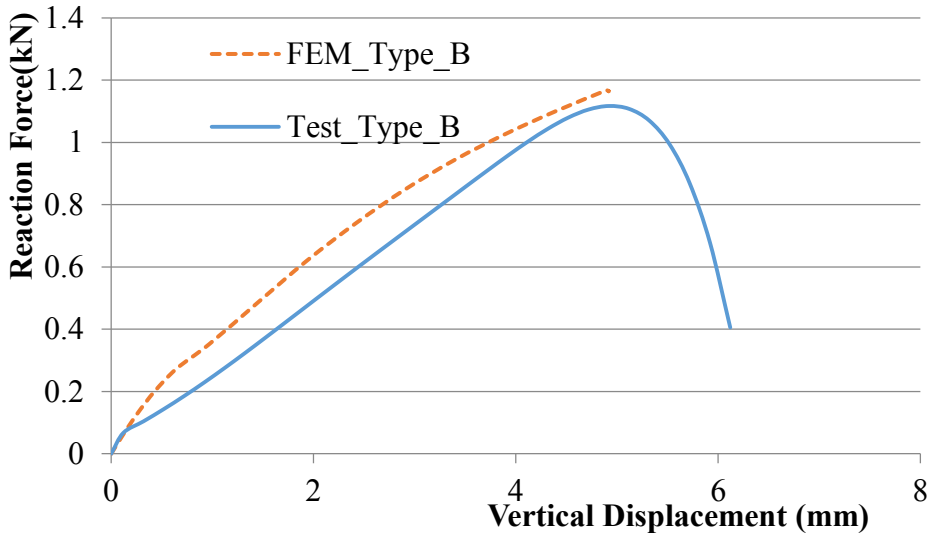

Figure C.23. Comparison of the FEM analysis with the laboratory test force-displacement relationships for the truss grip connection Type B

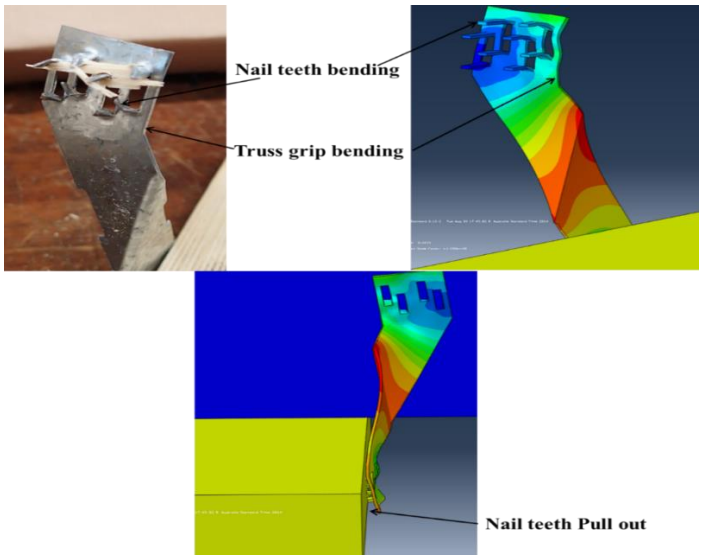

Figure C.24. Failure modes observed in the laboratory test and the FEM of the "Ideal" Truss grip connection Type B

Based on the FEM analysis, comparisons were made between the "Ideal" and defective truss grip connections force versus displacement behaviour, as shown Figure C.25. The strength and stiffness of the truss grip connection significantly reduces when the nail teeth are partially driven to the truss or top-plate. This reduces about 70% of the "Ideal" truss grip connection (Type B) strength and stiffness.

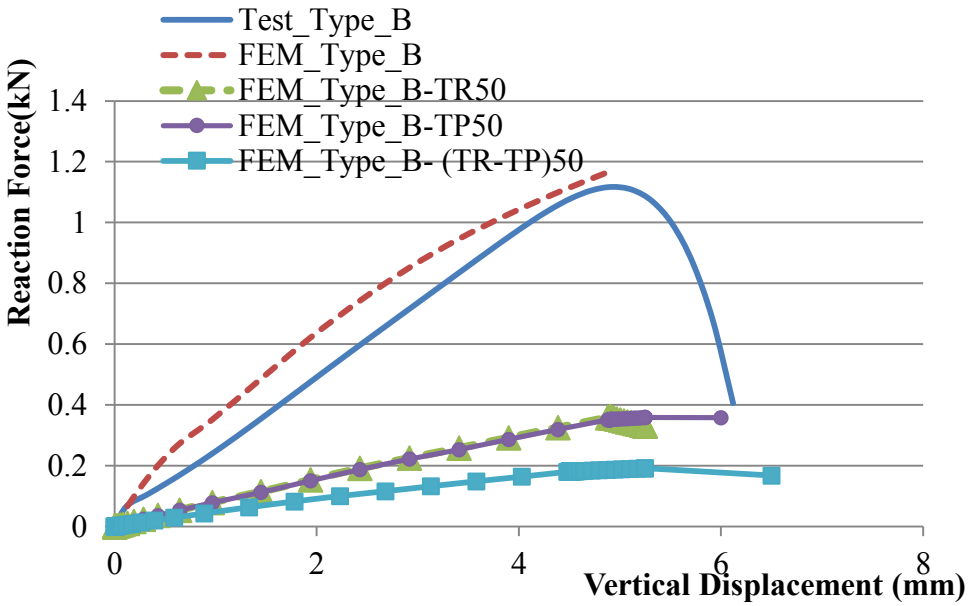

Figure C.25. Force- displacement relationships comparison between the "Ideal" and defective truss grip connections

C.6 Prediction of the design uplift capacity for the RWCs based on the FEM

FEM analysis gives a reasonable structural response of the triple grip and truss grip connections subject to uplift loading. Appendix D in the standard AS1720.1 (2010) specifies methods to determine the design uplift capacity from the force displacement relationship of these connections. Based on the FEM analysis, this study predicts the design uplift capacity of a hand nailed triple grip connection and truss grip connection with and without construction defects. The comparison of the design uplift capacities with standard and manufacturer's specification are listed in Table C.7 and shows that the design uplift capacity of "Ideal" triple grip connection based on the FEM was higher than the uplift capacity obtained from the experiments. The uplift capacity 1.5 kN was obtained when the "Ideal" triple grip connection subjected to wind load (i.e. angle load). This uplift capacity was about 55% less than the uplift capacity specified by the AS 1648.2 (2010) and about 50% less than the manufacture specification (MiTek (2014)). However, these uplift capacities specified by the standards and the manufacturer were obtained by vertical loading tests. The uplift capacity of the angle loading model were about 10% less than the maximum truss hold down force (1.68 kN) calculated for general truss region at wind speed 57 m/s (Chapter 3). This is indicates that the uplift capacity of the RWCs in the non-cyclonic regions houses are lower than the requested.

In Australian timber-framed house roof was pitched, thus that structure suffer from the combination of the vertical (y direction) and lateral (x direction) loads due to the windstorms. Thus, the standards and the manufacture's need to be consider the angle loading to determine the uplift capacity of the RWCs. Design uplift capacities of defective triple grip connections show good agreement between the FEM and experiments. The design uplift capacity of the "Ideal" truss grip connection obtained from the model also shows good agreement with design uplift capacity from the experiments. Based on the FEM analysis the design uplift capacity of the defective truss grip connections show that the partially driven nail teeth (i.e. 50% of the total length) on the top-plate or truss or both truss and top-plate gives about 70% of the "Ideal" connection (i.e. Type B) design uplift capacity.

Table C.7. Design uplift capacities of the RWCs

Design uplift capacity (kN)				
Detail	From AS1720.1 (2010) using experimental test	From AS1720.1 (2010) by using FEM	From AS 1648.2 (2010)	From MiTek (2014)
Hand nailed triple grip connections				
Type A (Ideal)	4.04	4.29	3.5	3.1
Type_A(+x)	-	1.58	-	-
Type_A(-x)	-	1.5	-	-
Defective hand nailed triple grip connections				
Type A-N1	3.39	3.27	-	-
Type A-N6	3.71	3.42	-	-
Type A-N9	3.96	3.63	-	-
Type A-(N1-N6)	2.58	2.44	-	-
Type A-(N1-N8)	2.32	2.38	-	-
Truss grip connections				
Type B (Ideal)	0.93	0.97	-	1.1
Defective Truss grip connections				
Type B-TR50		0.3	-	
Type B-TP50		0.3	-	-
Type B- (TR-TP)50		0.2	-	-

C.7 Summary and discussion

The response of triple grip and truss grip connections and single nail joints has been studied using laboratory tests and FEM analysis. The analysis included the design uplift capacity variation with a range of construction defects for the roof to wall triple grip and the truss grip connections. The advantage of a validated FEM will provide an economical means to assess the contribution of the many parameters that comprise the RWCs (e.g. stiffness, strength, stress, failure mode, different type of timber species, different type of

nails, etc.) along with the complex loading (i.e. tri axial loads, load and moment, combination of static and dynamic load, and etc.).

The results show the location of the nails defines the stiffness and failure modes of the triple grip connections. The stiffness of the triple grip connection also depends on the response of the nails located close to the center line of the loading action. Missing nails located close to the center line loading action was a common occurrence from the field survey (Chapter 3). The design uplift capacity for the "Ideal" truss grip connection is similar to laboratory test results. The partially driven nail teeth (i.e. 50% of the total length) on the top-plate or truss or both truss and top-plate reduced the strength, stiffness and design capacity by about 70% of the "Ideal" connection.

The roof to wall triple grip connection, subjected to a combination of the vertical and positive direction lateral load, the stiffness of the connection was about 15% higher than that of the connection subjected to the vertical and the negative direction lateral load. The RWC was subjected to a combination of the lateral and vertical loads, the uplift capacity was about 55% less than the only vertically loaded connection. Thus, the standards and the manufacturer should consider the uplift capacity combined with the lateral and vertical loads. The FEM analysis used in this study can be an effective alternative to load tests carried out in the laboratory to predict the structural response and design uplift capacity of the roof to wall triple grip and truss grip connections. With proper input parameters, these methods could also be used to predict uplift capacity and response of any timber metal nail joints. Based on the relative movement between truss and top-plate or rafter, this FEM also can quantify the residual strength of the RWCs after windstorm damage.

APPENDIX D: DETAILS AND MORE RESULTS OF FEM OF FULL-SCALE TEST STRUCTURE

D.1 Compression loading FEM of batten to truss connection

A batten to truss connection model was developed using ABAQUS (6.12-3) to determine the force displacement relationship when compression load is applied, as shown in Figure D.1. This model was assembled with the formation of individual components such as batten and truss. A two-node beam element (B31) was used to assemble the batten and an eight-node brick element (C3D8R) was used to assemble the truss. This model was only suitable to assess the compression loading effect on the batten to truss connections.

A surface to surface hard contact was enforced at each contact region between the batten and truss. Pin support was imposed on the bottom surface of truss and compression load was subjected at the batten to truss connection fastener locations. Applied load and the movement between the batten and truss were measured (Figure D.2). This force displacement relationship was used to develop the FEM full-scale test structure.

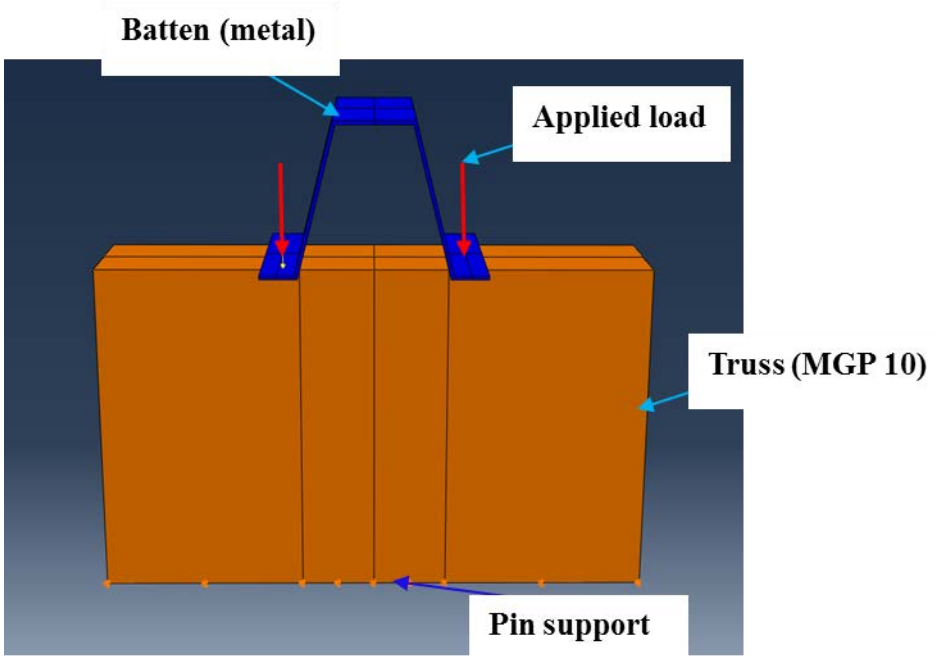

Figure D.1. FEM of batten to truss connection

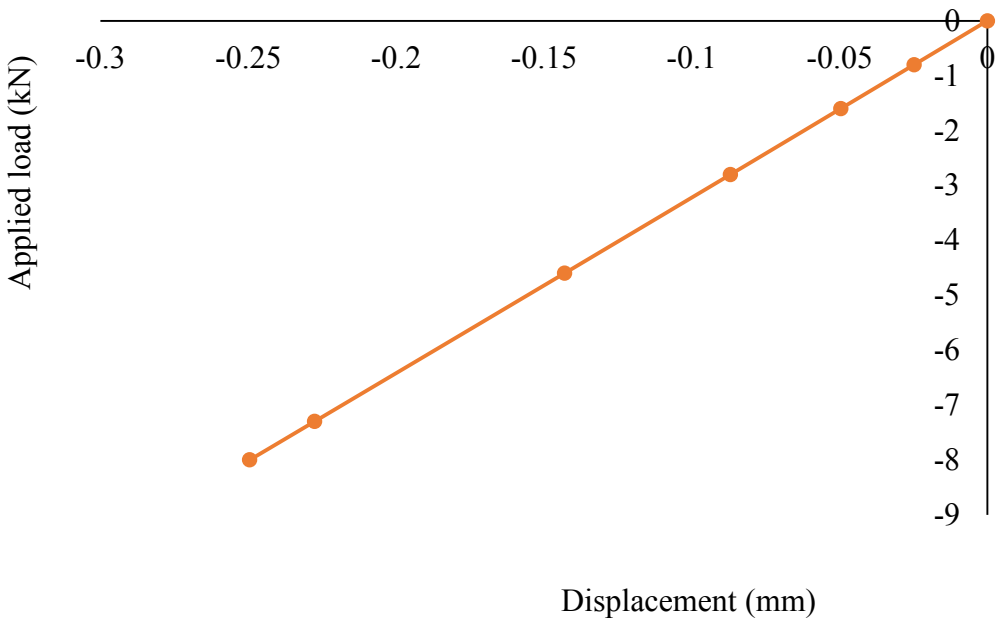

Figure D.2. Force displacement relationship of batten to truss connection when compression was load applied

D.2 Compression loading FEM of plasterboard to timber joint

A plasterboard to timber joint FEM was developed to evaluate the compression load effect (Figure D.3). The model consisted of two separate parts: plasterboard and truss. An eight-node linear brick element (C3D8R) and a four-node shell element (S4R) was used to assemble the truss and plasterboard respectively. This model only suitable to evaluate the compression loading effect. Pin supports were imposed along the bottom surface of plasterboard and compression load was subjected at the top surface of truss (Figure D.4). A surface to surface hard contact was enforced at each contact region between the plasterboard and truss. Applied load and vertical displacement (i.e. relative to support) of the truss were measured (Figure D.4). This force displacement relationship was used in the joint between the ceiling to truss bottom chord for the FEM full-scale test structure.

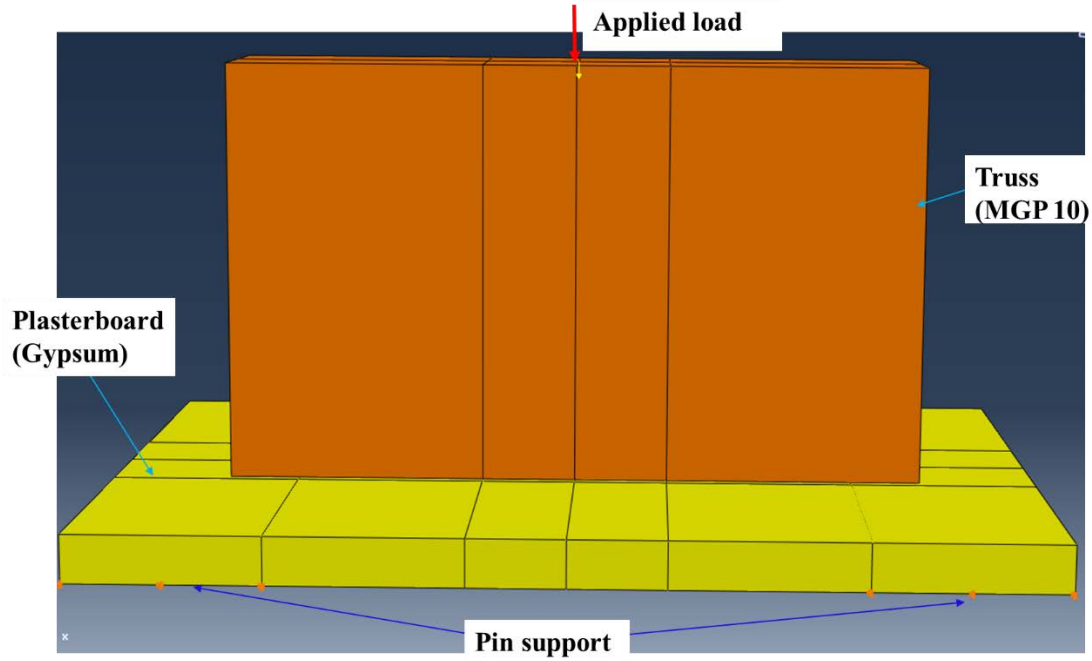

Figure D.3. FEM of plasterboard to timber joint

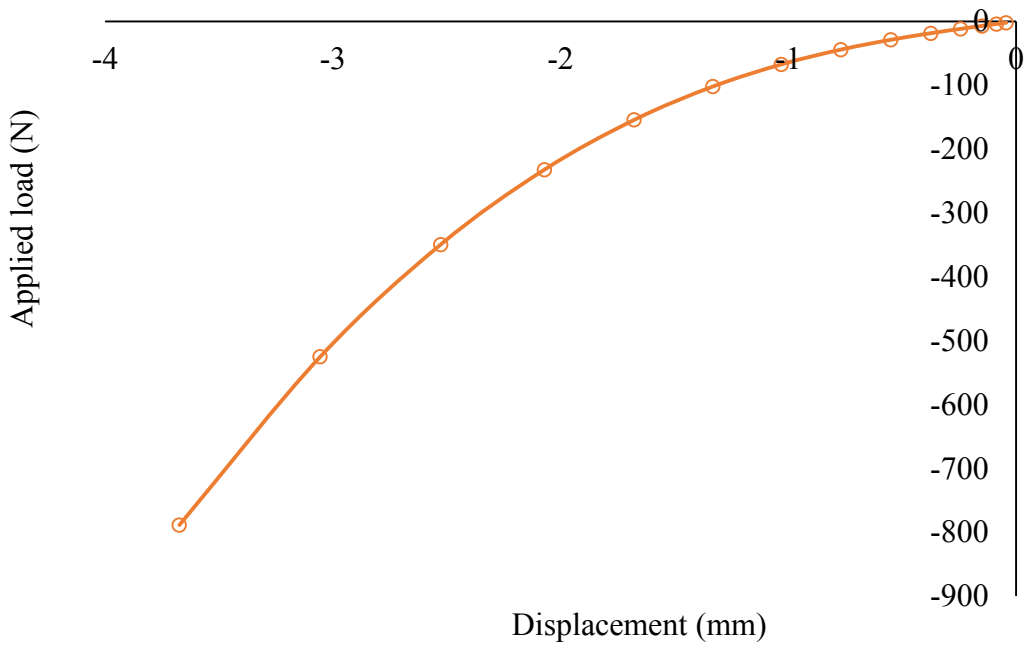

Figure D.4. Force displacement relationship of plasterboard to timber joint when compression was load applied

D.3 VRC comparison between the full-scale test and FEM

Table D.1 to D.7 shows the VRCs comparison between the full-scale test and FEM of the full-scale test structure.

Table D.1. VRCs comparison between the full-scale test and FEM at Stage S1

Stage S1	Loading side L					Non-loading side R				
Loading locations	**L.A**	**L.B**	**L.C**	**L.D**	**L.E**	**R.A**	**R.B**	**R.C**	**R.D**	**R.E**
Test_TA_B1	0.92	0.20	-0.08	-0.01	-0.02	-0.16	0.04	0.00	0.01	-0.05
FEM_TAB1	0.94	0.18	-0.07	0.00	0.00	-0.11	-0.01	0.00	0.02	-0.03
Test_TA_B2	0.81	0.19	-0.07	-0.01	-0.01	-0.08	0.05	-0.01	0.00	-0.05
FEM_TA_B2	0.87	0.17	-0.04	-0.01	-0.01	-0.06	0.00	0.00	0.00	0.00
Test_TA_B3	0.69	0.16	-0.06	0.00	-0.01	0.03	0.06	-0.01	0.00	-0.05
FEM_TA_B3	0.75	0.14	-0.09	0.00	0.00	0.08	0.04	0.00	0.00	0.00
Test_TA_B4	0.62	0.13	-0.05	-0.01	0.00	0.16	0.08	-0.02	-0.01	-0.06
FEM_TA_B4	0.63	0.12	-0.01	0.00	0.00	0.22	0.05	0.00	0.00	-0.08
Test_TA_B5	0.47	0.12	-0.04	-0.01	-0.01	0.28	0.09	-0.02	-0.01	-0.04
FEM_TA_B5	0.51	0.09	-0.02	-0.02	-0.02	0.35	0.07	-0.01	0.00	-0.03
Test_TB_B1	0.13	0.72	0.20	-0.06	0.00	-0.03	-0.09	-0.01	0.03	-0.06
FEM_TB_B1	0.09	0.83	0.17	-0.04	0.00	0.00	-0.06	-0.02	0.00	-0.04
Test_TB_B2	0.12	0.68	0.17	-0.05	0.01	-0.02	-0.05	0.01	0.03	-0.05
FEM_TB_B2	0.09	0.76	0.10	-0.02	0.00	0.00	0.00	0.00	0.00	0.00
Test_TB_B3	0.13	0.51	0.19	-0.06	0.00	0.02	0.04	0.02	0.02	-0.06
FEM_TB_B3	0.09	0.58	0.17	-0.01	0.00	0.01	0.06	0.00	0.00	0.03
Test_TB_B4	0.10	0.44	0.17	-0.03	0.00	0.02	0.13	0.05	0.03	-0.04
FEM_TB_B4	0.08	0.53	0.13	-0.01	0.00	0.01	0.17	0.02	0.00	0.00
Test_TB_B5	0.09	0.32	0.10	-0.03	-0.01	0.03	0.19	0.07	0.01	-0.04
FEM_TB_B5	0.11	0.39	0.08	-0.01	0.00	0.02	0.29	0.05	-0.01	0.00
Test_TC_B1	-0.05	0.30	0.48	0.36	-0.09	-0.03	0.00	-0.09	-0.01	-0.04
FEM_TC_B1	-0.08	0.24	0.52	0.30	-0.01	0.00	0.00	-0.04	0.00	0.00
Test_TC_B2	-0.05	0.26	0.48	0.28	-0.05	-0.02	0.04	-0.06	0.02	-0.05
FEM_TC_B2	-0.01	0.19	0.55	0.19	-0.03	0.00	0.07	-0.02	0.00	-0.01
Test_TC_B3	-0.02	0.21	0.42	0.24	-0.07	-0.04	0.07	0.01	0.05	-0.04
FEM_TC_B3	-0.01	0.14	0.48	0.17	-0.01	0.00	0.05	0.08	0.03	0.00
Test_TC_B4	0.00	0.17	0.34	0.20	-0.05	-0.02	0.10	0.08	0.07	-0.03
FEM_TC_B4	-0.01	0.15	0.40	0.18	-0.01	0.00	0.07	0.13	0.03	0.00
Test_TC_B5	0.00	0.14	0.28	0.16	-0.04	-0.03	0.14	0.14	0.12	-0.05
FEM_TC_B5	-0.01	0.08	0.36	0.09	-0.01	-0.02	0.09	0.24	0.09	-0.04

Table D.2. VRCs comparison between the full-scale test and FEM at Stage S2

Stage S2	Loading side L					Non-loading side R				
Loading locations	**L.A**	**L.B**	**L.C**	**L.D**	**L.E**	**R.A**	**R.B**	**R.C**	**R.D**	**R.E**
Test_TA_B1	0.74	0.37	0.08	-0.08	-0.14	-0.21	0.03	0.02	0.07	-0.05
FEM_TAB1	0.77	0.35	-0.03	-0.08	0.00	-0.08	0.01	0.01	0.00	-0.01
Test_TA_B2	0.68	0.35	0.02	-0.05	-0.11	-0.14	0.05	0.01	0.06	-0.03
FEM_TA_B2	0.74	0.28	-0.04	-0.06	0.00	-0.03	0.04	0.01	-0.01	-0.01
Test_TA_B3	0.61	0.34	0.00	-0.08	-0.11	-0.03	0.07	-0.01	0.06	-0.03
FEM_TA_B3	0.63	0.26	-0.03	-0.06	0.00	0.07	0.07	0.01	-0.02	-0.01
Test_TA_B4	0.54	0.29	0.03	-0.07	-0.14	0.07	0.13	0.00	0.05	-0.03
FEM_TA_B4	0.52	0.22	-0.02	-0.05	0.00	0.18	0.11	0.00	-0.02	-0.01
Test_TA_B5	0.40	0.24	0.05	-0.06	-0.14	0.15	0.18	0.00	0.04	-0.04
FEM_TA_B5	0.41	0.19	-0.01	-0.04	0.00	0.29	0.14	0.00	-0.03	-0.01
Test_TB_B1	0.30	0.30	0.39	0.07	-0.10	-0.04	-0.06	-0.08	0.04	-0.01
FEM_TB_B1	0.25	0.35	0.34	0.08	-0.04	-0.02	-0.03	-0.01	0.02	-0.01
Test_TB_B2	0.29	0.35	0.34	0.00	-0.10	0.01	-0.05	-0.07	0.04	0.01
FEM_TB_B2	0.24	0.40	0.30	0.03	-0.02	0.00	-0.02	-0.01	0.01	0.00
Test_TB_B3	0.26	0.30	0.29	0.02	-0.10	0.04	0.03	-0.03	0.05	-0.02
FEM_TB_B3	0.23	0.34	0.26	0.04	-0.04	0.07	-0.03	0.03	0.04	0.00
Test_TB_B4	0.18	0.28	0.21	0.05	-0.08	0.04	0.08	0.00	0.07	0.02
FEM_TB_B4	0.17	0.32	0.15	0.04	-0.02	0.05	0.13	0.07	0.03	-0.02
Test_TB_B5	0.19	0.21	0.17	0.03	-0.09	0.08	0.16	0.03	0.08	-0.01
FEM_TB_B5	0.15	0.24	0.12	0.05	-0.02	0.08	0.20	0.10	0.04	-0.03
Test_TC_B1	-0.02	0.27	0.46	0.28	-0.03	0.03	-0.03	-0.11	-0.02	0.00
FEM_TC_B1	-0.04	0.27	0.40	0.32	-0.06	0.02	-0.01	-0.08	0.00	0.02
Test_TC_B2	-0.07	0.26	0.45	0.31	-0.07	0.03	-0.01	-0.08	0.00	-0.01
FEM_TC_B2	-0.01	0.26	0.40	0.30	-0.03	-0.01	0.01	-0.01	0.02	-0.01
Test_TC_B3	-0.03	0.21	0.37	0.28	-0.05	0.07	0.01	-0.03	0.03	0.00
FEM_TC_B3	-0.04	0.23	0.33	0.26	-0.06	0.02	0.04	-0.03	0.05	0.01
Test_TC_B4	-0.06	0.18	0.27	0.24	-0.01	0.02	0.07	0.00	0.10	0.03
FEM_TC_B4	0.01	0.20	0.25	0.23	-0.01	-0.01	0.10	0.09	0.10	-0.01
Test_TC_B5	-0.01	0.15	0.21	0.18	-0.03	0.03	0.12	0.06	0.14	0.00
FEM_TC_B5	-0.08	0.12	0.17	0.15	0.09	0.06	0.09	0.09	0.11	0.06

Table D.3. VRCs comparison between the full-scale test and FEM at Stage S3

Stage S3	Loading side L					Non-loading side R				
Loading locations	**L.A**	**L.B**	**L.C**	**L.D**	**L.E**	**R.A**	**R.B**	**R.C**	**R.D**	**R.E**
Test_TA_B1	0.77	0.39	0.01	-0.07	-0.13	-0.18	-0.03	0.03	0.05	-0.02
FEM_TAB1	0.75	0.35	-0.01	-0.06	-0.02	-0.08	0.00	0.01	-0.01	0.00
Test_TA_B2	0.76	0.37	-0.02	-0.08	-0.11	-0.13	0.01	0.04	0.05	-0.01
FEM_TA_B2	0.71	0.31	-0.02	-0.05	-0.01	-0.03	0.03	0.01	-0.01	0.00
Test_TA_B3	0.71	0.28	0.00	-0.09	-0.12	-0.06	0.07	0.01	0.05	-0.03
FEM_TA_B3	0.61	0.27	-0.01	-0.05	-0.01	0.07	0.07	0.01	-0.02	0.00
Test_TA_B4	0.54	0.22	0.05	-0.04	-0.12	0.03	0.13	0.02	0.04	-0.03
FEM_TA_B4	0.50	0.23	-0.01	-0.04	-0.02	0.17	0.11	0.01	-0.02	0.00
Test_TA_B5	0.41	0.24	0.05	-0.05	-0.12	0.14	0.18	0.01	0.04	-0.02
FEM_TA_B5	0.40	0.19	0.00	-0.03	-0.02	0.27	0.14	0.00	-0.03	0.00
Test_TB_B1	0.31	0.43	0.30	0.03	-0.09	-0.03	-0.09	-0.07	0.05	0.02
FEM_TB_B1	0.23	0.48	0.25	0.09	-0.05	-0.01	-0.04	-0.02	0.00	0.00
Test_TB_B2	0.26	0.44	0.25	0.01	-0.07	-0.01	-0.05	-0.05	0.05	0.01
FEM_TB_B2	0.16	0.46	0.19	0.05	-0.04	0.03	-0.02	0.00	0.01	0.00
Test_TB_B3	0.24	0.37	0.21	0.07	-0.09	0.00	0.03	-0.03	0.07	0.00
FEM_TB_B3	0.18	0.41	0.17	0.04	-0.03	0.05	0.00	0.03	0.03	-0.01
Test_TB_B4	0.26	0.27	0.18	0.04	-0.09	0.06	0.09	0.01	0.06	0.00
FEM_TB_B4	0.16	0.32	0.16	0.06	-0.04	0.07	0.12	0.06	0.03	-0.01
Test_TB_B5	0.20	0.25	0.15	0.01	-0.07	0.11	0.15	0.04	0.06	0.01
FEM_TB_B5	0.14	0.24	0.13	0.06	-0.03	0.09	0.18	0.09	0.04	-0.02
Test_TC_B1	0.03	0.27	0.49	0.23	-0.04	0.03	-0.04	-0.12	0.00	0.03
FEM_TC_B1	-0.02	0.25	0.33	0.33	-0.03	0.01	-0.01	-0.05	0.00	0.01
Test_TC_B2	-0.05	0.28	0.49	0.22	-0.02	0.03	0.00	-0.09	0.00	0.01
FEM_TC_B2	-0.01	0.25	0.39	0.34	-0.04	0.01	0.00	-0.02	0.01	0.00
Test_TC_B3	0.00	0.22	0.31	0.32	-0.07	0.03	0.03	-0.03	0.05	0.01
FEM_TC_B3	-0.02	0.21	0.29	0.27	-0.03	0.00	0.04	-0.01	0.04	0.01
Test_TC_B4	0.03	0.16	0.24	0.26	-0.02	0.03	0.06	0.00	0.09	0.03
FEM_TC_B4	0.00	0.19	0.24	0.25	-0.02	0.00	0.08	0.09	0.09	0.00
Test_TC_B5	0.01	0.15	0.24	0.12	0.02	0.06	0.10	0.06	0.09	0.05
FEM_TC_B5	0.00	0.16	0.18	0.20	-0.01	0.00	0.12	0.14	0.14	-0.01

Table D.4. VRCs comparison between the full-scale test and FEM at Stage S4

Stage S4	Loading side L					Non-loading side R				
Loading locations	**L.A**	**L.B**	**L.C**	**L.D**	**L.E**	**R.A**	**R.B**	**R.C**	**R.D**	**R.E**
Test_TA_B1	0.71	0.31	0.06	-0.02	-0.06	-0.04	0.04	-0.04	0.02	-0.09
FEM_TAB1	0.71	0.37	0.00	-0.06	-0.02	-0.08	0.00	0.01	0.00	-0.01
Test_TA_B2	0.79	0.24	0.00	-0.05	-0.05	-0.04	0.05	-0.02	0.04	-0.06
FEM_TA_B2	0.67	0.33	0.00	-0.05	-0.02	-0.03	0.03	0.02	-0.01	-0.01
Test_TA_B3	0.66	0.24	-0.04	-0.05	-0.03	0.04	0.07	-0.02	0.04	-0.03
FEM_TA_B3	0.66	0.33	0.00	-0.05	-0.02	-0.02	0.03	0.02	-0.01	-0.01
Test_TA_B4	0.52	0.22	0.04	-0.04	-0.06	0.12	0.15	-0.01	0.04	-0.07
FEM_TA_B4	0.47	0.25	0.01	-0.04	-0.03	0.16	0.11	0.01	-0.02	-0.01
Test_TA_B5	0.37	0.20	0.07	-0.02	-0.07	0.21	0.20	0.00	0.03	-0.09
FEM_TA_B5	0.37	0.21	0.02	-0.03	-0.03	0.26	0.15	0.01	-0.02	-0.01
Test_TB_B1	0.29	0.44	0.22	0.05	-0.01	-0.03	0.01	-0.03	0.01	-0.07
FEM_TB_B1	0.23	0.48	0.25	0.09	-0.05	0.00	-0.06	-0.02	0.00	0.01
Test_TB_B2	0.25	0.52	0.18	-0.01	-0.01	-0.04	0.03	-0.01	0.03	-0.05
FEM_TB_B2	0.20	0.54	0.21	0.04	-0.03	0.02	-0.03	-0.01	0.02	-0.02
Test_TB_B3	0.19	0.44	0.16	0.03	-0.01	0.00	0.07	0.03	0.04	-0.03
FEM_TB_B3	0.17	0.47	0.17	0.06	-0.02	0.04	0.01	0.02	0.02	-0.01
Test_TB_B4	0.22	0.30	0.14	0.03	-0.02	0.04	0.14	0.04	0.06	-0.06
FEM_TB_B4	0.17	0.31	0.16	0.06	-0.03	0.08	0.10	0.05	0.03	-0.01
Test_TB_B5	0.17	0.22	0.12	0.05	0.00	0.07	0.20	0.06	0.08	-0.06
FEM_TB_B5	0.14	0.24	0.13	0.06	-0.02	0.10	0.17	0.08	0.04	-0.01
Test_TC_B1	0.08	0.26	0.35	0.26	0.04	-0.03	0.00	-0.02	0.02	-0.07
FEM_TC_B1	-0.01	0.25	0.37	0.34	0.03	-0.01	-0.02	-0.04	0.01	0.01
Test_TC_B2	0.01	0.26	0.40	0.21	0.00	-0.03	0.03	0.00	0.02	-0.06
FEM_TC_B2	-0.01	0.25	0.36	0.35	-0.03	0.02	-0.01	-0.03	0.00	0.01
Test_TC_B3	-0.01	0.25	0.31	0.26	-0.01	-0.02	0.06	0.03	0.08	-0.05
FEM_TC_B3	0.00	0.21	0.26	0.28	-0.02	0.01	0.03	0.01	0.06	0.01
Test_TC_B4	0.03	0.17	0.25	0.24	0.02	-0.02	0.10	0.08	0.11	-0.05
FEM_TC_B4	0.01	0.19	0.23	0.25	0.00	0.01	0.08	0.06	0.09	0.02
Test_TC_B5	0.02	0.14	0.16	0.16	0.05	0.00	0.13	0.11	0.15	-0.04
FEM_TC_B5	0.01	0.15	0.17	0.20	0.00	0.01	0.12	0.11	0.13	0.01

Table D.5. VRCs comparison between the full-scale test and FEM at Stage S5

Stage S5	Loading side L					Non-loading side R				
Loading locations	**L.A**	**L.B**	**L.C**	**L.D**	**L.E**	**R.A**	**R.B**	**R.C**	**R.D**	**R.E**
Test_TA_B1	0.65	0.36	0.08	-0.02	-0.08	-0.02	0.03	-0.02	-0.02	-0.08
FEM_TAB1	0.72	0.40	0.10	-0.05	-0.06	-0.06	-0.03	-0.02	-0.02	-0.05
Test_TA_B2	0.71	0.33	0.01	-0.06	-0.07	0.01	0.04	-0.01	-0.01	-0.06
FEM_TA_B2	0.76	0.35	0.08	-0.07	-0.06	-0.03	0.00	-0.04	-0.03	-0.04
Test_TA_B3	0.66	0.32	-0.02	-0.07	-0.07	0.03	0.08	0.01	0.01	-0.05
FEM_TA_B3	0.67	0.28	-0.09	-0.05	-0.03	0.04	0.05	0.04	0.03	-0.01
Test_TA_B4	0.46	0.27	0.04	-0.05	-0.07	0.12	0.14	0.02	0.01	-0.07
FEM_TA_B4	0.47	0.25	0.08	-0.07	-0.04	0.10	0.09	0.05	0.03	-0.02
Test_TA_B5	0.35	0.22	0.08	-0.03	-0.08	0.20	0.19	0.02	0.01	-0.07
FEM_TA_B5	0.37	0.20	0.07	-0.02	-0.06	0.17	0.14	0.05	0.02	-0.02
Test_TB_B1	0.31	0.39	0.25	0.07	-0.01	-0.02	0.01	-0.01	0.00	-0.05
FEM_TB_B1	0.26	0.41	0.27	0.10	-0.01	-0.01	-0.04	-0.03	0.00	-0.03
Test_TB_B2	0.29	0.41	0.22	0.01	-0.02	-0.02	0.02	0.00	0.01	-0.04
FEM_TB_B2	0.25	0.45	0.23	0.04	-0.01	0.00	-0.02	-0.01	0.02	-0.02
Test_TB_B3	0.22	0.34	0.20	0.04	-0.02	-0.02	0.06	0.03	0.04	-0.03
FEM_TB_B3	0.23	0.38	0.18	0.09	-0.02	-0.03	0.03	0.02	0.03	0.03
Test_TB_B4	0.20	0.26	0.16	0.05	-0.01	0.03	0.12	0.06	0.05	-0.04
FEM_TB_B4	0.19	0.29	0.15	0.08	-0.02	0.07	0.07	0.05	0.04	-0.01
Test_TB_B5	0.17	0.22	0.12	0.05	0.00	0.07	0.20	0.06	0.08	-0.06
FEM_TB_B5	0.15	0.25	0.12	0.07	0.00	0.11	0.12	0.07	0.05	-0.03
Test_TC_B1	0.12	0.24	0.34	0.25	0.04	-0.01	0.00	-0.01	-0.02	-0.07
FEM_TC_B1	0.07	0.23	0.34	0.28	0.08	0.01	-0.02	-0.05	-0.02	0.01
Test_TC_B2	0.06	0.25	0.37	0.23	0.02	-0.03	0.01	0.01	0.01	-0.04
FEM_TC_B2	0.07	0.21	0.31	0.25	0.08	0.02	-0.01	-0.03	0.00	0.02
Test_TC_B3	0.05	0.21	0.30	0.22	0.01	-0.02	0.05	0.05	0.04	-0.04
FEM_TC_B3	0.08	0.18	0.24	0.21	0.09	0.03	0.03	0.02	0.03	0.03
Test_TC_B4	0.06	0.16	0.21	0.19	0.05	0.00	0.09	0.09	0.08	-0.03
FEM_TC_B4	0.08	0.15	0.19	0.17	0.08	0.05	0.06	0.05	0.06	0.04
Test_TC_B5	0.07	0.13	0.16	0.13	0.04	0.02	0.11	0.12	0.11	-0.02
FEM_TC_B5	0.07	0.12	0.14	0.14	0.08	0.06	0.09	0.09	0.09	0.06

Table D.6. VRCs comparison between the full-scale test and FEM at Stage S6

Stage S6	Loading side L					Non-loading side R				
Loading locations	**L.A**	**L.B**	**L.C**	**L.D**	**L.E**	**R.A**	**R.B**	**R.C**	**R.D**	**R.E**
Test_TA_B1	0.49	0.45	0.23	-0.02	-0.17	-0.01	-0.01	-0.01	-0.02	-0.04
FEM_TAB1	0.49	0.42	0.15	0.00	-0.09	-0.06	-0.03	0.01	0.02	0.02
Test_TA_B2	0.52	0.48	0.21	-0.07	-0.20	-0.01	0.00	0.00	-0.01	-0.02
FEM_TA_B2	0.54	0.37	0.14	-0.01	-0.17	-0.03	0.00	0.02	0.03	0.02
Test_TA_B3	0.48	0.43	0.19	-0.08	-0.23	0.03	0.04	0.03	0.01	-0.02
FEM_TA_B3	0.53	0.30	0.13	-0.02	-0.15	0.02	0.04	0.04	0.04	-0.03
Test_TA_B4	0.36	0.34	0.16	-0.04	-0.16	0.11	0.10	0.05	0.00	-0.04
FEM_TA_B4	0.34	0.27	0.11	-0.01	-0.06	0.07	0.09	0.06	0.04	0.02
Test_TA_B5	0.28	0.26	0.13	-0.02	-0.11	0.19	0.16	0.07	0.00	-0.06
FEM_TA_B5	0.31	0.22	0.10	-0.01	-0.04	0.13	0.13	0.07	0.04	-0.02
Test_TB_B1	0.33	0.34	0.23	0.10	-0.02	-0.01	-0.01	-0.01	-0.03	-0.04
FEM_TB_B1	0.29	0.36	0.24	0.10	0.00	-0.03	-0.03	-0.02	0.00	0.01
Test_TB_B2	0.35	0.34	0.22	0.06	-0.06	0.01	0.01	0.01	-0.01	-0.04
FEM_TB_B2	0.27	0.33	0.22	0.09	0.01	-0.01	-0.01	0.00	0.02	0.01
Test_TB_B3	0.28	0.29	0.20	0.07	-0.03	0.02	0.03	0.03	0.02	-0.02
FEM_TB_B3	0.24	0.27	0.24	0.08	-0.01	0.02	0.03	0.03	0.04	-0.02
Test_TB_B4	0.23	0.24	0.16	0.06	-0.02	0.07	0.08	0.06	0.03	-0.01
FEM_TB_B4	0.20	0.25	0.15	0.07	-0.01	0.06	0.07	0.06	0.05	0.03
Test_TB_B5	0.20	0.22	0.14	0.04	-0.04	0.14	0.14	0.08	0.04	-0.01
FEM_TB_B5	0.16	0.18	0.15	0.07	-0.02	0.10	0.11	0.08	0.06	0.03
Test_TC_B1	0.19	0.22	0.23	0.19	0.15	-0.02	-0.01	-0.01	-0.02	-0.03
FEM_TC_B1	0.12	0.22	0.27	0.25	0.13	0.00	-0.02	-0.03	-0.02	-0.01
Test_TC_B2	0.16	0.21	0.21	0.20	0.13	-0.01	0.00	0.00	-0.01	-0.02
FEM_TC_B2	0.11	0.20	0.26	0.23	0.12	-0.01	0.00	-0.01	0.00	0.00
Test_TC_B3	0.12	0.17	0.19	0.18	0.13	0.02	0.03	0.03	0.03	-0.01
FEM_TC_B3	0.10	0.17	0.21	0.20	0.12	0.02	0.03	0.03	0.03	0.02
Test_TC_B4	0.11	0.15	0.15	0.15	0.12	0.04	0.06	0.06	0.06	0.02
FEM_TC_B4	0.09	0.14	0.17	0.16	0.10	0.04	0.06	0.06	0.06	0.04
Test_TC_B5	0.08	0.12	0.12	0.12	0.09	0.07	0.09	0.08	0.08	0.03
FEM_TC_B5	0.08	0.12	0.13	0.13	0.09	0.06	0.09	0.09	0.09	0.06

Table D.7. VRCs comparison between the full-scale test and FEM at Stage S7

Stage S7	Loading side L					Non-loading side R				
Loading locations	**L.A**	**L.B**	**L.C**	**L.D**	**L.E**	**R.A**	**R.B**	**R.C**	**R.D**	**R.E**
Test_TA_B1	0.47	0.44	0.23	-0.01	-0.16	0.01	0.00	-0.02	-0.05	-0.05
FEM_TAB1	0.51	0.42	0.16	-0.01	-0.10	-0.06	-0.04	0.00	0.02	0.03
Test_TA_B2	0.48	0.48	0.22	-0.07	-0.22	-0.01	0.00	-0.01	-0.01	-0.02
FEM_TA_B2	0.46	0.37	0.14	0.01	-0.09	-0.03	-0.01	0.02	0.03	0.03
Test_TA_B3	0.45	0.44	0.20	-0.06	-0.22	0.03	0.04	0.02	0.02	0.00
FEM_TA_B3	0.47	0.31	0.15	-0.02	-0.16	0.02	0.04	0.04	0.04	0.03
Test_TA_B4	0.33	0.33	0.15	-0.03	-0.13	0.13	0.11	0.06	-0.01	-0.05
FEM_TA_B4	0.34	0.27	0.11	-0.01	-0.06	0.07	0.08	0.06	0.04	0.03
Test_TA_B5	0.28	0.27	0.13	-0.03	-0.12	0.22	0.18	0.08	-0.02	-0.08
FEM_TA_B5	0.27	0.22	0.10	-0.01	-0.05	0.13	0.13	0.07	0.05	0.03
Test_TB_B1	0.33	0.33	0.22	0.09	-0.01	-0.01	-0.01	-0.02	-0.03	-0.04
FEM_TB_B1	0.30	0.35	0.24	0.10	0.00	-0.03	-0.03	-0.02	0.00	0.01
Test_TB_B2	0.33	0.33	0.21	0.07	-0.04	0.00	0.00	0.00	0.00	-0.02
FEM_TB_B2	0.28	0.33	0.22	0.09	0.01	-0.01	-0.01	0.00	0.02	0.02
Test_TB_B3	0.28	0.31	0.20	0.05	-0.06	0.03	0.04	0.03	0.02	0.00
FEM_TB_B3	0.25	0.35	0.18	0.08	-0.04	0.02	0.03	0.03	0.02	0.02
Test_TB_B4	0.24	0.26	0.15	0.05	-0.02	0.10	0.09	0.06	0.03	-0.01
FEM_TB_B4	0.21	0.24	0.15	0.07	-0.01	0.06	0.07	0.06	0.05	0.03
Test_TB_B5	0.18	0.19	0.12	0.05	-0.01	0.12	0.13	0.08	0.04	0.00
FEM_TB_B5	0.17	0.18	0.12	0.07	0.01	0.10	0.11	0.08	0.06	0.04
Test_TC_B1	0.17	0.22	0.22	0.22	0.15	-0.01	-0.01	-0.01	-0.02	-0.03
FEM_TC_B1	0.12	0.22	0.28	0.25	0.13	0.00	-0.02	-0.03	-0.02	0.00
Test_TC_B2	0.14	0.19	0.21	0.21	0.15	-0.01	0.00	0.00	0.00	-0.02
FEM_TC_B2	0.12	0.20	0.25	0.23	0.13	0.01	0.00	-0.01	0.00	0.01
Test_TC_B3	0.12	0.18	0.17	0.17	0.14	0.02	0.03	0.03	0.03	0.00
FEM_TC_B3	0.11	0.17	0.20	0.19	0.12	0.02	0.03	0.03	0.03	0.02
Test_TC_B4	0.09	0.16	0.15	0.15	0.10	0.04	0.08	0.06	0.05	0.02
FEM_TC_B4	0.09	0.14	0.17	0.16	0.10	0.04	0.06	0.06	0.06	0.04
Test_TC_B5	0.08	0.11	0.11	0.12	0.10	0.08	0.10	0.08	0.08	0.04
FEM_TC_B5	0.08	0.12	0.13	0.13	0.09	0.06	0.09	0.09	0.09	0.06

D.4 VRCs at the inter-component connections

Uplift load was applied perpendicular to the roof surface at the middle of roof cladding (i.e. between Batten B3 and B4, B4 and B5) in the FEM (P1 and P2, see Figure D.5). The vertical reaction forces were measured at the cladding to batten connections, batten to truss connections (see Table D8 to D10) and RWCs.

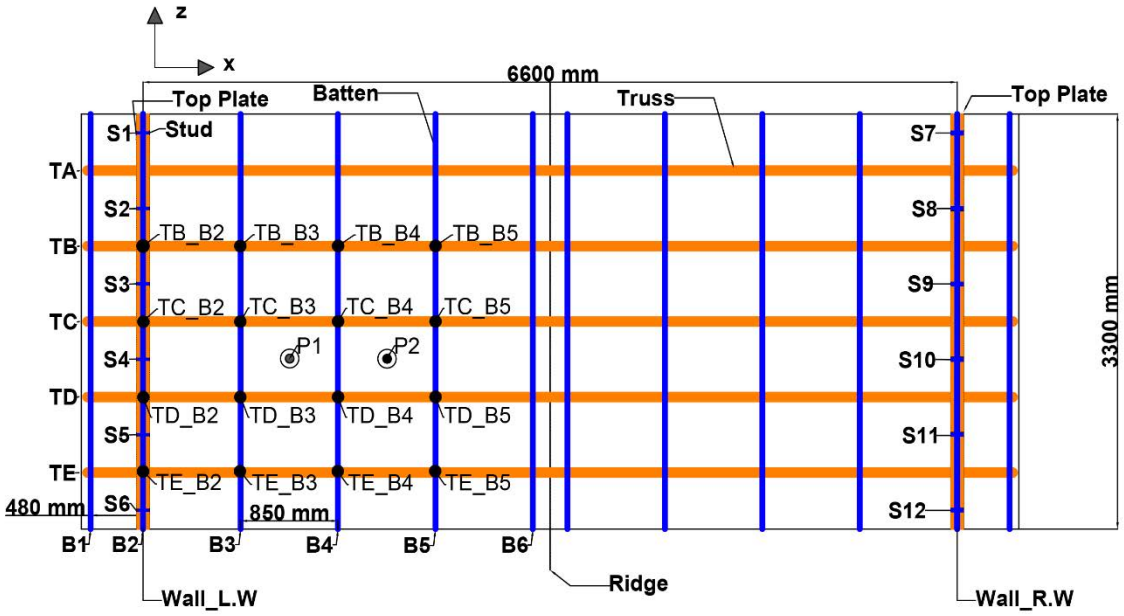

Figure D.5. Plan view of the FEM: showing the batten to truss connections, RWCs and loading locations (i.e. P1 and P2)

The VRC at batten to truss connections obtained when load was applied at location P1 in the FEM. These VRCs were compared with the VRCs of the experimental test of Jayasinghe (2012), (Table D.8), when the load was applied at P6,x (see Figure D.6). This table shows that the load distribution to the adjacent trusses through the batten to truss connections were similar in both FEM and experimental test of Jayasinghe (2012). However, the magnitude of the VRCs at the batten to truss connection in the FEM was about 10% less than the experimental test of Jayasinghe (2012). This was due to the differences in the RWC stiffness, batten member sizes, number of cladding to batten connections per corrugated sheet between the FEM and experimental tests. In the FEM, the triple grip connections were used as RWCs, while top-plates were fixed to the steel frame in the experimental test of Jayasinghe (2010). Thus, the stiffness of the RWCs was high in the experimental test of Jayasinghe (2010) compared to that of FEM. Three fasteners were used to fix a corrugated sheet in the FEM, whilst four fasteners were used per corrugated sheet in the experimental test of Jayasinghe (2012). These differences create the variations in the stiffness of the structural systems. This stiffness variation was the reason for the VRCs variation between the FEM and experimental test of Jayasinghe (2012). This VRC comparison between the FEM and experimental test of Jayasinghe

(2012) indicate that this FEM can predict the load sharing and influence coefficient of the batten to truss connection of the timber-framed house.

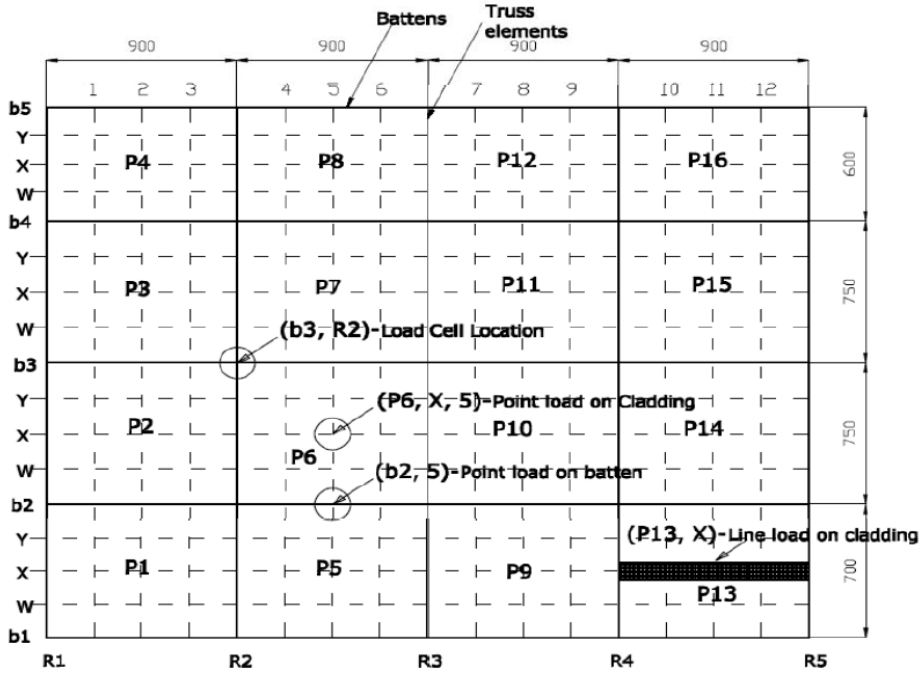

Figure D.6. Schematic diagram of the test stet up (Jayasinghe, 2012)

Table D.8. VRC of batten to truss connections comparison between FEM and experimental test of Jayasinghe (2012), when load was applied at P1

Reaction measured location		**Reaction coefficient**	
From FEM	**From Jayasinghe (2012)**	**From FEM**	**From Jayasinghe (2012)**
TC_B3	b2R2	0.22	0.25
TD_B3	b2R3	0.23	0.25
TE_B3	b2R4	0.02	0.01
TC_B4	b3R2	0.25	0.27
TD_B4	b3R3	0.25	0.26
TE_B4	b3R4	-0.01	0.03

Table D.9. VRC of batten to truss connections when load was applied at P1

Reaction locations	VRCs
TB_B2	-0.06
TB_B3	0.03
TB_B4	-0.01
TB_B5	0.02
TC_B2	-0.21
TC_B3	0.22
TC_B4	0.25
TC_B5	-0.05
TD_B2	-0.33
TD_B3	0.23
TD_B4	0.25
TD_B5	-0.06
TE_B2	-0.03
TE_B3	0.02
TE_B4	-0.01
TE_B5	0.00

Table D.10. VRC of batten to truss connections when load was applied at P2

Reaction locations	VRCs
TB_B2	-0.08
TB_B3	0.03
TB_B4	0.00
TB_B5	0.02
TC_B2	-0.13
TC_B3	-0.04
TC_B4	0.26
TC_B5	0.16
TD_B2	-0.24
TD_B3	-0.05
TD_B4	0.34
TD_B5	0.23
TE_B2	-0.05
TE_B3	0.02
TE_B4	-0.02
TE_B5	0.00

Tables D.11 and D.12 show the VRCs of the cladding to batten connection when load was applied at P1 and P2 respectively (Figure D.7). These tables show that the fasteners located closer to the loading locations experiences and shared the highest percentage of applied load to the battens. This indicates that the load sharing from the cladding to batten connections were function of connections stiffness, number of connections per corrugated sheet and the distance from the loading locations. Similar behaviour was found in the experimental study of Henderson (2010). The VRCs of the loaded side RWCs when load was applied at P1 and P2 are given in Table D.13 and D.14 respectively.

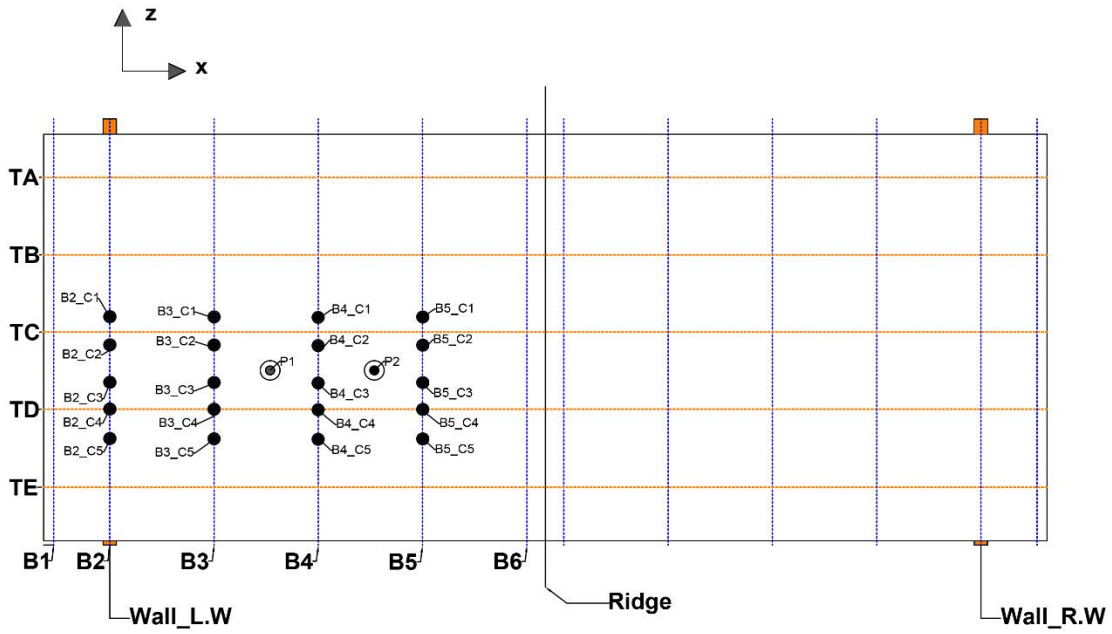

Figure D.7. Cladding to batten connection locations

Table D.11. VRC of cladding to batten connections when load was applied at P1

Reaction measured location	VRCs
B2_C1	0.00
B2_C2	0.01
B2_C3	-0.09
B2_C4	0.00
B2_C5	0.00
B3_C1	-0.02
B3_C2	0.13
B3_C3	0.42
B3_C4	0.00
B3_C5	0.00
B4_C1	-0.02
B4_C2	0.14
B4_C3	0.43
B4_C4	0.00
B4_C5	0.00
B5_C1	0.00
B5_C2	0.01
B5_C3	-0.08
B5_C4	0.00
B5_C5	0.00

Table D.12. VRC of cladding to batten connections when load was applied at P2

Reaction measured location	VRCs
B2_C1	0.00
B2_C2	0.00
B2_C3	0.00
B2_C4	0.00
B2_C5	0.00
B3_C1	0.00
B3_C2	0.01
B3_C3	-0.09
B3_C4	0.00
B3_C5	0.00
B4_C1	-0.02
B4_C2	0.14
B4_C3	0.43
B4_C4	0.00
B4_C5	0.00
B5_C1	-0.02
B5_C2	0.14
B5_C3	0.41
B5_C4	0.00
B5_C5	0.00

Table D.13. VRC of RWCs when load was applied at P1

Reaction measured location	VRCs
TA	0.03
TB	0.10
TC	0.14
TD	0.30
TE	0.09

Table D.14. VRC of RWCs when load was applied at P2

Reaction measured location	VRCs
TA	0.04
TB	0.09
TC	0.11
TD	0.25
TE	0.07

D.5 VRCs comparison to the FEM of test structure with and without construction defects

The FEM was developed with and without construction defects and the details of the FEMs given in Table D.15. The vertical reaction forces at the RWC were obtained from the FEMs. Figures D.8, D.9 and D.10 show the vertical reaction influence coefficients at Truss C's support L.C. These figures indicate that the load on Truss B was highly influenced the Truss C's support reaction compared to that of Truss D. This is because the number of batten to cladding fasteners in the tributary area of Truss B was higher than the tributary area of Truss D. This creates a higher load distribution on the cladding, in Truss B's tributary area compared to that of Truss D's tributary area. This was the reason the load on the Truss B is highly influenced by Truss C's support reactions.

Table D.15. Details of the FEM of with and without construction defects on the RWC

Details	
FEM 1	Using "Ideal" roof to wall triple grip connection for all the RWCs
FEM 2	Using single nail missing from the roof to wall triple grip connection for RWCs of Truss TC
FEM 3	Using two nails missing (i.e. one on the top-plate and one on the truss) from the roof to wall triple grip connection for RWCs of Truss TB and single nail missing roof to wall triple grip connection for RWCs of Truss TC

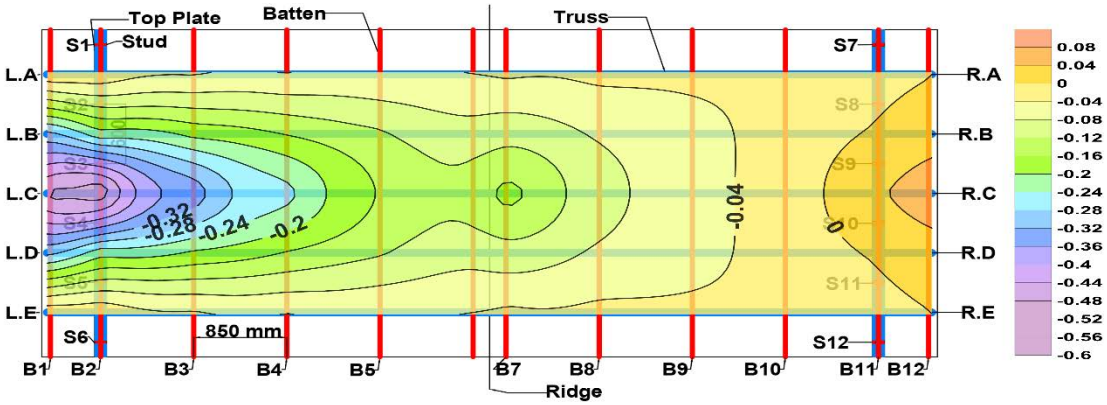

Figure D.8. Vertical reaction influence coefficient for Truss C support L.C obtained from FEM 1("Ideal RWC)

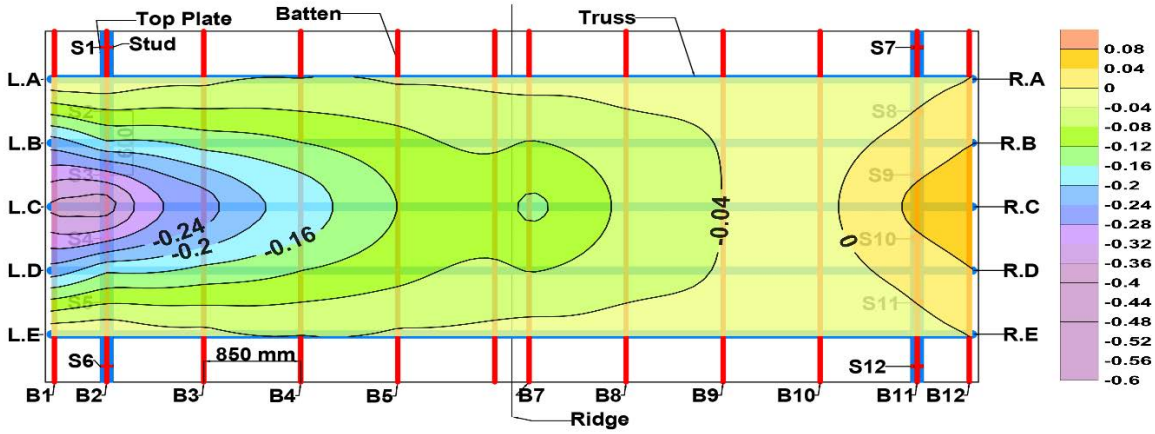

Figure D.9. Vertical reaction influence coefficient for Truss C support L.C obtained from FEM 2 (one defective RWC)

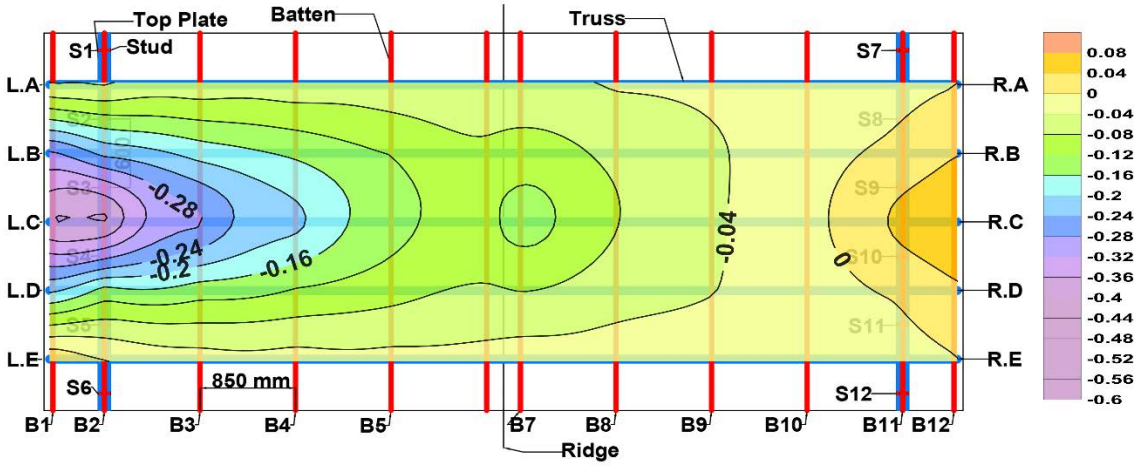

Figure D.10. Vertical reaction influence coefficient for Truss C support L.C obtained from FEM 3 (two defective RWCs)

Table D.16 shows the C_N of the general trusses of the contemporary representative house when 1 kPa uniform suction pressure was applied on the roof.

Table D.16. C_N at the RWCs of the general trusses when the uniform suction pressure (i.e. 1 kPa) applied on the roof

Detail	C_N									
	Side L					Side R				
	T1_L	T2_L	T3_L	T4_L	T5_L	T1_R	T2_R	T3_R	T4_R	T5_R
FEM 1	1.54	1.46	1.41	1.49	1.56	1.54	1.46	1.41	1.49	1.56
FEM 2	1.57	1.60	1.07	1.64	1.59	1.57	1.60	1.07	1.64	1.59
FEM 3	1.81	1.07	1.20	1.69	1.70	1.81	1.07	1.20	1.69	1.70

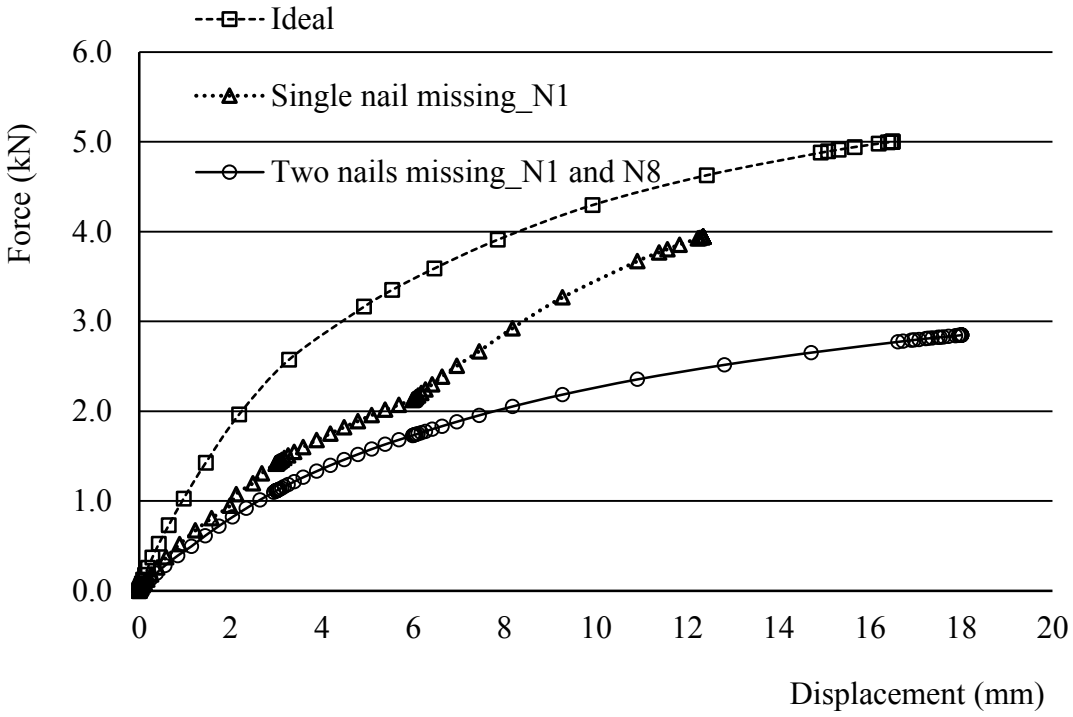

Figure D.11. Vertical force-displacement relationship for the "Ideal" and defective RWCs

D.6 Lateral load (i.e. horizontally perpendicular to ridge) response

In the FEM, a lateral load was applied to the wall (i.e. wall L) studs to compare the lateral load distribution to the non-loading side wall through the roof structure, ceiling and ceiling cornice with the full-scale test (Appendix B, Section B.4). The applied load and boundary conditions applied in this FEM were based on the full-scale test; pin and roller supports were imposed at the vertical and lateral load cells' locations respectively. These roller supports provided the lateral resistance of the structure. Figure D.12 shows the loading (i.e. S1_P1, S2_P2 and S3_P3) and lateral displacement measured locations (i.e. LD1, LD2, LD3, LD4, LD5, LD6, LD7, LD8 and LD9) in this FEM analysis. The locations where the lateral reaction forces are measured (i.e. L1 and L2), are shown in Figure D.13.

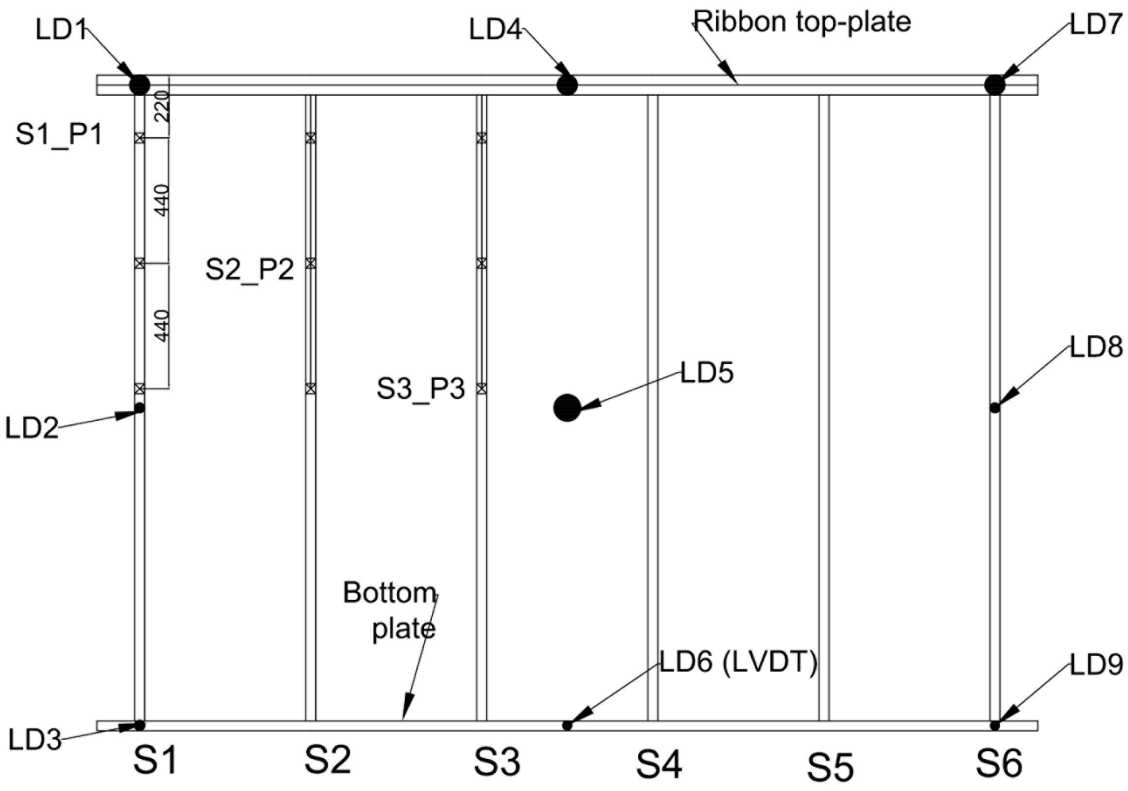

Figure D.12. Lateral loading (i.e. S1_P1, S2_P2 and S3_P3) and displacement measured locations

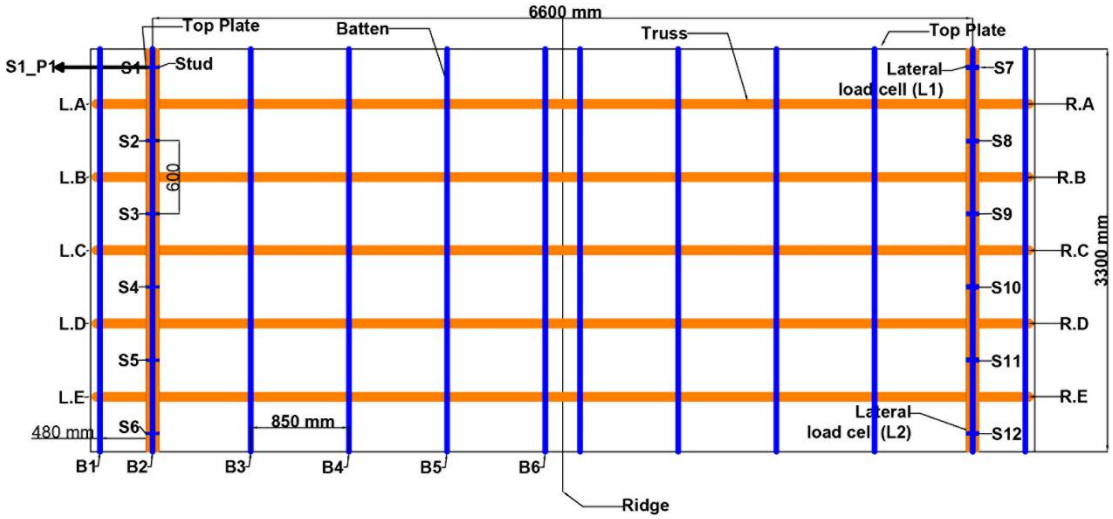

Figure D.13. Plane view of lateral loading of the FEM

Figure D.14 shows the comparison of the lateral load reaction coefficients (i.e. measured lateral reaction at the lateral load cells divided by applied load) between FEM and full-

scale test, when load was applied to the studs at S1_P1, S2_P2 and S3_P3. This figure shows that the lateral load reaction coefficients obtained in the FEM were higher than that of the full-scale test. The lateral stiffness of each RWC was same in the FEM but it varied in each RWC of the full-scale test. This was the reason for the high lateral reaction force obtained in this FEM. However, the FEM can predict the lateral load response and load sharing of the timber-framed structure with a variation of between 5% to 15% compared to full-scale test results.

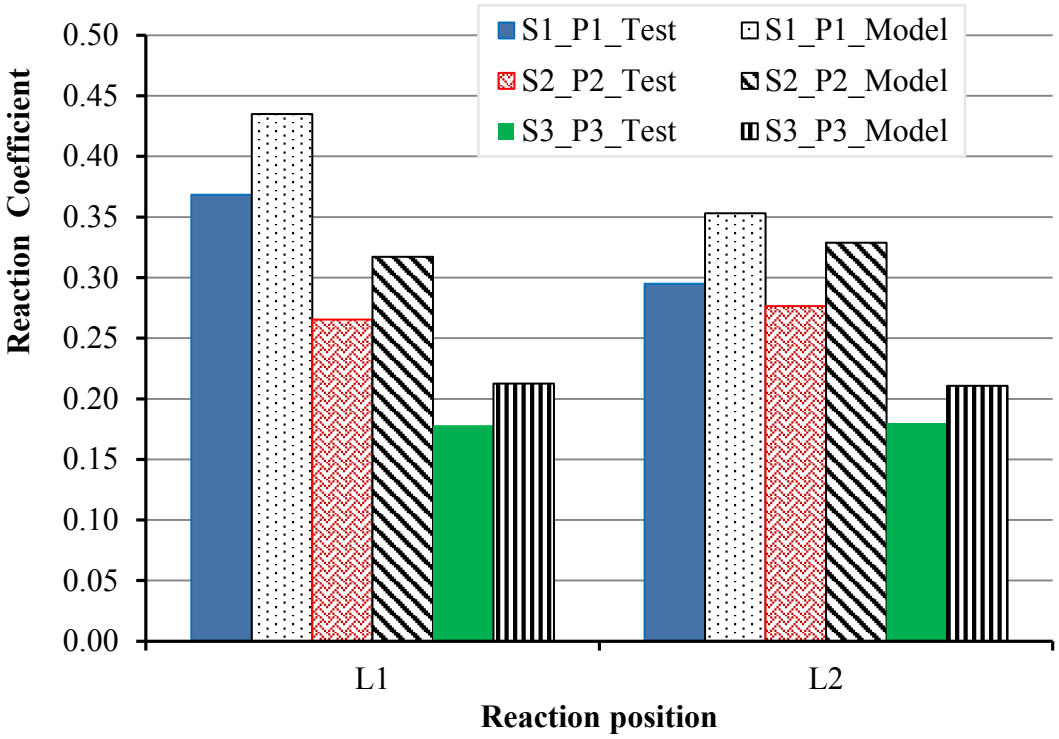

Figure D.14. Comparison of the lateral load reaction coefficients between FEM and full-scale test, when load was applied to the studs at S1_P1, S2_P2 and S3_P3

The lateral movement of the wall obtained in the FEM, when load was applied to the studs at S1_P1, S2_P2 and S3_P3, were compared with the full-scale test (Figure D.15). This figure shows the lateral movement of the top-plate (i.e. LD1, LD4 and LD7) and middle of the wall (i.e. LD2, LD4 and LD6) obtained in the FEM were less than the full-scale test. The lateral movement at the bottom plate (i.e. LD3, LD6 and LD9) were observed in the full-scale test but in the FEM it was minimal to zero. This could be the reason for the less lateral movement obtained at the top-plate and middle of the wall in the FEM compared to the full-scale test. This was also the reason for high lateral reaction

forces obtained in the FEM (Figure D.14). These less lateral movement and higher lateral reaction forces indicate that the lateral stiffness of the structural system in the FEM was higher than the full-scale test.

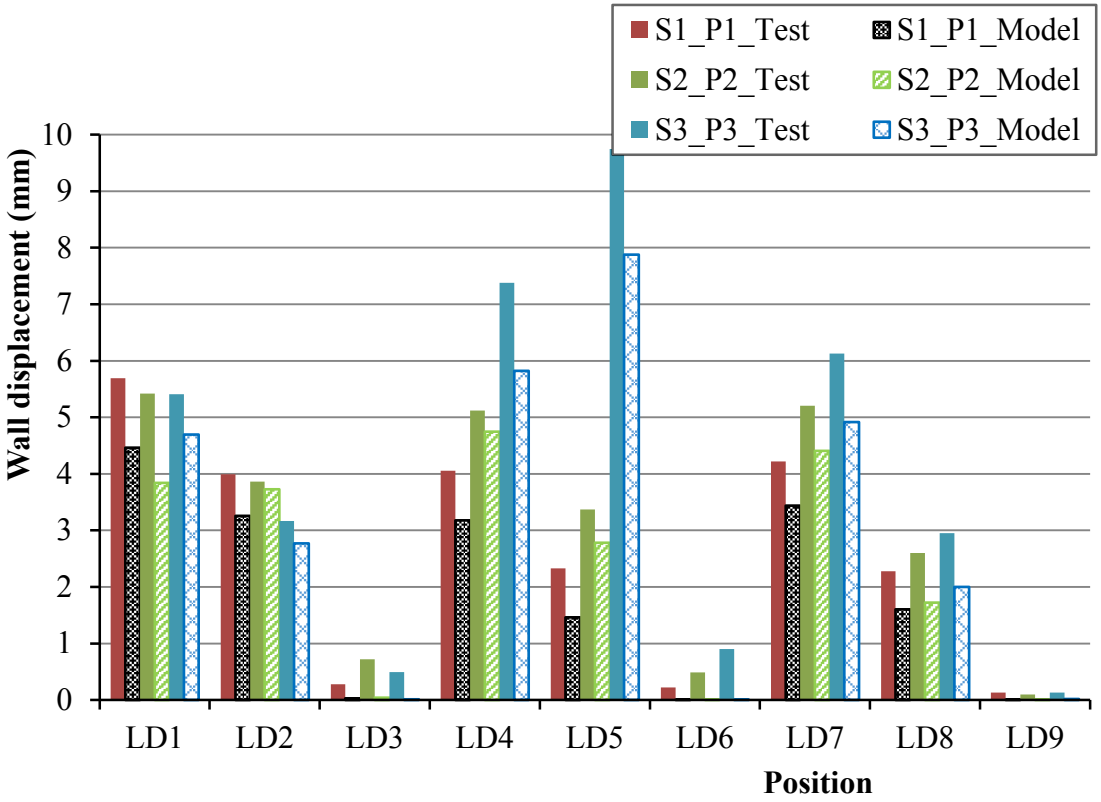

Figure D.15. Comparison of the lateral movement of wall (i.e. Wall L) between FEM and full-scale test, when load was applied to the studs at S1_P1, S2_P2 and S3_P3

D.7 Horizontal load response (parallel to the ridge line)

Horizontal load was applied to the web members of Truss A to compare the horizontal load sharing through the roof, wall, ceiling and ceiling cornice with the full-scale test (Appendix B, Section B.5). The locations of the loading and measured reaction forces and displacements were similar to the full-scale test. Pin and roller supports were imposed at the vertical and horizontal (i.e. L.H1, L.H2, L.H3 and L.H4) load cells' locations respectively. These roller supports resisted the horizontal movement of the top-plates and bottom plates, and were also used to measure the horizontal reaction forces.

Figure D.16 illustrates the comparison of horizontal reaction coefficients (i.e. measured horizontal reaction forces divided by applied load) between the full-scale test and FEM, when the horizontal load was applied at the web members of Truss A. This figure shows the horizontal reaction forces obtained in FEM were similar to the full-scale test.

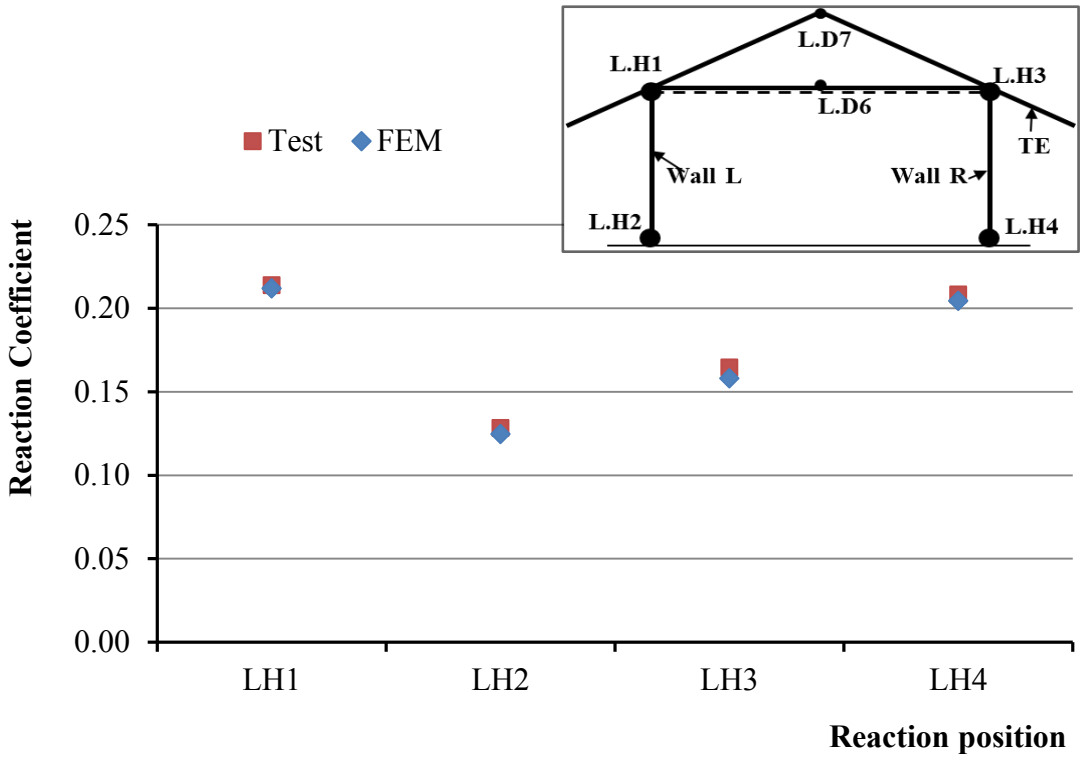

Figure D.16. Comparison of the horizontal reaction coefficients between FEM and full-scale test, when horizontal load was applied to the web members of Truss A

The horizontal flexibility (i.e. horizontal movement divided by applied load) obtained at the top-plates (i.e. L.D1 and L.D5), ceiling (i.e. L.D2 and L.D4), bottom chord of the Trusses A (i.e. L.D3) and E (i.e. L.D6) and apex of Truss E (i.e. L.D7) were compared with FEM and the full-scale test (Figure D.17). Figure D.17 shows that the horizontal flexibility obtained in the FEM at the top-plates (i.e. L.D5), ceiling (i.e. L.D4), bottom chord of Truss A (i.e. L.D3) were higher than that of the full-scale test. This figure also shows that the horizontal flexibility obtained in both bottom chord of the Trusses A (i.e. L.D3) and E (i.e. L.D6) were similar in the FEM but varied in the full-scale test. This is because the horizontal stiffnesses of each RWC of the FEM were the same, whilst they varied in the full-scale test.

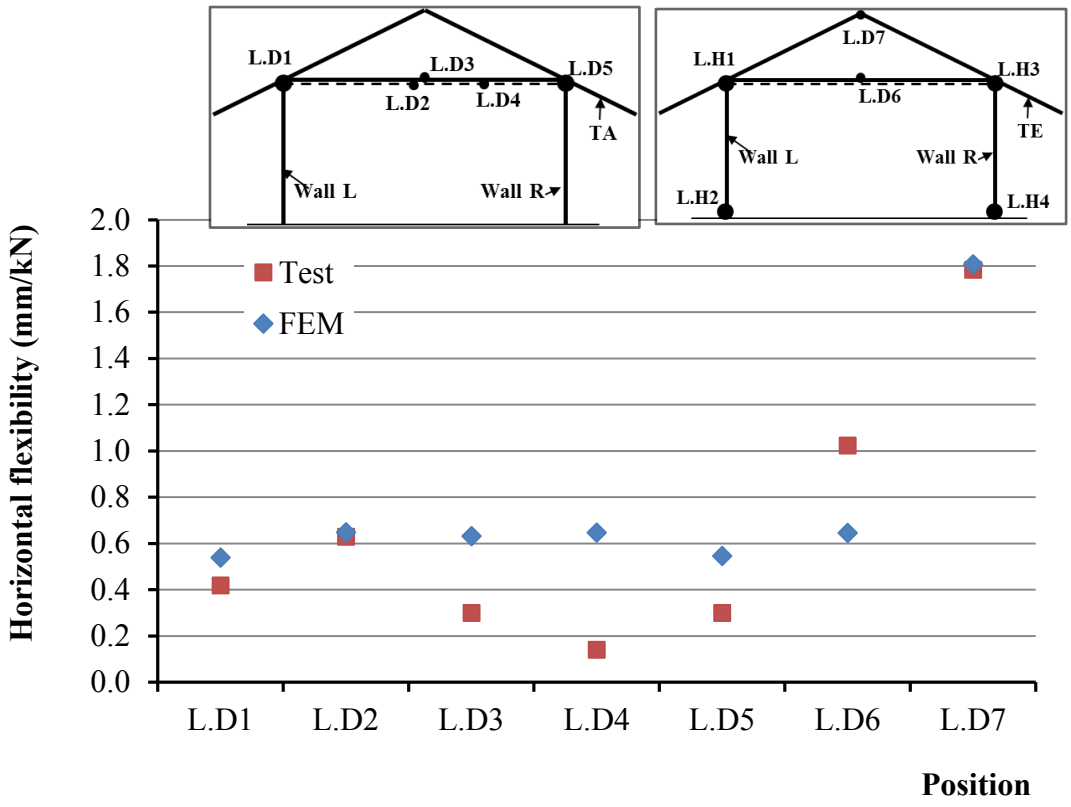

Figure D.17. Comparison of the horizontal flexibility between FEM and full-scale test, when horizontal load was applied to the web members of Truss A

The measured vertical reaction forces in the FEM and full-scale test were divided by the applied load and presented as reaction coefficients in Figure D.18. This figure shows the vertical reaction forces at the bottom plate's supports of the full-scale test were higher than that of the FEM. The horizontal flexibility of the trusses' bottom chords of the full-scale test was less than that of the FEM (see Figure D.17), indicating that the horizontal stiffness of the RWCs of the full-scale test were high compared to that of the FEM. This high stiffness induces high prying forces at the bottom plates' supports when the structural system was subjected to horizontal load compared to FEM. This is the reason for higher vertical reactions obtained in the full-scale tests compared to FEM. The FEM can predict the horizontal load sharing and structural response with about 10% to 15% variation compared to the full-scale test results.

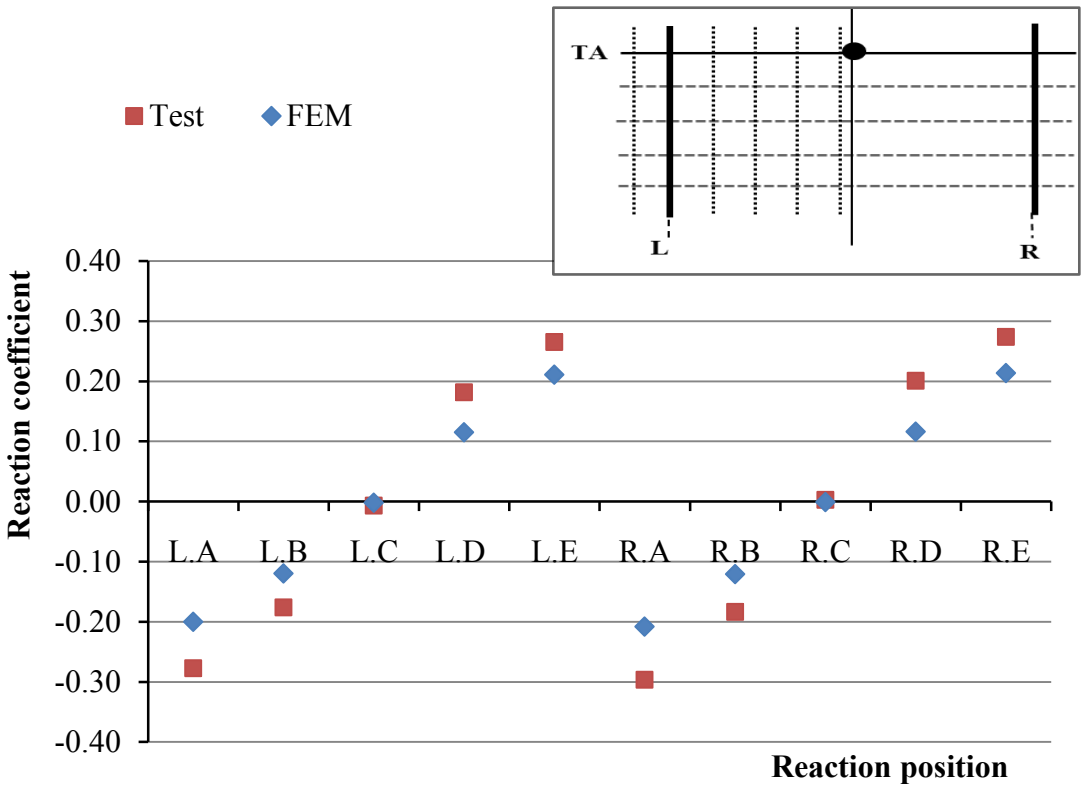

Figure D.18. Comparison of the vertical reaction coefficients between FEM and full-scale test, when horizontal load was applied to the web members of Truss A

APPENDIX E: WIND LOAD ANALYSIS

E.1 Pressure tap layout and the sample wind load calculation

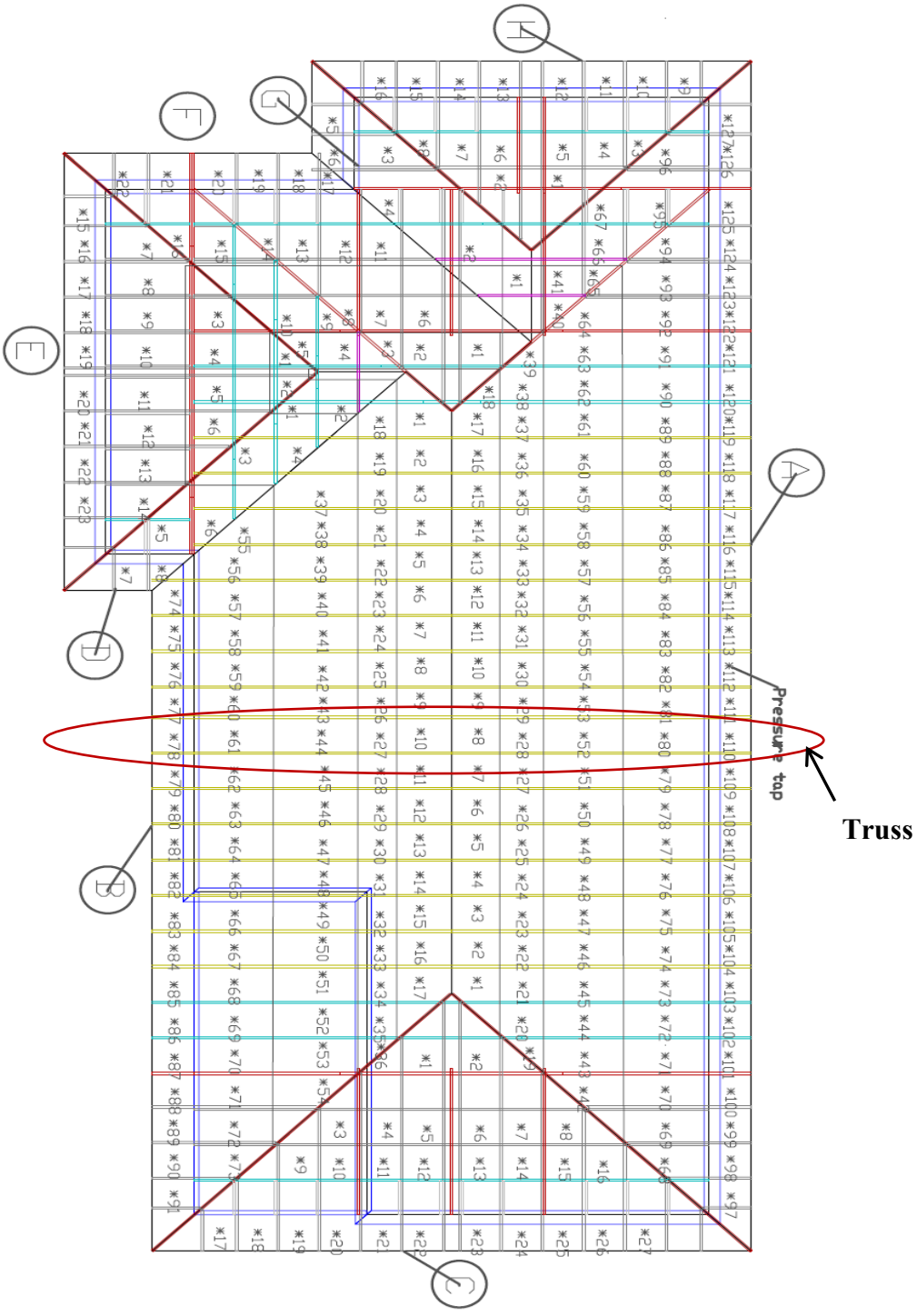

Figure E.1. Pressure tap layout for the representative house

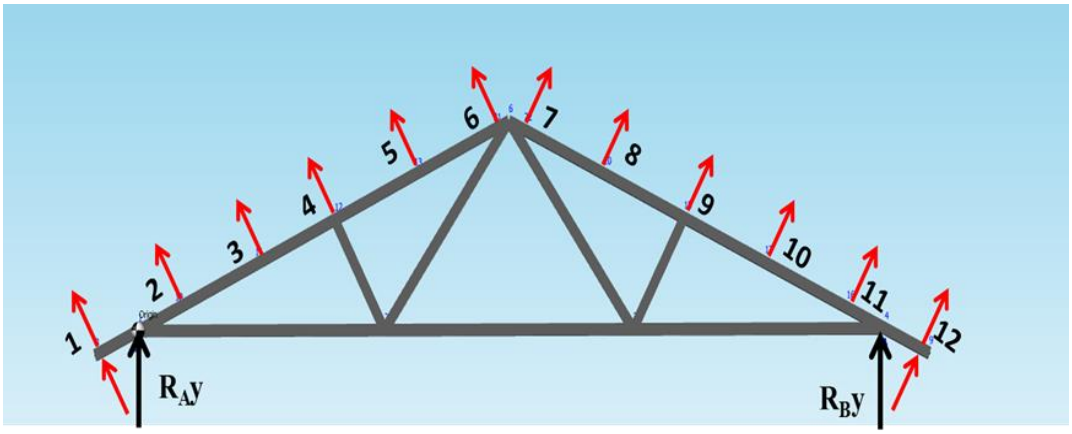

Figure E.2. Loading locations along the Truss A to calculate the Influence coefficient (β_i)

Table E.1. Influence coefficient (β_i) along the Truss A, obtained from single truss analysis

Position (Batten to Truss connection)	$R_{A}y$	$R_{B}y$
1	-0.99	0.06
2	-0.88	-0.05
3	-0.76	-0.17
4	-0.65	-0.28
5	-0.53	-0.40
6	-0.42	-0.51
7	-0.38	-0.55
8	-0.29	-0.64
9	-0.21	-0.72
10	-0.12	-0.81
11	-0.04	-0.89
12	0.05	-0.98

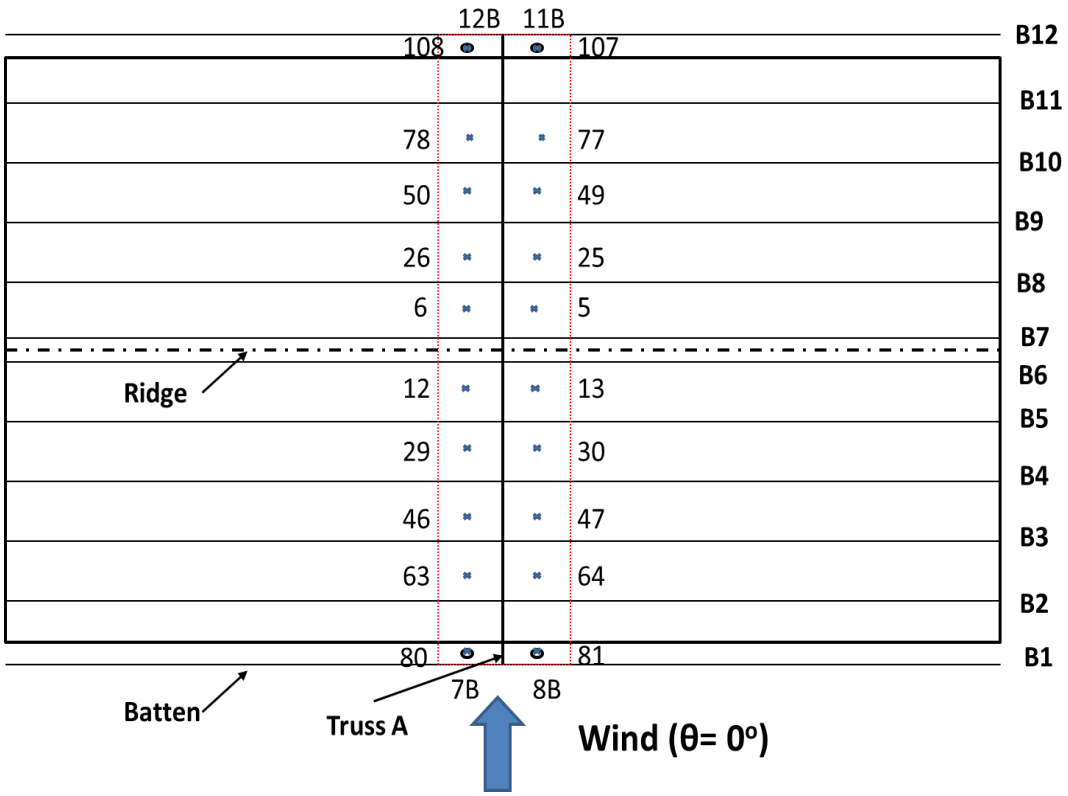

Figure E.3. Pressure tap layout along the Truss A

Table E.2. Mean wind load along the Truss A at wind direction 0°, obtained from wind tunnel studies

Position (Batten to Truss connection)	Pressure tap number	C_p mean at mid roof	Wind speed (m/s)	β_i	Tributary area (m^2)	Mean Wind load (N)	Total Mean Wind Load (N)
1	80	-0.18	57	0.99	0.29	-62.2	-123.7
	81	-0.18	57	0.99	0.29	-61.5	
1*	7B	0.27	57	-0.99	0.27	-87.1	-176.7
	8B	0.28	57	-0.99	0.27	-89.6	
2	63	-0.04	57	-0.88	0.54	20.7	246.3
	64	-0.03	57	-0.88	0.54	18.6	
	80	-0.18	57	-0.88	0.54	104.1	
	81	-0.18	57	-0.88	0.54	102.9	
3	63	-0.04	57	-0.76	0.54	17.9	75.7
	64	-0.03	57	-0.76	0.54	16.2	
	46	-0.05	57	-0.76	0.54	22.6	
	47	-0.04	57	-0.76	0.54	19.0	
4	46	-0.05	57	-0.65	0.54	19.1	90.4
	47	-0.04	57	-0.65	0.54	16.1	
	29	-0.07	57	-0.65	0.54	28.7	
	30	-0.06	57	-0.65	0.54	26.3	
5	29	-0.07	57	-0.53	0.54	23.6	128.7
	30	-0.06	57	-0.53	0.54	21.6	
	12	-0.12	57	-0.53	0.54	41.5	
	13	-0.12	57	-0.53	0.54	41.9	
6	12	-0.12	57	-0.42	0.36	21.7	43.7
	13	-0.12	57	-0.42	0.36	22.0	
7	6	-0.21	57	-0.40	0.36	36.2	71.9
	5	-0.21	57	-0.40	0.36	35.7	
8	6	-0.21	57	-0.38	0.54	52.1	208.3
	5	-0.21	57	-0.38	0.54	51.3	
	25	-0.21	57	-0.38	0.54	52.6	
	26	-0.21	57	-0.38	0.54	52.5	
9	25	-0.21	57	-0.29	0.54	39.4	158.9
	26	-0.21	57	-0.29	0.54	39.3	
	50	-0.22	57	-0.29	0.54	40.2	
	49	-0.21	57	-0.29	0.54	39.9	
10	50	-0.22	57	-0.17	0.54	23.9	94.0
	49	-0.21	57	-0.17	0.54	23.7	
	77	-0.21	57	-0.17	0.54	23.2	
	78	-0.21	57	-0.17	0.54	23.2	
11	77	-0.21	57	-0.05	0.54	7.4	31.2
	78	-0.21	57	-0.05	0.54	7.4	

	108	-0.23	57	-0.05	0.54	8.2	
	107	-0.23	57	-0.05	0.54	8.2	
12	108	-0.23	57	0.06	0.29	-4.9	-9.9
	107	-0.23	57	0.06	0.29	-5.0	
12*	12B	-0.12	57	-0.06	0.27	2.4	4.6
	11B	-0.11	57	-0.06	0.27	2.3	

E.2 Truss hold-down force using AS 1170.2.2011

Table E.3. Truss hold-down force obtained from AS 1170.2.2011 at wind direction 220°

Batten locations	Area (m^2)	β_i	C_{fig}	C_{dyn}	Wind speed (m/s)	Wind load (kN)
B1*	0.27	0.99	-0.50	1.00	57	-0.16
B1	0.29	-0.99	-0.60	1.00	57	0.24
B2	0.54	-0.88	-0.60	1.00	57	0.40
B3	0.54	-0.76	-0.60	1.00	57	0.35
B4	0.54	-0.65	-0.60	1.00	57	0.30
B5	0.54	-0.53	-0.60	1.00	57	0.24
B6	0.36	-0.42	-0.60	1.00	57	0.13
B7	0.36	-0.38	-0.33	1.00	57	0.05
B8	0.54	-0.29	-0.33	1.00	57	0.06
B9	0.54	-0.21	-0.33	1.00	57	0.05
B10	0.54	-0.12	-0.33	1.00	57	0.03
B11	0.54	-0.04	-0.33	1.00	57	0.01
B12	0.29	0.05	-0.33	1.00	57	-0.01
B12*	0.27	-0.05	0.75	1.00	57	-0.01
Hold-down force						1.68